CRANFIELD UNIVERSITY

SCHOOL OF AEROSPACE, TRANSPORT & MANUFACTURING (SATM)

PhD Thesis

Integrated Assessment of Parallel Hybrid Electric Aircraft Propulsion Architectures

Raj Ghelani

Academic Supervisors:
Dr. Ioannis Roumeliotis
Prof. Vassilios Pachidis
Dr. Christos Mourouzidis

Industrial Supervisors:
Dr. Marko Bacic
Mr. Justin Norman

October 2023

Cranfield University

School of Aerospace, Transport and Manufacturing

PhD Thesis

Academic Year: 2020 - 2023

Raj Ghelani

Integrated Assessment of Parallel Hybrid Electric Aircraft Propulsion Architectures

Academic Supervisors: Dr. I. Roumeliotis, Prof. V. Pachidis and Dr. C. Mourouzidis

Industrial Supervisors: Dr. M. Bacic and Mr. J. Norman

Submitted to the School of Aerospace, Transport and Manufacturing in partial fulfilment for the degree of Doctor of Philosophy in Aerospace Engineering at Cranfield University.

© Cranfield University, 2023.All rights reserved. No part of this publication may be reproduced without the written permission of the copyright owner.

Acknowledgments

First of all, I would like to express my gratitude to Prof. Vassilios Pachidis for offering me the opportunity to undertake such an exciting research project within the Rolls-Royce University Technology Centre (UTC) at Cranfield university. I would like to thank my main supervisor, Dr. Ioannis Roumeliotis for guidance and direction throughout the 3 years of PhD. Thanks are also due for Dr. Christos Mourouzidis and Dr Chana Anna Saias for their useful comments during the bi-weekly meetings and on publications.

I would also like to express my gratitude to Rolls-Royce for funding the current research project. I would like to thank my supervisors from Rolls-Royce, Mr. Justin Norman and Dr. Marko Bacic for their active involvement in the project, invaluable technical advice and guidance on research scope.

I would like to thank various colleagues from UTC, Dr. Stevan Van Heerden and Dr. David John Rajendran, for sharing their knowledge in thermal management and turbomachinery. I am indebted in particular to Dr. Ibrahim Eryilmaz, Dr. Mauro Righi and Mr. Daniele Obertino for their invaluable support at some pressing times on systems integration and performance. I would like to thank Dr. Devaiah Nalianda for providing the baseline version of ORION for me to build upon. I would also like to thank all the MSc students over the years who only made my experience richer.

I would also like to thank my officemates, Seyfettin, Dario, Pierre, Dimitrios, Stevan, Mauro and Sarath for making the office time a great one. Although we met only post the halfway stage due to Covid, it was good while it lasted. I would like to thank Seyfettin, Dario and Adriano for their friendship during the PhD, it definitely lightened my mood talking, joking with them.

I would like to express immense gratitude to my parents, for their unconditional love and support all these years. They never complained despite me staying away for them for the past few years and always kept motivating me. I will ever be grateful for it. I would like to thank various flatmates over the years for keeping the mood lively. I would like to thank my friends, Sachin, Juanito, John(Qihong), Anna and Pinakin besides many others for getting me through hard times and always having my back.

I dedicate this thesis to my Mother.

Abstract

Advisory Council for Aeronautical Research in Europe (ACARE) has published ambitious goals for reduction in emissions from aircraft applications by the year 2050. Hybrid-electric and alternative fuelled powerplants have been proposed as one of the major solutions to resolve this problem.

There has been significant industrial push to build and test viable hybrid-electric propulsion systems onboard aircraft and certify them for flight, with Rolls-Royce ACCEL, Airbus E-Fan X and Boeing SUGAR VOLT being some recent examples. Despite this, there exists significant uncertainty around the potential fuel burn benefits from these architectures across the different aircraft classes, the impact on gas turbine design, thermal management and aircraft integration, as well as fleet technology penetration. The work in open literature has focussed on individual aspects mentioned above but no study was found considering all these aspects in a common design and optimization loop. The aim of this thesis is to develop robust integrated design and optimization methods, to help industry examine future application scenarios in a more objective, systematic and therefore, more cost-effective manner.

The regional to single aircraft design space is explored with ATR 72, Fokker 100 and A320 being the baseline aircraft platforms. Initially, a design space exploration is performed for the Fokker 100 style airframe utilizing lithium ion batteries in a parallel hybrid configuration. The impact of hybrid gas turbine cycle redesign strategies are benchmarked and compared to retrofit hybrid gas turbine. A power management optimization loop is set up to optimize the power split for varying battery pack sizes and motor powers on different mission ranges. This sweep is also performed for varying technology levels on gas turbine, motor power density and battery energy density. It is demonstrated that the benefit from electrification improves with improvement in gas turbine technology level.

The integrated hybrid gas turbine cycle design and power management optimization ANN method is applied to all three aircraft platforms for EIS 2035 time frame.

The optimal power management strategies favour take-off and initial climb for redesigned gas turbines while they favour cruise for retrofit gas turbines. Incorporation of direct operating cost modules show retrofit hybrid systems having a lower direct operating cost as compared to redesigned hybrid systems owing to reduced gas turbine maintenance cost. The multi-mission method is applied to the test cases showing the penalty paid in carrying a fixed battery pack.

Two thermal management architectures, ram air-liquid coolant heat exchanger and vapour compression cycles are utilized to reject the heat load from the electrical systems. The design space of both the systems are first explored for varying levels on quantity of heat load, quality of heat load and flight mission conditions. The method to integrate optimal combinations of thermal management architectures in terms of, coolant mass flow rate, condenser pinch, condenser geometry and compressor pressure ratio is utilized and applied to different propulsion configurations. The full framework is also expanded to include proton exchange membrane fuel cells and hydrogen-powered gas turbines.

A final technological assessment is performed for the regional ATR 72 style aircraft platform for both thermal management architectures. A pure electric, battery and fuel cell powered aircraft with an optimal power split is identified as a suitable candidate against kerosene and hydrogen powered gas turbines to power EIS 2035 regional turboprop. While for single-aisle applications, there is a case for mild hybridization to reduce NOx and improve gas turbine operability at part load settings.

Contents

Acknowledgments v

Abstract vii

1 Introduction 1

1.1 General context . . . 1
1.2 Aim and objectives . . . 8
1.3 Contribution to knowledge . . . 9
1.4 Thesis outline . . . 10

2 Literature Review 13

2.1 Hybrid gas turbine cycle design . . . 14
2.2 PMS optimization and mission performance . . . 19
2.3 Thermal management strategies . . . 23
2.4 Existing Integrated frameworks . . . 25
2.5 Research questions . . . 26

3 Methodology 33

3.1 Overview of test cases . . . 33
3.2 Introduction . . . 35
3.3 Hybrid GT cycle design and weight assessment . . . 36
3.3.1 Hybrid GT cycle design . . . 36
3.3.2 GT weight assessment . . . 41
3.4 PMS optimization and integration ANN . . . 45
3.4.1 Integration ANN . . . 45
3.4.2 PMS optimization . . . 51
3.5 Direct operating cost . . . 53
3.6 Multi mission energy management . . . 56
3.7 Electrical systems modelling . . . 61

3.7.1 Introduction . . . 61
3.7.2 PMAD Modelling . . . 62
3.7.3 Battery pack Modelling . . . 68
3.7.4 PEM FC Modelling . . . 69
3.8 Ram Air HEX and VCC Modelling . . . 73
3.8.1 Compact HEX DP and OD modelling . . . 74
3.8.2 VCC HEX DP and OD modelling . . . 80
3.9 Integration of TMS into the framework . . . 84
3.10 ORION and Full framework at a glance . . . 88

4 Results **93**
4.1 Introduction . . . 93
4.2 HEPS Design space exploration . . . 98
4.2.1 Impact of GT cycle design . . . 98
4.2.2 Impact of assumptions on electrical systems . . . 104
4.2.3 Impact of optimal PMS . . . 111
4.2.4 Impact of GT technology level . . . 111
4.3 Integrated multi-mission assessment across aircraft classes . . . 116
4.3.1 Gas turbine cycle design . . . 116
4.3.2 PMS optimization and fuel burn benefit trends . . . 122
4.3.3 Multi mission assessment . . . 129
4.3.4 Direct operating cost trends . . . 136
4.3.5 Synthesis . . . 141
4.4 TMS design and optimization . . . 143
4.4.1 TMS design space . . . 143
4.4.2 TMS impact mission level . . . 153
4.5 Final Technology Evaluation . . . 155
4.5.1 LH2 GT . . . 155
4.5.2 LH2 GT PEM FC hybrid . . . 157
4.5.3 Regional Turboprop Architectural Comparison . . . 163

5 Summary, Conclusions & Future Work **169**
5.1 Summary . . . 169
5.2 Conclusions . . . 171
5.3 Future Work . . . 172
5.3.1 Modelling limitations . . . 172
5.3.2 Case studies . . . 174

Bibliography **177**

List of Tables

2.1 Parallel HEPS Integrated frameworks & studies. 29
2.2 Parallel HEPS Integrated frameworks & studies cont. 30
2.3 Parallel HEPS Integrated frameworks & studies cont.2 31

3.1 3-point cycle design parameters & variables 41
3.2 GT weight and sfc comparison 42
3.3 Hybrid and baseline component weight comparison 43
3.4 Hybrid engine surrogate inputs & outputs 46
3.5 Updated hybrid engine surrogate inputs & outputs 48
3.6 Neural network inputs 48
3.7 Surrogate optimizer settings 52
3.8 GA settings 53
3.9 Lifing model inputs 54
3.10 Direct operating cost assumptions 56
3.11 Battery cell characteristics used 69
3.12 Plate fin HEX design parameters 74
3.13 Comparison on same boundary conditions, HEX parameters 79

4.1 Fokker 100 aircraft and engine data 94
4.2 A320 aircraft and engine data 96
4.3 ATR 72 aircraft and engine data 97
4.4 BAe 146 aircraft and engine data 97
4.5 Comparison of baseline, retrofit hybrid and redesigned hybrid engine cycles 101
4.6 Electrical powertrain assumptions 105
4.7 Comparison of baseline, retrofit hybrid and redesigned hybrid engine cycles (EIS 2035) 113
4.8 SMR thrust requirements 117

4.9 EIS 2010 SMR GT cycle data 117
4.10 EIS 2035 SMR GT cycle data 118
4.11 EIS 2035 Turboprop GT cycle data 121
4.12 Comparison between redesigned and retrofit 123
4.13 PMS bounds 152
4.14 HY SMR thrust requirements 158
4.15 EIS 2010 SMR GT cycle data (KE and HY) 159
4.16 Parameter bounds 162

List of Figures

1.1 Domestic and International passengers in billions [1] 2
1.2 Predicted Aviation emissions and technology levers [2] 2
1.3 Fuel burn per pax nm trends from 1960 to 2014 [13] 4
1.4 Civil transport aircraft efficiency [12] 4
1.5 HEPS architectures [24] 5
1.6 Hybrid electric aircraft concepts from NASA: a) N3-X; b) ECO-150; c) STARC-ABL; d) SUGAR FREEZE [14] [28] 6
1.7 Predicted application of future technologies [29] 7
1.8 Predicted horizons [30] 8
1.9 Parallel hybrid applications[14] - A) UTRC hGTF[32], B)RR Liberty-Works EVE [31] 8

2.1 Traditional 3-point gas turbine cycle design process from Mourouzidis [80] 15
2.2 Fuel burn benefits for the hybrid GTF [32] 16
2.3 Physical integration architectures MIPH [25] 17
2.4 Potential surge margin benefits from electrification [26] 18
2.5 Parallel HEPS SUGAR VOLT Study [91] 20
2.6 Energy savings for 25000 lbs payload and 2500 hp motor for several mission ranges [57] 21
2.7 Variation of PMS for on 1500 nm [57] 21
2.8 Flight operational data for Boeing 737 [60] 22
2.9 Variation in adiabatic batteries temperature across flight mission [64] 24
2.10 E PASS Integrated framework from Cinar [88] 25
2.11 Parallel HEPS design loop [31] 26
2.12 HEPS Multi mission techno-economic assessment from Zhang [60] . . 28

3.1 Scope of Work 34

3.2 HEPS Architectures assessed . . . 35
3.3 Framework . . . 36
3.4 GT design points along mission . . . 37
3.5 Relationship between SFC, thermal, transfer and propulsive efficiencies, 2015 Rolls-Royce plc.[10] . . . 38
3.6 Fuel burn, drag and SFC curves for the Geared Fixed model.[80] . . . 39
3.7 3-point cycle design solving method . . . 40
3.8 Gas path validation . . . 42
3.9 Comparison of hybrid and non hybrid gas path . . . 43
3.10 Baseline GT trades for different specific thrusts . . . 44
3.11 Comparison of trends between hybrid and non hybrid GT . . . 44
3.12 GT-PMS ANN inputs & outputs . . . 46
3.13 Mission fuel burn . . . 47
3.14 Hybrid DP and OD deck method . . . 48
3.15 SMR test case ANN fits . . . 49
3.16 Regional turboprop test case ANN fits . . . 50
3.17 Comparison of optimal PMS trends (ANN vs TM) . . . 50
3.18 Comparison of trends GA vs surrogate . . . 52
3.19 Trends comparison with Trawick [57] . . . 53
3.20 HPT Lifing method[138] . . . 55
3.21 Impact of T/O temperatures on GT cycles to failure . . . 56
3.22 Impact of CR temperatures on GT cycles to failure . . . 57
3.23 Zhang design space example [60] . . . 58
3.24 Multi mission method . . . 59
3.25 Integrated multi mission schematic . . . 60
3.26 Off-design range utilization for narrow body aircraft [140] . . . 61
3.27 Basic PMAD schematic [25] . . . 62
3.28 PMAD schematic used . . . 63
3.29 Aircraft transmission system Turbo-electric example [144] . . . 63
3.30 Aluminium cables (kg/m) as a function of line voltage and power [143] 64
3.31 Comparison of different electric motor types [24] . . . 64
3.32 PMS motor topology . . . 65
3.33 PMS motor power density vs RPM generated curves . . . 66
3.34 Motor efficiency map against torque and RPM . . . 67
3.35 Inverter efficiency vs power . . . 68
3.36 Battery pack as defined in [24] . . . 69

3.37 Battery pack sizing method as in [91] . . . 70
3.38 Battery cell discharge rates . . . 70
3.39 PEM FC BoP . . . 71
3.40 Fuel cell schematic . . . 72
3.41 PEM FC efficiency . . . 73
3.42 Plate fin HEX [152] . . . 75
3.43 HEX design method . . . 76
3.44 HEX Off-design method . . . 77
3.45 Thermal power density - A) UTRC hGTF[70], B)Raj Ghelani . . . 79
3.46 Typical vapour compression cycle . . . 81
3.47 VCC design optimization . . . 82
3.48 VCC Off-design solving . . . 83
3.49 TMS Integration . . . 85
3.50 VCC packs per architecture . . . 86
3.51 Fuel cell HEX/VCC penalty . . . 87
3.52 Mission solving method for hydrogen fuel cell, battery, hydrogen GT . 89
3.53 HY PAX . . . 89
3.54 HEPS Aircraft Design Space . . . 90
3.55 Integrated framework . . . 91

4.1 Aviation emissions for 2022 by aircraft type [161] . . . 95
4.2 Fokker 100 payload range diagram validation against [162] . . . 95
4.3 A320 payload range diagram validation against [163] . . . 96
4.4 ATR 72 payload range diagram and spot point check against [160] . . 96
4.5 BAe 146 payload range diagram validation recreated from [164] . . . 97
4.6 Variation in T40 with power on-take at EOR on same thrust level . . 99
4.7 Variation in T30 with power on-take at EOR on same thrust level . . 99
4.8 Power on-takes for T/O and top of climb . . . 100
4.9 LPC operability vs on-take at EOR . . . 102
4.10 HPC operability vs on-take at EOR . . . 103
4.11 LPC operability vs on-take at TOC . . . 103
4.12 HPC operability vs on-take at TOC . . . 104
4.13 Payload vs battery energy densities for range of ranges . . . 105
4.14 Normalized delta energy (%) . . . 107
4.15 Normalized delta fuel (%) . . . 107
4.16 Battery weights vs range of ranges sweep for 0.5 MW retrofit . . . 108

4.17 Delta energy % for 0.5 MW . . . 109
4.18 Delta energy % for 1 MW . . . 110
4.19 % Delta fuel burn for 1153 kg battery pack . . . 110
4.20 % Delta fuel for 2307 kg battery pack . . . 111
4.21 Retrofit vs Optimal PMS . . . 112
4.22 % Delta fuel burn hTAY vs cTAY . . . 113
4.23 % Delta fuel burn, hybrid EIS2035 vs conventional EIS2035 . . . 114
4.24 Delta energy burn (%), hTAY vs cTAY . . . 115
4.25 Delta energy burn (%), hybrid EIS2035 vs conventional EIS2035 . . . 115
4.26 EIS 2010 SMR retrofit booster operating points, top of climb . . . 118
4.27 EIS 2010 SMR retrofit HPC operating points, top of climb . . . 119
4.28 Turboprop cycle design space without efficiency correction . . . 120
4.29 Turboprop cycle design space with efficiency correction . . . 120
4.30 Cruise T40 variation with degree of hybridization . . . 121
4.31 SMR Optimal PMS EIS 2035 (retrofit) . . . 123
4.32 SMR Optimal PMS EIS 2035 (redesigned) . . . 123
4.33 Battery pack weight variation across mission ranges (redesigned) . . . 124
4.34 Electrical power train weight variation across mission ranges (redesigned) 124
4.35 Motor power comparison on 1000 nm between redesigned and retrofit 125
4.36 SMR Optimal PMS EIS 2010 (retrofit) . . . 126
4.37 SMR Optimal PMS EIS 2010 (redesigned) . . . 126
4.38 Regional Optimal PMS (retrofit) . . . 127
4.39 Regional Optimal PMS (redesigned) . . . 128
4.40 Regional Optimal DOC PMS (retrofit) . . . 128
4.41 Percentage fuel burn benefit for SMR, regional turbofan and turboprop test case with varying battery energy densities . . . 129
4.42 SMR test case, 400 nm design range, redesign . . . 130
4.43 SMR test case, 600 nm design range, redesign . . . 131
4.44 SMR test case, 400 nm design range, retrofit . . . 131
4.45 SMR test case, 600 nm design range, retrofit . . . 132
4.46 Direct operating cost comparison, SMR . . . 132
4.47 Scenario 1, SMR . . . 133
4.48 Multi mission fuel burn benefit, SMR . . . 134
4.49 Scenario 2, SMR . . . 134
4.50 Overall fuel burn benefit, regional turboprop, Scenario 1 . . . 135
4.51 Overall fuel burn benefit, regional turboprop, Scenario 2 . . . 136

4.52 Direct operating cost comparison, Regional turboprop 137
4.53 Delta DOC trends for single variable variations 138
4.54 Delta DOC variation for redesigned 139
4.55 Delta DOC variation for retrofit 139
4.56 Delta DOC variation for retrofit for double overhaul cost 140
4.57 Optimal PMS ATR retrofit 140
4.58 Optimal PMS ATR redesigned 141
4.59 DOC vs Fuel burn benefit pareto 142
4.60 ATR 72 power profile 144
4.61 2 MW fuel cell cell DSE 144
4.62 1.5 MW fuel cell cell DSE 145
4.63 1 MW fuel cell cell DSE 146
4.64 0.5 MW fuel cell cell DSE 146
4.65 RA HEX energy penalty compared at ISA +15, +20 and +25 147
4.66 VCC energy penalty for FC loads, HP = 1.0, optimal PR 148
4.67 VCC energy penalty for FC loads breakdown, HP = 1.0, optimal PR 149
4.68 Energy penalty comparison between VCC sized for ISA 15 and 25 . . 149
4.69 VCC energy penalty comparison between fixed and optimal PR . . . 150
4.70 VCC energy penalty for FC with varying HP 150
4.71 Energy penalty comparison between Battery and Fuel cell 151
4.72 Optimal Parameters variation with sweep on PMS for Fuel cell splits 152
4.73 Penalty breakdown 153
4.74 PMS without TMS 154
4.75 PMS with TMS 154
4.76 Fuel burn due to TMS 154
4.77 Comparison of cruise esfc against core specific work [39] 156
4.78 Comparison of cruise esfc against core specific work highlighting LH2 switch temperatures [39] 157
4.79 PEM FC hybrid aircraft 158
4.80 Delta Fuel burn for FC wrt LH2 GT, CFM 159
4.81 Delta Fuel burn for FC wrt LH2 GT, CFM, no FC weight 160
4.82 Delta Fuel burn for FC wrt LH2 GT, GTF 160
4.83 Delta Fuel burn for FC wrt LH2 GT, GTF, no FC weight 161
4.84 Total Balance of power plant weight for complete fuel cell aircraft . . 162
4.85 Maximum payload vs range for 50% FC eta 163
4.86 Maximum payload vs range for 60% FC eta 163

4.87 Delta Fuel burn for FC wrt LH2 GT 165
4.88 Optimal PMS for BAT FC architecture 166
4.89 Payload comparison for all architectures 167
4.90 Delta EPX for all architectures 168

5.1 Future framework 175

Nomenclature

Equations

m_f	Fuel flow $[kg/s]$
r_n	Radius motor geometry for different subsections
ρ_n	Density of motor material for different subsections
R	Gas constant
ω_m	rotational speed of the rotor
m_m	Total motor mass
m_{AIR}	Air mass flow
E_0	Zero current voltage
L	Length
B	Fin width
X	Martinelli parameter
x	Vapour quality of refrigerant
CF	Plate fin correction factor
Ff	Boiling factor
$T_{cold,in}$	Inlet temperature of cold side
$T_{cold,out}$	Outlet temperature of cold side
$T_{hot,in}$	Inlet temperature of hot side
$T_{hot,out}$	Outlet temperature of hot side
V_c	Cell voltage
P_m	Motor power
P_{FC}	Fuel cell power
F	Faraday constant
v_{ag}	Air gap volume
D_M	Machine diameter
D_{AG}	Air Gap diameter
A_{AG}	Air Gap area
P_L	Motor losses
P_{shaft}	Shaft Power
P_{cool}	Motor cooling losses
AR_{HEX}	Aspect ratio HEX
eta_{mot}	Motor efficiency
U_{mot}	Motor voltage

n_{series}	Number of battery pack cells in series
$n_{parallel}$	Number of battery pack cells in parallel
E_{bat}	Battery pack energy
η_{FC}	Fuel cell efficiency
F	Faraday constant
Ff	Boiling nucleation factor
$\dot{m}_{H2}$	Hydrogen mass flow
$LMTD_i$	Logarithmic mean temperature difference of the i-th enthalpy interval
Q	Heat transfer
N_L	Number of cold layers of the HEX
PS	Plate spacing
A_F	Frontal area
FP	Fin pitch
H	Total height
Re	Reynolds number
Pr	Prandtl number
A_c	Cold side area
G_r	Refrigerant mass flux
h_conv	Convective heat transfer
d_h	Hydraulic diameter
B_g	Magnetic strength
$DragtoPow$	Shaft power for the thrust/drag
δP_{loss}	Pressure loss

Acronyms

ACARE	Advisory Council for Aviation Research and Innovation in Europe
ADP	Aerodynamic design point
ANN	Artificial Neural Network
AR	Aspect ratio
BoP	Balance of Plant
BPR	Bypass ratio
BWB	Blended wing body
CRZ	Cruise
CU	Cranfield University
DOC	Direct Operating Cost

DoH	Degree of hybridization
ECS	Environmental Control System
EIS	Entry into service
EOR	End of Runway
FPR	Fan pressure ratio
GT	Gas turbine
HE	Degree of hybridization by energy
HEPS	Hybrid electric propulsion systems
HEX	Heat exchanger
hFAN	Hybrid Fan
HP	Degree of hybridization by power
HPC	High pressure compressor
HPT	High Pressure Turbine
IATA	International Air Transport Association
IPC	Intermediate pressure compressor
LH2	Liquid hydrogen
MIPH	Mechanically Integrated Parallel hybrid
MTOW	Maximum take-off weight
NASA	National Aeronautics and Space Administration
NGV	Nozzle Guide Vane
NTU	Number of transfer Units
OPR	Overall pressure ratio
PMAD	Power Management and Distribution
PEM	Proton Exchange Membrane
PMS	Power Management Strategy
PO	Power off-take
PS	Power split
RSM	Response Surface Model
SoC	State of Charge
SMR	Short Medium range
TEEM	Turbine Electrified Energy management
TERA	Techno-Economic Risk Assessment
TOC	Top of Climb
TOW	Take-off weight
TMS	Thermal Management System
TSFC	Thrust specific fuel consumption

T30	High pressure compressor outlet temperature
T40	Combustion outlet temperature
T41	High pressure turbine rotor inlet temperature
VCC	Vapour compression cycle
VIGV	Variable Inlet guide vane
VSV	Variable Stator Vane
VTOL	Vertical take-off and landing
WS	Compressor pressure ratio split

Chapter 1

Introduction

This chapter provides the general context of the research, the path envisioned towards de-carbonisation and the design strategy of various aero-engine manufacturers and aerospace consortium to meet the ACARE flightpath 2050 requirements. An overview of different hybrid-electric architectures, electrification technologies and aircraft platforms is shown. The research gap is briefly highlighted and the chapter is concluded by listing the aims and objectives of the research, contribution to knowledge and thesis outline.

Contents

1.1 General context 1
1.2 Aim and objectives 8
1.3 Contribution to knowledge 9
1.4 Thesis outline 10

1.1 General context

Aviation remains a growing market despite the blip in fleet usage in the years 2020-2022, affected by COVID. In the forecast by IATA [1], the regional airline passenger demand for 2023 is back to 2019 levels as can be seen in Figure 1.1. But as the market consistently keeps growing, so do the emissions generated from aviation. Although current aviation emissions only amount to 3% of global carbon dioxide emissions but this value could well be in excess of 20% by the year 2050, provided rest of the sectors have been electrified [2]. Hence, it almost becomes imperative to develop airframe or propulsion technologies that have a big leap in terms of emissions and fuel burn reduction.

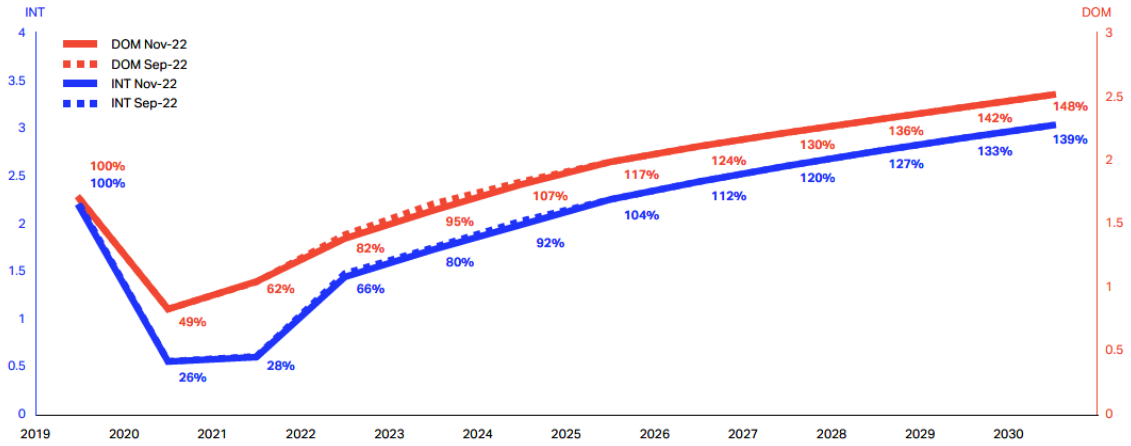


Figure 1.1: Domestic and International passengers in billions [1]

There has been increased effort put in by European Union and UK government in the form of various Clean Aviation [3],[4],[5], Flyzero [6] and independent consultant [2] projects to strategically investigate future decarbonisation technologies. Several proposals have been named in terms of potential pathways to reduce global warming impact of aviation until year 2050 shown in Figure 1.2.

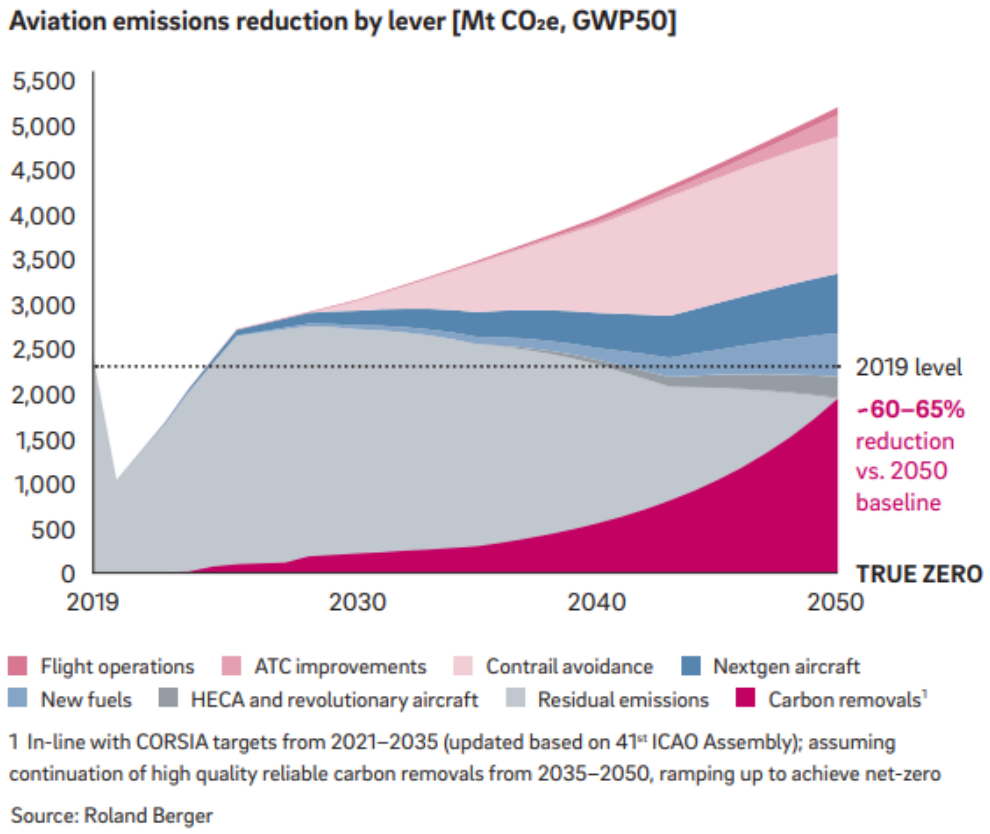


Figure 1.2: Predicted Aviation emissions and technology levers [2]

It can be seen from Figure 1.2, that the drop in global warming impact of aviation is envisioned to come from more optimal mission profiles to avoid contrails, new fuels, more optimally designed propulsion architectures & improvements to the airframe. The major chunk of reduction in global warming impact from aviation comes from avoiding contrails, this is due to the high global warming index of water vapour. The envisioned ways to reduce contrail formation are modified flight paths [7] and higher use of Sustainable Aviation Fuels [8]. In order to understand what could be the potential levers to improve overall aircraft-engine efficiency, it would be worth looking at the history of aviation. In the past 60 years of aviation (Figure 1.3, Figure 1.4), the improvement in airframe and engine efficiency has come in the form of evolutions rather than revolutions. The only big drop in fuel burn is only seen between 1969-1972 due to the introduction of Boeing 747 post which the drop in fuel burn has been slower. The baseline aircraft-engine post 1970s has remained a tube and wing configuration with increasingly lower specific thrust/higher bypass ratio turbofan engines (three-shaft, geared or direct drive). The improvement has come in the form of greater use of composites, winglets, morphing wings, higher aspect ratio for aircraft and better turbine cooling techniques and materials enabling higher core temperatures and pressures for the engine. The improvement in airframe-engine integration and installation methods have resulted in increased fuel burn benefit by utilizing lower specific thrust/high bypass ratio engines. Though 2010 onwards, the benefit achievable by these means have plateaued, leading to research into new airframe and propulsion architectures. These has further been well articulated by reports, papers from Cumpsty [9], Whurr [10], Epstein [11], and Kyprianidis [12].

The plateauing of baseline aircraft-engine efficiency has led to a very significantly increasing amount of studies in exploring different airframes, hybrid electric propulsion architectures and new fuels, as can be seen by the Clean Aviation investments and all the work from NASA over the years [14],[15],[16],[17][18]. NASA condensed all the research on unconventional airframes and hybrid electric architectures in a single presentation shown in 2017 [19]. The various aircraft configurations can be seen in the Figure 1.6 while the hybrid electric, completely electric or more electric propulsion architectures can be seen in Figure 1.5. There has also been a high number of studies on alternative fuels , especially on hydrogen, from Brewer [20] and number of Cranfield studies, Goldberg [21] and Verstraete [22], [23]. Although hydrogen would push to a volume constrained aircraft but the design process for optimization aircraft engine architecture would remain the same hence the conclusions on HEPS architectures could be assumed to hold true even with alternative fuels. Coming back

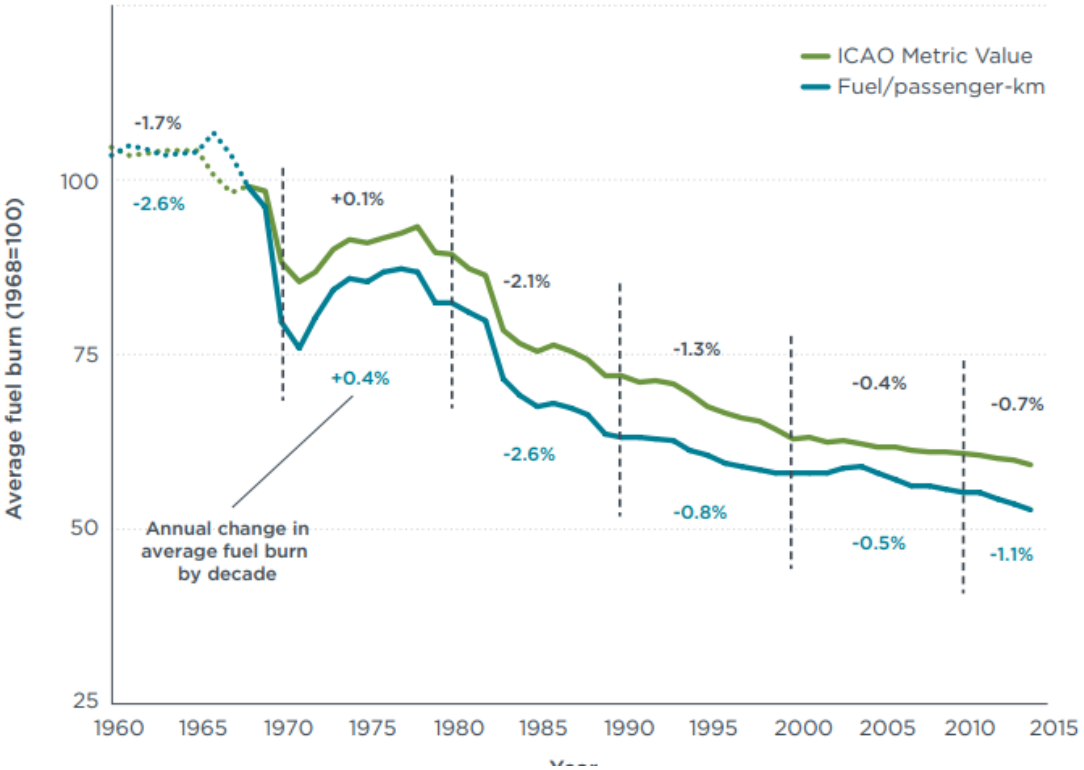


Figure 1.3: Fuel burn per pax nm trends from 1960 to 2014 [13]

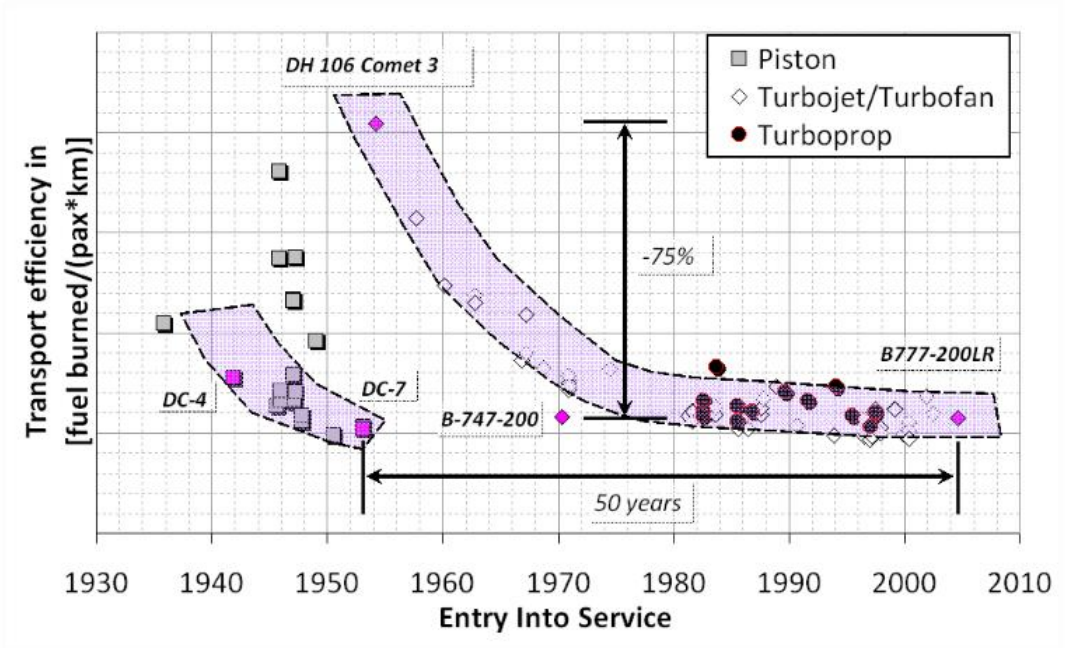


Figure 1.4: Civil transport aircraft efficiency [12]

to HEPS architectures and airframes, as that is the broad topic of research, it can be noticed that each architecture is tailored to a particular aircraft. Primarily the HEPS architectures could be Series, Parallel, Turbo-electric, Partial turo-electric,

combination of either of these or completely electric. Parallel architecture consists of a battery or a fuel cell powered motor, boosting the gas turbine by driving Fan, IPC or HPC shaft via a clutch or a gearbox. The potential advantage of utilizing such a configuration is that the baseline GT could be potentially pushed to higher thermal efficiencies by downsizing the core and also get a benefit in NOx and DOC.

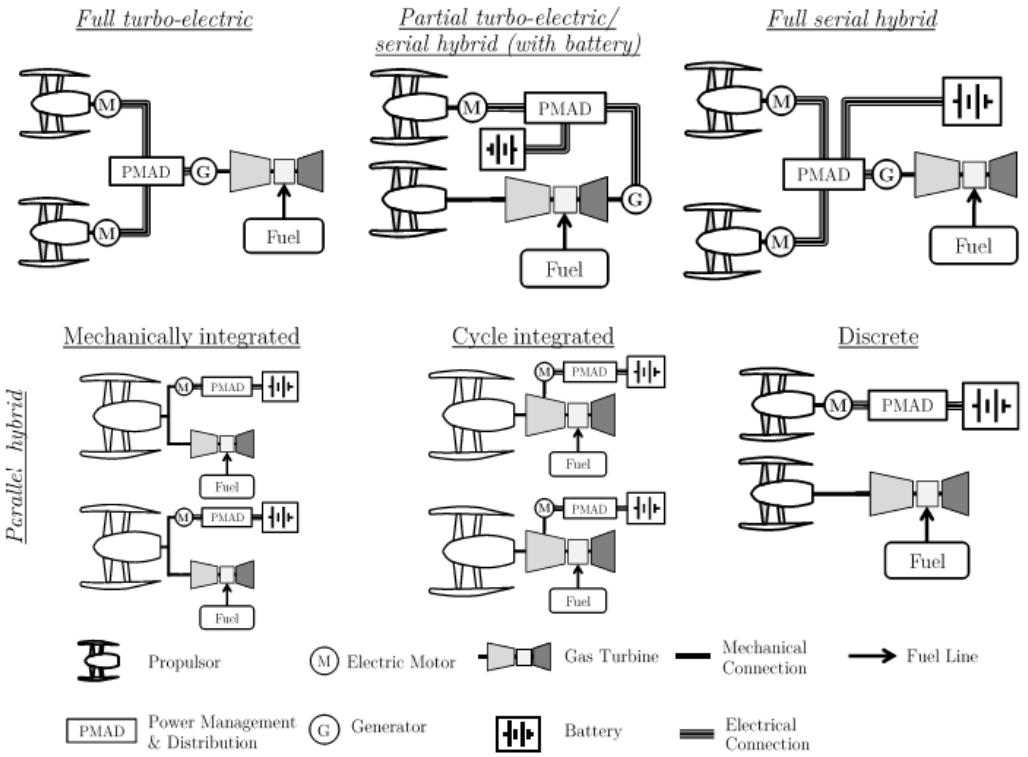


Figure 1.5: HEPS architectures [24]

Turbo-electric architecture consists of a gas turbine generator driving a series of motor-driven fans, thereby de-coupling the design of the fan and the gas turbine and utilizing the higher power density of the electric motors. Series architecture is primarily a turbo-electric architecture where a battery or fuel cell could be providing additional electric power to the distribution power thereby downsizing the gas turbine. Partial turbo-electric architecture is basically a parallel architecture, albeit mechanical power extracted from one of turbofan engines and then using generator-motor combination driving a third fan. Pure electric one is the simplest one as it is a fully electric battery or fuel cell powered architecture. More information on the architectures can be found in [16], [25] & [24]. If a look is now made at the airframes in the Figure 1.6, each of the airframe has been designed with a specific HEPS architecture in mind. The three study airframes were a A350 class BWB aircraft (N3-X) utilizing series/turbo-electric architecture, A320/B737 class Truss-based and high Aspect ratio aircraft utilizing

parallel hybrid architecture with batteries (SUGAR FREEZE, SUGAR VOLT) & A320 class boundary layer ingesting, partial turbo-electric aircraft (STARC-ABL).

It can be noticed that either of N3-X or STARC-ABL will need major modifications to the airframe and the electric generators, motors, inverters and cables in order of 10-15 MW or even greater [26], [27], [21], [18]. This heavy requirement of change in airframe and development of MW-scale PMD would push the entry into service to potentially post 2040-45, which would mean an interim solution would be needed to ease the transition to the ideal solution of blended wing body distributed propulsion turboelectric aircraft. This is where parallel hybrid-electric aircraft comes in, as it is the easiest to certify because the airframe doesn't require major changes and most of the airframe-engine could be reused. This is the reason why maximum of the studies in past 6-7 years have heavily focussed on parallel HEPS architectures. All the studies on parallel HEPS have been elaborated in detail in the Chapter 2 of the thesis. The ease of application and maximum chance of implementation on a real aircraft, is the primary motivation to pursue parallel HEPS architecture in this thesis.

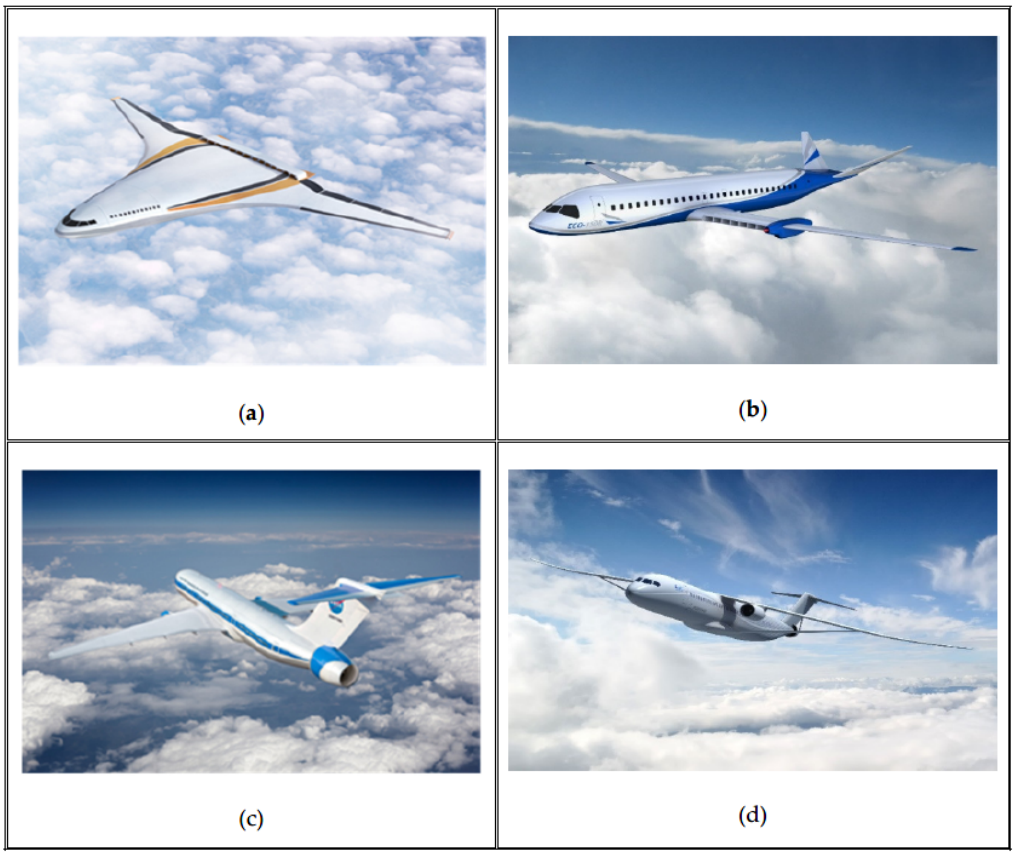


Figure 1.6: Hybrid electric aircraft concepts from NASA: a) N3-X; b) ECO-150; c) STARC-ABL; d) SUGAR FREEZE [14] [28]

Given that Parallel HEPS remains the architecture most likely to be implemented,

the question still remains that which technology would one utilize in a parallel architecture, Li-ion batteries or PEM fuel cells or Solid Oxide fuel cells or any other Metal-air battery chemistry. It also remains to be understood which aircraft class could this potentially be applied to, regional, 19-seater communal, SMR Turbofan or where. There has been plenty of scenario analysis done by consultants or by Clean Aviation projects, two of the outcomes is shown below in Figure 1.7 and Figure 1.8. It can be seen from Figure 1.7 that for an EIS 2035-40, Battery powered hybrid-electric aircraft have a potential of only 165 pax on maximum of 1000 km, with the rest of flight segments run on Synfuels or hydrogen.

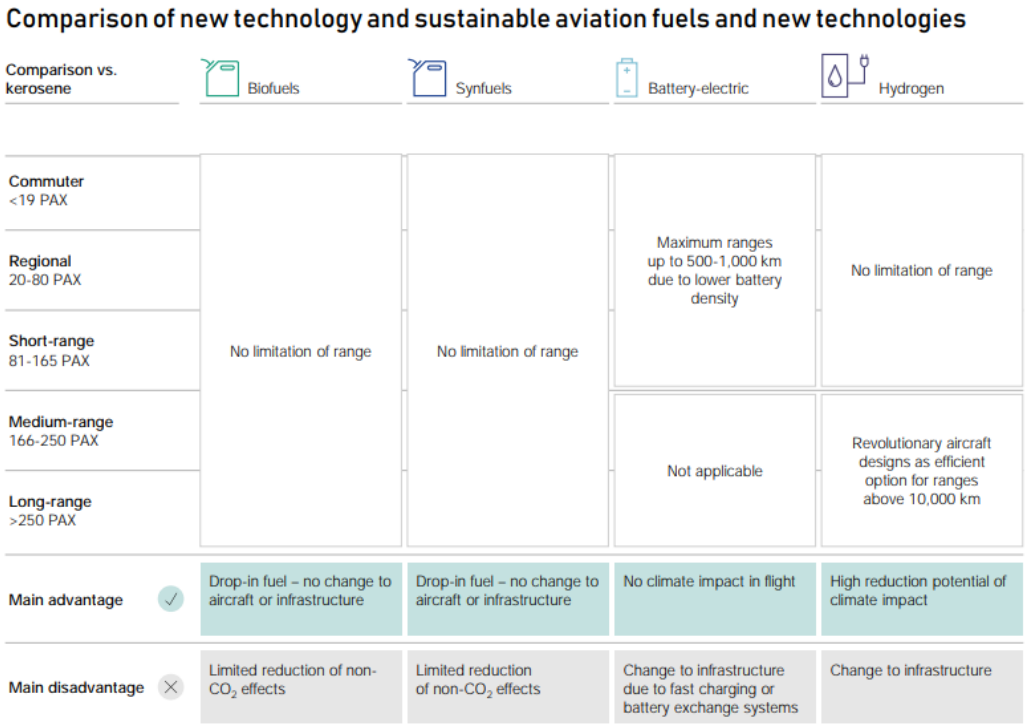


Figure 1.7: Predicted application of future technologies [29]

While the outcome from Figure 1.8, also shows the application of parallel HEPS only for regional and SMR. But all of these studies, ignore the implications of parallel HEPS on the direct operating cost, gas turbine design and thermal management. The studies which deals with more detailed aspects of the propulsion architecture have been done by Perullo [31], Lents [32] & Seitz [25]. There have been many other studies too, but these 3 were the only studies found which tried to bring as many elements of propulsion architecture into question. All 3 studies utilize a MIPH configuration, visualized in Figure 1.9. But even in these studies what has been missing is the integration of optimal PMS and cycle design and comparison across a full regional SMR aircraft design space.

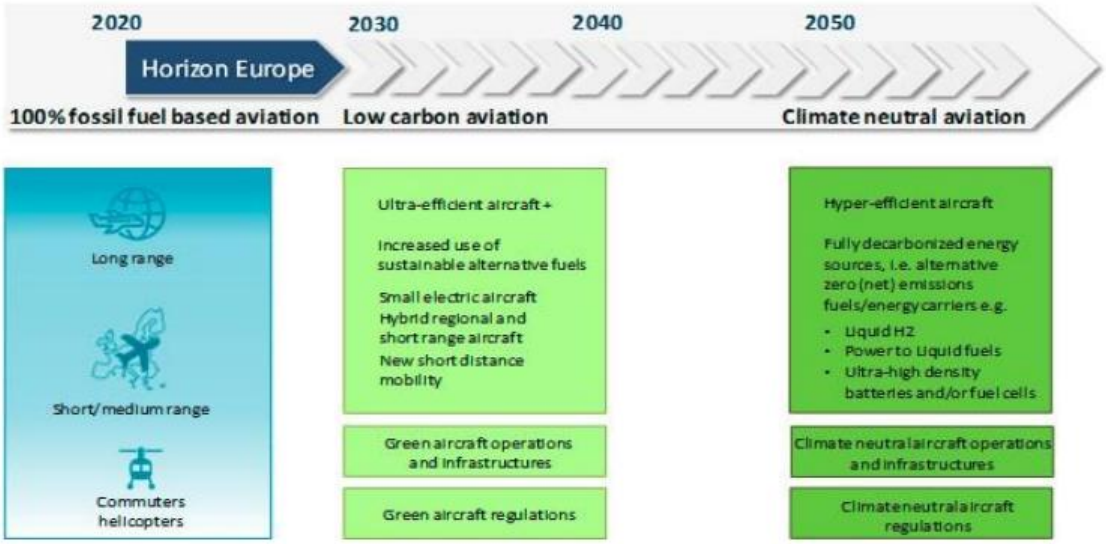


Figure 1.8: Predicted horizons [30]

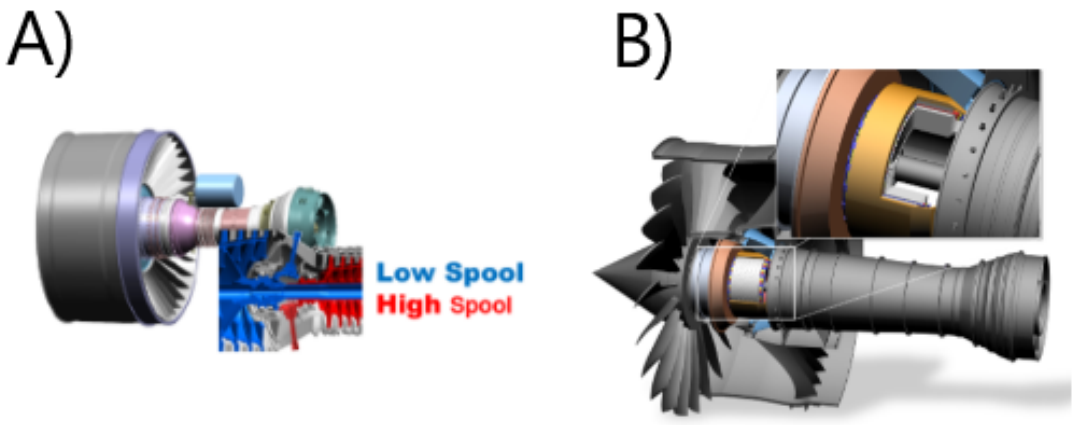


Figure 1.9: Parallel hybrid applications[14] - A) UTRC hGTF[32], B)RR LibertyWorks EVE [31]

The thesis will focus on assessment of MIPH parallel HEPS configuration utilzing fuel cells or batteries across the aircraft deisgn space. The aim & objectives are clearly stated in the next subsection.

1.2 Aim and objectives

The literature review conducted on existing work on hybrid electric propulsion revealed research gaps on the impact of electrification on gas turbine cycle design, thermal management system design and energy management optimization. To resolve

these gaps, the main aim of this thesis is to develop robust integrated design and optimization methods, to help industry assess future hybrid electric application scenarios in a more robust and systematic manner. The developed methods should be capable to provide a comprehensive assessment of hybrid electric architectures considering the design flexibility offered by electrification. The objectives of the research to achieve the aim are summarized as below:

- Address the limitations of existing performance tools, modify/develop in-house methods and framework to assess HEPS architectures.
- Integrate gas turbine cycle design and power management optimization methods and explore the full aircraft design space with varying technology levels on electrical powertrain, gas turbine and batteries for HEPS architectures.
- Develop a multi-mission assessment method for HEPS and implement direct operating cost, acquisition cost, and turbine life models inside the whole framework.
- Develop methods to optimize power management strategies along the mission profile considering the impact of thermal management strategies.
- Perform a similar design space exploration with hydrogen fuel cells and gas turbines and compare with battery powered HEPS architectures including different thermal management strategies.
- Perform a final synthesis of the technologies evaluated and provide guidelines for potential application of HEPS architectures.

1.3 Contribution to knowledge

This the third doctoral thesis submitted within the Cranfield UTC focussing on parallel hybrid electric aircraft propulsion architectures [33][34]. The elements of the developed HEPS framework which have been novel additions to previous UTC studies include the following:

- Addition of ANN/interpolation based design/off-design hybrid engine deck generation embedded within ORION.
- Addition of 3-point gas turbine cycle design solving method within ORION and also extended to hybrid and hydrogen gas turbine cycles.

- Development of integrated power management and gas turbine cycle optimization method.
- Development of vapour compression cycle and ram air heat exchanger design and optimization methods.
- Integration method for thermal management, energy management and gas turbine cycle.

The developed framework was also utilized in the ATI Flyzero project as part of the Cranfield University team for performance modelling of hydrogen, hybrid-electric regional and SMR aircraft [35]. The major contribution of this thesis to existing work in open literature can be summarized as follows:

- Assessment of parallel HEPS architectures across different aircraft classes with varying technology level & degree of redesign on gas turbine.
- Development of vapour compression cycle optimization method as part of hybrid electric propulsion framework.
- Integration method for thermal management, energy management and gas turbine cycle design.
- Identification of optimal power splits between fuel cell, gas turbine, battery accounting for off-design flight missions, providing a more comprehensive propulsion configuration assessment.

The contribution to knowledge of this thesis has been disseminated in one published [36], one accepted [37], two under preparation [38], [39] journal articles, three conference papers [40] [41] [42] and three MSc co-supervised thesis [43], [44], [45].

1.4 Thesis outline

The **Introduction** chapter of the thesis provides a general context of the work, a brief on the existing hybrid electric concepts, aim & objectives of the thesis and contribution to knowledge.

The **Literature Review** chapter of the thesis provides a compact literature review focussing on different aspects of the technology, gas turbine cycle design & operability, power management optimization, aircraft design and thermal management system design. The research gaps are identified from all the previous parallel HEPS

studies. The research questions are summarized at the end of the chapter, laying the foundation for methodology development and targeted results.

The **Methodology** chapter of the thesis explains all the methods developed or utilized as part of the research. Gas turbine cycle design methods are described, showing the rationale to go for a solver based approach. The extension of the 3-point design method to account for hybridization is shown and is followed by the development of ANN based "design & off-design" hybrid engine deck. Energy management optimization algorithms, electrical system, direct operating cost modules & multi-mission approach is described. The modules for design and optimization of ram air HEX and VCC are described. Finally, the HEX, VCC optimization & overall integration method is shown.

The **Results** chapter of the thesis is divided into 5 sub chapters covering different aspects - **Introduction**, **Design space exploration**, **Multi mission analysis across aircraft classes**, **Thermal management systems design** & **Technology synthesis**. The **Introduction** has the validation data for all the aircraft models assessed in this thesis. The **Design space exploration** sub-chapter shows the impact of gas turbine cycle redesign, power management optimization, engine technology level & electrical systems technology level for a parallel hybrid Fokker 100 style test case. The **Multi mission analysis across aircraft classes** sub-chapter expands the integration method to all 3 aircraft platforms, showing the trends for optimal PMS for minimization in fuel burn, direct operating cost & energy consumption. A multi-mission analysis is utilized to show select the optimal design configuration. The **Thermal management systems design** sub-chapter starts initially with a design space exploration of ram air HEX & VCC architectures for battery, motor and fuel cell temperature heat loads. The final integration is applied to the test cases to show the variation in multi-mission outcome with inclusion of TMS. The **Technology synthesis** sub-chapter includes a holistic comparison between kerosene gas turbine, hydrogen gas turbine, battery powered parallel HEPS, fuel cell powered parallel HEPS & pure electric configuration for the regional turboprop test case.

The **Conclusions & Future work** chapter of the thesis summarizes all the major conclusions of the thesis & provides recommendations for future work.

Chapter 2

Literature Review

This chapter provides a compact literature review of various aspects of parallel hybrid electric aircraft propulsion and highlights the research gap. After identification of the research gap, the chapter is concluded by summarizing the research questions.

Contents

2.1 Hybrid gas turbine cycle design **14**

2.2 PMS optimization and mission performance **19**

2.3 Thermal management strategies **23**

2.4 Existing Integrated frameworks **25**

2.5 Research questions **26**

In the previous chapter, it was the identified that parallel HEPS architecture is the most likely architecture to be implemented for EIS 2030-35 airframe. Hence the literature review focuses heavily on parallel HEPS studies though conclusions from other architecture studies have also been shown in order to emphasize the research gap. Extensive work has been done in the open literature in the field of hybrid electric aircraft propulsion, with varying levels of fidelity. The work has ranged from conceptual design, detailed systems design to experimental flight testing. Conceptual design exercises have included elements of hybrid electric aircraft design [46], [47], [48], [49], gas turbine cycle design [32], [50], [51], [52], [53], electric powertrain design [54], [24], power/energy management optimization [55], [56], [57], [58], [59], DOC and mission optimization [60], [31], and thermal management system design [61], [62], [63], [64], [65]. Detailed system design studies have focussed on transient/operability

assessment of hybrid engine [66], [17], [67], [68] and some aspects of off-design operation of thermal management [69], [70] along the aircraft mission. The experimental flight testing have been performed for bespoke testing of MW-scale motors [71], [72] inverter or for thermal management systems [73] or a full aircraft level testing. The aircraft level testing has been done for turbo-electric HEPS architecture, Airbus E-Fan X [74] and also various VTOL aircraft utilizing electric architectures [75], [76]. The research is a hybrid between conceptual design and detailed system design, with the aim being to bring detailed design elements of thermal management systems, gas turbine cycle design, power management optimization in a preliminary design loop. Aircraft redesign, transient simulations and any level of experimental tests are not performed in the research hence the literature review is divided into 4 sections targeting the research gap, gas turbine cycle design, power/energy management optimization, thermal management system design hybrid electric propulsion and existing integrated design & optimization frameworks. In the end a full table is shown, which summarizes all studies found on parallel HEPS configuration, their conclusions and limitations. Based on the limitations, research gap is identified and research questions are formulated.

2.1 Hybrid gas turbine cycle design

In this section, conclusions and methods utilized by studies focusing on hybrid engine cycle design are summarized. The main objective of an aircraft gas turbine cycle design process is to identify an optimal combination of fan pressure ratio, fan diameter, bypass ratio, compressor pressure ratio split, overall pressure ratio, & turbine entry temperatures to minimize an objective function comprising fleet level fuel burn, operating cost & component life. Multi-point 2.1 design approaches have been utilized for non hybrid gas turbine optimization, either with a Newton Raphson or secant solver-based[77][78][79] targeting a jet velocity ratio or genetic algorithm based approach[80][81]. One of the examples of a 3-point cycle design process is shown by in Figure 2.1, the 3 points being Mid Cruise (CRZ), Max Climb (MCL or TOC) and End of runway (EOR). But how would these methods need to be modified with application of electrical power? How have other studies on open literature approached this?

Addition of mechanical torque via motor powered from electrical storage systems provides flexibility to the gas turbine design but also complicates the selection process due to constraints coming from energy & power splits for design & off-design flight

missions. Providing electrical power during demanding flight segments of take-off (End of runway) & initial climb (MCL) would enable core to run at higher temperatures and pressures, at mid cruise (in case no power is applied at this point). Higher core temperature and pressure would increase thermal efficiency and also enable smaller core sizes, subsequently leading to greater fuel efficiency. On the flip side, it will also result in reduced gas turbine life & greater thermal management penalty. In the case that a reverse strategy is applied, that is providing power during Mid cruise(CRZ) would result in lower thermal management penalty & lower electrical power train weights. The trade-off mentioned here regarding the impact of power management strategy on cycle design was not addressed in any literature, but still some work has been done to address the impact of electrical power on gas turbine cycle method & selection. The major work on hybrid cycle design has been done by Lents [32], [64], Seitz [25], Sahoo [50], [28], Perullo [31] and Sielemann [52], [53].

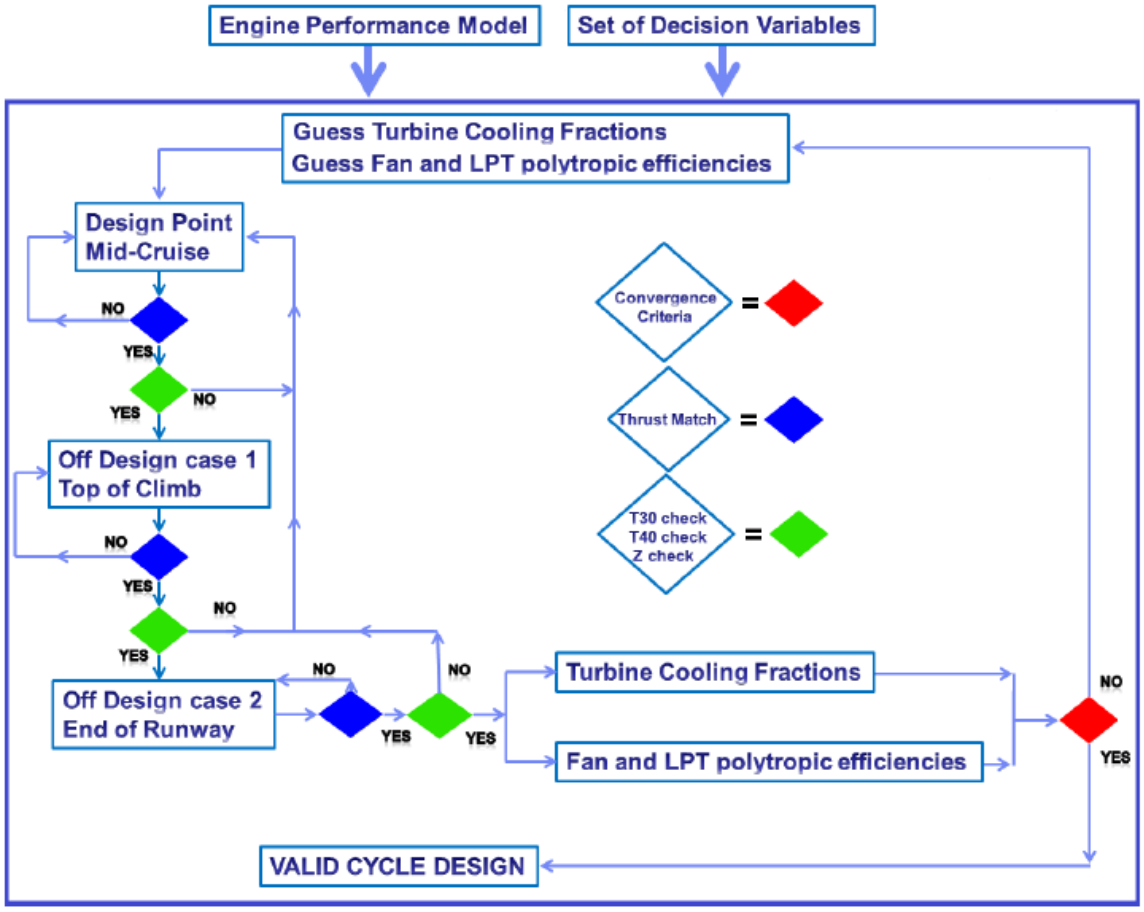


Figure 2.1: Traditional 3-point gas turbine cycle design process from Mourouzidis [80]

The study from Lents et al [32] focussed on B737-class aircraft powered by low specific thrust parallel hybrid electric engines for entry into service 2035. Lents used

an approach where the bypass ratio/core size was modified by providing a fixed take-off & climb motor power on-take without any cruise power on-take. This resulted in a cycle level TSFC benefit of a 2.3% when providing 2.1 MW power on-take at EOR and 0.7 MW power on-take at MCL. The total fuel burn benefit was estimated to be 6% with respect to baseline non hybrid gas turbine assuming 2035 entry into service and 1000 Wh/kg battery energy density, as can be seen in Figure 2.2. It can be noted from Lents study is that although the assessment is done for varying technology levels on motor, inverters power density and battery energy density, but power management strategy and thermal management system design is kept fixed.

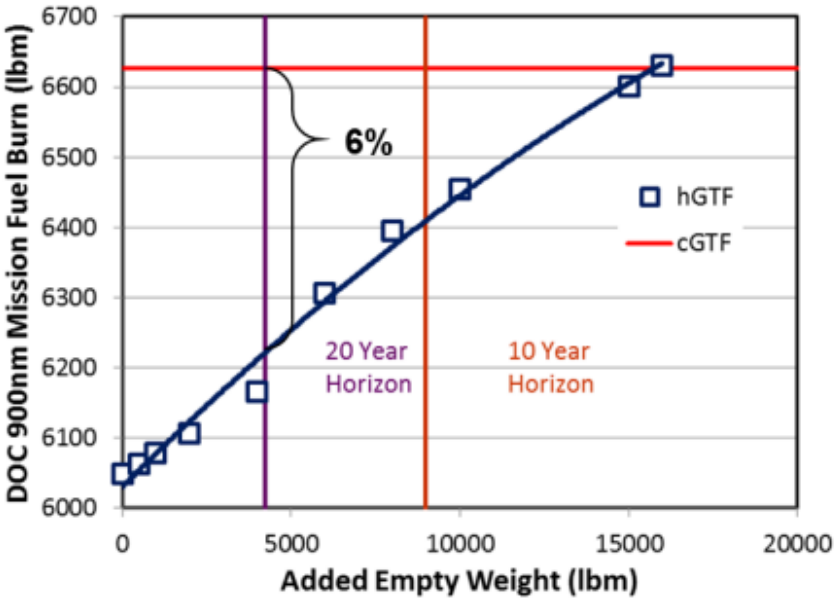


Figure 2.2: Fuel burn benefits for the hybrid GTF [32]

The studies from Sahoo et al [50] [82] and Sielemann et al [52][53] utilize same approaches as Lents to hybrid gas turbine cycle design again with a fixed pre-defined power management strategy. [50] showed a difference of 3.6% benefit in fuel burn on 500 nm for an A320-class aircraft between core-optimized (reduced core size) and hybridised (same engine as baseline engine) gas turbines. [82] focussed also on the same test case and showed 0.5% fuel burn benefit by simply re-sizing the turbine cooling flows upon provision of 500 kW electrical power at take-off and also showed the operability benefits from electrification at part load settings. [52] & [53] used same approaches for hybrid cycle approach as [32] but accounted change in electrical power train weights and efficiency with change in shaft speed due to change in specific thrust. A slightly more modified approach was shown by Seitz [25], where he looked at different locations of mounting the electrical motor, all within MIPH configurations as

seen in Figure 2.3. Seitz also performed all gas turbine cycle redesign studies for A320 class aircraft and aircraft too was redesigned for different degrees of hybridization, the conclusions on fuel burn are estimated to be at the same level as Lents studies. Ultimately, it was found that the electric motor located in the fan hub was the most suitable physical integration to have low motor weights due to being connected on the faster LP shaft and also the ease to remove the heat loads. A 6.6% fuel burn benefit was found on 500 nm for 1000 Wh/kg battery energy density with respect to baseline non hybrid aircraft. Again, even in this study, the limitation still exists that different power management strategies and thermal management strategies aren't explored. Several studies have also looked at gas turbine operability on electrification.

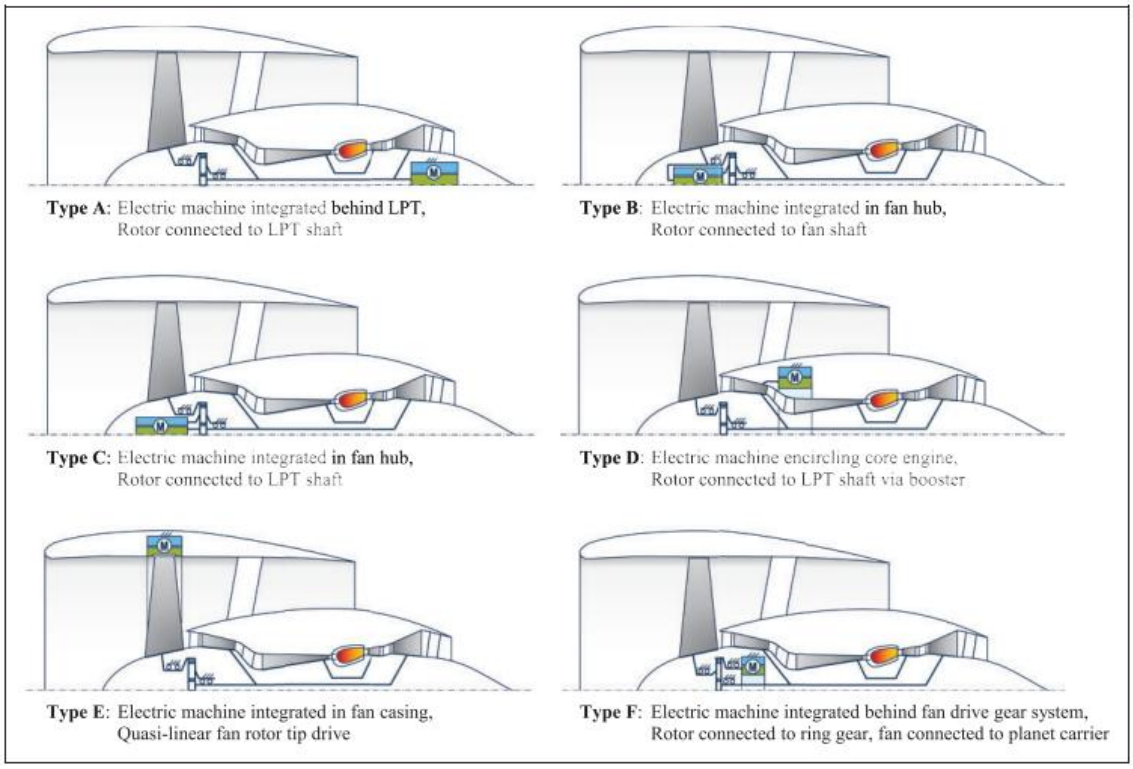


Figure 2.3: Physical integration architectures MIPH [25]

Kang et al [83] presented the impact of power on-takes on LPC, Fan and HPC operability, with reduction in LPC surge margin with high power on-takes on LP shaft. The studies from NASA on TEEM [17],[26], hFAN [67] showed the potential reduction in transient stack for both LP & HP compressors during acceleration and deceleration by providing electrical power on both shafts strategically throughout the flight mission. Similiar concepts of powering different gas turbine shafts to improve gas turbine operability by electrification have also been highlighted in [84], [85], [82] & [68]. The fundamental outcomes from all these studies are the same showing the

ability of electrical shaft powers to replace handling bleed valves or variable stator vanes. The potential transient surge margin benefits on application of different power splits to the LP and HP shaft can be seen in Figure 2.4.

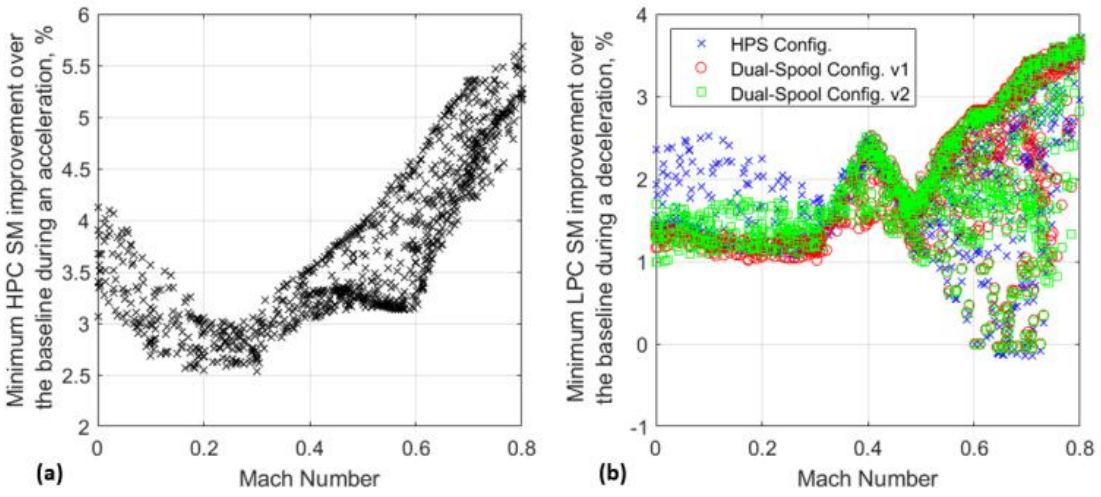


Figure 2.4: Potential surge margin benefits from electrification [26]

From all the studies summarized above it can be clearly seen that significant work has been done on parallel hybrid engine cycle design & operability assessment for a pre-defined power management strategy. But the design studies suffer from the following limitations, In Lents' study [32], no change is made to the design point fan pressure ratio and overall pressure ratio with increasing bypass ratio, and neither are the mass flows at top of climb conserved. This leads to a slight overestimation in fuel burn benefit for hybrid cycle as the higher drag and weight due to a bigger fan diameter is not accounted for. In subsequent studies focussing on a cycle design, [82], [52] & [53], the aircraft mission performance is assessed for a pre-defined power management strategy rather than optimizing the two systems together and exploring the design space. This also holds true for studies from Seitz [25]. Gas turbine cycle designs for different power management strategies have been explored to some extent in study by [31], but the individual benefits coming from these two are not quantified and no trade-offs are identified. The question regarding whether or not one would redesign gas turbine cycle upon electrification remains open. It is indicated that to fully assess the potential benefits of electrification in performance, life and cost, the cycle design should be directly coupled with the energy management optimization and varying technology levels on either sides. This approach is essential to provide a realistic fuel burn and operating cost benefit from electrification considering all the constraints and system interdependencies. Hence, the analysis from the first

section of the literature review, the broad research gap that shows up is the design of gas turbine with varying power management strategies and the inclusion of direct operating cost to determine benefits of retrofit against redesigned gas turbine.

2.2 PMS optimization and mission performance

Carrying on from previous section, this section contains literature review of parallel HEPS design space parametrization methods, power/energy management optimization methods & HEPS mission assessment across different aircraft classes. The parallel HEPS studies have focussed on both regional turboprops as well as SMR turbofan aircraft. Antcliff et al[15] analysed mission performance for an EIS 2030, ATR 42 style regional aircraft utilizing parallel hybrid architecture with lithium ion batteries. The study utilized NASA FLOPS[86] for aircraft performance analysis, lookup tables for modelling the gas turbine and fixed efficiency, specific power and energy density for electrical components. The study assumed a fixed degree of hybridization for all flight phases and the gas turbine was scaled with degree of electrification without optimizing power management strategies or considering aspects of gas turbine cycle redesign. The study concluded battery pack energy density of 500 Wh/kg to have same energy consumption as baseline non hybrid aircraft, thus identifying a break even energy density point. Similar approaches, albeit with increasing modelling fidelity for electrical systems, have been utilized by [47][87][46] for performing regional turboprop mission analysis. Cinar [47], [88], Cinar [89], performed a series of studies looking at smaller less than 19-seater turboprops utilizing either completely electric, series and parallel hybrid configurations. Even in her studies, the gas turbine cycle is scaled and no power management optimization is performed but electrical systems modelled in significant detail.

Moving on to the SMR or regional turbofan studies, The SUGAR VOLT[90][91] study was performed by NASA focussed on a parallel hybrid electric truss based B737 class aircraft. Electrical system models (Switched reluctance models for motor, battery pack modelling) were developed and integrated in NPSS with gas turbine component characteristics, resulting in "hFan (hybrid fan)" system models. SUGAR VOLT study was detailed in terms that it includes all elements of the propulsion system, thermal management system design and aircraft design, but the element of power management optimization in the design loop has been missing. The work from Perullo et al [31] carried on the SUGAR work, using the same aircraft and propulsion models and performed the analysis at a mission level for a sweep of battery sizes.

The main conclusion from the paper was a 25% fuel burn benefit with a 22500 lb. battery pack on 900 nm, at reduced payload relative to the baseline aircraft. The mission analysis was performed without optimizing power management strategies and accounting for thermal management penalty, but the aspects of cycle design and direct operating cost were covered.

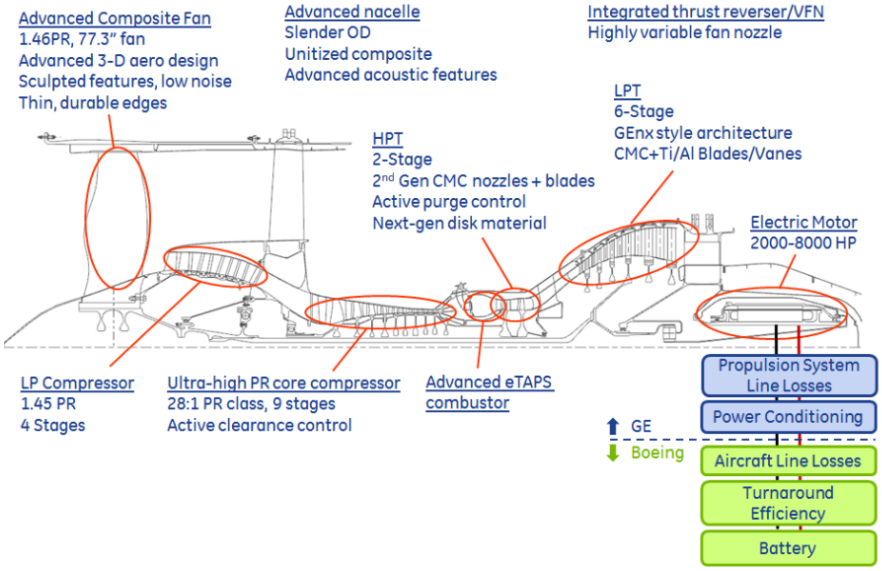


Figure 2.5: Parallel HEPS SUGAR VOLT Study [91]

In order to extend the studies from Perullo and bring elements of power management optimization into the game, Trawick[57][92] optimized power management strategies for all the battery weights and mission ranges shown in [31]. The work from Trawick was found to be defining work in power management optimization in open literature hence has been explained in greater detail. Trawick utilized various different optimization algorithms to get optimal power distribution along the mission. These included dynamic programming, global optimization and model predictive control. A fuel burn benefit ranging from 0.1-0.8% was obtained from optimizing power management strategies relative to full climb power strategy as can be seen in Figure 2.6. Different optimization techniques, global optimization, dynamic programming, optimal control and constant power (Figure 2.7) were utilized with marginal difference in fuel burn obtained from each method but varying simulation times. The major conclusion from Trawick's study was that the major factors which drive an optimal power management strategy is the battery resistance, variation in aircraft weight and change in gas turbine sfc/efficiency with thrust ratings. Trawick found that the cruise on-take in terms of non dimensional power dominated but in actual power, take-off and initial climb had higher power on-take distributions. This power management

strategy can be seen in optimal control in Figure 2.7. What can be again noticed is that the gas turbine cycle design and thermal management system design are not redesigned for each power management strategy, again showing another research gap.

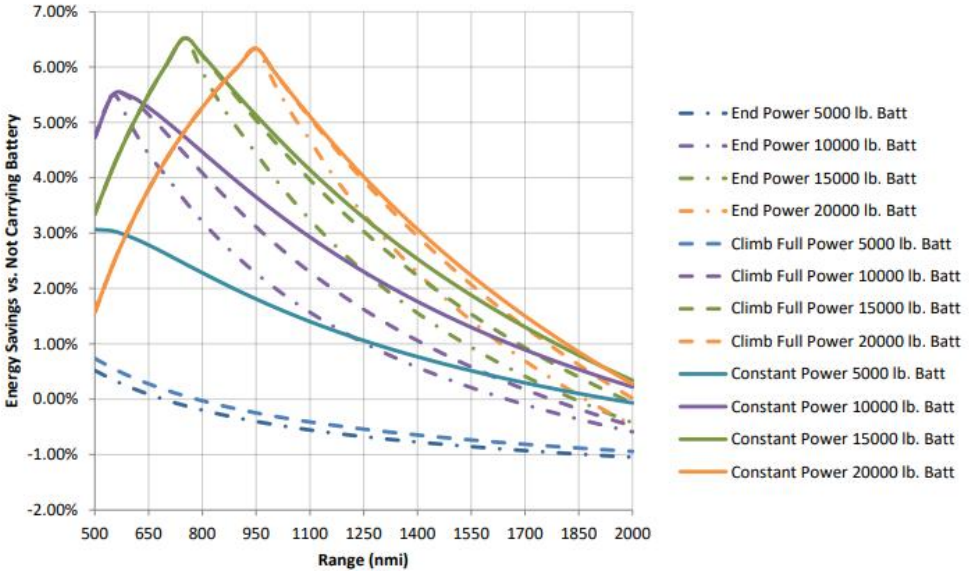


Figure 2.6: Energy savings for 25000 lbs payload and 2500 hp motor for several mission ranges [57]

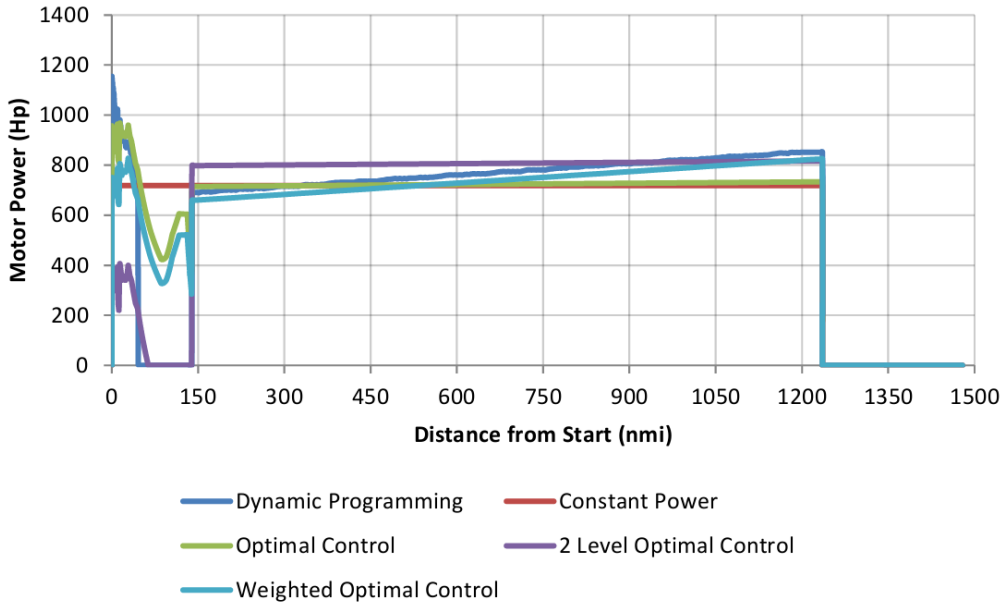


Figure 2.7: Variation of PMS for on 1500 nm [57]

Trawick's work was the starting point of all power management studies and the design space was parametrized on the basis of battery weight and motor power. Similar approach of parametrizing the parallel HEPS design space on the basis

of degree of hybridization by power (motor weight) & degree of hybridization by energy (battery weight) has been explored further in [47][87][49][93][94][95] without optimizing power management. The studies from Donateo et al[96] and Zhang et al[55][97] reduced the design space to only variable, that is degree of hybridization by power for different flight phases. Subsequently, if the design space is parametrized in such a way, battery size becomes a fall-out design variable. Donateo [96] first optimized the power management strategy on design missions for a rotorcraft test case and then applied on-line PMS optimization for off-design flight missions. The series of work from Zhang [97], [55], [60] look at application of different energy management optimization algorithms and also perform optimization of the electric powertrain keeping in mind off-design mission performance. The energy management studies [97] from her concluded a fuel burn reduction ranging from 8% to 45%, depending on battery energy density for B737 style aircraft. This study [60] added elements of direct operating cost and carbon taxation in a multi-mission framework, with the final selection of power management strategy accounting for airline operator's fleet planning. A flight cluster for B737 using CFM 56 engines is shown in Figure 2.8 which was developed from public available fleet data. There have also been studies which have looked at application of convex optimization, model predictive control & set based techniques for optimizing PMS [59][98][58] for hybrid electric aircraft, with all methods summarized in literature review from [99].

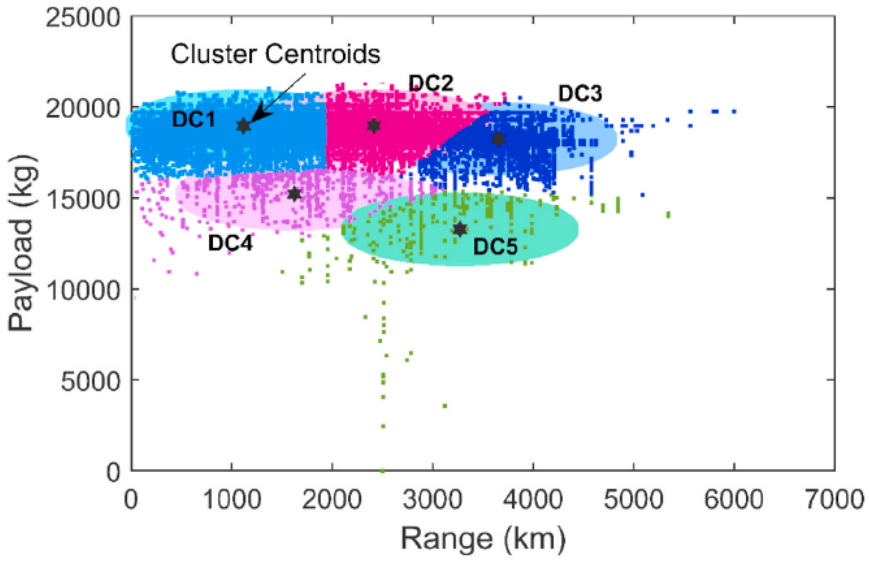


Figure 2.8: Flight operational data for Boeing 737 [60]

One thing which is common in all these power management and mission perfor-

mance studies is that the power/energy management optimization is performed on a fixed "retrofit" gas turbine and without accounting for thermal management penalty. The question arises whether the power management distribution shown in [57][60] change if the gas turbine cycle & thermal management design is simultaneously modified in the loop? What would be the potential modifications to existing modelling methods to account for simultaneous design & optimization of all systems for HEPS architectural assessment?

2.3 Thermal management strategies

The last element of integrated frameworks for HEPS propulsion systems, is the thermal management systems. The work done in open literature regarding them has been summarized in this section. Due to the operational temperature of batteries being at 293-308 K, there exists no temperature gradient to dump the heat to either of the terminal heat sinks - fuel or air for take-off or partial climb flight segments. To overcome this, various thermal management methods for batteries have been considered. These include air cycle machine, vapor cycle machine, phase change material, thermoelectric cooling, vortex tube among others[62][100][42]. Kellerman et al [62] designed a cooling system for a 19-seater hybrid electric battery powered aircraft, utilizing thermoelectric cooling module as a heat pump technology, and showed that the energy penalty due to thermal management varied from 2% to 16%. This was primarily driven by battery pack allowable temperature, outside air temperature and battery efficiency. It must be noted that vapor cycle machine as a thermal management system is ignored in Kellerman's work[62] without performing a sizing exercise and using power density assumptions from ground applications. The work from Lents & Rheaume et al [32],[64],[65] & [101] performed a series of studies focusing on B737-class parallel hybrid-electric aircraft. As mentioned before A predefined power management strategy of take-off and climb 2.1 MW power on-take resulted in a fuel burn penalty of 0.75% due to the ram air-liquid coolant heat exchanger. It was assumed though in these studies that the batteries are pre-cooled on the ground and the battery pack is let heat up till a given altitude, after which it reaches maximum allowable temperature. It can be seen in Figure 2.9, the rise in battery pack temperature for varying battery energy density and fixed power and heat capacity. As the battery energy density increases, it becomes increasingly tougher to keep the pack at same temperatures as the heat flux is much higher. Again, the study from Rheaume, uses a liquid coolant ram air heat exchanger and not a vapour

compression cycle cooling loop. Kellerman et al[63] performed a similar analysis for a partial turboelectric A320-class aircraft with a puller fan and compact heat exchanger and concluded a fuel burn penalty in the order of 0.29%.

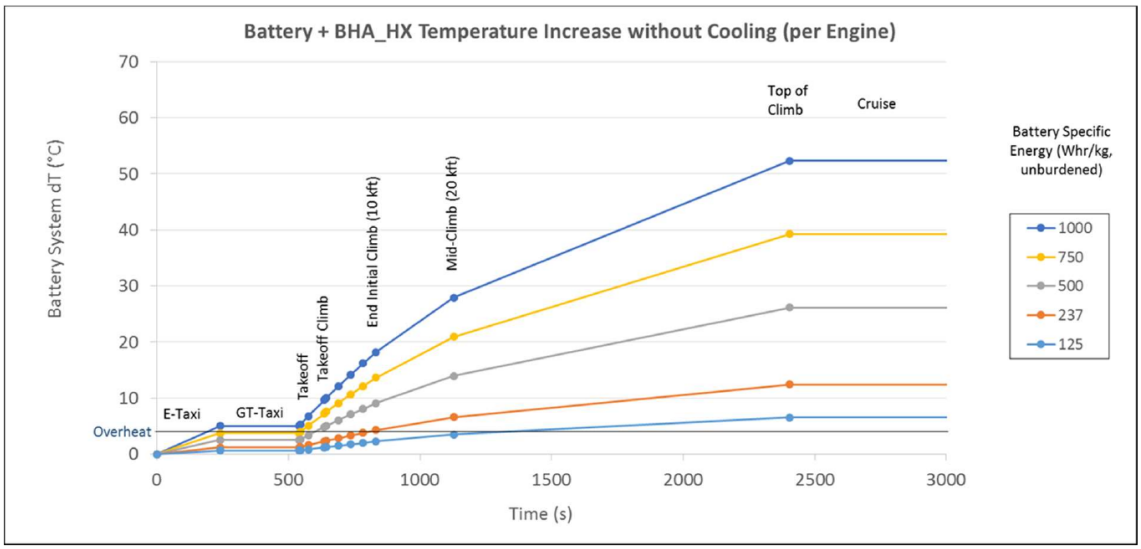


Figure 2.9: Variation in adiabatic batteries temperature across flight mission [64]

Chapman et al [70],[102] & [69] showed a method to design a preliminary plate fin heat exchanger for aero applications and used an aircraft specific objective function to select the optimal heat exchanger design. The problem with such an approach is it neglects off-design behavior of the selected TMS design hence leading to overall non-optimality across the aircraft mission. An approach was developed from Lents[103] to account at each flight point the contribution of TMS to drag, weight & power penalty. But this method can only be applied to direct ram air heat exchangers and not for other TMS architectures. It can be clearly noticed from all these studies is that there is no explicit integration of thermal management strategies with power management strategies, as all these studies design for a pre-defined power split and aircraft hybrid gas turbine design. The only study which was found to integrate these two elements was done by Elder et al [61], but this too designed thermal management strategy for a fixed motor power on a variable battery pack. To the author's knowledge, very limited work addresses the design, optimization & sizing of thermal lift or vapour compression cycles for HEPS aircraft as has also been highlighted in the literature review by Heerden [42]. The question that arises is would inclusion of thermal management design within propulsion optimization loop change the selection of the propulsion system? The need to consider impact of thermal management systems at the conceptual design phase especially for fuel cell powered aircraft is highlighted by Dragan[104], as the penalties arising from TMS can be as high as 16% of baseline

energy consumption.

2.4 Existing Integrated frameworks

In the previous sections, the literature on each of the individual elements of the HEPS propulsion design was reviewed. In this section, a complete summary of integrated frameworks that have been employed in studies from academic institutions, aerospace consortium & industries for analysis of parallel HEPS concepts for regional or SMR aircraft is shown. The division is done on the basis of the institution with sub division by framework or aircraft platform type. Only those studies have been considered which are novel and repeated studies have been excluded. This complete summary of all major parallel HEPS studies can be found in Table 2.1, Table 2.2 & Table 2.3. The major frameworks developed that to cover more elements of the propulsion have been the ones developed by Cinar [47], Zhang [60] and Perullo [31]. These are visualized in Figures 2.10, 2.12 and 2.11 respectively.

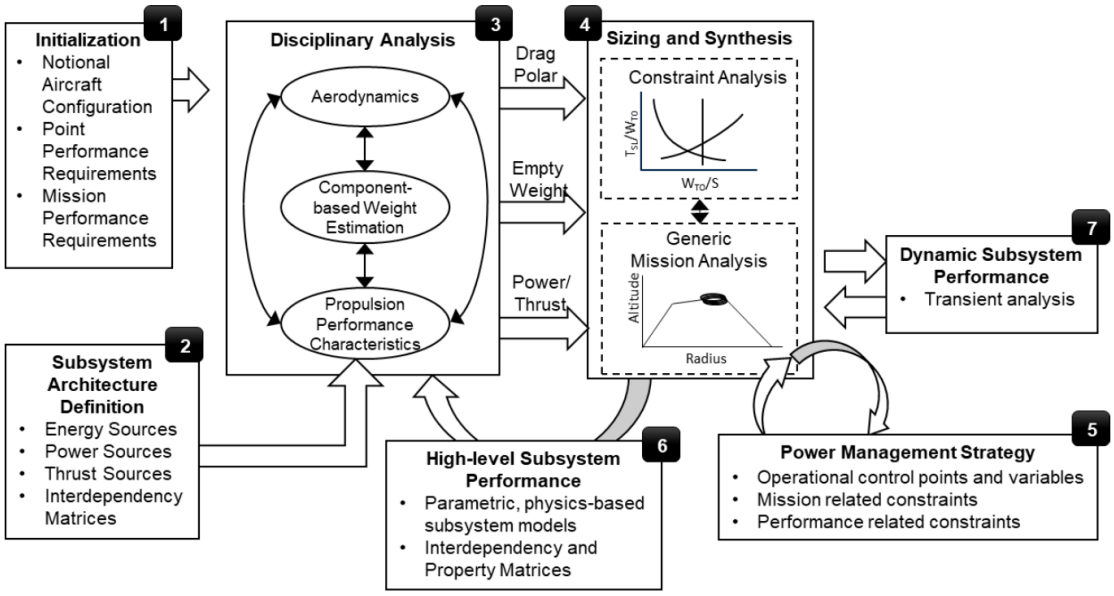


Figure 2.10: E PASS Integrated framework from Cinar [88]

Cinar puts all the elements, electrical systems and gas turbine in optimization loop and performs design space exploration for parallel HEPS but simply scaling the gas turbine. Zhang extends this and performs a multi-mission energy optimization assessment but keeping the gas turbine fixed. Perullo does put the gas turbine cycle and power management in a common optimization loop, but the benefits coming from the two parameters are not separated. It can be clearly noted that the clear theme

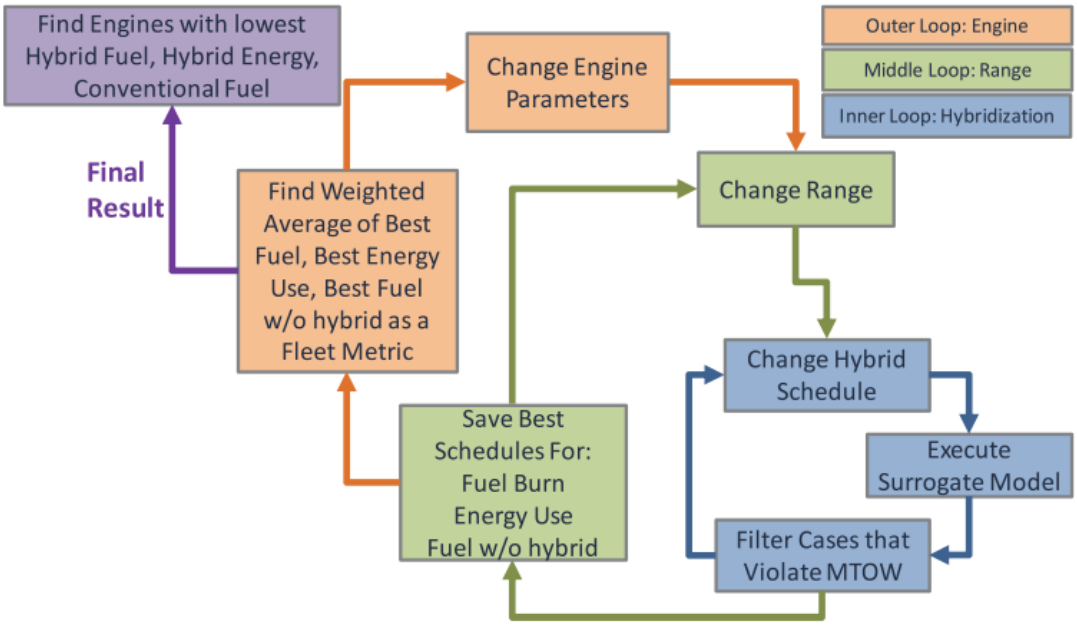


Figure 2.11: Parallel HEPS design loop [31]

common in all these studies is that the gas turbine, power management optimization & thermal management systems are not part of a common design and optimization loop. The literature review also showed limited number of studies on comparison between fuel cell and battery powered HEPS architectures. Hence, in order to make a consistent assessment & comparison between different design combinations of fuel cell, gas turbine & batteries across aircraft classes, it is necessary that all element are in the common optimization loop. This would allow to capture maximum synergies between the systems and extract maximum energy benefit. This essentially becomes the top level aim of the research and the research questions are further summarized in the next section.

2.5 Research questions

The main aim of the dissertation is to develop methods to provide a comprehensive assessment of parallel HEPS architectures across aircraft classes. The develop of such methods and integration of gas turbine cycle, power management and thermal management in an integrated framework would answer the following unanswered or partially answered research questions:

- What is the maximum benefit that can be obtained by redesigning the engine cycle with hybridization as compared to simply retrofitting the gas turbine with electrical power?

- Do the potential benefits from hybridization increase or decrease with improvement in gas turbine technology?
- What is the optimal motor power and battery size for a given mission range to minimize fuel burn, energy consumption and direct operating cost?
- How do power management strategies differ for cycle redesigned and retrofitted gas turbines and for different objective functions?
- How do the fuel burn and direct operating cost benefits vary between different aircraft classes?
- What maximum fuel burn and direct operating cost benefit can be obtained when considering all the constraints imposed by electrification on a realistic off-design mission cluster?
- How does an integrated approach comprising all aspects related to the cycle redesign and energy management optimization change the outcome of the selection of propulsion system configuration and the expected benefit from electrification?
- What is the impact of different TMS architectures on the performance of HEPS architectures and does it change the selection itself?
- How to simultaneously design and optimize TMS architectures as part of the full HEPS framework?
- What is the optimal implementation strategy of PEM fuel cells, Li chemistry based battery packs alongside gas turbine across aircraft classes?

The next chapter describes the methodology developed in order to answer the research questions.

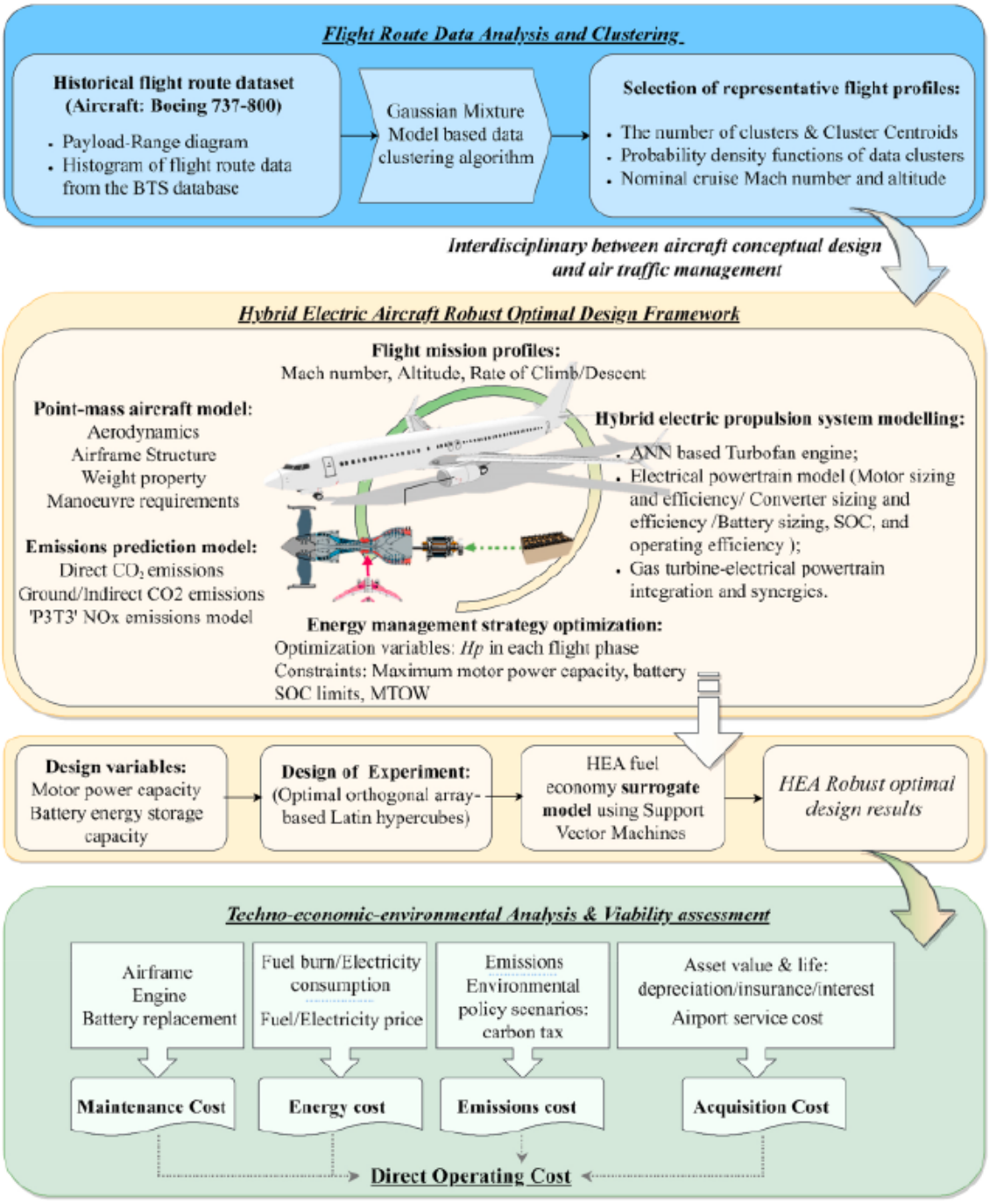


Figure 2.12: HEPS Multi mission techno-economic assessment from Zhang [60]

Study	References	Modelling Methods	Contribution to knowledge	Limitations
CU	[97][55][60]	GT - ANN + Turbomatch ES - Motor maps, Battery pack TMS - not considered AP - SUAVE	Optimal PMS methods Multi mission assessment	No GT integrated design No TMS integrated design
	[95][105][106][107]	GT - Turbomatch, propeller - BEMT ES - Motor maps, Battery pack TMS - not considered AP - CU in-house	Design space exploration Integration of VRS & PMS	No TMS integrated design No GT integrated design
	[83][108][109][66]	GT - AMESIM ES - AMESIM TMS - AMESIM AP - AMESIM	Transient HEPS assessment TMS Modelling	No optimal PMS integrated design No GT integrated design
NASA	[15]	GT - sfc/efficiency MAPS ES - fixed efficiency,power density TMS - not considered AP - NASA FLOPS	Early HEPS Regional Turboprop study Design mission impact & DOC	No optimal PMS integrated design No TMS integrated design
	[69][70][68][102]	GT - N/A ES - N/A TMS - DSE & Sizing AP - N/A	HEX Design Ram Air TMS Airframe Integration	No GT integrated design No optimal PMS integrated design
	[90][91]	GT - NPSS ES - Motor maps, Battery pack TMS - sized AP - in-house framework	Addresses most design aspects HEPS Airframe Integration accounted	No optimal PMS integrated design Test case specific work
	[26][17]	GT - NPSS ES - Simulink TMS - not considered AP - N/A	Transient HEPS assessment Potential energy management benefits	No TMS integrated design No multi-mission assessment
RR Indianapolis	[31][110][111][56]	GT - NPSS ES - Motor maps, Battery pack TMS - GTHEAT AP - in-house framework	Hybrid EVE cycle design Mission optimization & DOC	No optimal PMS integrated design Test case specific work
UTRC	[32][101][103][64]	GT - NPSS ES - Motor maps, Battery pack TMS - REHEAT AP - in-house framework	GT redesign impact benchmarked TMS impact benchmarked	No optimal PMS integrated design Test case specific work

Table 2.1: Parallel HEPS Integrated frameworks & studies.

Study	References	Modelling Methods	Contribution to knowledge	Limitations
Georgia Tech	[47][88][89]	GT - sfc/efficiency maps ES - Simulink TMS - not considered AP - in-house framework	Transient limits of electrical systems Development of aircraft design framework	No GT integrated design No TMS integrated design
	[57][92]	GT - NPSS Surrogates ES - Motor maps, Battery pack TMS - not considered AP - in-house framework	PMS Optimization impact benchmarked Comparison of PMS optimization methods	No TMS integrated design No GT integrated design
Oxford	[59]	GT - sfc/efficiency maps ES - Motor maps, Battery pack TMS - not considered AP - in-house framework	Application of MPC & Convex optimization PMS Optimization impact benchmarked	No GT integrated design No TMS integrated design
Stanford	[112][113]	GT - N/A ES - models developed TMS - not considered AP - in-house framework	Al air batteries aircraft impact Developed Li-ion detailed models	No GT integrated design No TMS integrated design
Bauhaus Luftfahrt	[51]	GT - ANN + in-house codes ES - Motor maps, Battery pack TMS - power density AP - in-house framework	PEM fuel cell A/C impact Water injection synergies	No GT integrated design No TMS integrated design
	[25]	GT - ANN + in-house codes ES - Motor maps, Battery pack TMS - power density AP - in-house framework	GT redesign with HEPS Comparison of different shaft locations	No optimal PMS integrated design No TMS integrated design
	[63][62]	GT - N/A ES - N/A TMS - Thermoelectric, Ram air AP - N/A	Development of TMS sizing models HEX sizing	No GT integrated design No optimal PMS integrated design
Malaarden & Modelon	[50][82][52][53]	GT - in-house codes ES - models developed TMS - power density AP - in-house framework	GT redesign impact Motor weights modified with location	No optimal PMS integrated design No TMS integrated design
FUTPRINT50	[114][58][115][116]	GT - in-house codes ES - fixed efficiency, specific density TMS - not considered AP - in-house framework	PMS optimization impact benchmarked Development of models	No GT integrated design No TMS integrated design

Table 2.2: Parallel HEPS Integrated frameworks & studies cont.

Study	References	Modelling Methods	Contribution to knowledge	Limitations
TU Munich	[54][85]	GT - sfc,efficiency maps ES - models developed TMS - power density AP - in-house framework	Development of Electrical system models Ducted Fan vs parallel hybrid	No optimal PMS integrated design No TMS integrated design
	[49]	GT - sfc,efficiency maps ES - Motor maps, Battery pack TMS - power density AP - in-house framework	Aircraft Design framework developed Ducted Fan vs parallel hybrid	No TMS integrated design No optimal PMS integrated design
	[117]	GT - sfc/efficiency maps ES - efficiency, power density assumptions TMS - not considered AP - in-house framework	Development of hybrid DOC modules Impact of carbon taxation	No propulsion design No multi mission performance
TU DELFT	[48][46][87][118]	GT - sfc/efficiency MAPS ES - Motor maps, Battery pack TMS - power density AP - in-house framework	HEPS Architectural comparison HEPS Aircraft Sizing method	No optimal PMS integrated design No TMS integrated design
Maryland	[119]	GT - N/A ES - models developed TMS - power density AP - in-house framework	PMS between fuel cell & battery Potential for electric VTOL	No TMS integrated design No optimal PMS integrated design
UMichigan	[120][61]	GT - in-house codes ES - fixed efficiency, specific density TMS - sized AP - in-house framework	TMS integration with GT Thermoacoustic chiller impact	No GT integrated design No multi-mission assessment
RMIT	[121]	GT - sfc,efficiency maps ES - efficiency, power density assumptions TMS - not considered AP - in-house framework	Comparison across aircraft classes Potential for VTOL	No propulsion integrated design No multi-mission assessment
AUTh	[122]	GT - N/A ES - efficiency, power density assumptions Aft Fan TMS penalty & DSE AP - N/A	TMS Sizing & Performance Potential for VTOL	No GT integrated design No TMS integrated design

Table 2.3: Parallel HEPS Integrated frameworks & studies cont.2

Chapter 3

Methodology

This chapter comprises all the methods developed or utilized in the research to achieve the overarching aim & objectives. The overall framework is first introduced, followed by detailed description of various elements of the framework and ultimately how they are integrated together.

Contents

3.1 Overview of test cases 33
3.2 Introduction 35
3.3 Hybrid GT cycle design and weight assessment 36
3.4 PMS optimization and integration ANN 45
3.5 Direct operating cost 53
3.6 Multi mission energy management 56
3.7 Electrical systems modelling 61
3.8 Ram Air HEX and VCC Modelling 73
3.9 Integration of TMS into the framework 84
3.10 ORION and Full framework at a glance 88

3.1 Overview of test cases

A short overview of all the aircraft test cases and the HEPS architectures modelled are summarized in this section. The reason that all the test cases are summarized here is that validation of different modules of the framework are performed on various test case and are shown in the methodology section. The Scope of work is shown in

Figure 3.1, and it can be seen that three aircraft classes are assessed in this study with 3 different HEPS architectures (Battery powered parallel HEPS, fuel cell powered parallel HEPS and battery-fuel cell electric hybrid architecture) (architectures shown in Figure 3.2).

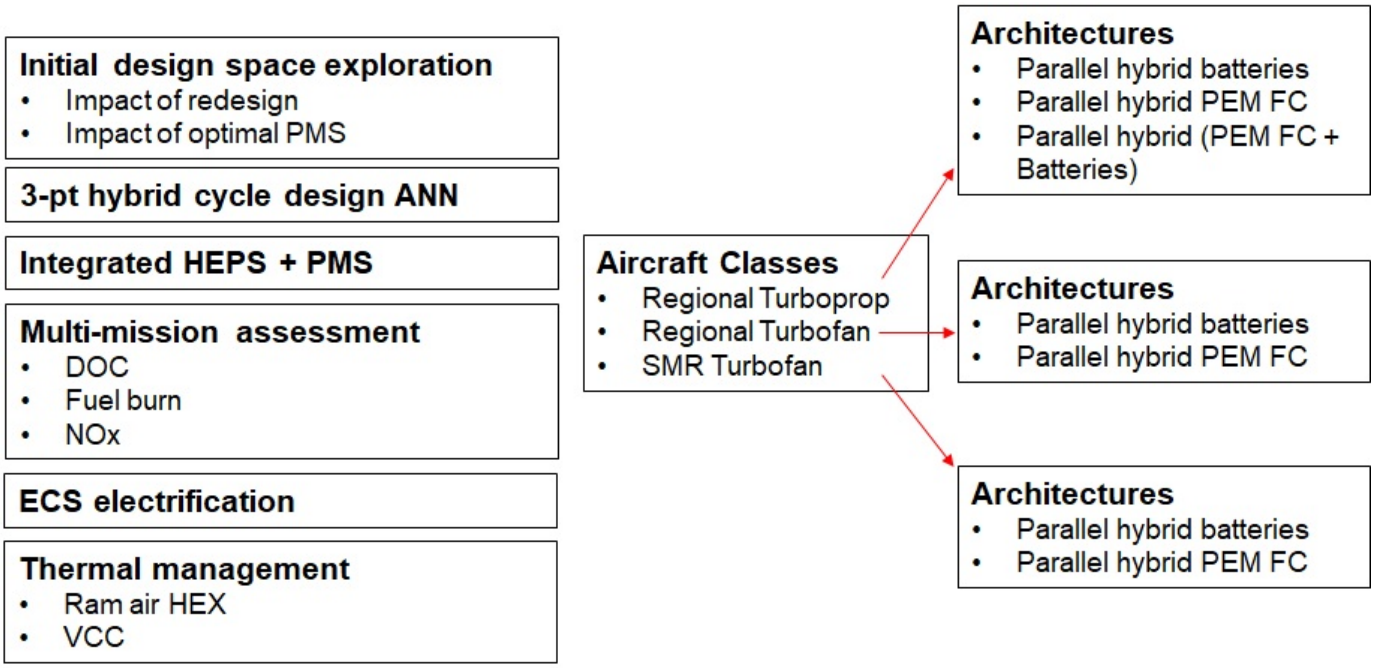


Figure 3.1: Scope of Work

For all aircraft, two baseline GT are developed, one corresponding to the EIS of the aircraft and another for EIS 2035. This is done to understand how benefit from hybridization changes with change in GT technology. The HEPS design space is explored to benchmark the impact of gas turbine redesign, assumptions on electric power train density, optimal PMS and GT technology in section 4.2. The integrated multi mission assessment is shown in the section 4.3, while the TMS design space and architectural comparison is shown in section 4.4.1 and 4.5.3 respectively. The ECS electrification was a side study and was a deliverable to the sponsor, hence isnt a part of the thesis. Coming to the validation elements shown in this chapter. The gas turbine cycle design embedded solver is validated against trends from EPIDOSYS [80], the gas turbine weight and gas path ATLAS model is validated for EIS 2035 GT for SMR aircraft shown by Perullo [31]. The standalone optimal PMS optimizer trends are compared and validated against Trawick's trends [57]. The validated aircraft-engine models are shown in Section 4.1 of chapter 4. The thermal management modules are compared against HEX trends from Chapman [70] and all ANN modules are trained with regression error target in mind. Validating each module of the

framework essentially gives confidence that integrated framework is capable of giving correct trends. The next section starts with introduction of the framework.

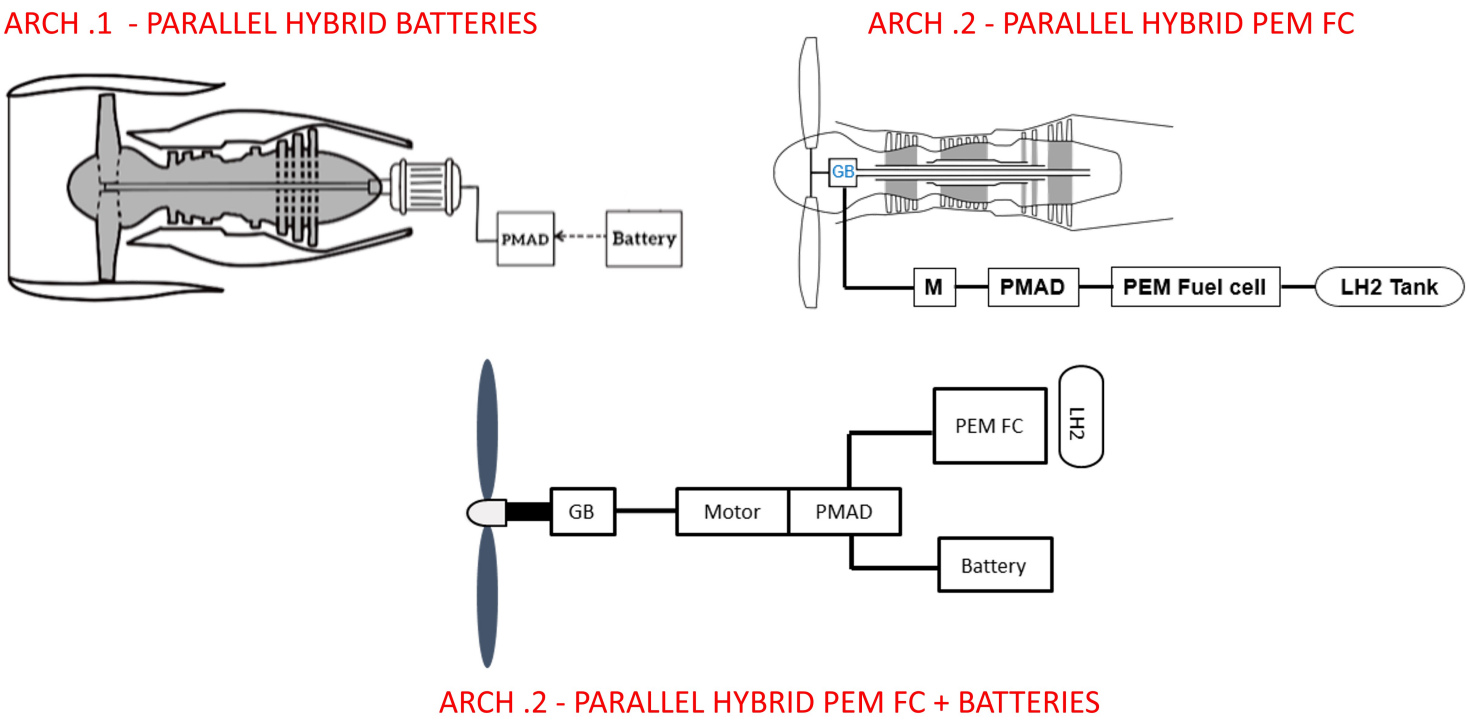


Figure 3.2: HEPS Architectures assessed

3.2 Introduction

The framework developed in this research include modules for gas turbine cycle design, direct operating cost calculations, electrical system models, power management integration ANN, multi mission energy management, ram air & vapour compression cycle design & optimization, TMS integration & aircraft modelling approach. The framework can be visualized in 3.3.

At the centre of the framework is the energy management optimization loop which calls aircraft mission performance code, ORION, which in turn calls rest of the modelled elements. The gas turbine performance, weights, diameter and length and thermal management performance are provided as surrogates during the mission run, while the electrical systems are modelled as simple equivalent circuit models. The outputs from the mission run are then fed to HESTIA which then calculates the HP turbine rotor replacement cycles which allows for the calculation of direct operating cost depending on battery weight, cycles, fuel burn and carbon emissions. Once all

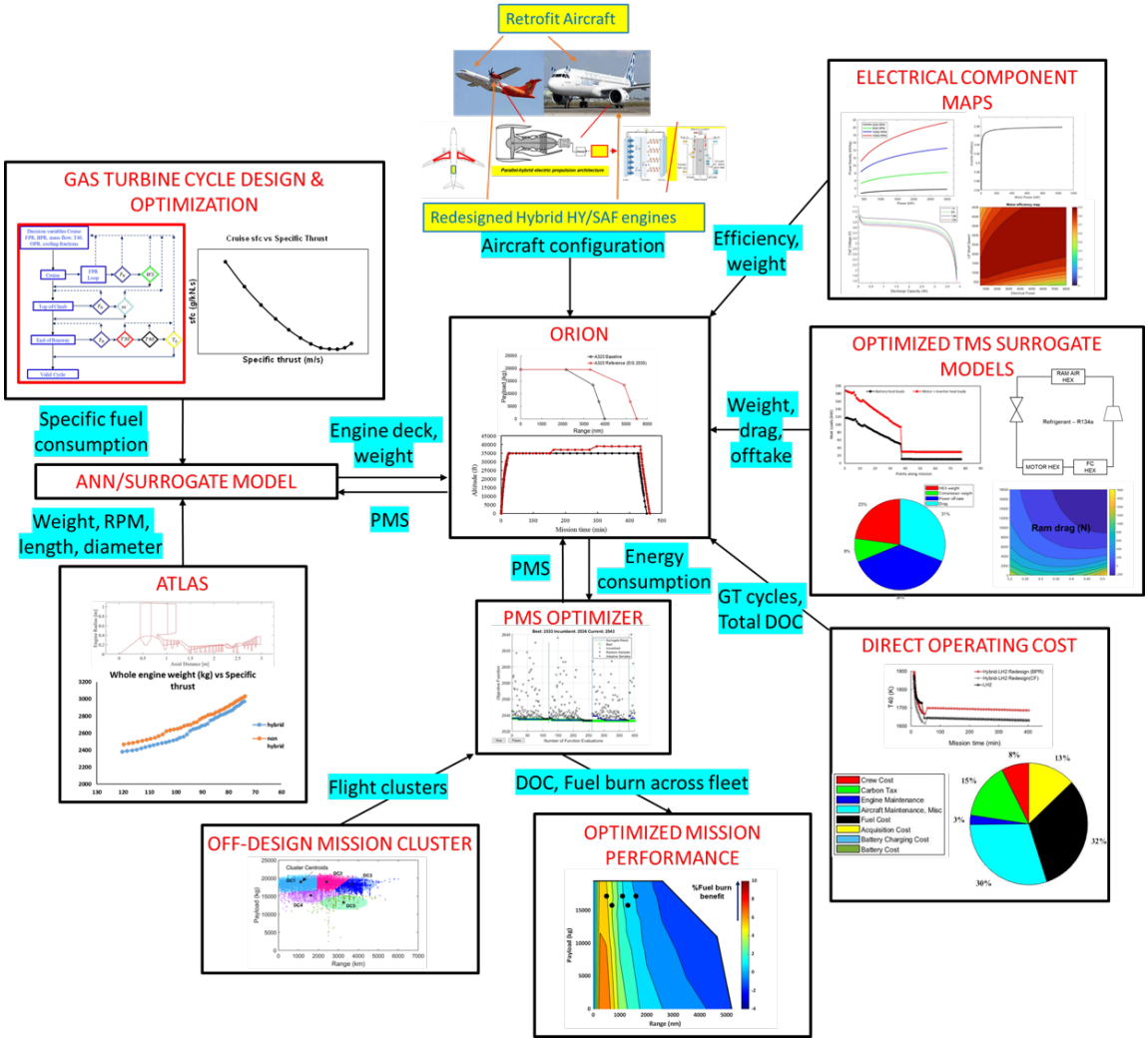


Figure 3.3: Framework

the attributes of the powertrain are known, multi mission optimization algorithm is utilized to get the optimal energy management strategy which in essence gives us the optimal propulsion configuration. The next sections describe each of the individual modules of the framework, ending with the aircraft design space.

3.3 Hybrid GT cycle design and weight assessment

3.3.1 Hybrid GT cycle design

This section of the chapter describes the method used for both the turboprop and turbofan hybrid engine cycle design. The cycle design process is initially developed for separate flow turbofan engines as this has been the primary focus of current existing fleet and is predicted to be the major propulsion system for EIS 2035 despite

the efforts on Open Rotor and distributed propulsion system. But the method to get an hybridized version of a baseline cycle remains the same irrespective of the baseline with a few more changes. Traditionally, for aircraft gas turbines, multi-point design approaches have been utilized [77][78][79][80]. The key points along an aircraft flight mission which constraints the gas turbine cycle are: Top of Climb (TOC), End of Runway (EOR), Maximum Take-off at hot and high conditions (MTOHH), One Engine Inoperative (OEI), Maximum Continuous thrust (MCT) & Sea-level static conditions (SLS) as shown in Figure 3.4.

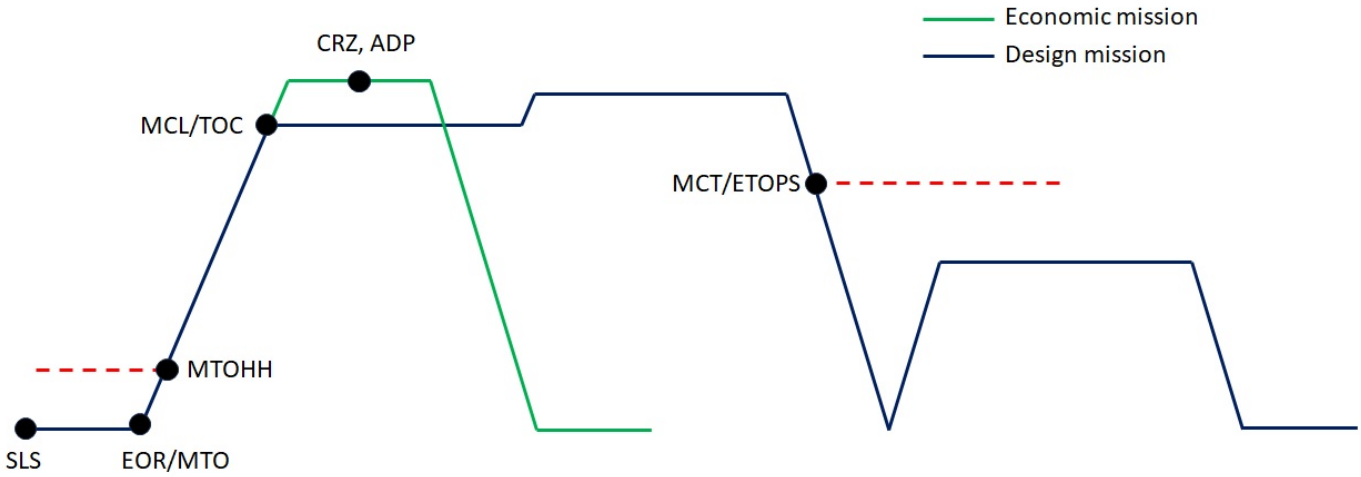


Figure 3.4: GT design points along mission

The key design points are Mid Cruise (CRZ) and Aerodynamic design point (ADP), CRZ being the design for the whole engine and ADP being the design point for compressors. The rest of the points along the mission act as constraints for The TOC thrust is calculated from CRZ thrust in order to maintain a certain rate of climb (300 ft/min for Turbofans and 500 ft/min for Turboprops), the EOR thrust is rated at End of Runway typically for ISA+15 or ISA+25 conditions. While MTOHH, MCT, SLS, OEI constrain a real engine in terms of compressor surge margins, turbine deterioration, lifing & engine starting. ADP is defined as the aerodynamic design point for compressors to maintain a working line and may or may not coincide with CRZ. The information regarding MTOHH, MCT, SLS, OEI & ADP is only obtained after sufficient cycling between airframer and engine OEM hence only 3 points, TOC, EOR and CRZ are part of a cycle design loop at a conceptual level. This leads to a 3-point gas turbine design followed by most work published in open literature [77][78][79][52][53][123]. Primarily, the aim of the 3-point gas turbine cycle design is to optimize specific fuel consumption at cruise while satisfying the turbine NGV & rotor inlet temperature (T40 & T41 respectively), compressor outlet temperature (T30),

OPR constraint (top of climb) & fan diameter. The ratio of cold nozzle velocity to hot nozzle velocity is the parameter which dictates the optimization of specific fuel consumption. The engine cycle can be defined by following variables : BPR, FPR, OPR, Fan diameter, T40 (Combustion outlet temperature), gear ratio & compressor pressure ratio spilt. The selection of compressor work split is dependent on many factors : secondary system power off-takes, bleed requirements, LP, HP compressor transient stack & engine starting hence at a conceptual level, this can be extrapolated from existing engines of same class. The gear ratio is a fall-out variable dependent on fan diameter, top of climb fan frontal axial mach number/Qa, LP turbine ANsq limit & axial mach number. For a given fan diameter or specific thrust, there can be only one combination of FPR & BPR to give optimum jet velocity ratio [79][81]. Hence, the whole engine cycle optimization filters down to three design variables: fan diameter, OPR & T40. Whurr et al characterized the design space as a function of these three variables to show the selection dependent on fuel burn, direct operating cost/turbine life & NOx emissions[10].

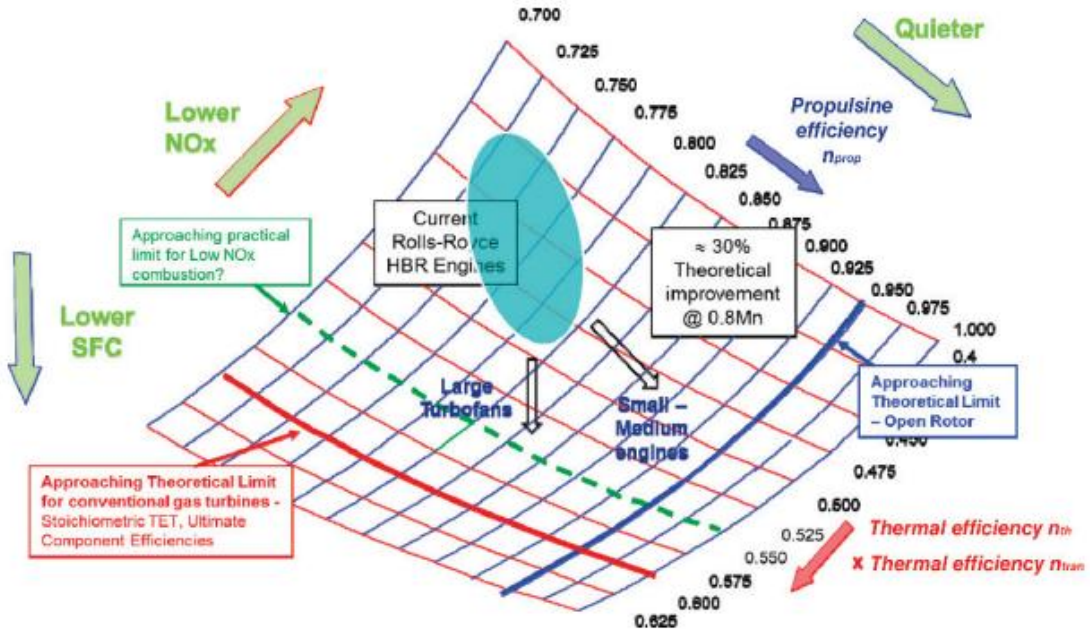


Figure 3.5: Relationship between SFC, thermal, transfer and propulsive efficiencies, 2015 Rolls-Royce plc.[10]

Higher T40's and T30's only increase the sfc benefit upto a limit constrained cooling flow effectiveness, high pressure turbine life and Time on Wing. The fan diameter or specific thrust selection requires a full aircraft mission to be run to get the optimal balance between weight, drag and sfc exchange trades as performed in [81][80][124].

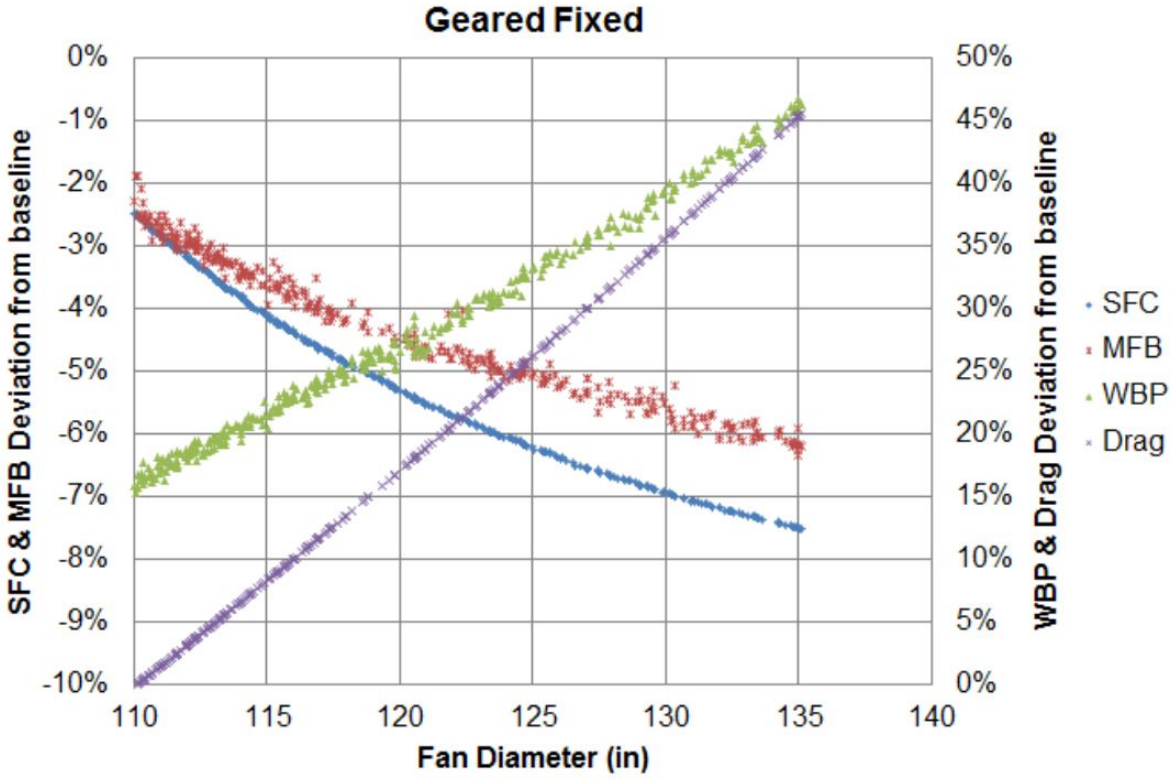


Figure 3.6: Fuel burn, drag and SFC curves for the Geared Fixed model.[80]

Adding electrical power to any shaft of the gas turbine changes the design space as every power management strategy alongside the original variables of OPR, T40 & specific thrust changes the design space distinctly. The cycle optimization problem no longer remains a 3 variable problem but evolves into a 6 variable problem at the very least and also the mission fuel burn has an additional impact from battery, motor & inverter weights. The traditional approach that has been utilized to select an engine cycle most suitable for aircraft mission is to first develop a pareto front of engine cycles optimized for specific fuel consumption and specific thrust with target T40 and OPR as constraints. These set of engine cycles are then run for a steady aircraft mission run and finally the cycle is selected depending on objective function of fuel burn, NOx and operating cost [80]. But this approach is no longer feasible as the design space has multiplied exponentially due to power management strategies, hence a modified approach is needed. The method would to simply create a dataset of solved cycles for each target T40, OPR, fan diameter and motor powers for the three points and then train a surrogate of these optimized engine cycle parameters as a function of these variables. This surrogate hybrid engine designs are then called for aircraft mission runs with power management strategy optimized. The cycle design

process for each PMS, T40, OPR, & fan diameter is can be visualized in Figure 3.7 with the variables and parameters noted in Table 3.1.

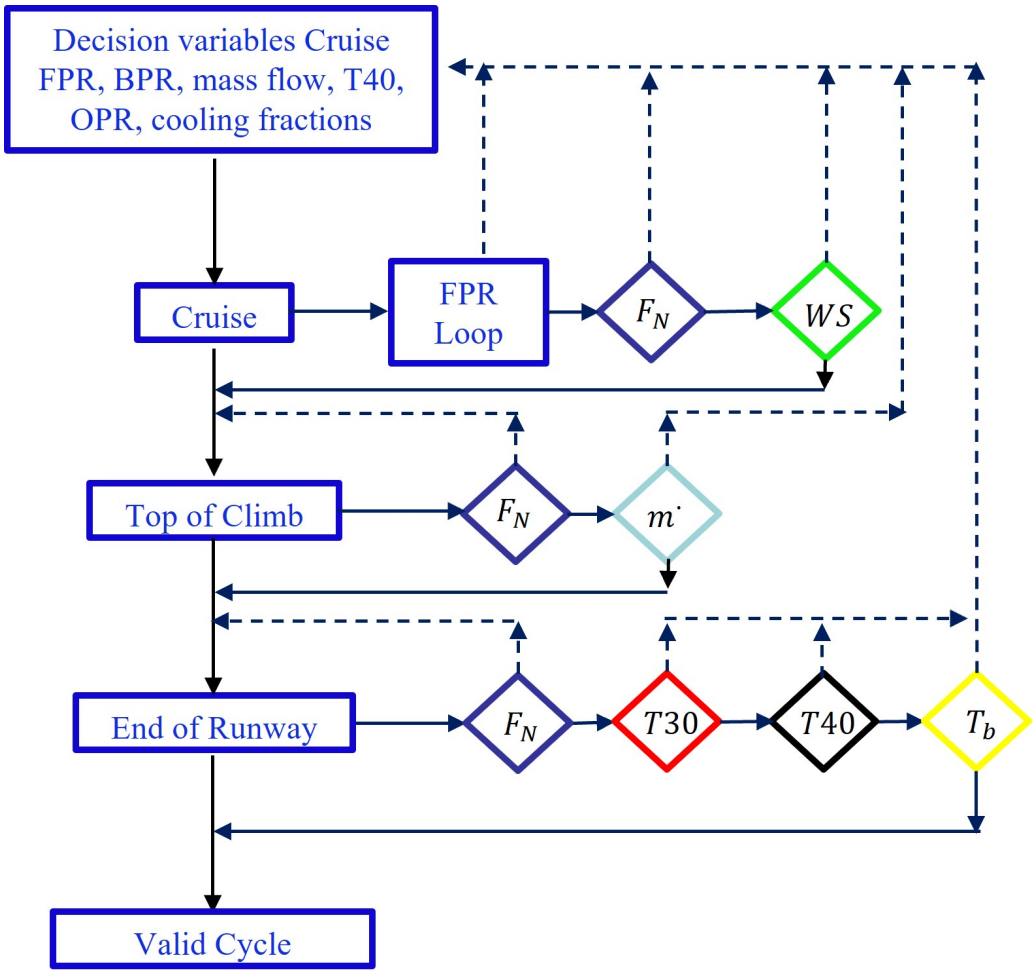


Figure 3.7: 3-point cycle design solving method

A secant method based solver is utilized to match the variables to target parameters (Table 3.1). The combination of BPR and FPR are varied to match the jet velocity ratio and top of climb mass flow, the Cruise T40, mass flow and OPR to match MTO T40/T41, CRZ thrust and T30 at MTO respectively. An extra variable of top of climb motor power on-take is used as a variable to have the same lifing/temperature rating as baseline non hybrid gas turbine for a given take-off power on-take. This is only imposed for the initial design exploration results but not otherwise. Constraints are also imposed on take-off and cruise power on-take to have 15% LPC, HPC surge margin as a transient stack. Cruise power on-takes are also constrained to avoid excessive HP turbine rotor temperatures and potential creep failure.

The GT cycle design process and solving method for each power management strategy, thrust requirements, target temperatures and pressures has been described

Parameters	Variables
Cruise thrust	Cruise FPR
Top of climb thrust	Top of climb LPT spool speed
Top of climb HPT rotor temperature	Top of climb on-take
Take-off thrust	Take-off LPT spool speed
Take-off T30	Cruise OPR
Take-off T40	Cruise T40
Top of climb inlet mass flow	Cruise inlet mass flow
Cruise target jet velocity ratio	Cruise BPR
Take-off rotor & NGV temperatures	Cooling fractions

Table 3.1: 3-point cycle design parameters & variables

above. The next sub-section deals with the GT weight assessment module for the top level requirements and different design variables.

3.3.2 GT weight assessment

For every baseline gas turbine cycle assessed further in all the studies, two main hybridized versions of this baseline are assessed, retrofit and redesigned hybrid GT. The retrofit GT means that the same baseline GT is used and it is simply hybridized by maintaining operability limits on the booster and fan. Hence, the weights and dimensions of the retrofit GT is the same as the baseline GT as the same physical engine is reused. While in the case of redesigned GT, because the baseline GT is modified, the weight needs to be modified in order to have a fair comparison between retrofit, redesigned and baseline at a mission level. There have been various methods used in open literature, to estimate the gas turbine weight at a conceptual level. They have either been single [125][126], two [127], three, four [128] variable correlations or component by component weight calculation methods [129] [130], with varying level of detail and accuracy.

Primarily, all the major previous HEPS studies [47][24][87][32] except [31][91] have either utilized weight correlations or not changed the weight at all with electrification. The approach which has been followed is a step up from these approaches to get a correct back to back difference between retrofit and redesigned hybrid GT engines, hence a component-weight based approach is followed. ATLAS is an in-house component by component gas turbine weight analysis developed by Lolis [130] and has been validated against NASA's WATE tool [129]. In order for the tool to be used for SMR EIS 2035 Geared engine studies, it was best to use the code and compare against results of the same technology level and thrust class from open literature [31]. So,

EIS 2035 baseline kerosene GT gas path was obtained using ATLAS and compared against the gas path from for EIS 2035 from Perullo. This alignment would show if we are in the correct ballpark of pressure ratio split, sfc, weight and length of the GT. This alignment is shown in Figure 3.8.

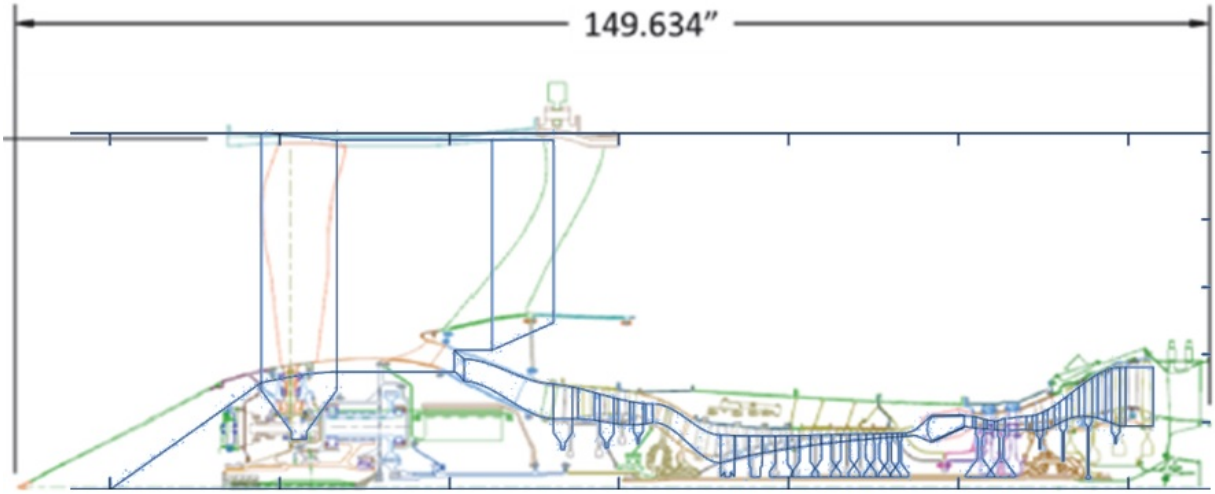


Figure 3.8: Gas path validation

It can be seen that the hybrid gas path with 3500 HP is well aligned with Perullo's EVE study with 3 stages LP compressor, 10 stages HP compressor, 2 stage HP turbine and 4 stage LP turbine correctly matched. But how about weight and cycle parameters between the two studies. The comparison of the these parameters are shown in Table 3.2.

Parameters	EIS 2035 SMR MODEL	Perullo EVE Study	Delta
Hybrid 3500 HP GT weight (kg)	2150	2249	4.4%
Baseline GT OPR (TOC)	50.7	51	0.3
Baseline GT FPR (TOC)	1.44	1.45	0.1

Table 3.2: GT weight and sfc comparison

Given that the match is within 5% and ATLAS has baseline GT models also well aligned for CFM 56 and turboprop engines [130], this model is now lined up for all the hybrid studies. The comparison of the hybrid gas path with the baseline gas path is shown in Figure 3.9. The main changes are the increase in the swan neck length to accomodate the electric motor while the hybrid core is smaller (due to higher BPR, smaller core size described in cycle design section 4.2) and shorter due to a less loaded HP compressor (this is discussed in operability section within 4.2).

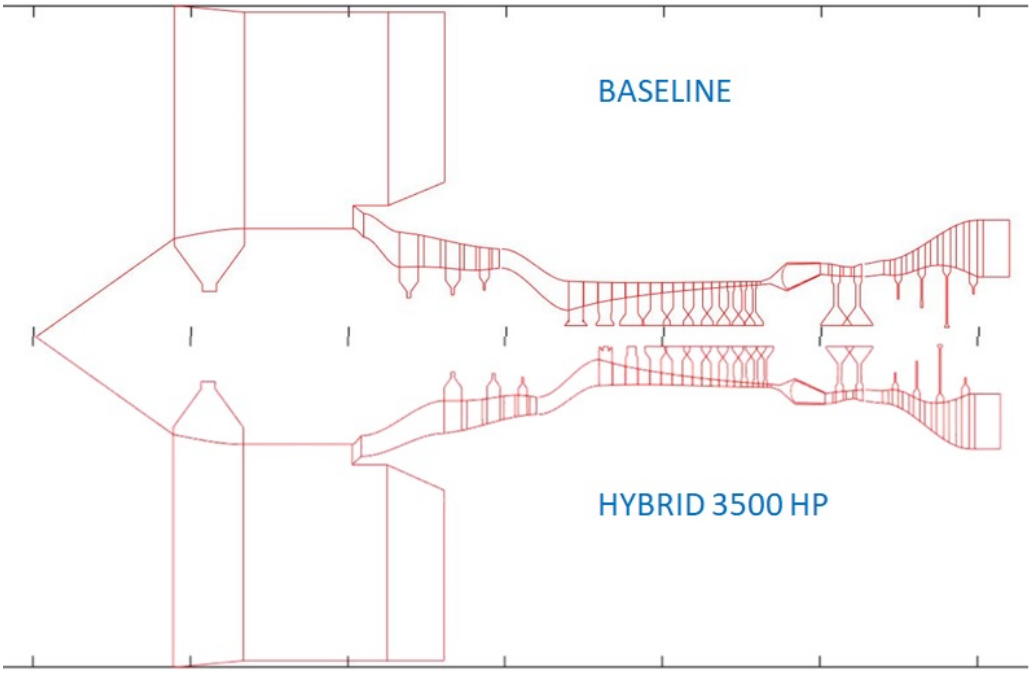


Figure 3.9: Comparison of hybrid and non hybrid gas path

Component	Hybrid	Baseline	Delta
Fan	789	784	0.6%
IPC	78	96	18.7%
HPC	214	284	24.6%
HPT	70	93	24.7%
LPT	126	146	13.9%

Table 3.3: Hybrid and baseline component weight comparison

The component by component weight comparison between hybrid and non hybrid GT is shown in Table 3.3, again highlighting the difference due to smaller core size of 17%. A final comparison is done between hybrid (1 MW power) and non hybrid GT cycle sfc, BPR, whole engine weight against specific thrust are shown in Figure 3.11, below. The T40, T30, BPR, sfc trends (Figure 3.10) across specific thrust are also shown and these align well with variations from EPIDOSYS (found in [80]).

It can be seen that the T40, T30 targets are consistently met by the solver across the range of specific thrusts and the increasing T40 at CRZ across the spectrum. The trends of hybrid GT are similar to non hybrid GT but coming at a drop of sfc due to cycle redesign (described in detail in Results section). It can also be seen that the weight on hybrid GT is 5% lower than baseline GT on an average specific thrust. Finally, as the cycle design trades, weights and gas path has been validated, these methods and models are used right through all the studies. The next section deals with the development of ANN of GT design and off-design performance to integrate

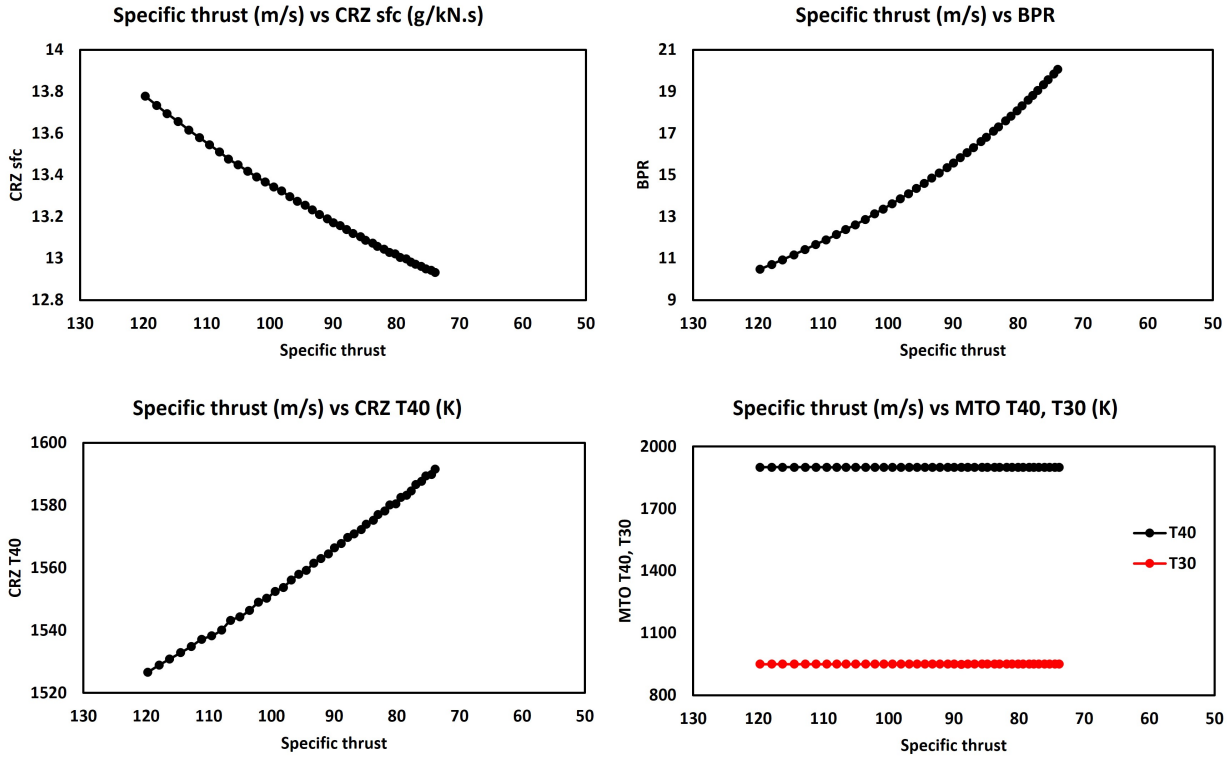


Figure 3.10: Baseline GT trades for different specific thrusts

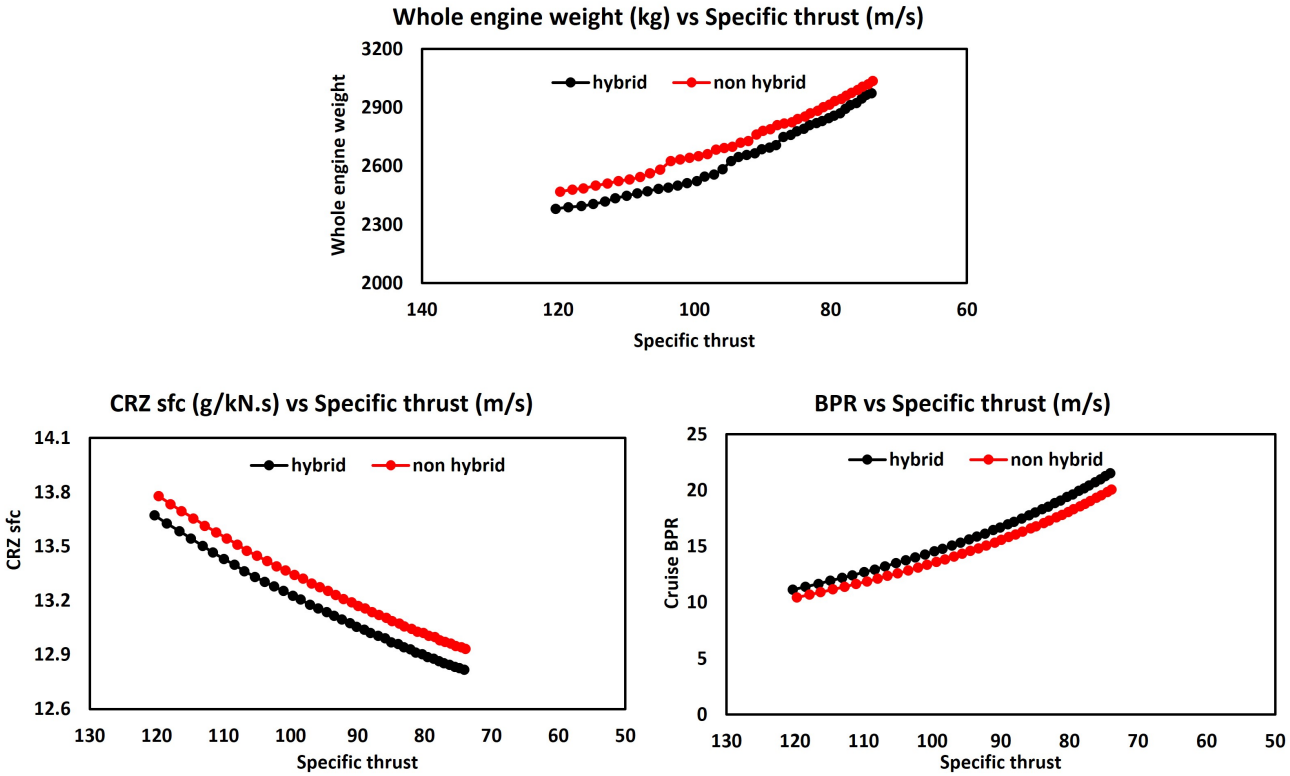


Figure 3.11: Comparison of trends between hybrid and non hybrid GT

into the framework.

3.4 PMS optimization and integration ANN

This section is divided into two sub-sections - Integration ANN and PMS optimization. The first part deals with the development of GT design and off-de sign surrogate model to be implemented in the multi-mission framework and the corresponding validation approach. The second part deals with the PMS optimization method employed and the validation of the trends.

3.4.1 Integration ANN

This sub-section of the chapter describes the surrogate method used for integrating the power management strategies with gas turbine cycle design. The main aim of the surrogate is not just to get variation of cycle design performance as a function of PMS but also to get off-design performance variation. The need to get off-design performance is to bypass the use of Turbomatch (Cranfield University gas turbine performance tool) when running the mission every time. So, the ideal process would be that once a dataset of redesigned engine cycles is developed, they are run for a series of off-design flight conditions and motor powers to create a complete hybrid engine deck model. The surrogate is created by training on the dataset and finally integrated into aircraft mission-power management optimization loop. The inputs and outputs of such a neural network are noted down in Table 3.4 and shown in Fig 3.12 and equation 3.1.

$$[Thrust, sfc, T30, T41, GTWeight, LPPower] = f(T/ODoH, CLDoH, CRZDoH, FlightpointDoH, TargetT40, TargetT30, Flightaltitude, Mach, Fan\ diameter, LPSpoolspeed) \tag{3.1}$$

It can be noticed that the database is trained and developed on 10 inputs (T40, T30 and fan diameter being cycle variables, T/O Hp, Climb HP and CRZ HP being PMS variables, Altitude, Mach, Off-design HP and Spool speed being the mission variables. Because the number of inputs are so high, it isn't feasible within the timescale and accuracy that ANN be trained on that, so a decision was taken in order to bypass some of the inputs. The 3 inputs which could potentially be passed are

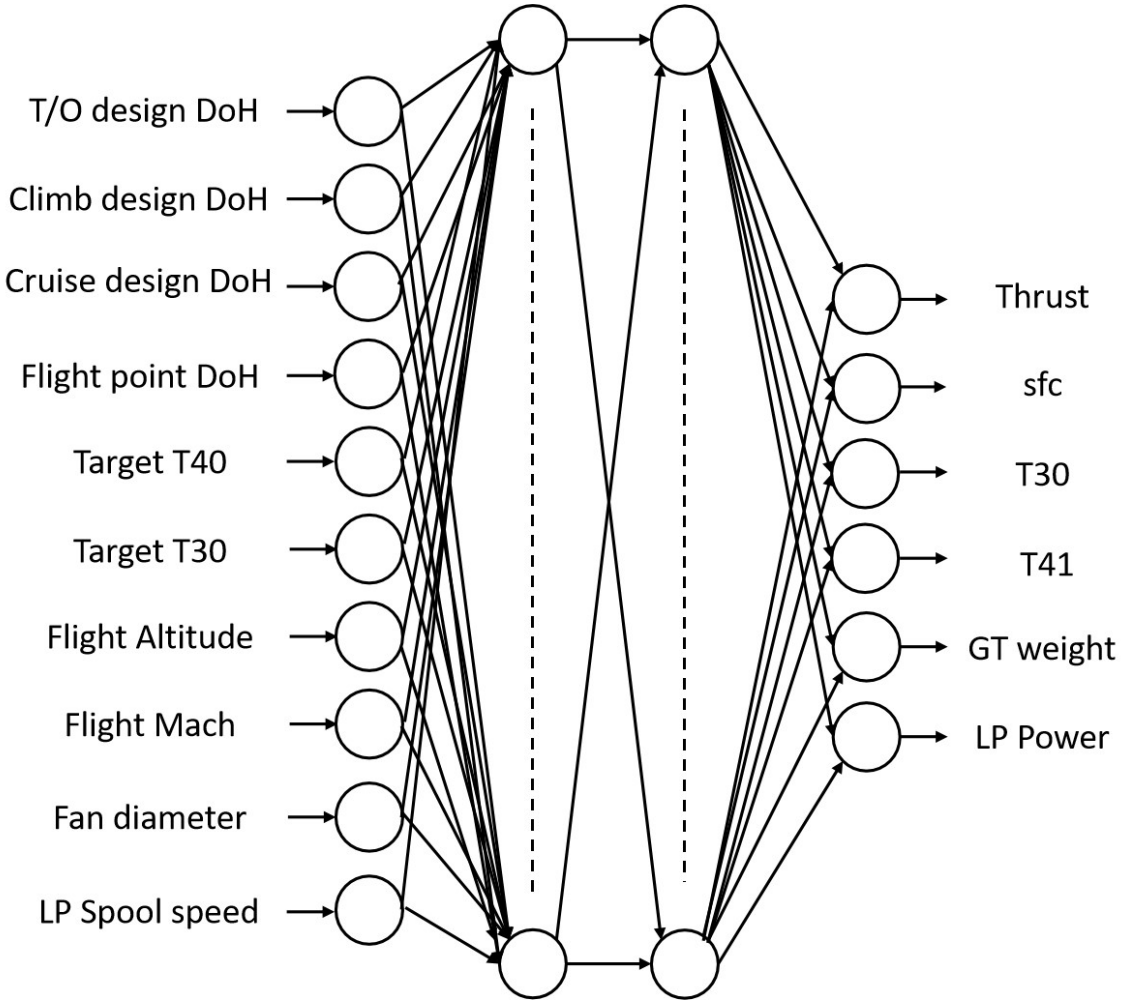


Figure 3.12: GT-PMS ANN inputs & outputs

Inputs	Outputs
Climb design DoH	
Cruise design DoH	
Take-off design DoH	T30
Off-design DoH	Specific fuel consumption
Fan diameter	Thrust
Target T40	T41
Target T30	LP Shaft power
Altitude	GT weight
Fan spool speed	
Mach	

Table 3.4: Hybrid engine surrogate inputs & outputs

the core T40, T30 and fan diameter. The T40 and T30 are technology and material capability parameters, hence it is accepted that the hybrid GT be designed at the same core capability as the baseline GT. So when designing hybrid variants of all

GT's modelled in this study (all 3 classes, 2010 and 2035), they are designed for the same target temperatures. It is likely that designing for same temperatures, may not be optimal for both fuel burn and direct operating cost for very high degrees of hybridization, as the trade for core size and component efficiency would plateau (this is discussed in Section 4.3). But the assumption is fair enough for low degrees of hybridization. It needs to be understood if optimal fan diameter would indeed be different between hybrid and baseline aircraft-GT. In order to get this answer a comparison of mission fuel burn was done for SMR aircraft on 2500 nm for hybrid (1 MW) and baseline GT with varying specific thrust. This comparison of mission fuel burn can be seen in Figure 3.13, it can be clearly seen that both the fan diameters have the same optimal fan diameter on design mission (the constraint in fan diameter imposed by landing gear length). So, even assuming that hybrid and non hybrid aircraft have same optimal fan diameter is a good one. But can these be rationalized?

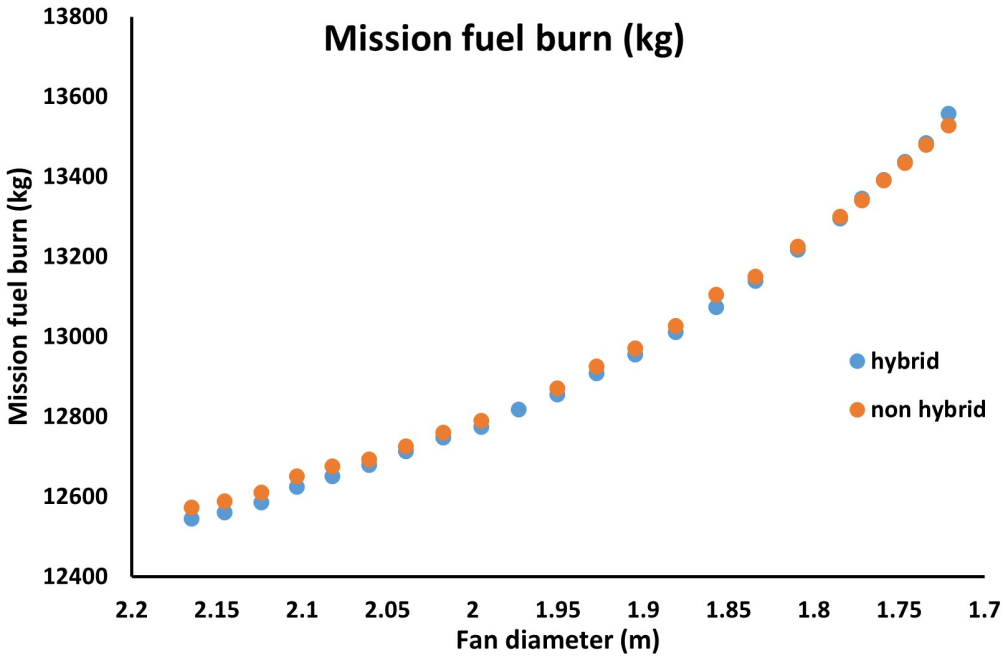


Figure 3.13: Mission fuel burn

The equation 3.2 shows how a change in fan diameter wrt to a baseline changes the fuel burn depending on sfc, weight and drag slope. Where a,b and c are the respective trade slopes. What can be noticed in Figure 3.11, that the slopes of sfc, weight and drag are similar for hybrid with the curve offset by a value driven by benefit in sfc and reduction in core size. Hence, rationally, all hybrid variants will have same level of fan diameter, T40 and T30 as baseline GT.

$$[Total fuelburndelta] = (\%sfcdelta) * a + (\%dragdelta) * b + (\%weightdelta) * c \quad (3.2)$$

The approach is then modified such that the optimization on T40, T30 and fan diameter is performed only for the baseline GT and then for each PMS, the cycle is optimized and then run off-design for series of flight conditions, ultimately generating a complete database. The updated set of inputs and outputs are shown in Table 3.5 and the final process is shown in Figure 3.14.

Inputs	Outputs
Climb design DoH	LP Shaft power
Cruise design DoH	T41
Take-off design DoH	T30
Off-design DoH	Specific fuel consumption
Altitude	GT weight
Fan spool speed	Thrust
Mach	

Table 3.5: Updated hybrid engine surrogate inputs & outputs

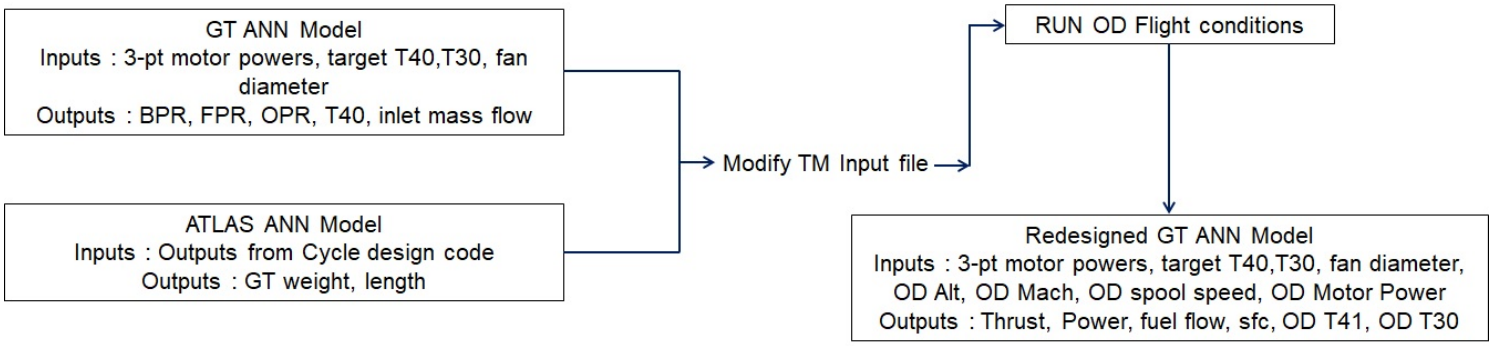


Figure 3.14: Hybrid DP and OD deck method

Parameter	Value
Number of Neurons in each hidden layer	10
Maximum Epochs	1000
Training data	70%
Validation data	15%
Testing data	15%
Number of layers	2

Table 3.6: Neural network inputs

To create the full engine surrogate, a feedforward neural net is trained using

Lavenberg Matequardt algorithm [131]. The neural network approach is utilized over an interpolation based approach to preserve the trend of the dependence of the outputs on the input parameters. The problem though is unlike interpolation based approaches, fitted function wont pass through all given output variables. Hence it is necessary that the maximum error across the whole dataset between trained values and input values be less than 3% to capture both the trends and real values. These approaches have been used for retrofitted gas turbine engines quite extensively as in [97],[57][132], hence LM is used in this research too.

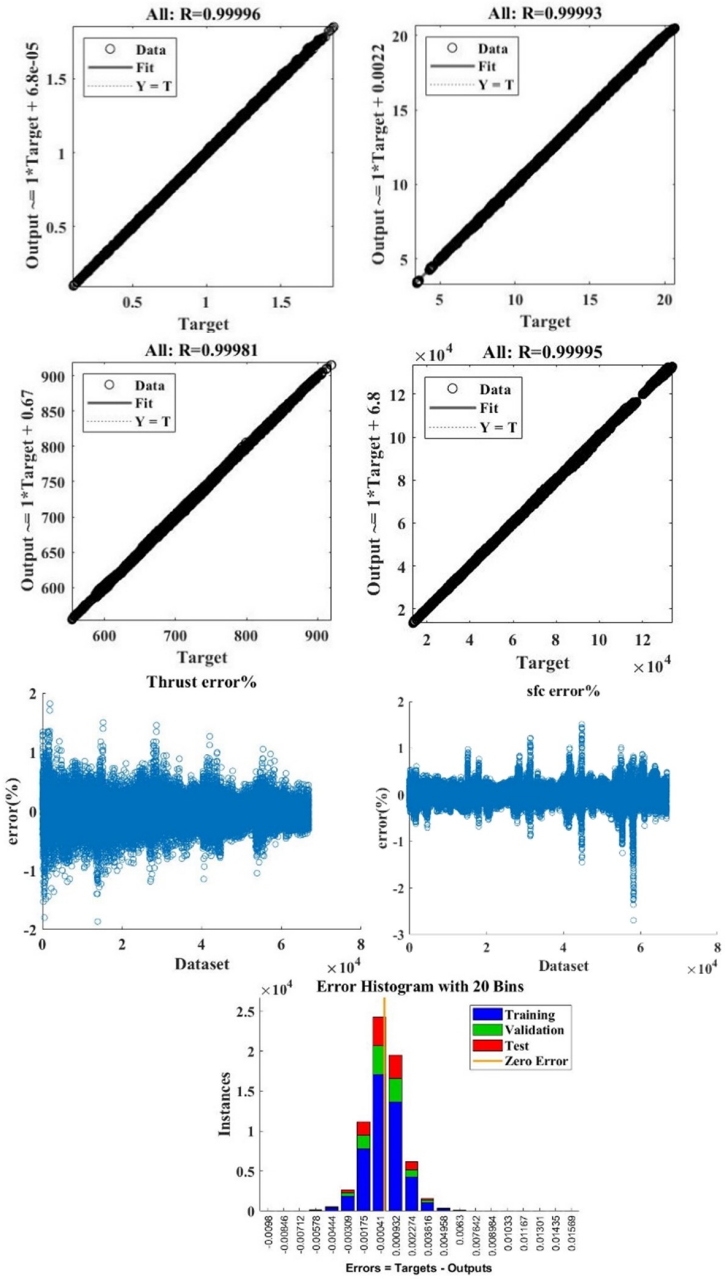


Figure 3.15: SMR test case ANN fits

A large dataset of around 16,000 inputs was run for SMR test case, the errors can be seen in 3.15. While the fits for Turboprop test case can be seen in Figure 3.16. The curves are well fitted to the data as can be noticed from R-squared value and global percentage errors. The final set of ANN inputs are seen in Table 3.6.

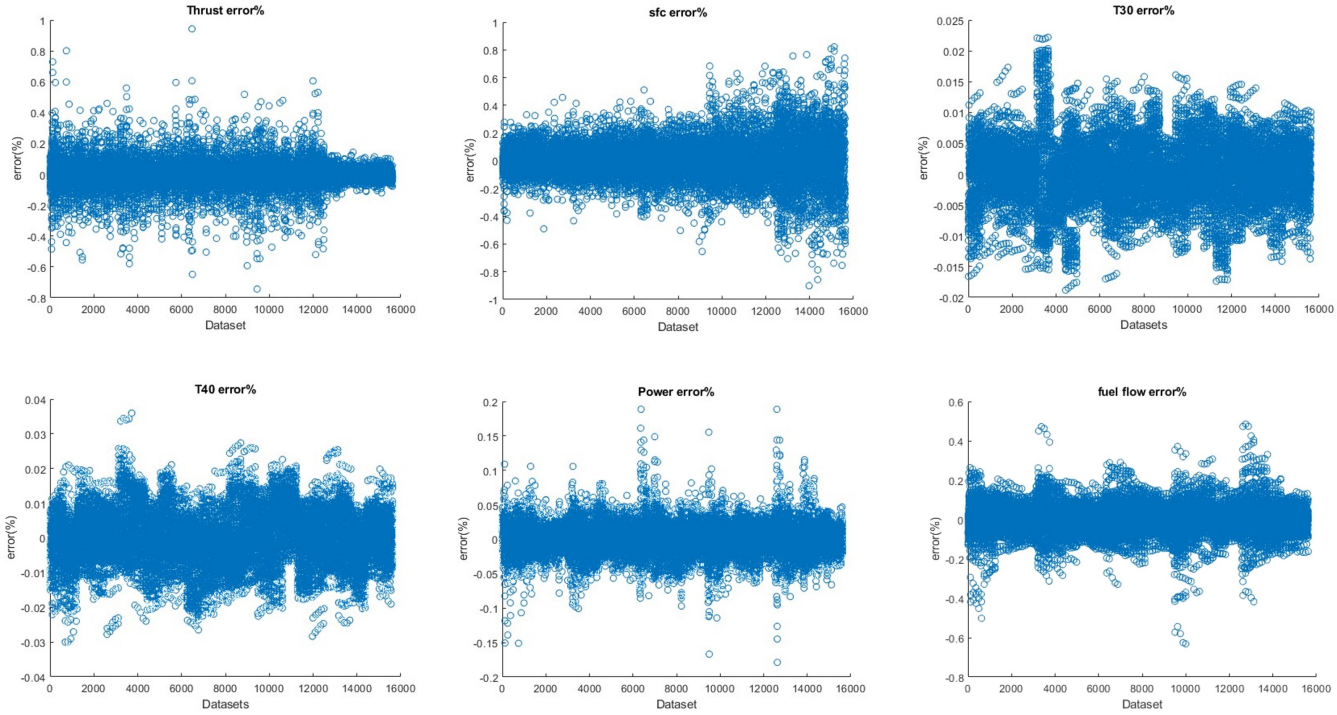


Figure 3.16: Regional turboprop test case ANN fits

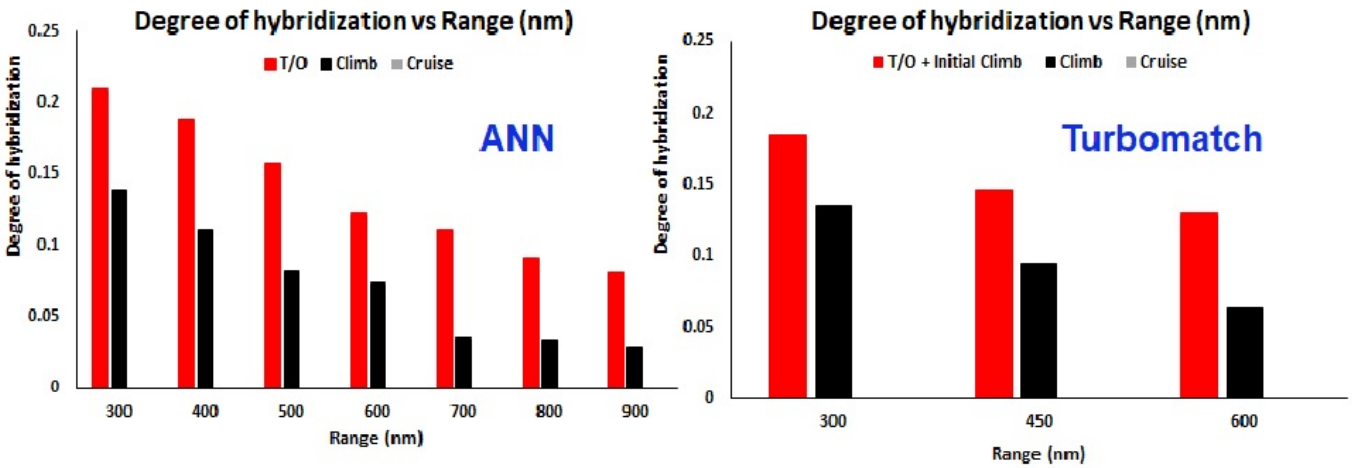


Figure 3.17: Comparison of optimal PMS trends (ANN vs TM)

Once the data is fitted, an optimal PMS validation study was run (the method

is described in the next sub-section) and the trends were developed. The trends were then compared against if Turbomatch was used directly. This comparison is shown in Figure 3.17, showing the alignment in optimal PMS trends. These trends are described in detail in the results section hence only validation is shown here. The trends suggest that the ANN captures the design behaviour as well as the off-design behaviour hence can reproduce the same optimal power management strategies.

3.4.2 PMS optimization

This subsection deals with the setup of the PMS optimizer, methods used and the validation of trends. The optimizer is setup within each mission run to optimize the power split between motor and gas turbine while satisfying the battery state of charge and aircraft MTOW constraints. The formulation of PMS optimizer is shown in Equation 3.3.Where essentially the fuel burn over the whole mission is minimized while targeting a battery minimum state of charge requirement and matching aircraft take-off weight constraints.

$$
\begin{aligned}
&min(\sum_{t=0}^{FT} m_f dt) \\
&s.t. \\
&HP_{climb_{max}} \geq HP_{climb} \geq 0 \\
&HP_{takeoff_{max}} \geq HP_{takeoff} \geq 0 \\
&HP_{cruise_{max}} \geq HP_{cruise} \geq 0 \\
&MTOW \geq TOW \\
&Battery_{SOC_{end}} \geq 20\%
\end{aligned}
\tag{3.3}
$$

Two methods are primarily utilized for the optimization process, genetic algorithm optimizer and surrogate based optimizer. There have been smarter optimization methods used before in optimal PMS studies, like model predictive control [60] or convex optimization [59]. These methods work well if the design space is convex with one global optima, which is indeed the case with retrofit HEPS as the trade is between battery efficiency and aircraft weight distribution. But the integration of GT design and thermal management increases the complexity of the design space thereby having local optimums, hence these methods are not utilized in this study, instead global optimization approach is used. Genetic algorithm [133] is quite popular method used in most engineering problems, due to the ability to capture non-linear and non-convex

objective functions and it has also been used often in PMS studies [57], [55]. Due to the integrated cycle design and power management strategy optimization inherently being a non-linear function, genetic algorithm was initially utilized. But the genetic optimization algorithm has high overheads due to extremely high time required for the solutions to converge. To solve this problem, a surrogate-based optimization method [134] (available with MATLAB library as surrogateopt) was also utilized. The method uses radial basis interpolation to define a utility function continuously from various objective function runs. The convergence from both these methods for the same example fuel burn minimization case on mission range of 400 nm for Fokker 100 is shown in Figure 3.18. It was found that both the methods ultimately picked very close fuel burn values and power distributions. But the surrogate-based optimizer performing the same within 400 function calls while GA optimizer requiring over 600 function runs. The settings used for GA optimizer can be found in Table 3.8 while settings used for surrogate-based optimizer can be found in Table 3.7.

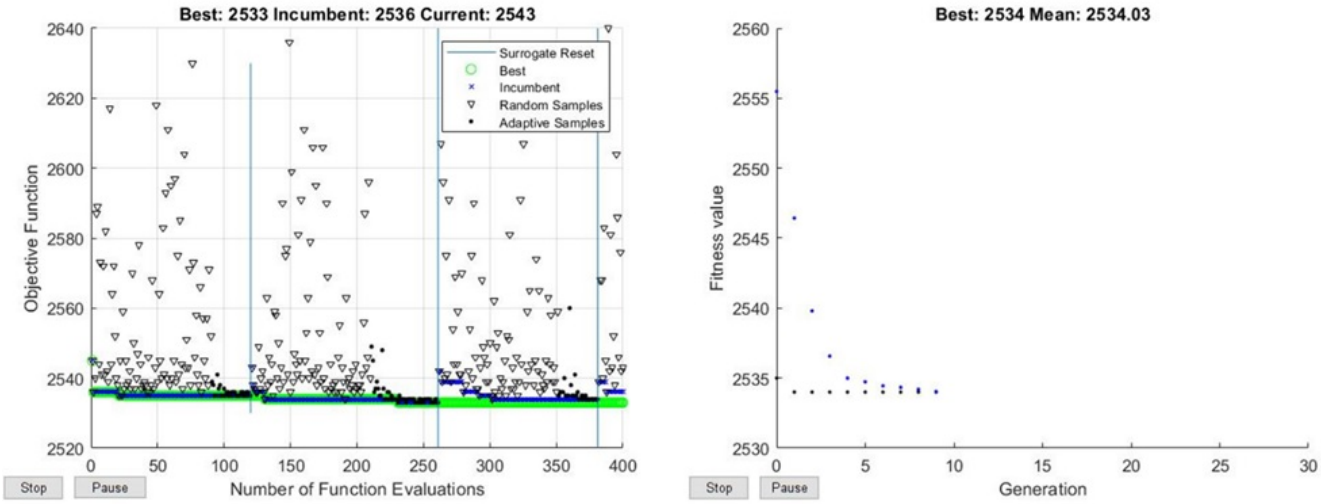


Figure 3.18: Comparison of trends GA vs surrogate

Parameter	Value
Maximum Function Evaluations	400
Minimum Surrogate points	50

Table 3.7: Surrogate optimizer settings

This concludes the section regarding the optimizer setup and method used but how about the validation and comparison of trends. It has been shown that multiple studies in the past have been looking optimal PMS trends for retrofit GT's [57], so a comparison is made on a common setup of battery efficiency, mission, payload and

Parameter	Value
Population Size	80
Maximum Number of Generations	30
Crossover fraction	0.8
Elite count	10
Mutation function	'adaptfeasible

Table 3.8: GA settings

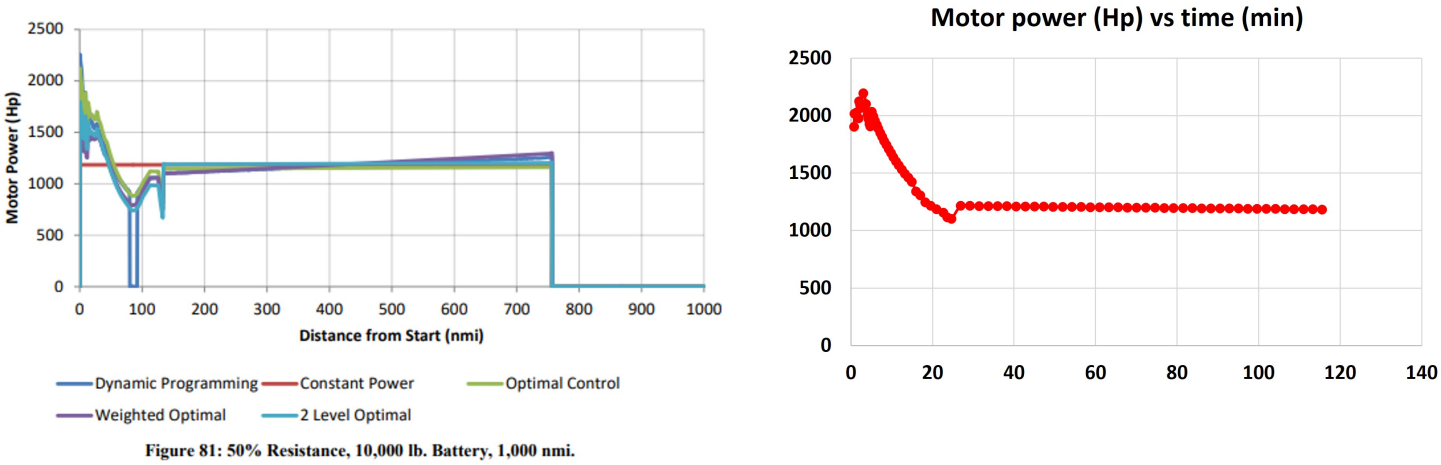


Figure 3.19: Trends comparison with Trawick [57]

constraint assumptions. The comparison of optimal PMS trend for retrofit GT is shown in Figure 3.19. The optimal PMS trend for SMR EIS 2035 model on same range aligns very well with optimal control outcomes from Trawick. This concludes the development of ANN and optimization setup. Next section discuss the Direct operating cost estimation module.

3.5 Direct operating cost

This section includes the method utilized for estimating the direct operating cost of all retrofit, redesigned HEPS architectures for all three aircraft classes. The total operating cost for an airline typically consists of the following costs[135]:

- Fuel cost.
- Flight and cabin crew cost.
- Aircraft maintenance cost.
- Engine maintenance cost.

- Aircraft leasing cost.
- Emission cost.
- Taxes, fees and user charges.
- Insurance cost.

As the main aim of this research is to compare both sets of retrofit and redesigned parallel HEPS architectures against baseline non hybrid architectures, extra systems cost needs to be accounted for. The additional cost for HEPS architectures includes the following:

- Electrical powertrain cost.
- Battery acquisition cost.
- Battery replacement cost.

The major reduction that the HEPS architectures could potentially bring in operating cost could be by virtue of reduced fuel cost, emission cost and engine maintenance cost. It is assumed in the study that rest of the aircraft maintenance cost, crew cost, insurance and taxes would remain same for HEPS aircraft as the baseline. Also, besides the operating cost, the acquisition cost of hybrid electric aircraft would be expected to be greater than baseline aircraft by 10-30%[136]. In order to correctly account for the engine maintenance cost for different power management strategies, HESTIA has been utilized. HESTIA is an HPT rotor lifing module used extensively as part of TERA framework in previous lifing studies performed by CU in previous integrated airframe engine studies[137][138]. HESTIA essentially estimates the failure of HPT rotor blades and disks by three failure modes: fatigue, creep and oxidation, and then estimates the cycles to failure for each mode by using Miner's Law (to account for different flight segment ratings).

Inputs
T41 along mission profile
T30 along mission profile
Mission time
Cooling effectiveness
Blade and disk heights
HP shaft speeds

Table 3.9: Lifing model inputs

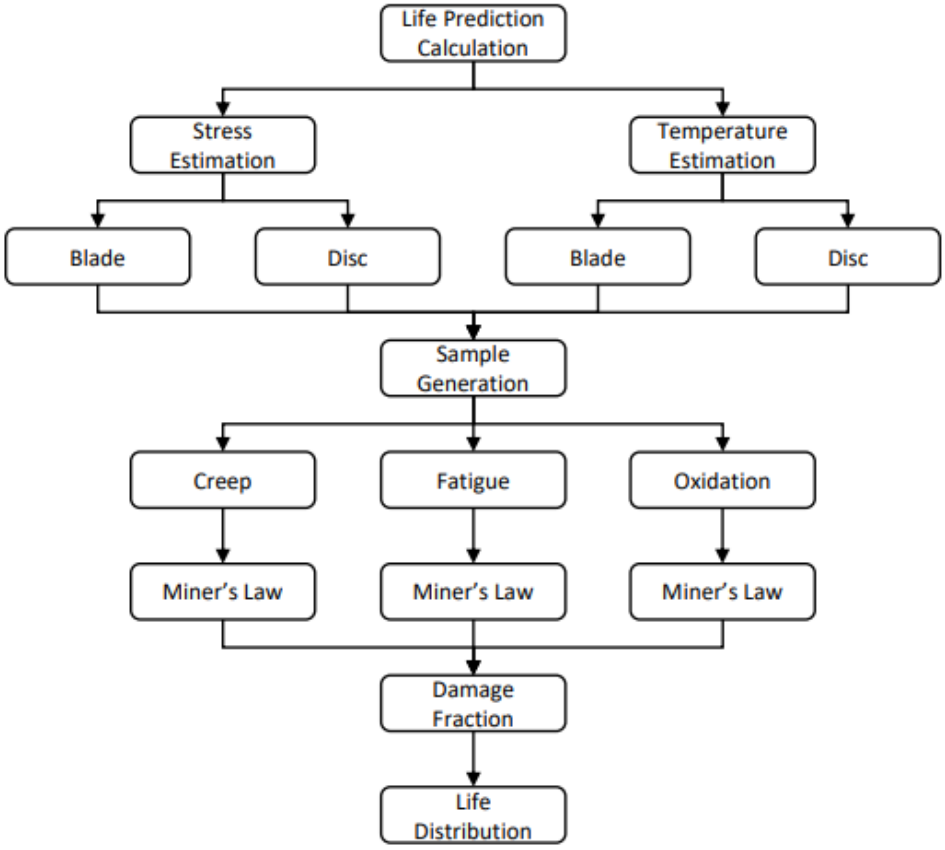


Figure 3.20: HPT Lifing method[138]

The blade and disk heights and geometries were generated from ATLAS and fed into HESTIA and finally giving the output of cycles to failure for different PMS and GT cycle designs. Another surrogate is created for the engine maintenance cost from HESTIA assuming that the replacement of HPT rotor drives the number of shop visits and constitutes 80% of the engine maintenance cost[135].

The inputs for the lifing surrogate is summarized in Table 3.9. All the inputs utilized for estimating the direct operating cost for all HEPS configurations is summarized in Table 3.10. Some initial trends are shown in Figure 3.21 to highlight the effect of change in cycles to failure for change in MTO blade metal temperatures at fixed cooling fractions for SMR test case. A drop of 50 rotor blade metal temperature (translates to roughly 120 K in T41) in MTO and initial climb rotor temperatures effectively doubles the time of wing keeping the same cooling flow fraction which shows the potential benefit from electrification.

Another set of trends are also shown to see what could be potential impact of CRZ power on-take on cycles to failure in Figure 3.22. The power on-take at CRZ has negligible impact on time on wing highlight the downside of powering CRZ for retrofit case.

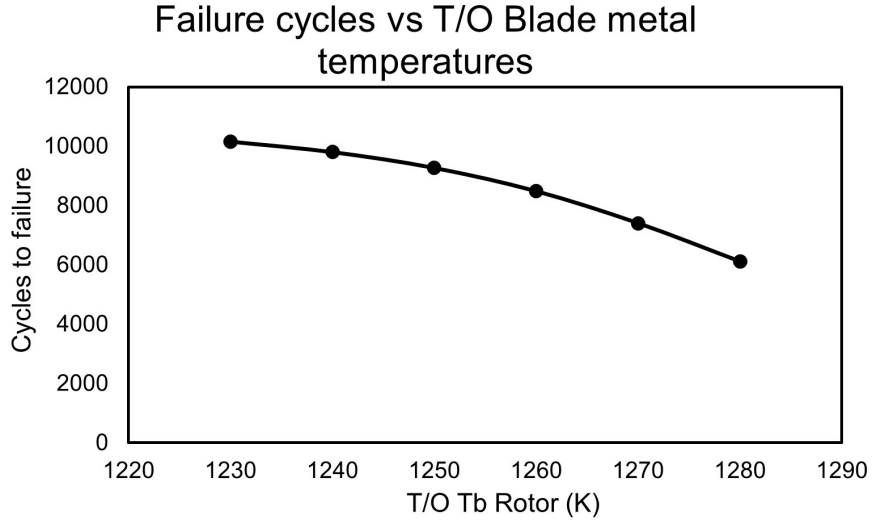


Figure 3.21: Impact of T/O temperatures on GT cycles to failure

Inputs	Outputs
Battery charging cost ($/kWh)	0.15
Carbon tax ($/ton)	240
Battery cycles	500
Total aircraft cycles (SMR)	60000
Cost per shop visit ($ mill)	2.1
Total aircraft cycles (Regional turboprop)	72000
SMR economic mission (nm)	500
Regional turboprop economic mission (nm)	300
Acquisition cost ($ mill)(Regional turboprop)	26
Acquisition cost ($ mill)(SMR)	108.4
HPT blade material	Inconel 738
HPT disk material	Rene95
Thermal barrier coating (K)	130
Acquisition cost increment - hybrid variants	10%

Table 3.10: Direct operating cost assumptions

3.6 Multi mission energy management

The previous sections dealt with the method to integrate optimal PMS and GT cycle design in the common design loop but the issue with such an approach is that the propulsion system is optimized and modified on each aircraft mission. In a realistic aircraft operational scenario, it is unlikely that the operator would even put a new battery pack in every flight mission, let alone mount a different electric power train. This section of the chapter focuses on the method utilized for multi-mission assessment of HEPS architectures. The main aim behind performing a multi mission

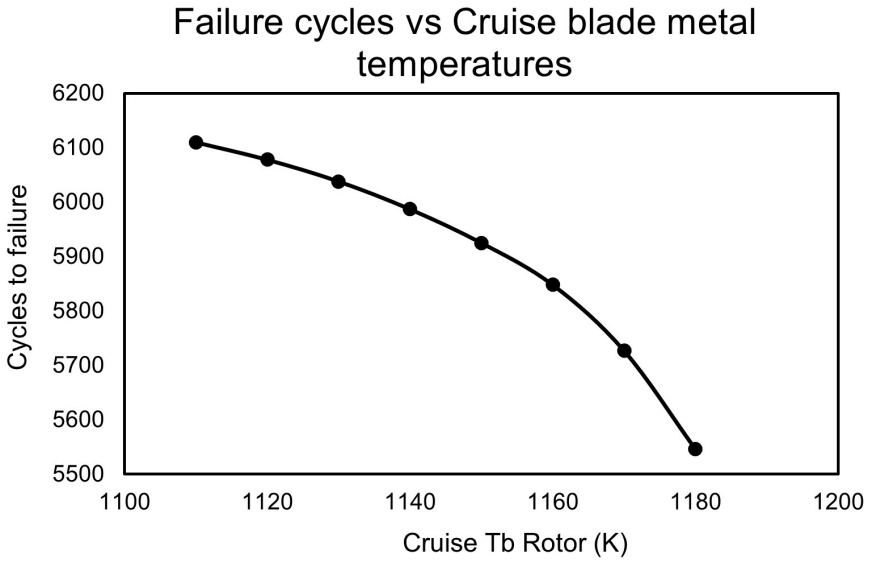


Figure 3.22: Impact of CR temperatures on GT cycles to failure

assessment is to identify the combination of battery pack, electric power train and gas turbine cycle which will consume the lowest fuel, energy or operating cost, considering a realistic off-design mission cluster. Typically, for a conventional fuel powered GT aircraft, off-design mission distribution has limited impact on the selection of the cycle due to insignificant variation in thermal and transfer efficiency. This is because the as the aircraft flies lighter at lower off-design ranges, a higher cruise altitude is selected, thereby pulling the cycle close to same non dimensional thrust. But this is not the case with hybrid electric aircraft as batteries are essentially a dead weight if the aircraft is flown at lower ranges with not enough mission time to discharge the batteries[40][31]. An approach to multi-mission assessment was shown by Zhang et al[60] and applied to parallel hybrid B737-style aircraft. The design space was characterized by battery weight and motor power with power management of each combination of the two variables optimized one each off-design mission range. An example of how the design space is characterized can be seen in 3.23. The limitation of such an approach is that it ignores the constraints on power management strategy imposed by thermal management systems.

As the design is characterized by battery energy available and motor power, when the power management is optimized at each mission range, the operating temperatures of electrical systems will be different every mission, leading to reduced life, cost and harmful operation. As a potential improvement on this work, if thermal management system becomes part of the multi-mission framework, the design space at the very least becomes a 25-dimensional RSM optimization problem. The five variables being

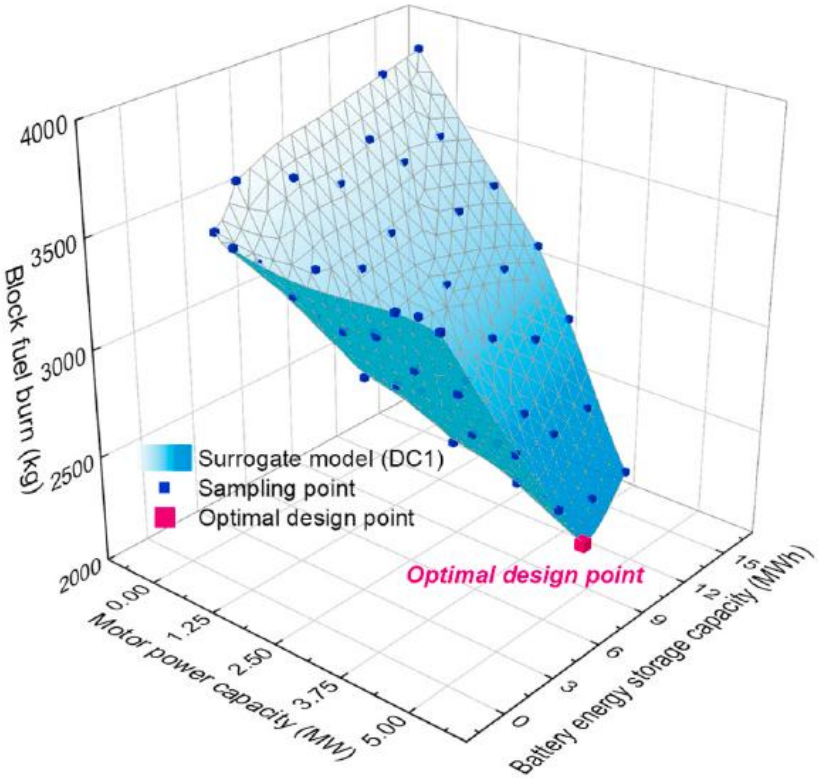


Figure 3.23: Zhang design space example [60]

battery weight, motor power, take-off, climb & cruise degree of hybridization at atleast 5 off-design mission ranges. The increased dimensionality of the design space makes the RSM computationally very expensive and inapplicable to analyse architectures at a conceptual level. It becomes very clear that a more integrated quick multi mission method is required to identify the complete optimal propulsion system across all potential mission clusters flown by the aircraft fleet. In order to achieve this, a new method to reduce the design space and account for fleet allocation is proposed. The proposed method is shown in Figure 3.24 and shown graphically in Figure 3.25.

As can be seen in Figure 3.25, the main steps include the development of baseline current technology and EIS 2035 aircraft-engine models, implementation of integrated ANN method to get optimal propulsion configuration for a grid of design "range" and payload combinations and finally applying multi mission approach. The multi-mission method requires a set of off-design mission cluster and then optimization of power management strategy of each propulsion configuration at each of these off-design mission points. Expanding more on the sentences above, the selection process for the whole propulsion system follows a grid based approach where design degree of hybridization for 3 flight phases is optimized for a mesh of range and payload.

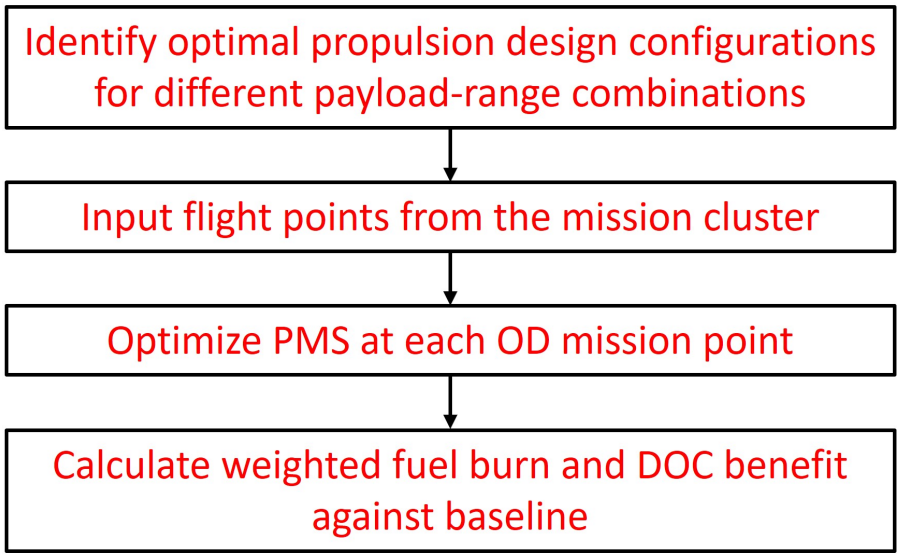


Figure 3.24: Multi mission method

When degree of hybridization is optimized for three flight phases, implicitly battery weight and electrical power train weight is selected. As the thermal management system is also a part of the optimization loop, the constraints can then be imposed at off-design missions. Once the set of design optimized systems are obtained for each payload-range combination, they are then run for a series of off-design missions and the solution which minimizes fuel burn, direct operating cost or energy consumed.

To obtain the off-design mission cluster for SMR aircraft is directly utilized from the study by Zhang [60], where a centroid based clustering technique was used. Zhang collected the fleet data for the target aircraft (B737-8 in that case), flown by US carriers[139] and the clustering technique was applied on that data. The aim was to identify mission points which were representative of the full cluster and to also identify the collective intensity at those points. Zhang identified those off design mission points which are highlighted in Figure 2.8. Similarly, the data for ATR 72 was collected from the same source and the data is shown in Figure3.25. Limited data was found for ATR 72 to perform clustering approach, hence most common flights were directly used and considered to be representative of the fleet. The trend of aircraft being underutilized in terms of maximum range capacity was seen for both aircraft, thereby showing the potential of application of electrification. This trend of narrowbody and regional aircraft being under-utilized compared to their design range has also been highlighted in studies from Flyzero, in Figure 3.26. Essentially A320 designed for around 2400 nm is flown at a mission cluster concentrated around 500-800 nm, signifying heavy off-design usage of the aircraft.

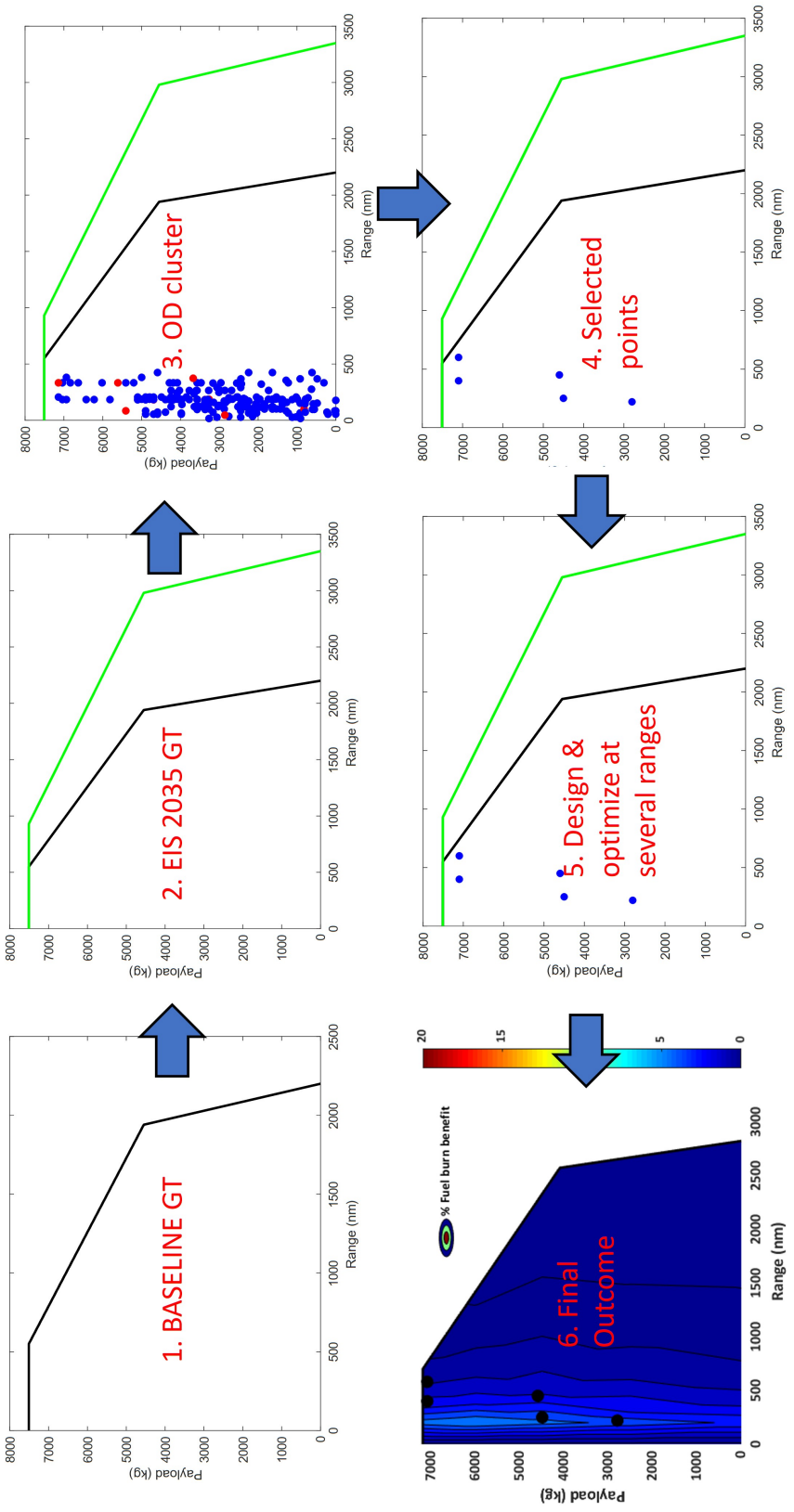


Figure 3.25: Integrated multi mission schematic

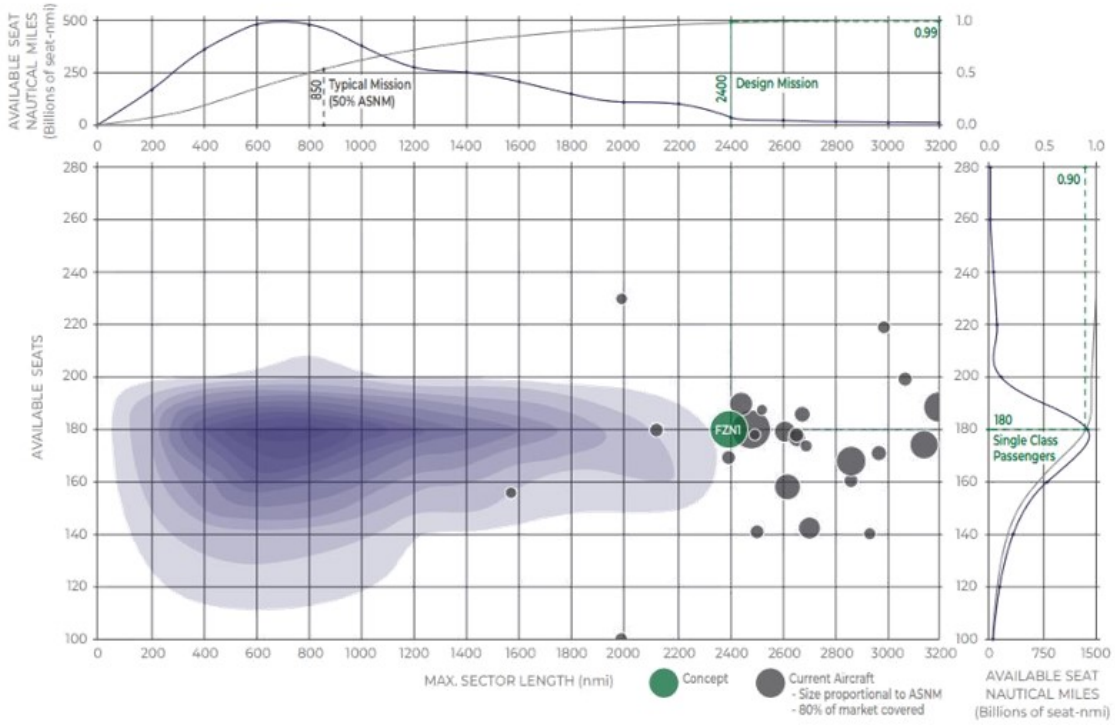


Figure 3.26: Off-design range utilization for narrow body aircraft [140]

3.7 Electrical systems modelling

Various electrical system models are utilized in this research in order to model the HEPS architectures. This section of the chapter describes the modelling methods applied for simulating motor, inverters, battery pack and PEM fuel cell weight estimation and performance.

3.7.1 Introduction

As mentioned in the Scope of work section at the start of this chapter, primarily three architectures are being looked at and these are shown in Figure 3.2, which is use of PEM fuel cell and battery in a parallel hybrid configuration with turbofan/turboprop gas turbine (using either Jet-A or hydrogen) or a fully electric battery and fuel cell turboprop configuration. In order to have a correct back-to-back comparison between these 3 architectures for different power management strategies, it was necessary that a suite of electrical weight and efficiency models be used rather than fixed design point efficiency used by multiple previous studies [50], [95], [64]. Given that the focus of the study in the development of integrated design methods, the models developed by previous relevant studies have been adapted in this study. Each

of the individual models have been described separately in the subsections below.

3.7.2 PMAD Modelling

The PMAD (power management and distribution system) typically consists of a number of switches, AC-DC bidirectional inverter, electrical energy source, DC-DC converter and electrical motor as can be seen in Figure 3.27. In this study, a simplified PMAD schematic has been used which is shown in Figure 3.28. Before even describing the modelling methods, it is necessary to understand the reasoning behind the PMAD schematic.

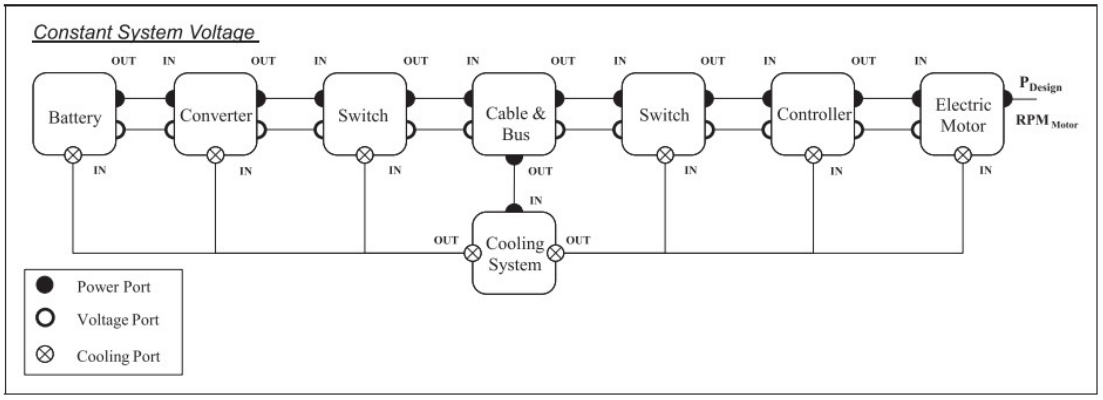


Figure 3.27: Basic PMAD schematic [25]

The batteries and fuel cells pack and stack level voltage is restricted by multiple reasons, structural integrity of the stack, arcing, thermal runaway [141], [142]. The major reason to go for extremely high transmission voltages is to reduce the current density as the weight varies proportional to current density [143]. Designing for higher pack voltages would mean reduced requirement for DC-DC converters hence overall leading to a lighter transmission system. But the restrictions due to arching, and structural integrity eventually drop the line and pack voltage respectively. There were a series of studies from Vratny and Pornet et al [54], [24], [49] which modelled similar parallel HEPS architectures for single aisle aircraft. They did a sweep on line voltages and concluded that the mass optimum for aluminium cables and converters and risk from arcing come at a line voltage of 2000 VDC. In this study as the level of power is in the same ballpark, this number is directly utilized as the line voltage for all the architectures with battery pack at 800 VDC [142] and fuel cell stack at 1000 VDC [141] respectively. It is presumed that the inverter will be either integrated with the motor or will be placed closer to the motor leading to a complete DC supply

thereby reducing wiring length. This approach has also been taken by turboelectric architecture study by Ibrahim et al [144], Figure 3.29.

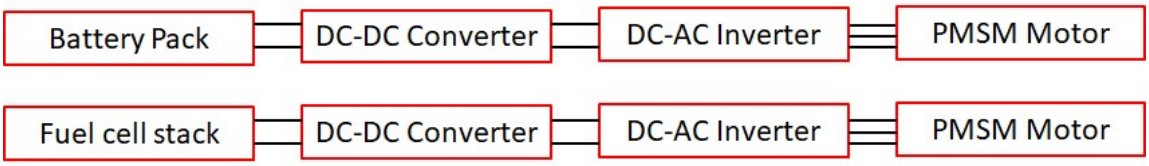


Figure 3.28: PMAD schematic used

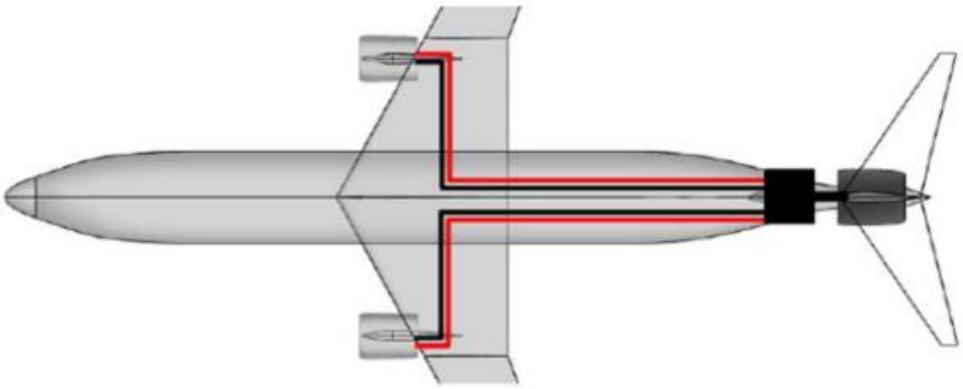


Figure 3.29: Aircraft transmission system Turbo-electric example [144]

That concludes the short discussion on selection of line voltages and PMAD architectures. To model the cabling system, aluminium cables are used assuming a "kg/m" relation as derived by Stuckl [143], shown in Figure 3.30. Moving on to the modelling of motors and inverters, as has been shown in the literature review, extensive work has been done on the modelling, testing and use of electrical MW scale electrical motors, generators and inverters for hybrid-electric or full electric aircraft propulsion. Primarily, EMF can be generated by Permanent magnets (PM) or by induction via coils, and motor architectures are categorized depending on the EMF generation [24]. The most common electric motors used in hybrid and fully electric vehicles are Asynchronous Motor (ASM), Switched Reluctance Motor (SRM) and the Permanent Magnet Synchronous Motor (PMSM). Vratny[24] produced a figure on comparison between different motor types on the basis of Efficiency, Torque Density, Mass and Inverter complexity, adapted from data originally produced by [145]. The comparison is shown in Figure 3.31, showing the power/torque density and efficiency benefits of PMSM over other motor types. The higher TRL level and lesser control complexity of permanent magnet motors makes it most likely solution for near-term aviation electrification.

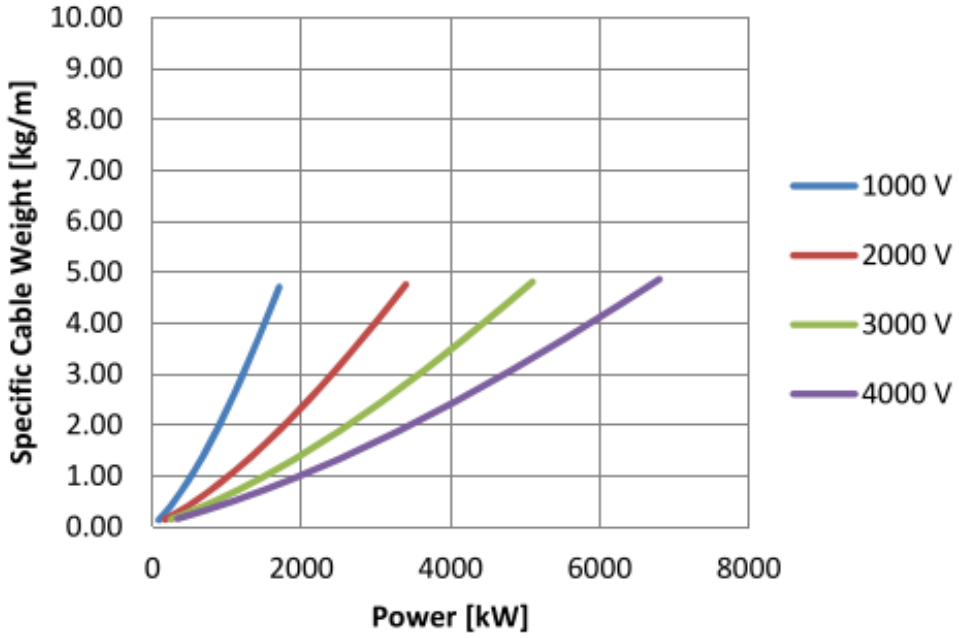


Figure 3.30: Aluminium cables (kg/m) as a function of line voltage and power [143]

Electric Motor Type	ASM	SRM	PMSM
Efficiency	0	0	+3
Torque Density	0	0	+1
Mass	0	+1	+3
Inverter Complexity	0	-3	-1

-3 strongly negative; -1 negative ; 0 neutral; +1 positive; +3 strongly positive

Figure 3.31: Comparison of different electric motor types [24]

Essentially, the sizing of an electric motor is based on torque density with several approaches taken by previous studies. Some studies assume a fixed power density irrespective of the RPM and actual power as in [33], [34], [50] or analytical component by component methods utilized by Vratny [24], [146], [49] or scaling of the weight and efficiency based on aspect ratio from previously designed electric motors [144], [147]. The first approach will not sufficiently capture the trade-offs when performing the integrated power management optimization, while the second approach requires far too many parameters like number of slots, pole pairs, conductors per slot making it difficult to do a correct assessment across different RPMs. Hence the third approach is utilized in this study, where the motor weight is estimated by scaling on previously sized permanent magnet motor geometries to avoid guessing detailed motor parameters for every torque and RPM combination. The total weight is calculated as follows

from Equation 3.4, while keeping an outer rotor motor configuration shown in Figure 3.32. The densities for rotor, stator, shafts and magnets are taken from Appendix A.2 of [24] while the baseline outer diameter, air gap diameter and active length are taken from for a 1 MW motor rotating at 14000 RPM from [31]. The machine air gap volume is calculated using equation 3.5, and is then used to calculate the air gap diameter 3.7, machine diameter 3.6 and air gap area 3.8 using equation. Once the air gap diameter, machine diameter and length are obtained, the weight equation is directly used.

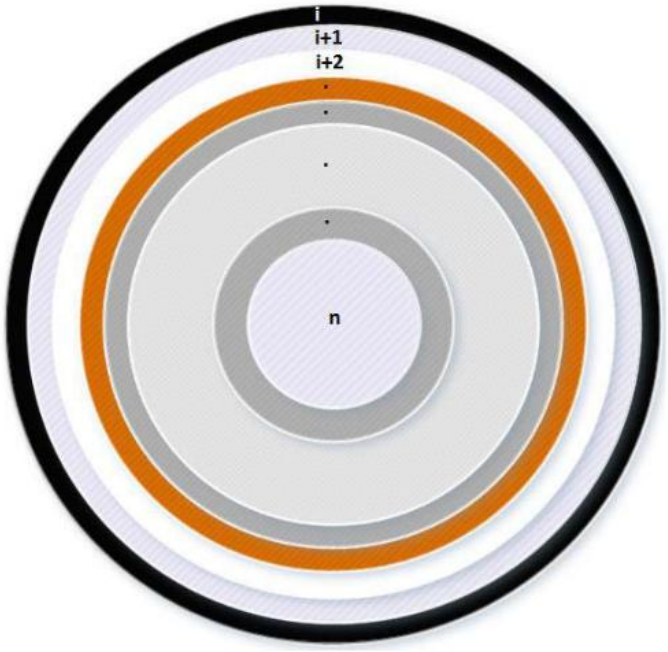


Figure 3.32: PMS motor topology

$$m_m = \pi r_n^2 L \rho_n + \pi r_{i+1}^2 L \rho_{i+1} + \sum_{j=1}^{n-1} \pi (r_i^2 - r_{i+1}^2) L \rho_i \tag{3.4}$$

$$v_{ag} = P_m / (\omega_m K_\omega B_g A_L 2^{0.5}) \tag{3.5}$$

$$D_M = R_{MAG} D_{AG} \tag{3.6}$$

$$D_{AG} = (4v_{ag}R_{DL}/\pi)^{1/3} \tag{3.7}$$

$$A_{AG} = \pi D_A G L \tag{3.8}$$

For a sweep of RPMs and sizing powers, the calculated power densities are shown in Figure 3.33. These trends align well with the trends from Vratny [24], showing a good comparison between different methods and placing the motor weight in the right ballpark.

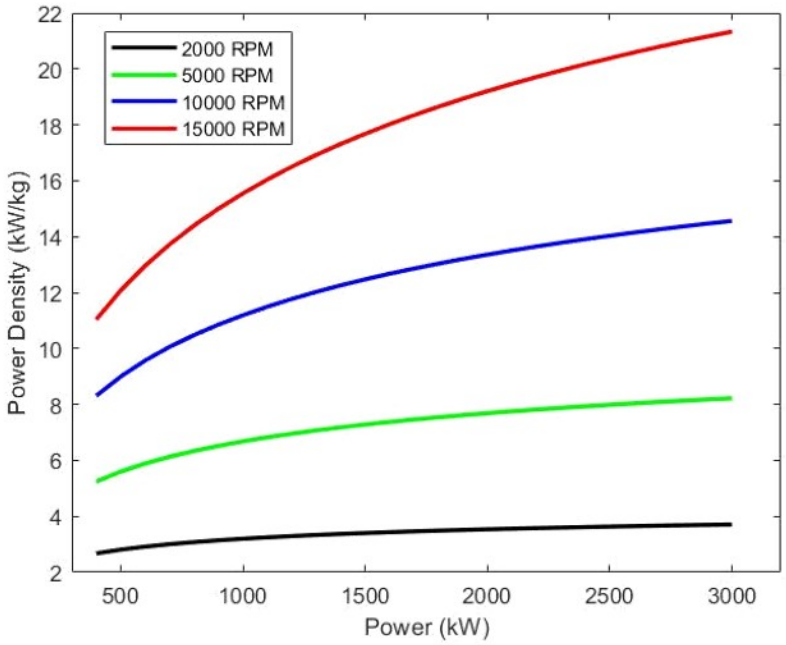


Figure 3.33: PMS motor power density vs RPM generated curves

Moving on to the motor efficiency calculations, in a PMS motor, five main type of losses occur, which are summarized below:

- Stator core losses
- Armature losses
- Friction and windage losses
- Stray load losses
- Miscellanous losses

The motor efficiency is calculated using equation 3.9, where $\sum P_L$, is the summation of all the losses in the motor summarized above. P_{Cool} is the losses due to cooling system for the motor which is assumed to be zero.

$$eta_{mot} = P_{shaft}/(P_{shaft} + P_{Cool} + \sum P_L) \tag{3.9}$$

The losses are scaled on a reference distribution of PM losses initially on maximum power [24] and later on off-design torques and RPM to get a full map of electrical motor efficiency across the power envelope. The equations for scaling all the PM losses are directly taken from [24] and a map is developed. For one of the test cases, the scaled efficiency map is shown in Figure 3.34. The basic variation in motor efficiency against torque and RPM matches well against trends from [91], validating the implementation. This concludes the weight and efficiency calculations for electric motor, for inverter, a fixed power density is assumed depending on the technology level, while the efficiency is modelled as a function of max current or max power.

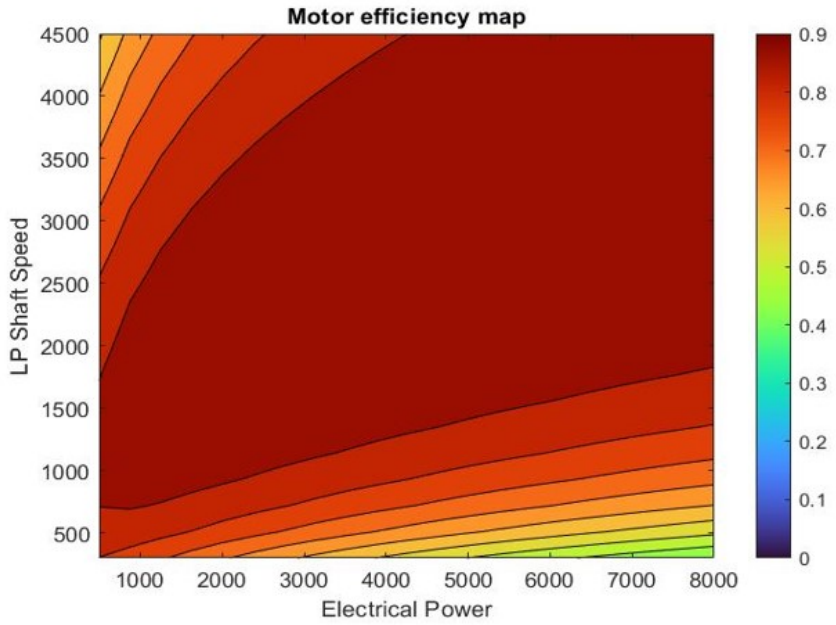


Figure 3.34: Motor efficiency map against torque and RPM

The motor input voltage is calculated using shaft rotational speed and no of pole pairs, ultimately giving the output current requirement from the inverter while the input current 3.10 is based off assuming a voltage of 1800 VDC as described previously. The main losses in a Voltage source inverter (VSI) are the conduction and switching losses which are dependent on the number of parallel and series modules as described in [24]. The exact same method is followed to get the final efficiency

variation against off-design motor power, shown in Figure 3.35. In reality, a more correct estimation of efficiency would be by calculating the switching frequency right through the flight mission but considering the level of fidelity, a simple efficiency vs power trade is considered.

$$I = 1.414 P_{design} / (eta_{mot} U_{mot} cos\phi 1.732) \tag{3.10}$$

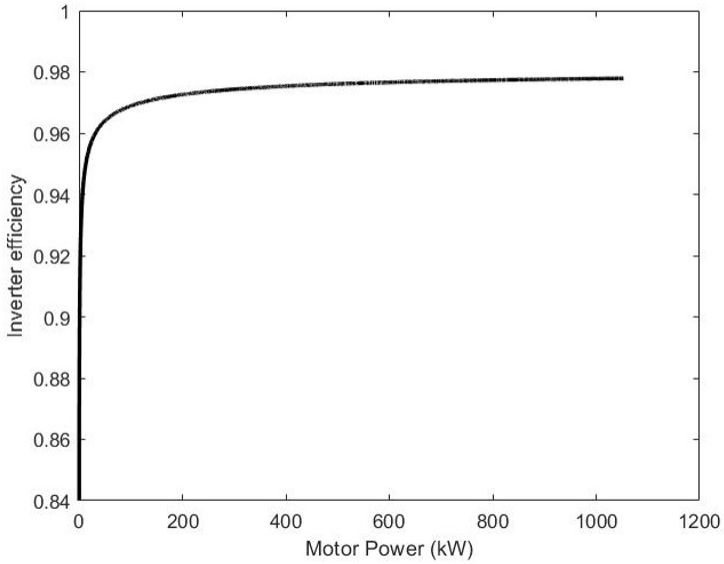


Figure 3.35: Inverter efficiency vs power

This concludes the PMAD modelling sub-section, the next sub-section deals with battery pack modelling.

3.7.3 Battery pack Modelling

The battery pack consists of modules of cells connected in series and parallel (shown in Figure 3.36) to achieve the peak current and total capacity requirement. The cells in series and parallel are calculated using the equations below 3.11 & 3.12, effectively the cells in series sized to match the maximum voltage and cells in parallel sized to match the maximum current or capacity. The cells in series and parallel are consistently iterated until the correct battery size is found, the pack sizing method is directly adapted from SUGAR VOLT study [91] and is shown in Figure 3.37.

$$n_{series} = [V_{target} / V_{cell}] \tag{3.11}$$

$$n_{parallel} = [E_{bat}/(Capacity_{cell}U_{target})] \tag{3.12}$$

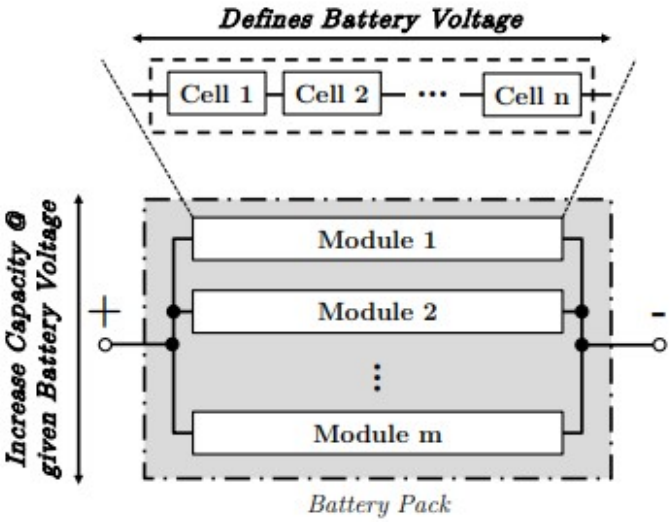


Figure 3.36: Battery pack as defined in [24]

Parameters	Value
Nominal Cell Voltage (V)	3.6
SoC (%)	20
Specific Energy Density (Wh/kg)	250
Specific Power (W/kg)	1.2
Capacity (Ah)	3.3

Table 3.11: Battery cell characteristics used

Within the sizing framework, the cell voltage is varied with state of charge using correlations defined in [47] and the cell capacity, open circuit voltage and temperature characteristics are obtained from [148]. The cell characteristics used are defined in Table 3.11.

The developed discharge rates at the cell level can be seen in Figure 3.38. That ends the discussion on battery pack modelling and next sub-section deals with PEM FC modelling.

3.7.4 PEM FC Modelling

In this thesis, only Proton exchange membrane fuel cells are considered and Solid oxide fuel cells haven't been considered. There have been a number of studies in the

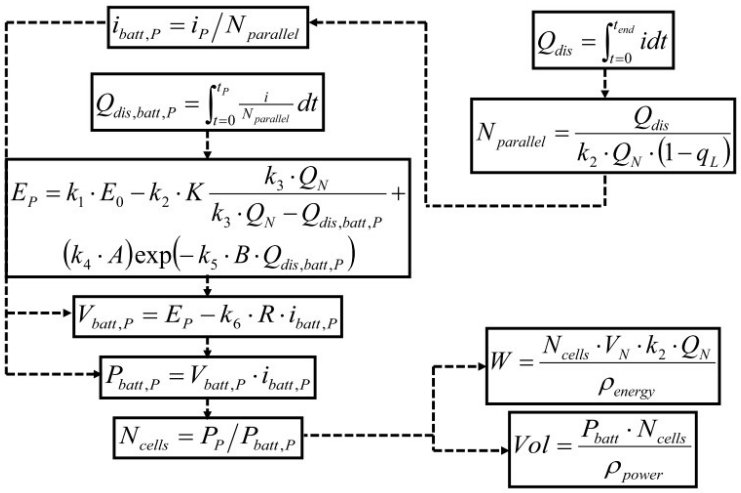


Figure 3.37: Battery pack sizing method as in [91]

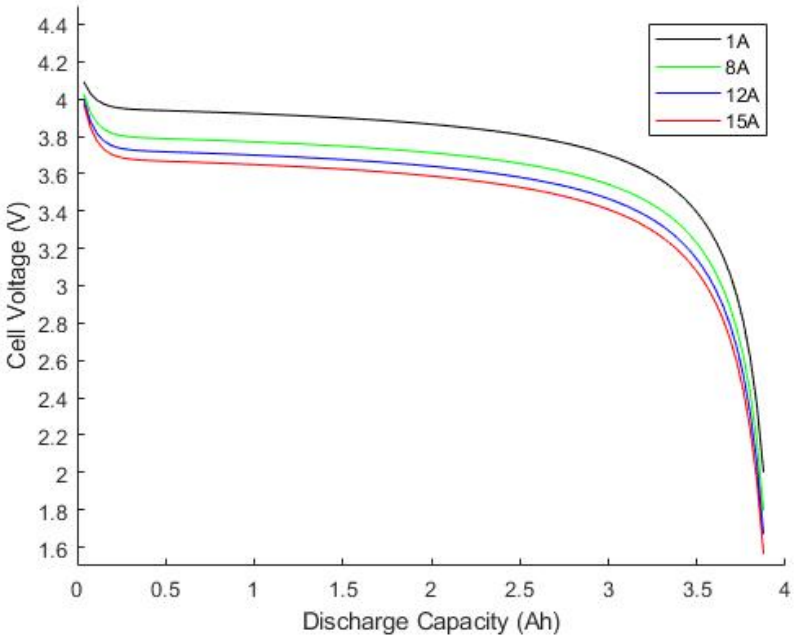


Figure 3.38: Battery cell discharge rates

past which have looked combination of solid oxide fuel cells and gas turbine but the low power density of SOFC make them unlikely to be implemented in the near future [149]. PEM fuel cell and all the sub-systems are together called balance of plant(BoP) [141]. The sub-systems include the LH2 tank, shell and tube HY heat exchangers, air compressors, humidifiers, exhaust waster management systems and finally, VCC/ram air heat exchangers for rejecting waste heat from fuel cell, seen in Figure 3.40.

The modelling of the whole balance of plant has been in few other fuel cell studies like in [141], [119] & [149]. But all these studies were sizing studies on a fixed power

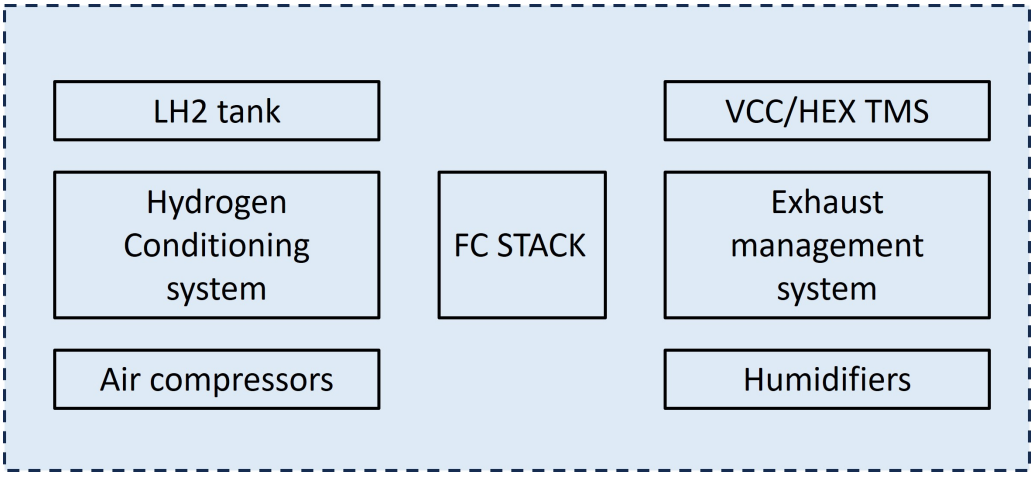


Figure 3.39: PEM FC BoP

management strategy. Given that the scope of the present study is vaster than all the previous studies, it was decided that the fuel cell power density and peak efficiency numbers will be used from previous studies but the thermal management systems, be it ram air HEX or VCC will be sized additionally on these numbers. From all the studies above and also from [33], a total balance of plant power density number of 1-1.5 kW/kg is the maximum expected number for 2035 EIS MW-scale PEM fuel cell [149]. In this study, a stack power density of 3 kW/kg, with thermal management system, tank weight and compression penalty added on top of this, which brings the total power density number in the correct ballpark. As can be seen from Figure 3.40, the compression power for the air intake is taken from the fuel cell itself (it is assumed that a small battery will be needed to provide the initial compression energy). And also as will be described later, even the VCC compression power and drag power is taken from the fuel cell itself (meaning that the fuel cell is over-sized). The LH2 tank is modelled using a gravimetric density number ranging from 0.40-0.60 depending on fuselage/tank diameter [39]. So essentially, the total balance of plant number is calculated using fixed fuel cell stack power density, TMS weight and LH2 tank weight.

Given that the elements of TMS sizing is discussed in the next sections of these chapter, the final part of this section deals with the PEM FC efficiency vs power density trade-off curve and fuel consumption equations. It is assumed that air comes at a pressure of 2 bar for all test cases. Typically the efficiency of the fuel cell increases with air input pressure [33], and 2 bar is the number selected which provides a good balance between efficiency and compression power. The voltage of the fuel cell depends on current density and is computed using a polarization model and

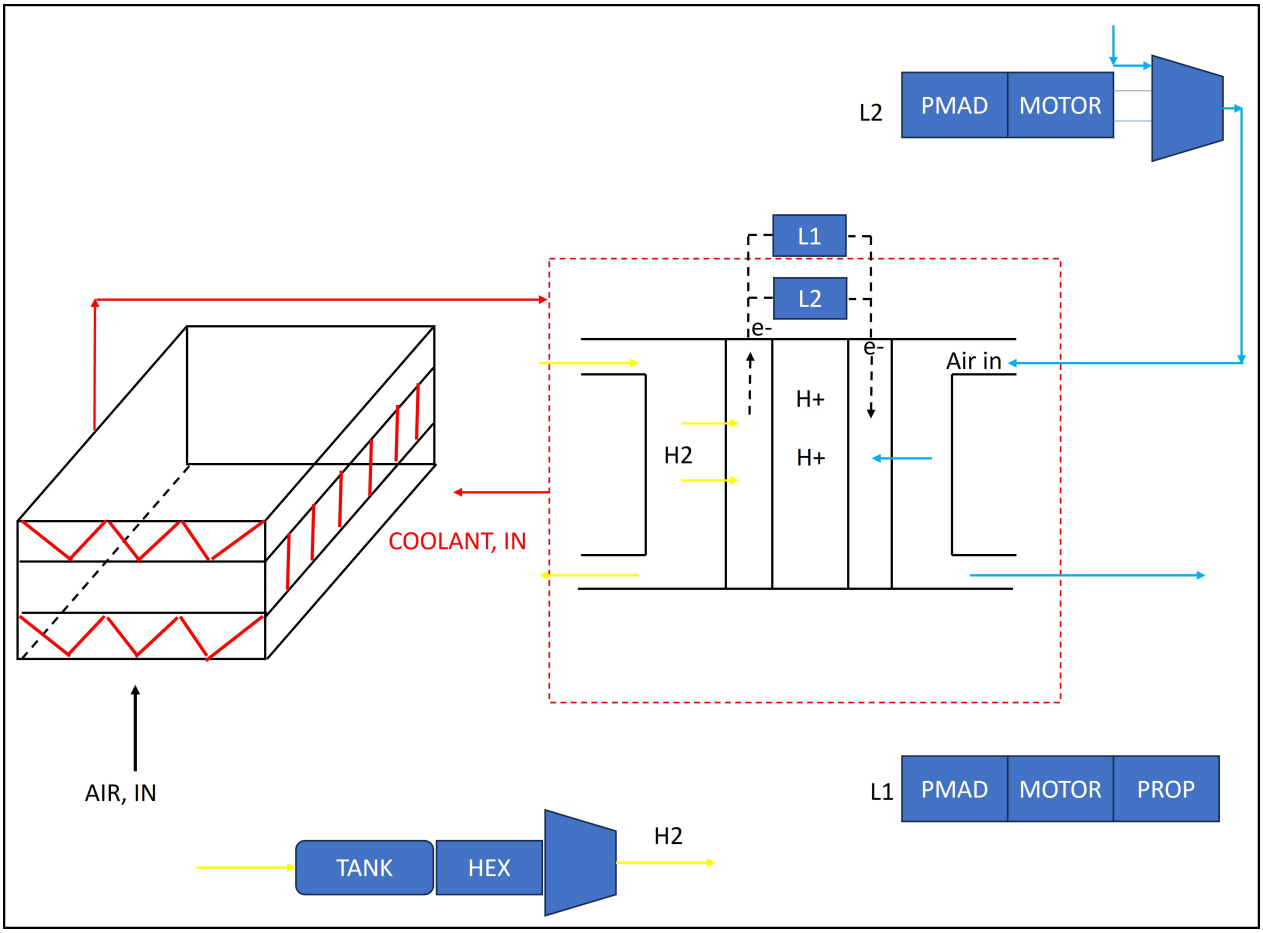


Figure 3.40: Fuel cell schematic

can be seen in Equation 3.13. The curve is created using some of the leakage and limit current numbers from [141], and is visualized in 3.41. It can be that higher the current density of the stack, lower is the efficiency,and the design point is placed such that a sizing point efficiency of 0.49 is targeted, the curve is recreated when the fuel cell is run off-design. The efficiency and fuel consumption are calculated using equations 3.14, 3.15 & 3.16.

$$V_c(j) = E_0 - \frac{\delta s}{2F}(T - T0) + \frac{RT}{2F} ln(\rho_{H2} {\rho_{o2}}^{0.5}) - \frac{RT}{2\alpha F} ln(\frac{j + j_{leak}}{j_0}) - rj - cln(\frac{j_{lim}}{j_{lim} - j - j_{leak}}) \tag{3.13}$$

$$\eta_{FC} = \frac{V_c * \mu_f}{1.482} \tag{3.14}$$

$$\dot{m_{H2}} = \frac{P_{FC}}{1.2 * 10^6 \eta_{FC} F} \tag{3.15}$$

$$\dot{m_{air}} = 34.78\dot{m_{H2}} \tag{3.16}$$

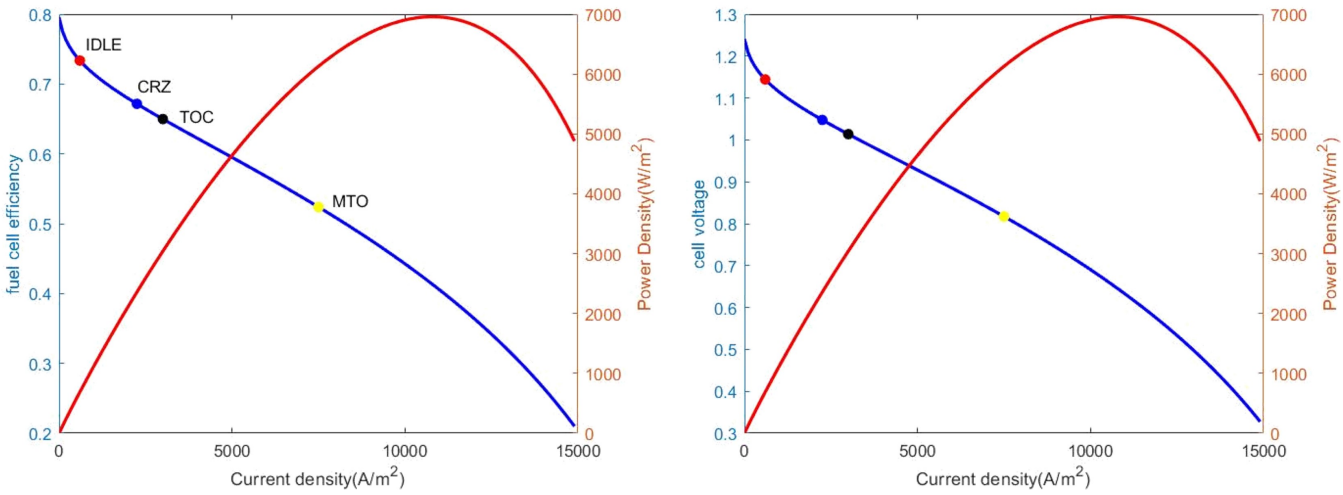


Figure 3.41: PEM FC efficiency

That concludes the full section on Electrical systems modelling, now the discussion moves to modelling of the ram air HEX and VCC and how the weight, off-take and drag penalties are accounted for in the mission loop.

3.8 Ram Air HEX and VCC Modelling

The main methods for design point and off-design modelling for Ram Air - liquid coolant heat exchangers and "thermal lift" Vapour compression cycles is presented in this section. The integration of these models via surrogate models and the development of objective function within the aircraft performance loop has been described in the next section. The major objective behind designing both type of thermal management architectures is to understand if there is a requirement of thermal lift cycles for fuel cell, electrical motor/generators and inverters. In order to have a fair comparison between the two thermal management architectures, it is necessary that the comparison is done between two optimized systems for a given heat load. The modelling of vapour compression cycles is simply an extension the of the baseline heat exchanger modelling hence the heat exchanger modelling is described initially. While considering both the thermal management architectures, the liquid cooling loop through the battery or fuel cell is not modelled (the evaporator is modelled but it is understood that there will be a liquid-refrigerant heat transfer loop) and only the heat transfer to air side is modelled.

3.8.1 Compact HEX DP and OD modelling

In all the studies performed for the air side heat transfer (condenser-air side for VCC), a plate fin heat exchanger is utilized (shown in Figure 3.42). The decision of going for a plate fin HEX model is the compactness of it, delivering a high heat transfer surface area to volume ratio. The modelling of the plate fin HEX is based on the series of work done by different authors on for 2-phase plate fin heat exchangers [150], [151], [152] and [153]. The existing works in open literature from Kellerman [63], [62], Chapman [69], [102] which have modelled HEX for hybrid-electric applications have either used effectiveness-NTU approaches which makes it unsuitable to be used for phase change applications. Even the corresponding studies from Kosters [154] and Dragan [104] which have modelled phase modelled HEX, no information is provided on how the phase change HEX is modelled and how the VCC loop is controlled. The Flyzero study [35] where author was part of the team, the HEX for the fuel cell was proprietary information of Reaction Engines with no shared information. Hence, it was decided that a simple VCC design method will be built from scratch with phase change HEX modelling methods applied from non-aircraft applications [150], [151]. The single phase HEX model is validated against trends from both Dragan [104] and Kellerman [63]. The methodology followed for design point modelling for the HEX model is shown in the flowchart 3.43, while for the off-design modelling is shown in 3.44. As explained before, a modified LMTD approach is used instead of effectiveness-NTU approach and the implementation is discussed within the explanation of the ram air HEX loop.

Parameters	Value
Fin thickness (mm)	0.1
Fin lance length (mm)	2.1
Plate spacing (mm)	0.5
Height to width ratio front face)	1
Fin pitch (cold) (mm)	2
Fin height (cold) (mm)	10

Table 3.12: Plate fin HEX design parameters

The main optimization variables for the HEX design include the coolant mass flow, frontal area of the HEX and the pinch temperature difference (this could be effectiveness but a pinch temperature is used as a way to control it) between cold end exit and hot end inlet. The mass flow of the cold side and length of the HEX are fall-out variables for a given heat load and pinch temperature. Once an assumption is made on the fin type (offset fin type assumed in all the cases), pitch and the height

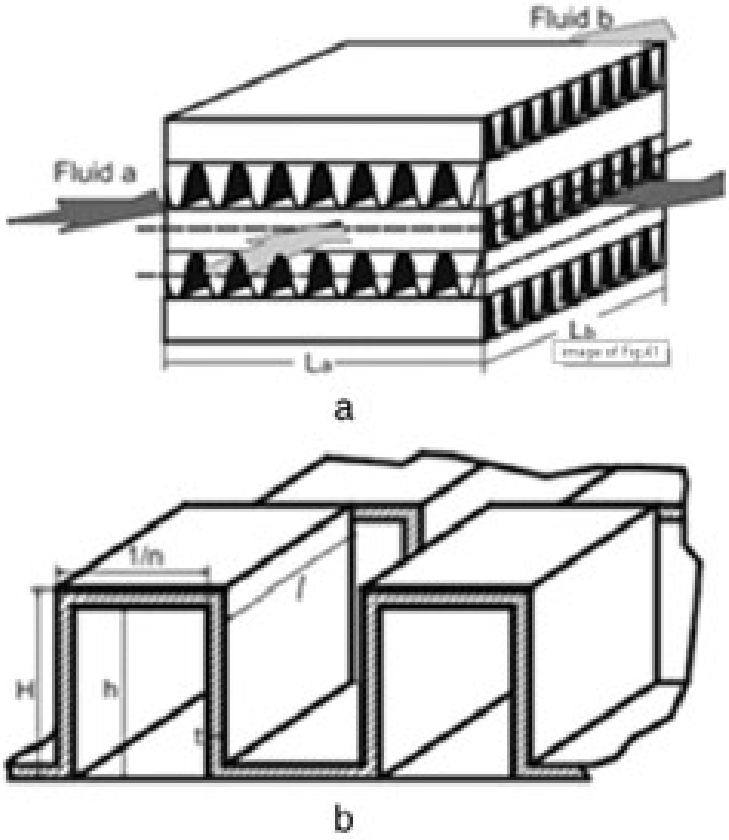


Figure 3.42: Plate fin HEX [152]

besides the main optimization variables mentioned above, the weight, pressure loss and full HEX design is obtained. It can certainly be argued that the fin parameters should also be a part of the optimization loop but that would increase the computation exponentially as the fin optimization would be within the main HEX optimization which is ultimately envisioned to be a surrogate model within the power management mission optimizer. The selection of fin parameters for all the fluids utilized - water-glycol mixture and air, is made from the various references utilizing plate fin heat exchanger designs [150],[151],[152],[153]. This would guarantee a certain level of optimality by balancing pressure loss, heat transfer, targeted reynolds number and ease of manufacturing. The main heat exchanger design parameters are summarized in Table 3.12. It is assumed that the number of cold layers is one greater than the number of hot layers and the number of cold and hot layers are iterated until the height and width matches the frontal area.

By utilizing the pinch temperature the exit temperature of the cold stream is known which then allows for the calculation of logarithmic mean temperature difference which can be calculated using the equation below. A secant method based solver is then employed to vary the length in order to match the LMTD error within

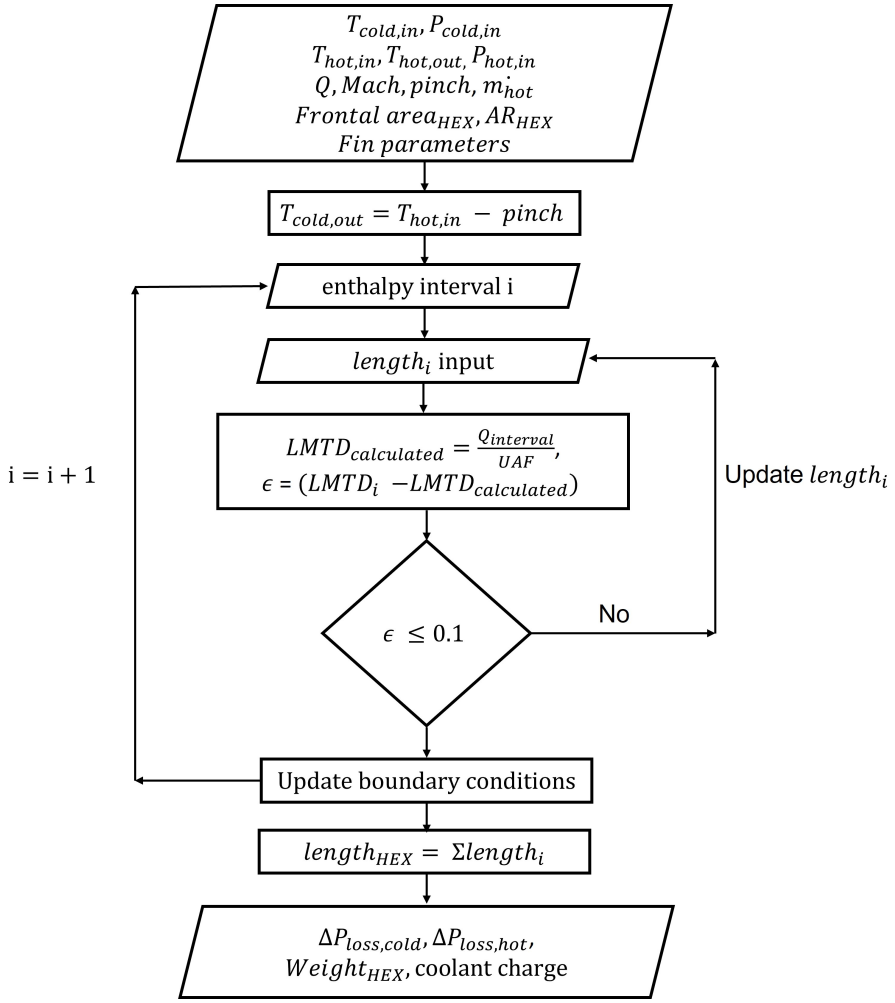


Figure 3.43: HEX design method

convergence. Once the length of the HEX is obtained, and the frontal area and fin sections being already known, the full HEX geometry is known. As the HEX geometry is known, now it can be utilized for off-design analysis. For the off-design heat load analysis, the unknowns of the HEX now remain the end temperatures of the two streams - hot and cold. The design process now gets reversed as the pinch temperature is unknown while length of the HEX is known. The same solver is utilized once again but now the pinch temperature is guessed and varied to match the LMTD error.

$$N_L = \frac{H - PS - FH_{hot}}{FH_{cold} + FH_{hot} + 2 * PS} \tag{3.17}$$

$$Q = KA(CF)\delta T_{LM} \tag{3.18}$$

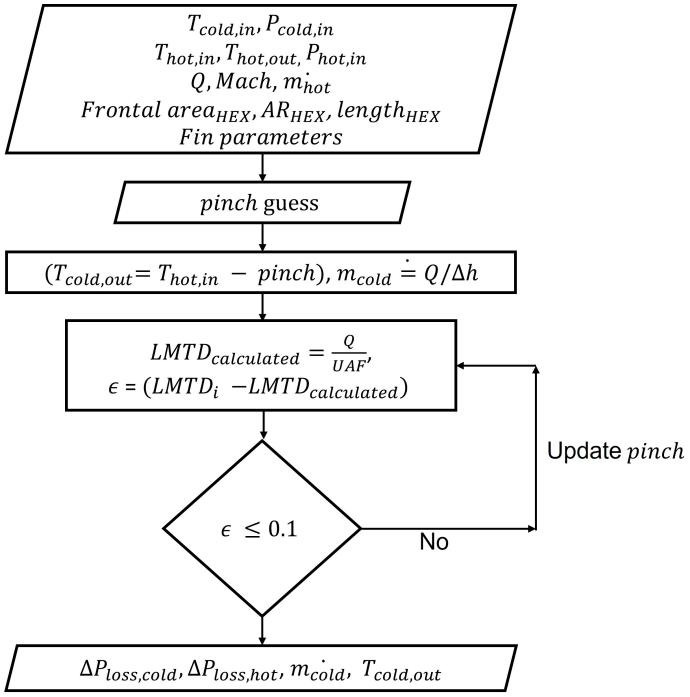


Figure 3.44: HEX Off-design method

$$Q = m_h c_{p,h}(T_{h,i} - T_{h,o}) = m_c c_{p,c}(T_{c,o} - T_{c,i}) \tag{3.19}$$

$$\delta T_{LM} = \frac{[max(T_{h,i} - T_{c,o}), (T_{h,o} - T_{c,i}) - min(T_{h,i} - T_{c,o}), (T_{h,o} - T_{c,i})]}{ln(\frac{max(T_{h,i} - T_{c,o}), (T_{h,o} - T_{c,i})}{min(T_{h,i} - T_{c,o}), (T_{h,o} - T_{c,i})})} \tag{3.20}$$

$$A_F = (FH_{cold} - B) * (1 - 1/(FP * B)) * W * N_L \tag{3.21}$$

$$d_h = \frac{4 * L * (FH_{cold} - B)}{(2 * ((FP - B) * L + (FH_{cold} - B) * L + (FH_{cold} - B) * B) + B * (FP - B) - B * B)} \tag{3.22}$$

$$Re = \frac{m_{AIR} * d_h}{\mu * A_F} \tag{3.23}$$

The colburn and friction factors are calculated using the equations below, which are essentially regressed factors for offset strip fins as described in [150].

$$j = 0.6522Re^{-0.5403}(c/b)^{-0.1541}(t_f/x)^{-0.1541}(t_f/c)^{-0.0678} \\ *[1 + 5.26910^{-5}Re_{1.34}(c/b)^{0.504}(t_f/x)^{0.456}(t_f/c)^{-1.055}]^{0.1} \quad (3.24)$$

$$f = 9.6243Re^{-0.7422}(c/b)^{-0.1856}(t_f/x)^{0.3053}(t_f/c)^{-0.02659} \\ *[1 + 7.66910^{-8}Re_{4.429}(c/b)^{0.920}(t_f/x)^{3.767}(t_f/c)^{0.236}]^{0.1} \quad (3.25)$$

Once the colburn and friction factors are calculated, the heat transfer coefficient and the corresponding pressure drop across the heat exchanger are calculated using equations below. Where the prandtl number, viscosity and other fluid properties are obtained using MATLAB embedded tool Refprop [155].

$$h = \frac{m_f C_p j}{A_c Pr^{2/3}} \quad (3.26)$$

$$\delta P = \frac{2fm_f^2 L}{\rho * d_h * {A_c}^2} \quad (3.27)$$

The series of equations from 3.17 to 3.25 are enough to model the cold/air side of the HEX, a correspondigly similiar set of equations are used to model the hot end too (water in ram air HEX case or R134a/sCO2 in VCC case). For modelling the heat transfer coefficients on the coolant side, the single phase heat transfer coefficients are taken from [156], which are CFD obtained data for heat transfer coefficients for water throught offset fins. (Equation 3.28 and 3.29)

$$j_{hot} = 0.6728 * (Re^{-0.585}) \quad (3.28)$$

$$f_{hot} = 9.736 * (Re^{-0.72}) \quad (3.29)$$

Post the calculation of heat transfer coefficient and frontal geometry calculations of both sides, the total enthalpy is divided into enthalpy intervals and the length is iterated until the enthalpy interval is met, where, the total heat transfer and the corresponding log mean temperature difference is given by equations 3.30 and 3.31. As previously explained before, the methods are summarized in Figures 3.43, 3.44.

$$UA = \frac{1}{(\frac{1}{\eta_{fin} * h_{cold} * A_{cold}}) + (\frac{1}{\eta_{fin} * h_{hot} * A_{hot}})} \quad (3.30)$$

$$\delta T_{LM} = -Q_{total}/UA/CF \tag{3.31}$$

Both the method and the numbers are validated against corresponding studies from [104] and [70]. On the same boundary conditions, the HEX thermal power density is compared in Figure 3.45 & also against fuel cell study by Dragan [104] in Table 3.13. Both the trends and weight, length numbers align well and are within 10% variation with both the studies showing a well validated HEX methodology.

Parameters	Dragan	Ghelani
Heat Load (MW)	9.27	9.27
Length (m)	0.21	0.18
Coolant charge (kg)	116	89
HEX weight (kg)	1080	1120
HEX pressure loss (%)	6.6	6.3
Area (sq.m)	10.56	10.56

Table 3.13: Comparison on same boundary conditions, HEX parameters

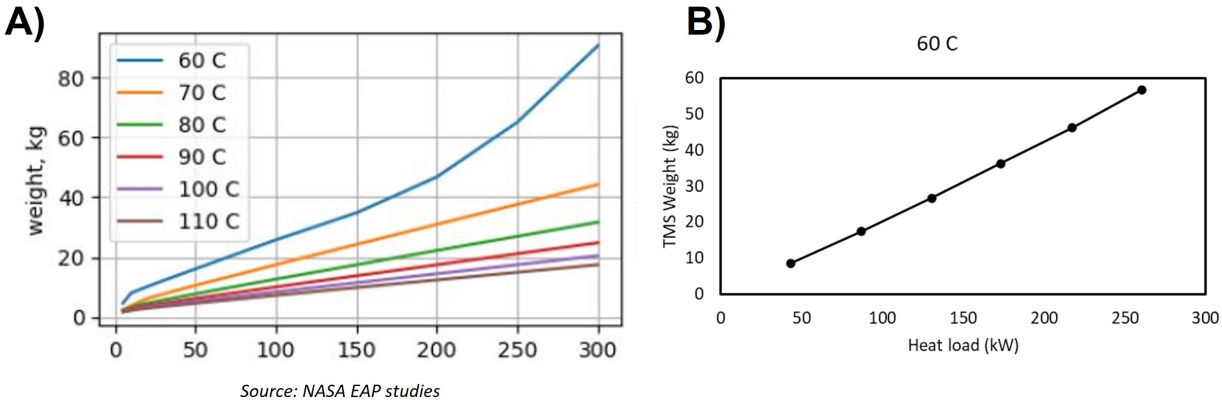


Figure 3.45: Thermal power density - A) UTRC hGTF[70], B)Raj Ghelani

Now that the design and validation of the HEX is shown, the real question that should arise is how the heat exchanger methodology is utilized to estimate it's impact on fuel burn and for which point in the flight envelope is the HEX designed for? The impact of HEX on the aircraft fuel burn/energy consumption has been done in previous studies but the question on where in the flight envelope would a HEX be sized for, is not a straightforward question. The reason for the complexity is there are many variables at play here: altitude, Mach, ISA rating and heat loads through the flight profile. For example, dumping a certain fixed MW of heat will result in a bigger heat exchanger at higher altitude. Despite increased temperature difference

enabling greater heat transfer, reduced air density & pressure has a greater impact on the size of heat exchanger. If the heat load is scaled with pressure as in the case of typical gas turbine heat load, the greater temperature difference will certainly be the impact variable. The fact that the electrical systems don't have heat load variation like a gas turbine adds the complexity. The integration of the heat exchanger models with whole framework to resolve the questions mentioned above is described in the next section. Before that the extension of these HEX models to be utilized in the vapour compression cycle loop is described in the next sub-section.

3.8.2 VCC HEX DP and OD modelling

Vapour compression cycles have long been utilized for military applications (high flight Mach applications) owing to the requirement of dumping heat loads with no or low temperature difference with atmosphere. But the application of vapour compression cycles for civil aerospace applications has been limited as the typical gas turbine heat loads have significant temperature difference with atmosphere and control complexity of VCC can be avoided. But the emergence of high low quality heat loads arising from electric or hybrid electric aircraft or geared turbofan propulsion systems has led to increased studies focussing on VCC. The main aim of VCC is to provide the necessary "thermal lift" to reduce the area and the installation drag of the HEX but it comes at the expense of increased complexity of pumping high refrigerant flows, control increased weight and very high power off-takes. If a proper comparison is done between ram air HEX and VCC, then they need to both be optimized for fuel burn for the given mission to give us a true number. In order to optimize and design vapour compression cycles for fuel burn, 3 level of loops are created and they are summarized as follows:

- Method to simulate design & off-design performance of VCC with different compressor pressure ratios.
- Optimizer wrapped around the VCC model which optimizes combined design & off-design performance for fuel burn or energy consumption penalty.
- A surrogate model trained on the results obtained from the optimizer by performing a correct accounting of drag, power off-take and weight.

The method to simulate design & off-design performance is described below while the optimizer and surrogate model is described in the next sub-section. The method

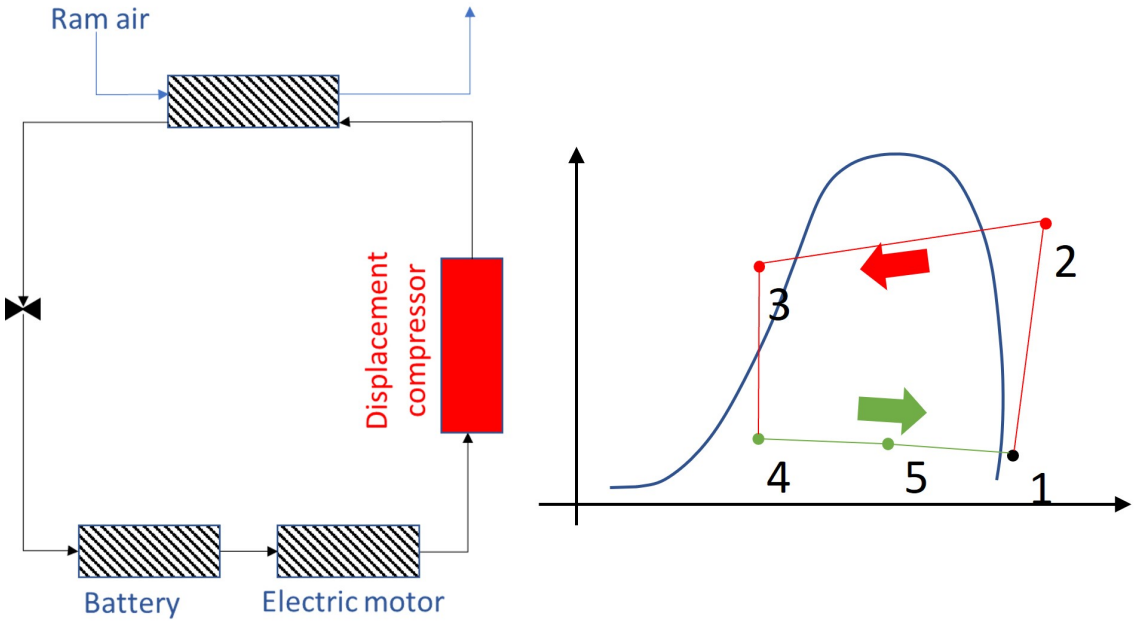


Figure 3.46: Typical vapour compression cycle

to simulate design & off-design performance of VCC is basically an extension of the ram air HEX modelling in previous sub-section albeit the the addition of vapour compression cycle and 2-phase heat exchange modelling. In order to model the phase change across the plate fin HEX model, the heat transfer coefficient is modified depending on whether the coolant is in superheated vapour, 2-phase or liquid state. The estimation of heat transfer coefficient for 2-phase heat transfer is difficult due to multiple modes of existing heat transfer, convective heat transfer and nucleate boiling term [156]. The modelling is dependent on the vapour quality, for the single phase mode, the same heat transfer correlations are used as explained in previous section as they hold true also for R134a, while the 2-phase is modelled specifically for R134a. The 2-phase heat transfer coefficient is calculated using set of equations from 3.32 to 3.36.

$$h_{conv} = j_{rl} G_r c_{pl} {Pr_l}^{-2/3} F f (1-x)^{0.8} \tag{3.32}$$

$$Ff = 2.35(1/X + 0.213)^{0.736} \tag{3.33}$$

$$X = ((1-x)/x)(\frac{f_l \rho_v}{f_v \rho_l})^{0.5} \tag{3.34}$$

$$G_{eq} = G[(1-x) + x(\rho_l/\rho_v)^{0.5}] \tag{3.35}$$

$$\delta P = f_r * 2 * (G_{eq}^2) * L/(rho_l * d_h) \tag{3.36}$$

The vapour compression cycle can be visualized in Figure 3.46. The cycle consists of evaporation, compression, condensation and expansion in a closed loop cycle. Evaporation is the phase where the refrigerant picks up the heat from the heat source, followed by compression where the refrigerant enters in a superheated gaseous state and is compressed until enough pinch temperature is found against the sink and this is followed by condensation. Condensation is where the heat transfer takes place between the refrigerant and air and finally the liquid is expanded back to the evaporation inlet conditions.

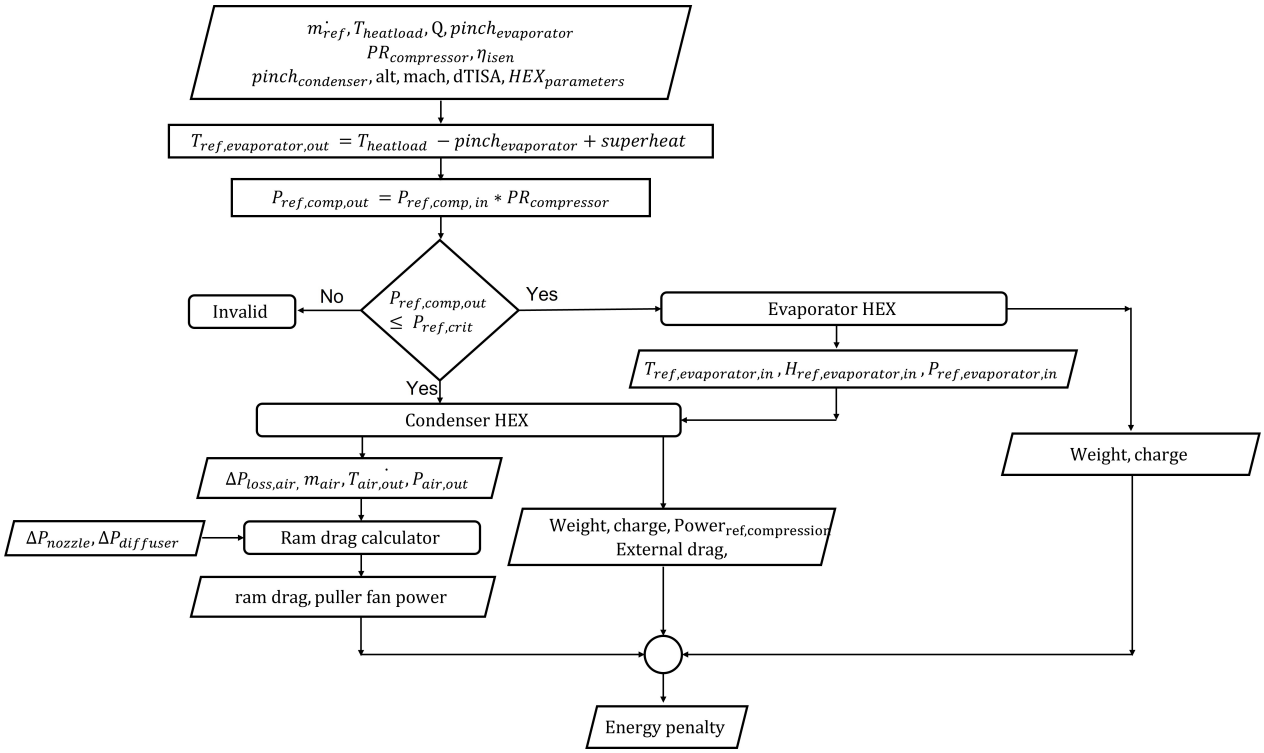


Figure 3.47: VCC design optimization

The main variables which define the vapour compression cycle are: compressor pressure ratio, condenser pinch, condenser frontal area and refrigerant mass flow. The pinch temperature at the evaporator is assumed to be a technology level estimate and because this part of the system is meant to be kept in the cargo area, there are no implications on external drag. Hence, lowest possible pinch temperature (10 K) is selected as the value at the evaporator side. Within the vapour compression cycle, it

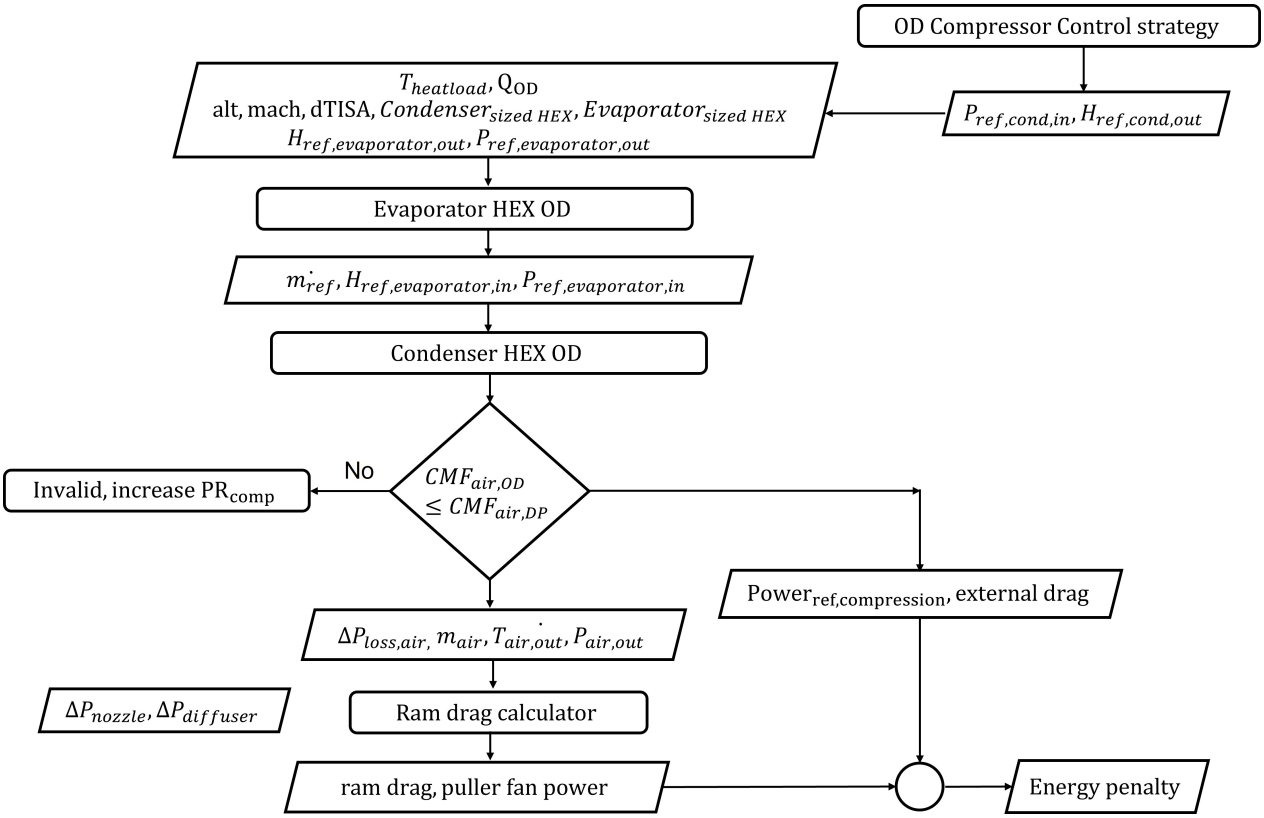


Figure 3.48: VCC Off-design solving

is very likely that certain parts of the cycle are sized for a different flight point in the mission. The evaporator is sized for max heat loads, compressor for maximum work or pressure ratio and condenser is sized for length to achieve the pinch temperature. Once the four design variables are provided besides the altitude, Mach and heat load variations across the mission profile, the design sizing of VCC is started. In all designs, the point 1 (compressor inlet) is always kept fixed (depending on operating temperature) by assuming superheat temperature over the saturated curve to keep the refrigerant in gaseous state entering into the compressor. The point 2 (condenser inlet) is dictated by the pressure ratio, 4 (evaporator inlet) is dictated by the design mass flow while the pressure drop between 3 & 4 is dictated by a combination of condenser frontal area and pinch.

Secant solver based solving scheme is used to vary the length of the condenser HEX to match the pinch temperature and which in essence is driven by the exit enthalpy at point 3. At the condenser side of the cycle, the same HEX module described in previous sub-section is extended by incorporating 2-phase heat transfer coefficients. At the evaporator side of the cycle, a tube fin HEX module is developed and implemented within framework. For the compressor side, a reciprocating piston is assumed with

constant isentropic efficiency. It is highly likely that a centrifugal compressor would actually be used within hybrid-electric aircraft for EIS 2035 onwards but the control complexity would make the implementation difficult. Once the complete design cycle is obtained, the energy consumption penalty is calculated by normalizing power off-take, drag and weight of the full system with respect to overall aircraft's power, drag and weight requirement. This concludes the discussion on design and sizing of ram air HEX and VCC thermal management systems. Next section looks at the method to integrate these designs with the framework and accounting of drag, weight and off-take penalty of TMS at a mission level.

3.9 Integration of TMS into the framework

This section constitutes the methods to integrate both thermal management architectures - Ram Air Liquid coolant HEX & Vapour compression cycle with the whole framework. In the previous sections, design and off-design solving methods were shown for both the TMS architectures. But for what quality, quantity of heat loads should the architecture be designed for? How would the power management change the TMS design and corresponding penalty? How to optimize the VCC for off-design conditions? The methods to answer these forms the crux of this section. The main ways by which TMS affects the aircraft mission fuel burn or energy consumption is by external drag, internal pressure loss drag, weight and compression, fan power consumption or by pump power consumption. In the case of the ram air HEX, the external drag is contributed by the installation of the HEX on the aircraft, the internal drag contributed by the pressure loss through the nozzle, diffuser and the HEX. In the case that the flow can't be expanded through the nozzle owing to high pressure loss in HEX, a pusher fan is considered to push the flow out. The pumping power is also accounted for in order to maintain the pressure across the ram air HEX-coolant loop. The power consumed by the fan and the pumping power is accounted by sizing a separate electrical powertrain and over-sizing the battery pack or hydrogen tank (in case of PEM fuel cell hybrid). The weight of the full unit consists of HEX weight and the coolant weight with the weight of fluid pumps not accounted for. In case of the VCC system, the external drag consists of the installation drag of the HEX at the condenser side while the evaporator side is assumed to be installed within the cargo section of the aircraft hence contributing to no drag. The internal drag consists of the pressure loss drag through the HEX at the condenser side while the pressure loss at the evaporator side HEX is accounted for by extra compression. The

weight of the VCC consists of the weight of the HEX at both end of the cycle, the compressor, motor and coolant weight. The power of the fan at condenser side and the compressor power both are accounted for and cycled in the loop. An example of an accounting for a fuel cell case can be seen in Figure 3.51.

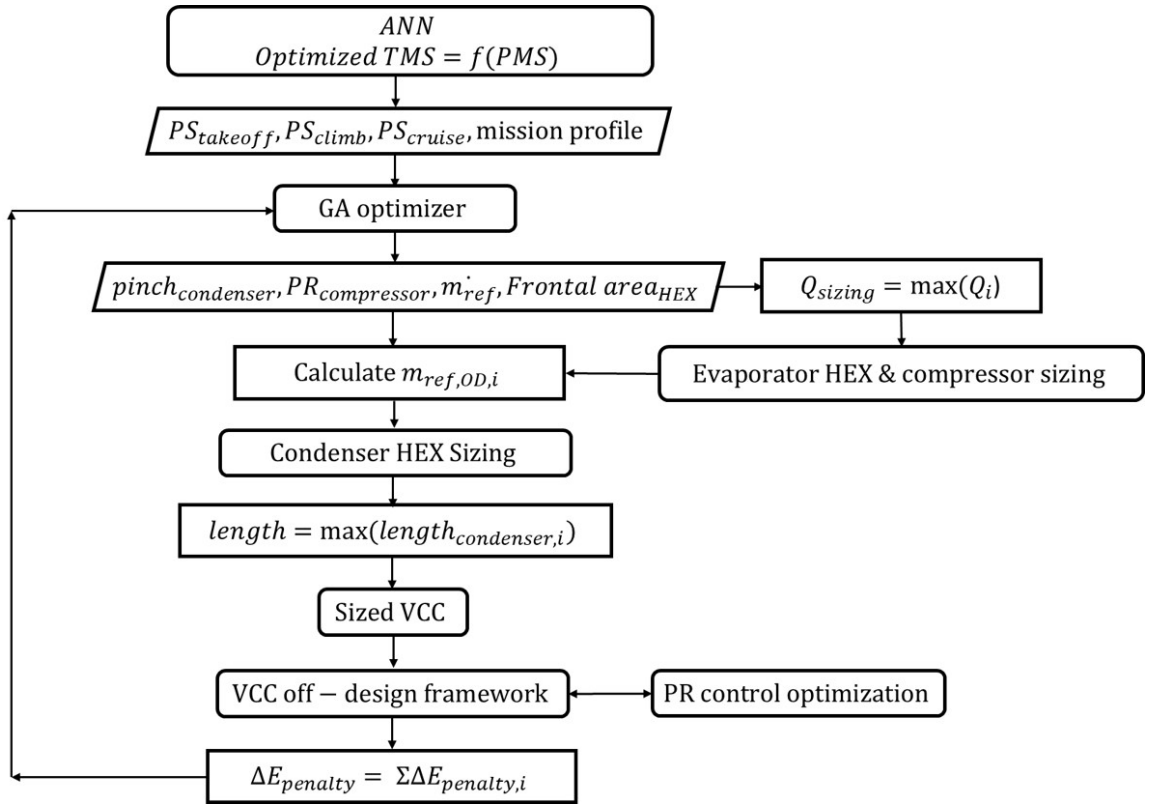


Figure 3.49: TMS Integration

Before explaining the details in Figure 3.49, it is important to understand how is the accounting done within each architecture and how the VCC packs are utilized. Essentially there exists three options, 1. when all electrical systems within an architecture are in the same evaporative coolant loop, 2. when each electrical load has a different refrigerant pack and 3. when a cascaded cycle is used making the best use of different working temperatures of the heat loads. The option 1 is the simplest but essentially the least efficient as it forces a high temperature heat load (like fuel cell) to require pressure ratio of a low quality heat load (like battery). It was initially found that the penalty arising from such a pack was far too high, hence was discarded. The option 2 is the one where each heat load is in a different refrigerant loop, enabling a more efficient energy penalty but subsequently increasing the complexity. Option 3 is potentially the one which should be the most efficient and should be pursued in future (explained in detail in future work), but is not pursued in this work.

Given that the option 2 is the one which is pursued, essentially separating each

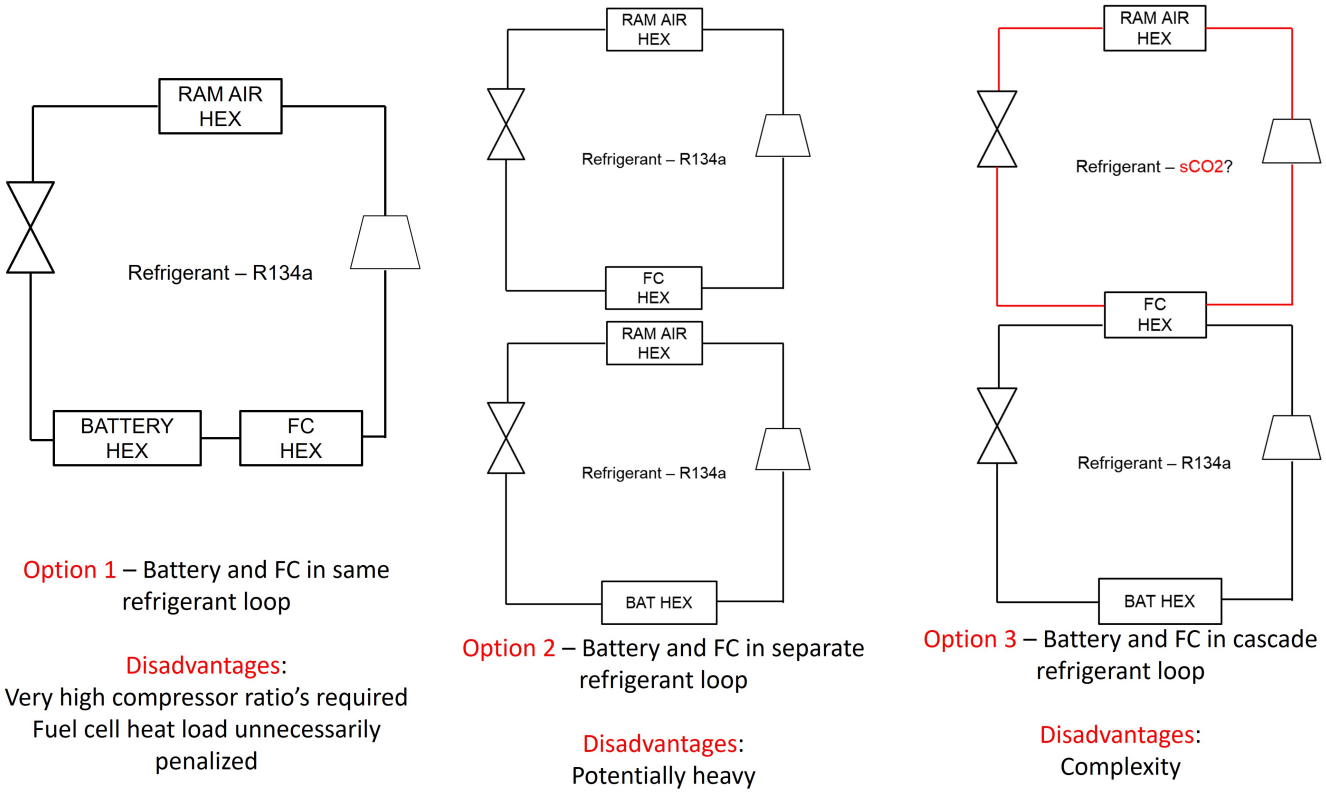


Figure 3.50: VCC packs per architecture

electrical system in a different loop simplifies the energy penalty calculations. It is assumed that the compression/drag power is accounted for over-sizing the fuel cell or battery pack within each architecture. Now, if a look is now made at Figure 3.49, the main steps are the creation of ANN trained on thermal management penalty as a function of PMS, and the overall energy penalty accounting design and off-design behaviour across a mission profile. The same ANN method described in section 3.4 is utilized to develop the correlation shown in Equation 3.37. The drag, power off-take and weight accounting is broken down into energy penalty factors and power penalty factors. The energy penalty factors are calculated using Equations 3.38, 3.39 and 3.40, while the peak power (used to oversize the fuel cell/battery by power) is done using equation 3.41. The points "i" are flight points along the mission profile. The mission profile is broken down into smaller segments to capture the drag and power variation with altitude and Mach. The penalty factors are calculated in such a way that the system (fuel cell or battery) under assessment is oversized by this penalty factor. It is hydrogen fuel consumption in case of fuel cell and battery pack size in the case of batteries. It should be noted that in all the cases the external drag is calculated assuming square wing mounted HEX drag coefficient obtained from Hoerner [157].

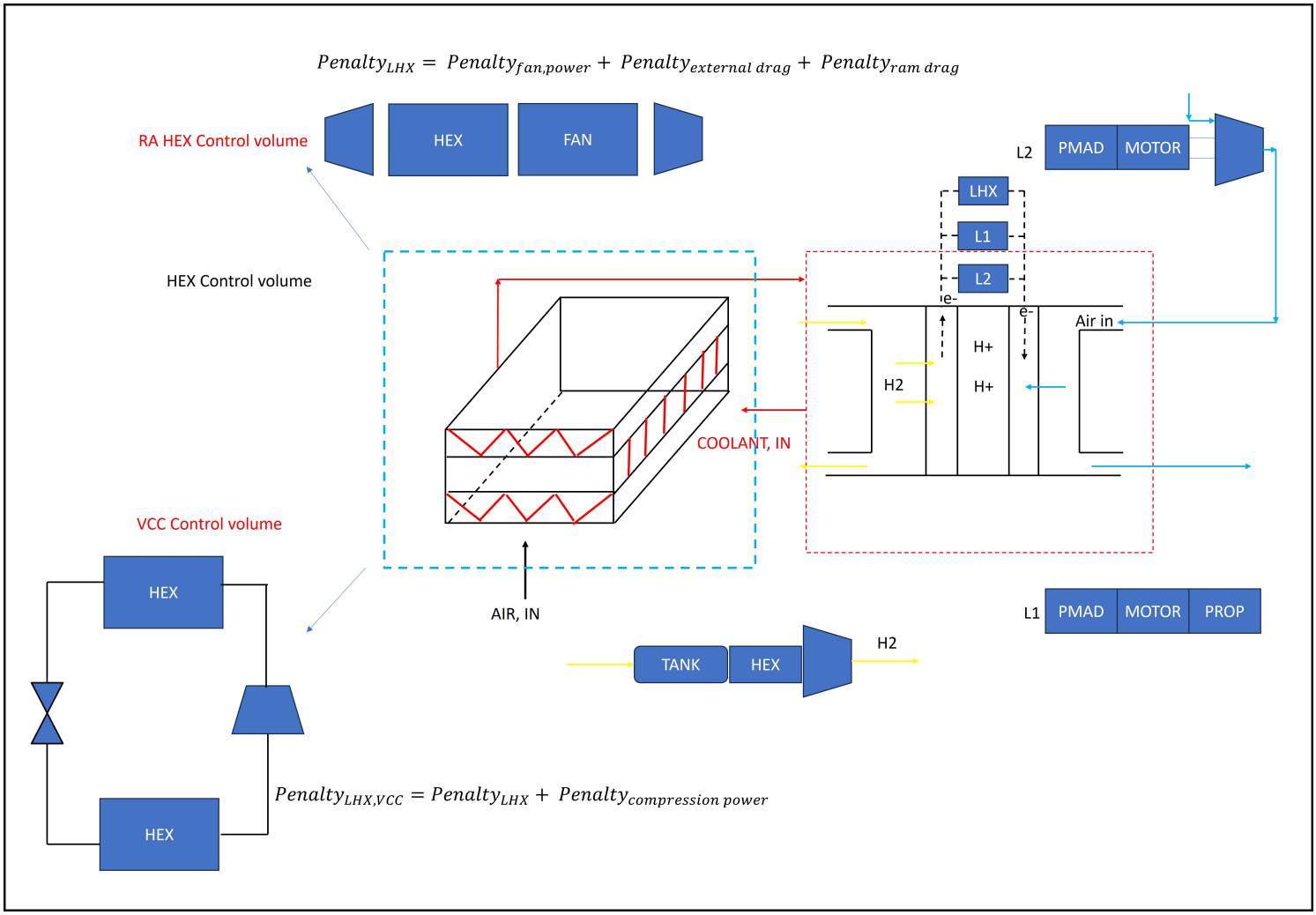


Figure 3.51: Fuel cell HEX/VCC penalty

$$[penalty_{NWT}, weight, penalty_{P_{max}}] = f(H_{P,MTO}, H_{P,MCL}, H_{P,CRZ}) \tag{3.37}$$

$$penalty_{off-take} = \frac{\sum_{i=1}^{n} PO_i dt}{\sum_{i=1}^{n} P_{system,i} dt} \tag{3.38}$$

$$penalty_{drag} = \frac{\sum_{i=1}^{n} (DragtoPow_{shaft_i} dt / \eta_{transmission})}{\sum_{i=1}^{n} P_{system,i} dt} \tag{3.39}$$

$$penalty_{NWT} = penalty_{drag} + penalty_{off-take} \tag{3.40}$$

$$penalty_{P_{max}} = (max(PO_i) + max(DragtoPow_{shaft_i}))/max(P_{system,i}) \quad (3.41)$$

Once the penalty factors are estimated, the optimizer is setup as described in 3.49 to minimize the energy penalty. It needs to be understood that the penalty factor used to get the optimal designs when training the ANN also account for the weight penalty but cannot account for the payload penalty as described in Figure 3.55. This is a slight drawback which is described in future work, and can be resolved by putting multiplying factors on the weight. Presently, though the design is selected by putting equal multiplying factors on all 3: drag, weight and off-take. The rest of the off-design calculations are done the same way as described in previous section. The final framework when integrated with rest of all the elements is seen in Figure 3.55, which iterates on the payload to meet the MTOW constraint. The final framework is concluded in the section 3.10, where all the inputs and outputs are summarized. Before that, a small section on hydrogen aircraft iterations are design space are described in next section.

3.10 ORION and Full framework at a glance

This section deals with the mission run setup within ORION and how the baseline kerosene and hydrogen aircraft performance is done. ORION is CU's aircraft performance tool, similar in logic to NASA FLOPS [86]. The validation of the kerosene aircraft models is shown in Section 4.1, hence only the method to develop hydrogen counterparts of the baseline kerosene aircraft is described here. All the HY aircraft have tanks stored in fuselage in place of pax. In this study, the extension of fuselage is not considered, hence the payload is traded against tank length/fuel volume. All the results in section 4.5.3 follow the solving scheme shown in Figure 3.52. optimization is done on a fixed mission range as shown in Figure 3.52, with the optimizer identifying the power splits between different propulsion components albeit with hydrogen tank length as the constraint. The key addition when assessing any hydrogen powered fuel cell or gas turbine are the tanks volumetric constraint. Effectively, the optimization scheme remains the same as previous discussed in Section 3.4 but simply put pax are also internally iterated in ORION during the mission run. An example of trade-off between pax against fuel capacity for the regional turboprop can be seen in Figure 3.53. The pax comes out in the factor of 6 as the tanks cover the full fuselage

diameter.

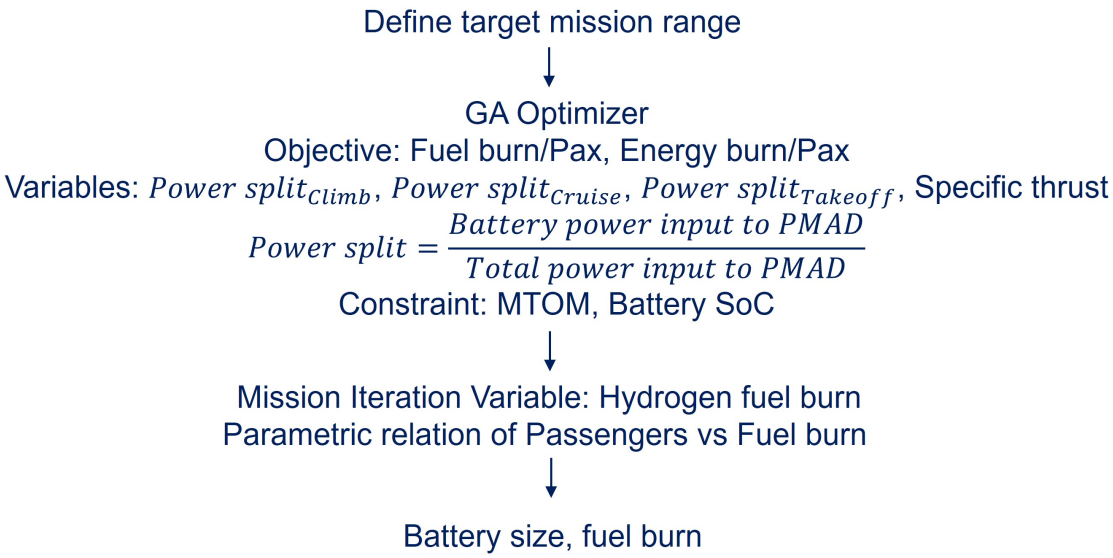


Figure 3.52: Mission solving method for hydrogen fuel cell, battery, hydrogen GT

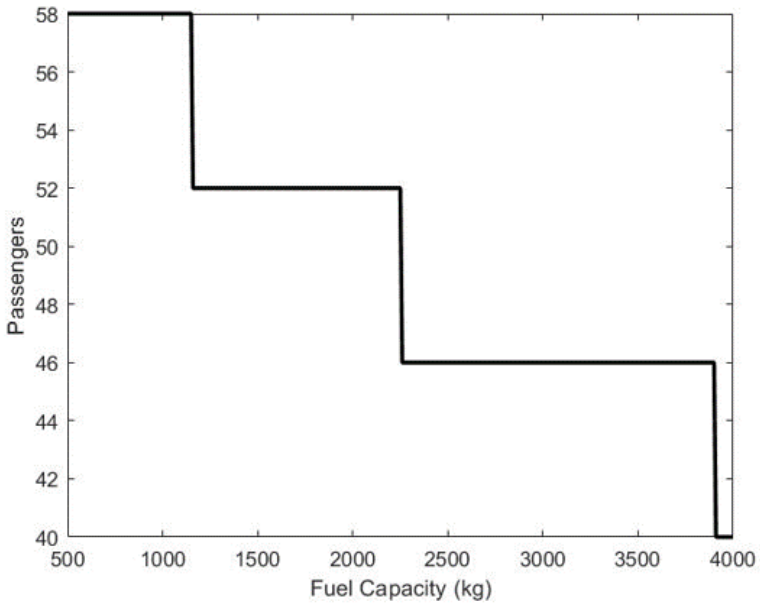


Figure 3.53: HY PAX

The details on hydrogen aircraft are also described in Chapter 4.5.3. Finally the aircraft design space analyzed is described. Essentially 4 aircraft models have been developed, being SMR turbofan (A320), 2 regional turbofan (Fokker 100 and BAe 146) and regional turboprop (ATR 72). The reasoning behind their selection and architectures assessed for each are described in Section 4.1. All parts of the

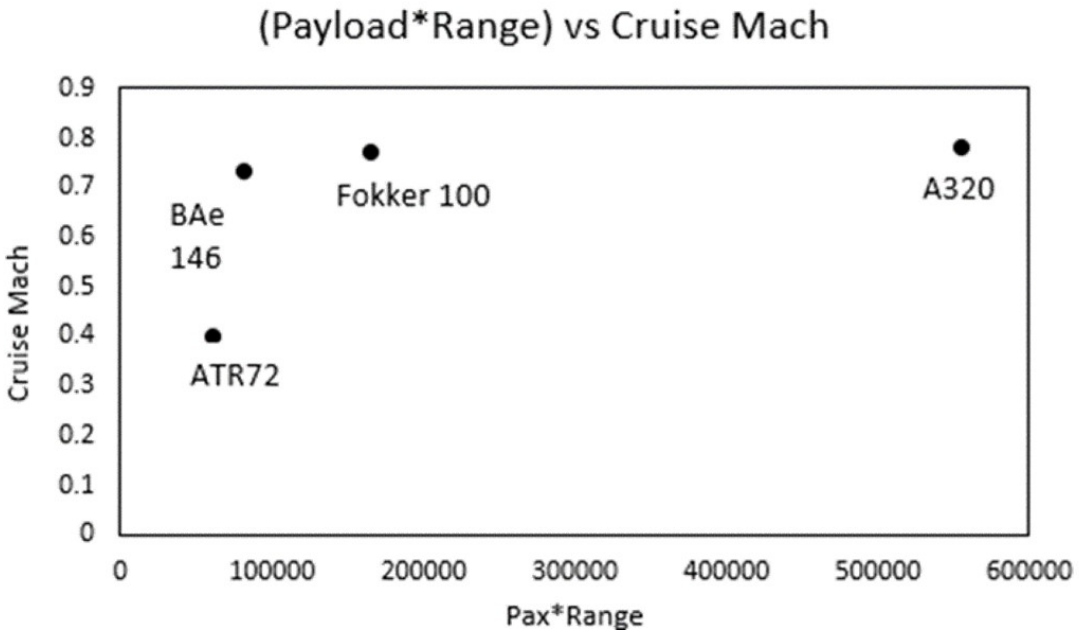


Figure 3.54: HEPS Aircraft Design Space

framework have now been discussed besides the propeller and fan modelling. The propeller modelling is done by directly utilizing methods developed by Giannakakis [158], hence not described in the thesis. That concludes the discussion on all elements of the framework, leading us to finally summarize how the integration is done and the mission simulations are performed. Initially an aircraft type, EIS and architecture to be assessed are selected, following which the optimization is done for each propulsion "design" range. Each range as described in multi mission framework is optimized for fuel burn or energy penalty per pax. During each mission run, the gas turbine performance, fuel cell and battery performance ANN surrogates are utilized following which the TMS ANN is also added to the framework. The internal iterations are performed in ORION such the MTOW and volumetric constraints are met. The complete algorithm is shown in Figure 3.55 and the various steps described can be seen. It needs to be understood that the full framework with TMS is only used right at the end of results section, and rest of the sections are various fragment of this overall framework. That concludes the the methodology chapter of the thesis and next chapter discusses the key results.

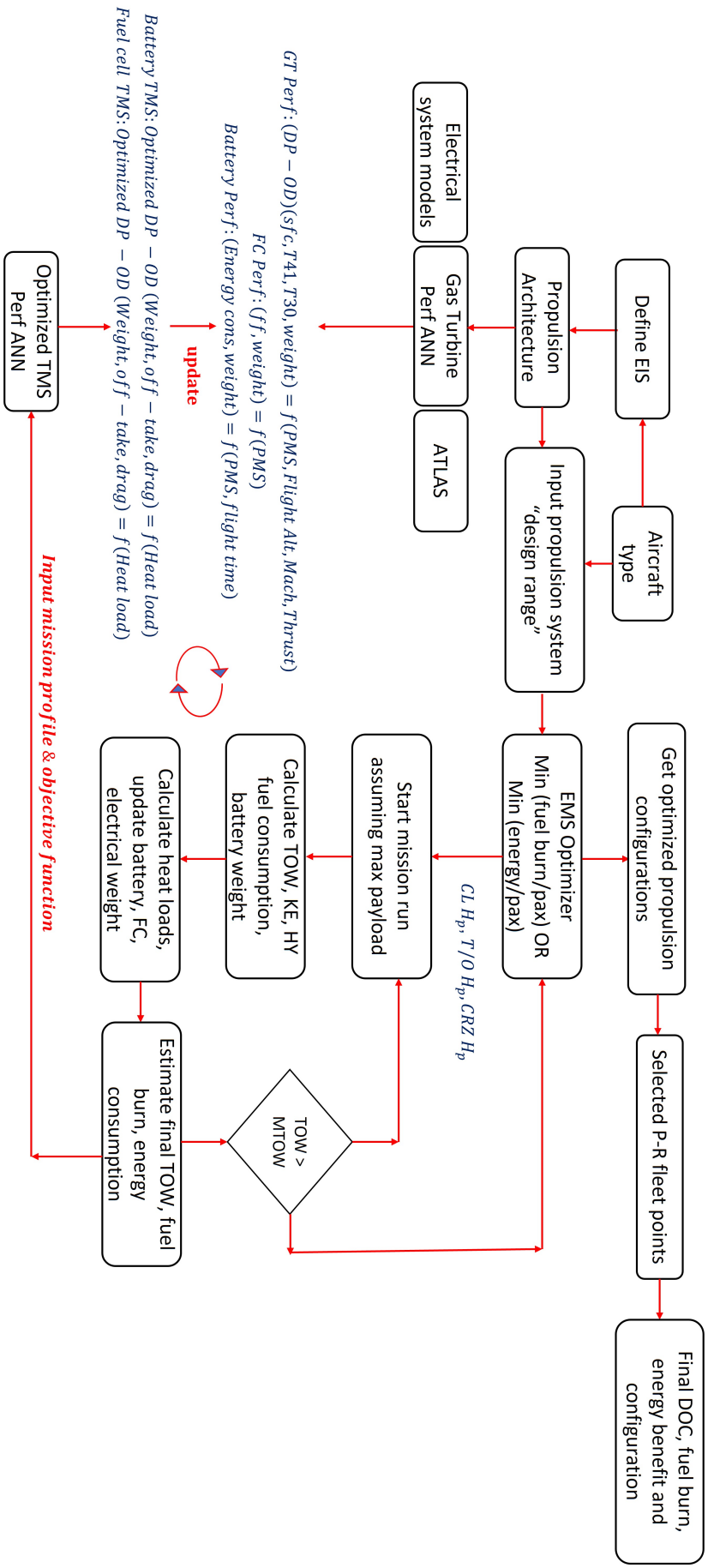


Figure 3.55: Integrated framework

Chapter 4

Results

This chapter comprises all the major results produced during the research. The results start with design space exploration for the regional turbofan test case followed by the integrated multi mission results across the design space, thermal management systems design space results and ultimately a final technology comparison for the regional turboprop case.

Contents

4.1 Introduction 93
4.2 HEPS Design space exploration 98
4.3 Integrated multi-mission assessment across aircraft classes 116
4.4 TMS design and optimization 143
4.5 Final Technology Evaluation 155

4.1 Introduction

Primarily, four aircraft have been modelled and assessed in this research based on public available data. These are based on BAe 146, Fokker 100, A320 Neo and ATR 72. These aircraft were strategically chosen to cover the regional and single aisle aircraft design space. The reason why A320 Neo was chosen as the one of the test cases and has been explored the most in this study, is the high utilization of A320 and B737 family. Aviation emissions from all aircraft type in 2022 was summarized in a study by Statista as shown in Figure 4.1. It can been that A320-200 and B737-800 family contribute to almost 25% of aviation emissions, meaning that electrifying them would be of maximum potential due to the large scale of usage. Hence, the decision to go for

A320 Neo as the primary aircraft test case. The comparison between electrification on Fokker 100 and A320 Neo would give the impact of change in designed payload and range of the aircraft. While electrifying ATR 72 would give the impact of change in Flight speed, when comparing against Fokker 100 electrification numbers. Modelling BAe 146 would give the potential of electric fan concepts (in line with Airbus E-Fan X study [74])and also help compare electrification on 4 engine aircraft against a twin (Fokker 100). Despite Fokker 100, ATR 72 and BAe 146 being older airframes which have been in service for more than 30 years, the reason to model them was driven by the sponsor of the project. All of these aircraft have the potential to be retrofitted by an hybrid-electric power train and would give the sponsor a chance to understand impact of electrification in case of entry into service before 2030. Besides modelling A320 Neo and Fokker 100 and comparing impact of electrification on them, would also account for the improvement in aircraft technology. For all four aircraft, a baseline engine performance model is created in Turbomatch using a combination of public available information [159][160] and assumed appropriate technology level provided by the sponsor. The engine deck is then generated, assuming standard climb rates and engine rating, a payload range diagram is modelled and validated. Once the payload range diagram validation is done, the aircraft model is then utilized by updating technology level on engine, and finally utilized for electrification cases. The payload range validation (4.2, 4.4, 4.3, 4.5) and baseline aircraft gas turbine information (4.1, 4.2, 4.3, 4.4) can be seen below for all four aircraft.

Max Ramp Weight (kg)	45909
Max Payload Range (nm)	1425
Max Payload (kg)	10750
Cruise sfc (g/kN.s)	19.47
Cruise BPR	3.06
SLS Thrust (kN)	68.5
T/O T40 (K)	1411

Table 4.1: Fokker 100 aircraft and engine data

The results shown in the next sections all correspond to either of the four aircraft and are performed keeping following objectives and order in mind.

- The first objective was to explore the parallel hybrid design space with batteries and to differentiate the impact coming from cycle redesign, motor power, battery weight, mission range, gas turbine, motor, battery technology level & PMS optimization. The design space exploration is performed for the regional

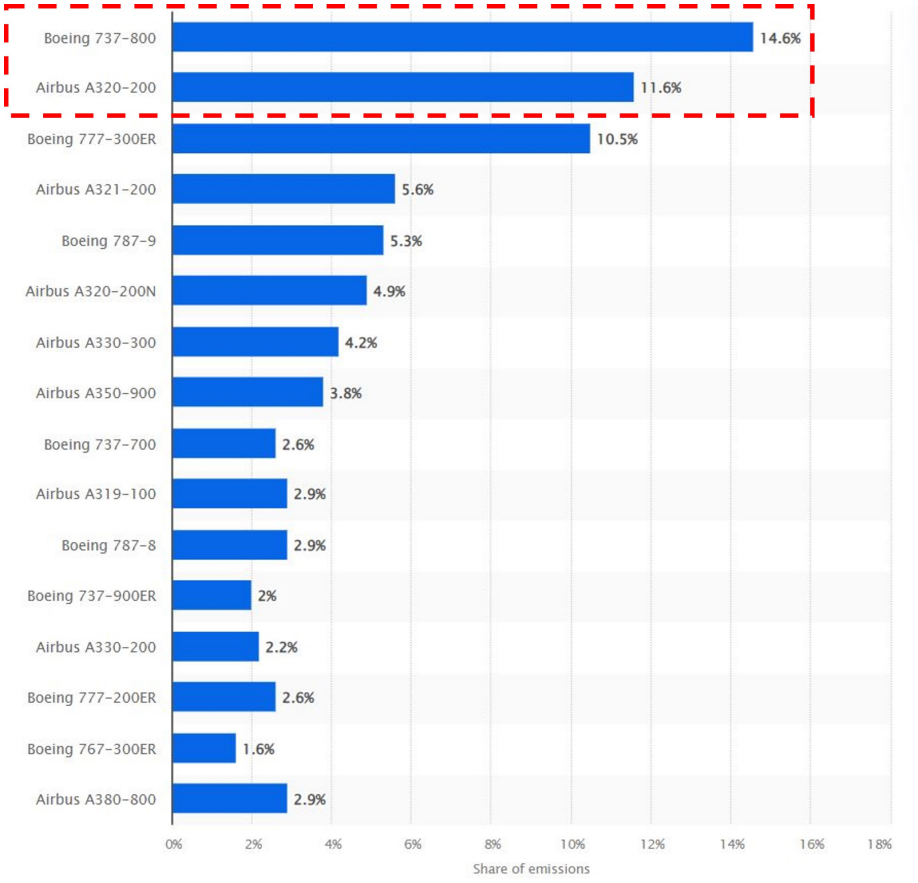


Figure 4.1: Aviation emissions for 2022 by aircraft type [161]

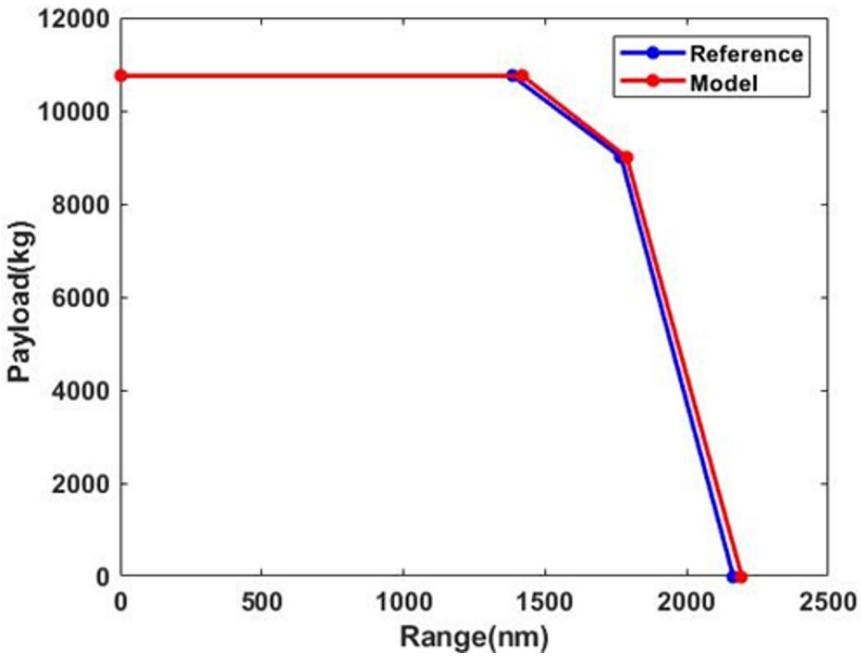


Figure 4.2: Fokker 100 payload range diagram validation against [162]

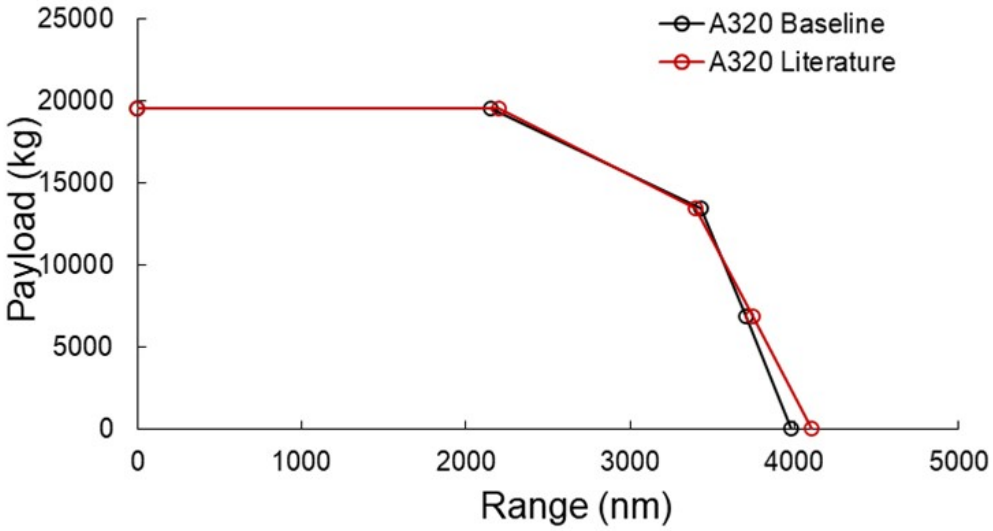


Figure 4.3: A320 payload range diagram validation against [163]

Max Ramp Weight (kg)	78400
Max Payload Range (nm)	2200
Max Payload (kg)	19500
Cruise sfc (g/kN.s)	16.5
Cruise BPR	6.1
SLS Thrust (kN)	120
T/O T40 (K)	1641

Table 4.2: A320 aircraft and engine data

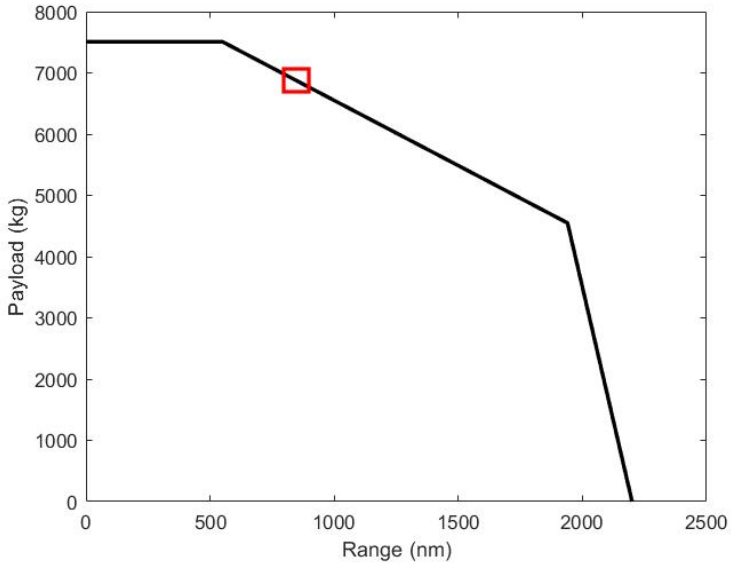


Figure 4.4: ATR 72 payload range diagram and spot point check against [160]

Max Ramp Weight (kg)	22968
Max Payload Range (nm)	825
Max Payload (kg)	7100
Cruise sfc (g/kN.s)	12.2
SLS Thrust (kN)	31
T/O T40 (K)	1320

Table 4.3: ATR 72 aircraft and engine data

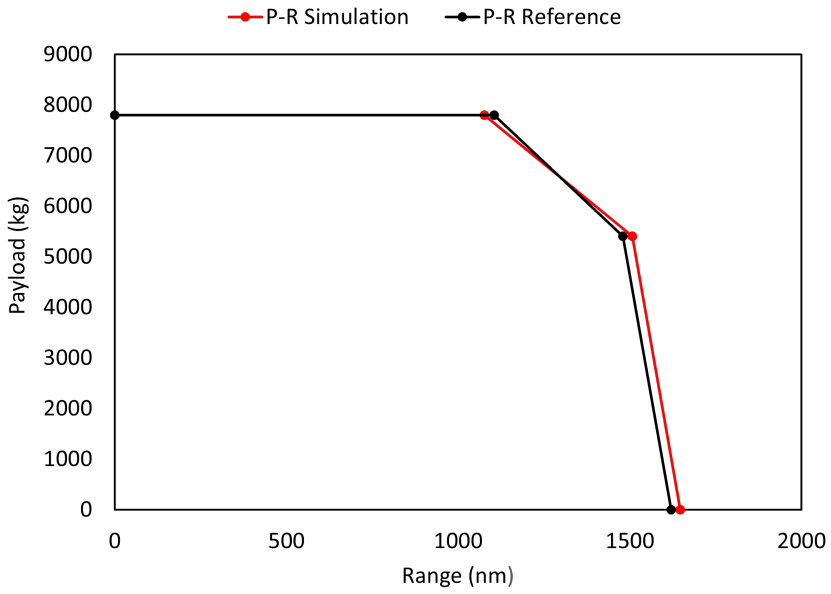


Figure 4.5: BAe 146 payload range diagram validation recreated from [164]

Max Ramp Weight (kg)	38102
Max Payload Range (nm)	1105
Max Payload (kg)	7800
SLS Thrust (kN)	31.1
Max zero fuel weight (kg)	21800

Table 4.4: BAe 146 aircraft and engine data

turbofan test case, Fokker 100. The reason this exploration is not performed for all test cases as the conclusions regarding impact of these parameters will hold true irrespective of the aircraft platform to be assessed.

- Once the conclusions on the impact of technology level and bounds of the design space are obtained, they are applied across all platforms with modifications, and a full integrated assessment is performed. The integrated assessment is used to obtain the difference between retrofit and redesigned HEPS in terms of block fuel, block energy, direct operating cost and power management strategies. The

integrated method is then subjected to a multi mission assessment to get final fuel burn and direct operating cost benefit scenarios. Ultimately, a synthesis is performed to understand the trade-off between direct operating cost and fuel burn and the expansion of it across aircraft classes.

- The next 2 set of objectives now try to implement TMS architectures within the integrated framework. The 3rd objective deals with the design space exploration of both TMS architectures, to understand the impact of the selection of TMS design on weight, ram drag, external drag and power consumption. The addition of all these parameters ultimately constitutes the energy consumption penalty. Post the design space exploration of the thermal management architectures, the impact of them are also quantified for the battery powered architectures.
- The final subsection of results deals with a technology comparison on the regional turboprop test case, where a fuel cell battery hybrid architecture is compared to battery gas turbine HEPS architecture and hydrogen GT and kerosene GT. The advantages of using vapour compression TMS are shown over ram air HEX for cooling fuel cell architectures.

4.2 HEPS Design space exploration

This sections deals with the objective 1 of the results, design space exploration for parallel HEPS architecture on Fokker 100 platform. The key design parameters are impact of cycle design (retrofit vs redesign), battery weight (degree of hybridization by energy), motor power (degree of hybridization by power), technology level (gas turbine temperatures, component efficiencies, specific thrust, battery energy and power density, motor and inverter power density). All the results in this section correspond to Architecture 1 within Figure 3.2.

4.2.1 Impact of GT cycle design

The impact of electrification on the baseline engine cycle is described in this sub-section. A comparison is made between retrofit and redesigned engine. The retrofit engine simply means there is no change to the baseline engine and the engine is de-rated for the phases of flight where the motors provide power to the LP shaft, as described in Section 3.3. The retrofit hybrid engine will have potentially a turbine life benefit and NOx reduction compared to the baseline due to the lower turbine work requirement and hence lower turbine entry temperatures. Application of motor

power to the LP shaft of the TAY 651 style engine model within TURBOMATCH gives the following trends. Figures 4.6 and 4.7 show the drop in T40 and T30 on the same thrust level at EOR/take-off conditions with varying degrees of hybridization. Every 1 MW motor power on-take leads to a drop in T40 by 41 K and a drop in T30 by 5 K. The retrofit engine data are provided in Table 4.5. This reduction in T40 and T30 at take-off gives some margin to redesign the cycle to smaller core sizes and higher OPRs at cruise. This will lead to improvement in core efficiency (owing to higher temperatures) and lower specific fuel consumption. An engine cycle redesigned to take advantage of this flexibility is called the redesigned hybrid engine.

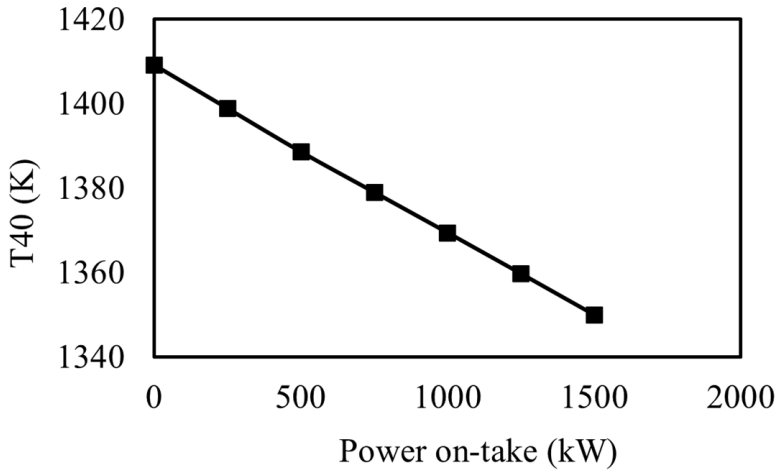


Figure 4.6: Variation in T40 with power on-take at EOR on same thrust level

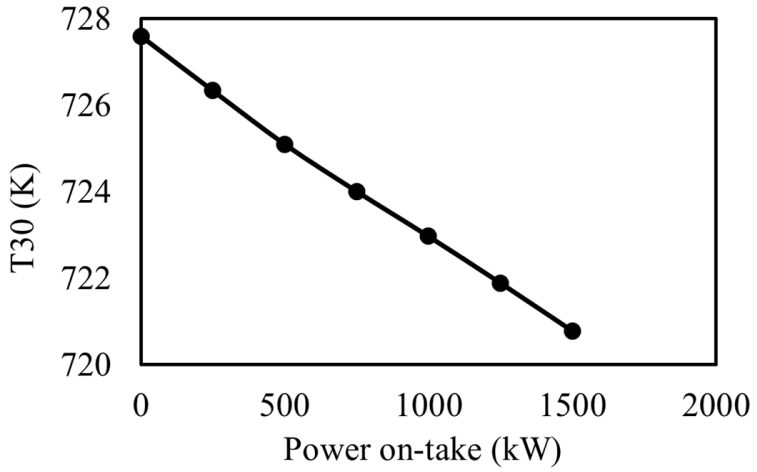


Figure 4.7: Variation in T30 with power on-take at EOR on same thrust level

The method for engine cycle design described in section 3.3 is utilized to develop an engine cycle redesigned according to electrification. The comparison of the three

engine cycles – baseline, retrofit, and redesigned hybrid is presented in Table 4.5. The trade off is simply put between the lower sfc, smaller core size of the redesigned engine against the lower take-off and climb temperatures of the retrofit engine. Before bringing elements of direct operating cost into the calculation, it was necessary that the redesigned hybrid engine have the same HP turbine rotor blade metal temperatures through take off & climb as the baseline, hence the top of climb power on-take was varied to match the take-off power on-take. For the redesigned cycle, the power on-take is found to be 400 kW at top of climb to have the same blade temperatures as the baseline for 1 MW.

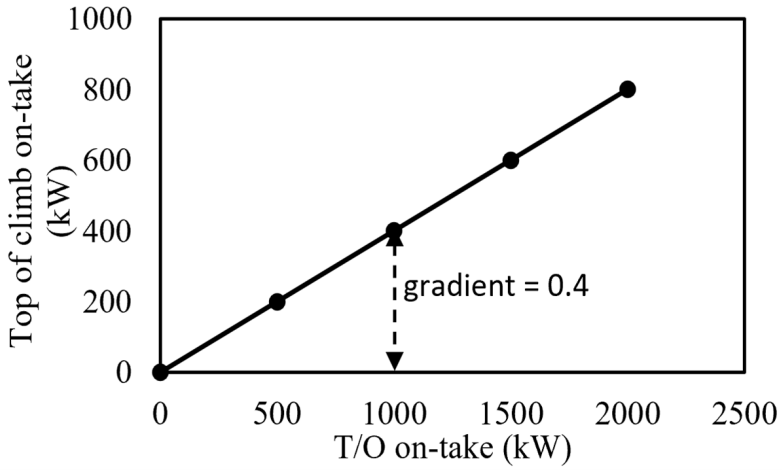


Figure 4.8: Power on-takes for T/O and top of climb

All three cycles are compared at the same thrust levels as the maximum take-off weight constraint is maintained. Because the MTOW is maintained, effectively the MCL and MTO would remain the same, though the CRZ thrust would vary owing to constant battery weight against reducing fuel weight. This CRZ thrust increase could help extract even more sfc benefit as thrust ratios would come closer, but is assumed that this is a secondary effect as compared to the core redesign benefit hence ignored. For the redesigned hybrid case, the increase in design point T40 and OPR increases the thermal efficiency at cruise. Thereby reducing cruise specific fuel consumption by 0.7% relative to the baseline engine. Based on the outputs from ATLAS, the redesigned engine is also 7% lighter than the baseline engine due to the reduced core size. Though the ratio of top of climb to take-off on-take of 0.4 obtained from Figure 7 is not too different from Lents [18] (0.35), it heavily depends on gas turbine technology level and thrust ratios.

The other factor to consider during gas turbine cycle design exercise is also the

Parameter	Baseline	Retrofit, delta		Redesigned, delta	
CR BPR	3.06	3.06	0	3.329	8.8%
CR tsfc (g/kN.s)	19.475	19.475	0	19.34	-0.7%
CR OPR	16.6	16.6	0	17.01	2.5%
CR T40 (K)	1160	1160	0	1198	38
T/O T40 (K)	1411	1369	-42	1411	0
T/O T30 (K)	728	723	-5	728	0
TOC mass flow (kg/s)	80.3	80.9	0.7%	80.3	0
CR on-take (kW)	0	0	0	0	0
TOC on-take (kW)	0	400	400	400	400
T/O on-take (kW)	0	1000	1000	1000	1000

Table 4.5: Comparison of baseline, retrofit hybrid and redesigned hybrid engine cycles

impact on compressor steady state operability. It would always be ideal to get the limits kept for LP or HP compressor transient stack from a proper transient model accounting for thermal soakage, deterioration, starting torques and bleeds and VIGV schedules([84],[66],[17]). But this is out of scope for this study, hence a 15% transient stack is assumed as the minimum possible surge margin for the compressors. It was discussed that as the motor shaft power increases, there is a linear decrease in T40 and T30, which means a linear improvement in the cruise specific fuel consumption for the redesigned engine cycles with an increasing degree of hybridization. But this high degree of hybridization by power provided at take-off, climb and cruise though will ultimately be limited by the impact on the operability of the gas turbine components. The LP compressor moves towards surge on application of on-take for any phase of flight. This is particularly more prominent if higher motor power is provided to the LP shaft as seen in Figure 4.9. The HPC operating point change with power on-take is shown in 4.10. If the HP shaft was powered instead of the LP shaft, the trend would be reversed. The behaviour is similar to a typical power off-take from HP spool in aero-engines with the raised HP compressor working line on increasing power off-takes from HP spool [165]. The trend for the effect of power on-take of off-take on the LP compressor or booster becomes much more aggressive in the case of a 2-spool geared or non-geared architecture as the speed is dictated by the Fan/LPT system to achieve a given target thrust. This leaves the Booster with lower corrected mass flow rate (due to lower core temperatures) on a higher corrected speed, leading to reduced surge margin. These trends align well with previous conclusions from [83], [17], [84], [50] regarding LP compressor surge and HP compressor overspeed. Regarding the redesigned gas turbine, two options do exist, one would be to keep the same CRZ operating point and constrain take-off and climb power by surge margin or push

CRZ to a lower point and target higher powers. The first option is utilized to get maximum sfc benefit from a given power on-take and also to avoid flutter risk by pushing CRZ lower. Hence, the operating characteristics will remain the same for redesigned engine cycle as the retrofit as the cruise design point surge margin is kept the same and no electrification is assumed to be provided at that point. Though, as will be seen further, on-takes are also used during CRZ but no CRZ on-take does give the maximum bound on take-off and climb on-take. The other decisions to also avoid going to higher powers is the greater physical size of the motor and inability to fit within the core engine and ultimately also the greater difficulty to remove the level of heat loads.

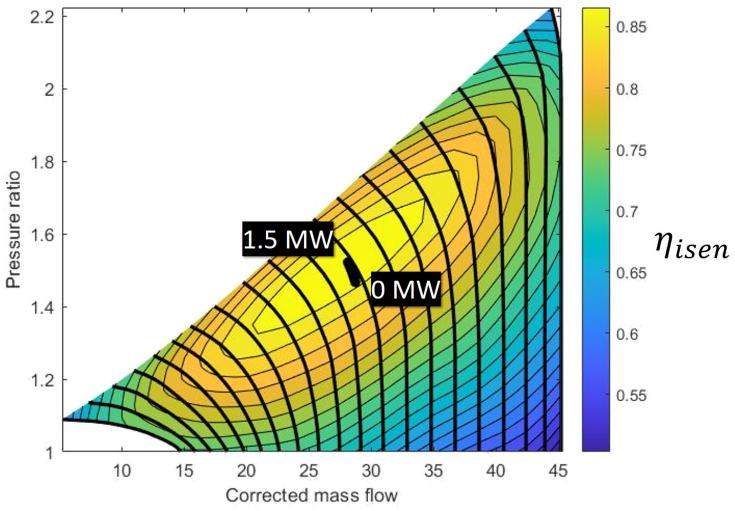


Figure 4.9: LPC operability vs on-take at EOR

This discussion concludes on the potential cycle level benefit that can be obtained from redesign enabled by electrification, but this isn't necessarily the optimal engine when looked at from a mission level. This is because, although the ratio of top of climb to take-off power of 0.40 is ideal from an engine cycle design and operability point of view but is not ideal from a power management strategy point of view. In the literature review done previously, it was concluded from Trawick's work [57], that the power management distribution would depend on three factors: variation of aircraft weight along the mission, battery discharge rates, and motor-inverter efficiency. From the battery stack model described in the methodology section, higher discharge rates/ currents will reduce the efficiency of the battery, keeping the discharge rate low is a critical factor for both performance and life.

The variation in motor-inverter efficiency with percentage power/current is typically low, from models described again in the methodology section. It can be

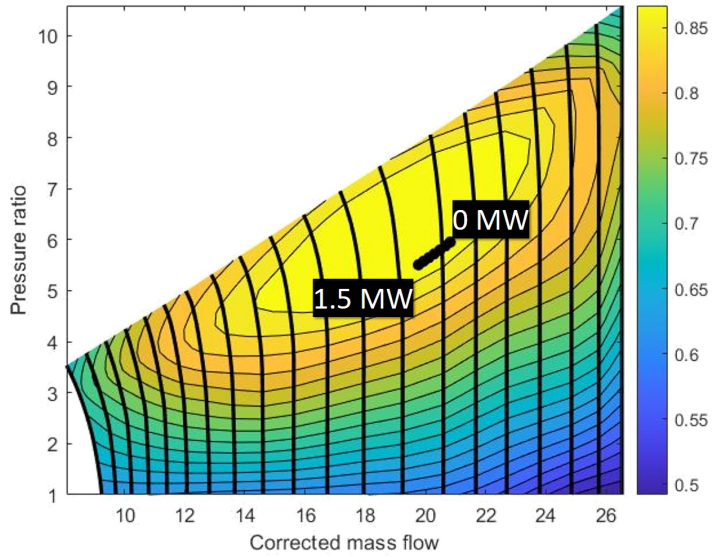


Figure 4.10: HPC operability vs on-take at EOR

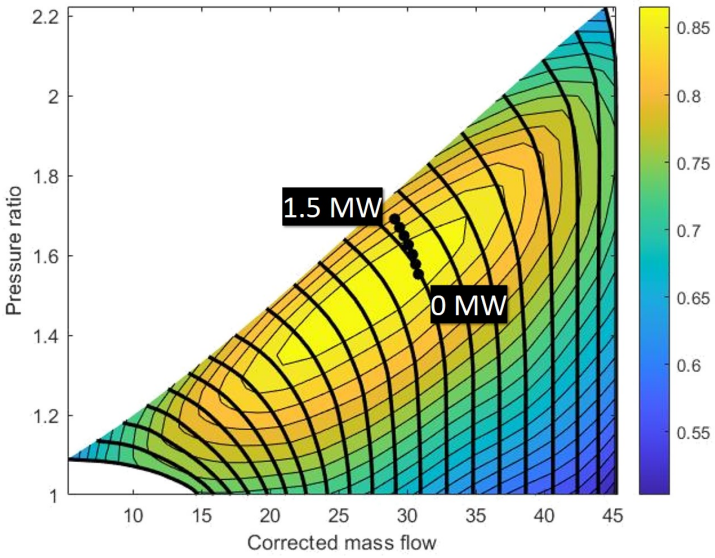


Figure 4.11: LPC operability vs on-take at TOC

concluded that the battery discharge rates, and aircraft weight variation are driving factors in the selection of a power management strategy. Hence, the ideal power management strategy would be to utilize a fraction of the maximum available power throughout the flight, powering mostly cruise, to have lower battery discharge rates and get lighter earlier in the mission. These inferences are also backed up by other PMS optimization studies from [55][58][59]. However, such a power management distribution tilted in favour of CRZ will leave no chance to perform core size reduction and harness the sfc reduction. Hence, the integration of power management

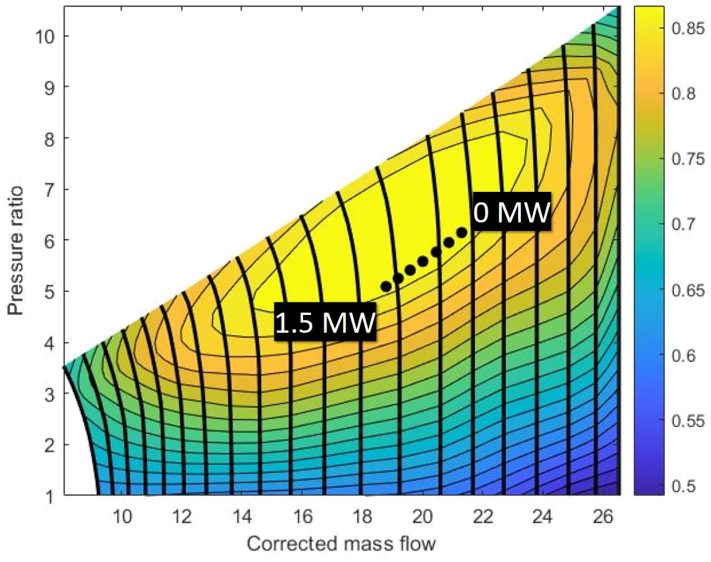


Figure 4.12: HPC operability vs on-take at TOC

optimization and cycle design is required to get optimal combined dual benefit and identify trade-offs in an agnostic manner.

4.2.2 Impact of assumptions on electrical systems

Now that the potential benefits of redesigned hybrid have been identified at a cycle level, it is required that these be quantified at a mission level, and the impact of assumptions on electrical systems be benchmarked. The main assumptions on electrical systems include the battery energy density, battery available energy/weight & motor power. The sweep on all the 3 variables is done for both retrofit and redesigned GT on multiple off-design mission ranges.

Sweep on battery energy density for fixed battery energy and motor power

The major uncertainty around the impact of electrification comes from the battery pack energy density assumptions. In order to quantify this uncertainty, the battery energy density at the pack level is swept for three values, 250, 500 and 750 Wh/kg, with 250 Wh/kg being the current pack level numbers while 750 Wh/kg being the maximum potential EIS 2035 energy density number [166]. The data used for baseline, redesigned and retrofit GT are the ones summarized in Table 4.5. The sweep of battery energy densities are performed with current technology assumptions on the motor and inverter power density and with fixed battery energy, sized to provide 1 MW power during take-off and climb.The complete powertrain efficiency

(battery, motor, inverter and cables) considered for the design point is 0.86, with no superconducting technology considered for the electrical motors. The motor and thermal management power densities are summarized in Table 4.6 for both state of the art and 2035 assumptions. For the sweep of battery energy densities, state of the art assumptions are used while 2035 assumptions are used for the sweep of battery weights and motor power.

Parameter	Current	2035
Motor Power density (kW/kg)	7	13
Inverter Power density (kW/kg)	11	19
TMS Power density (kW/kg)	0.7	1.2
Battery Power density (kW/kg)	1.2	2

Table 4.6: Electrical powertrain assumptions

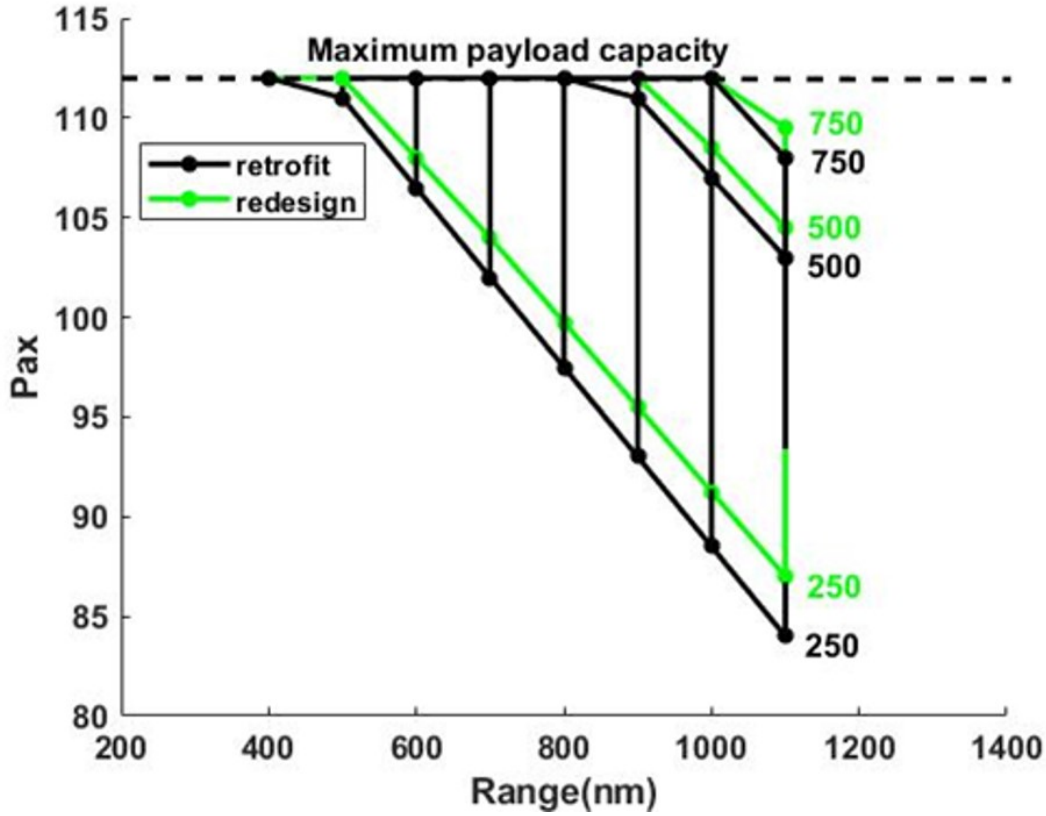


Figure 4.13: Payload vs battery energy densities for range of ranges

Starting with the results, it can be seen from Figure 4.13, that payload needs to be reduced with an increase in mission range to meet the ramp weight constraint for mission ranges above 1000 nm and all energy densities considered. For battery energy density of 250 Wh/kg, there is a consistent penalty in the payload for all mission

ranges considered except for missions shorter than 400 nm. While for battery energy energy density of 500 Wh/kg, there is a penalty in payload post 800 nm to maintain the weight constraint. There is no penalty in payload till 1000 nm for 750 Wh/kg for both retrofit and redesigned case studies. It is observed that the redesigned hybrid case results in lower penalty in payload than the retrofit hybrid for all mission ranges. This is attributed to 7% lower engine weight and lower specific fuel consumption, resulting in lower fuel burn. Two new parameters are defined to compare energy and fuel economy, accounting for the penalty in payload and range, named as Normalized energy and Normalized fuel. These are defined in equations 4.1 and 4.2 respectively. The terms Normalized delta energy and fuel are delta of normalized energy and fuel with respect to the baseline non hybrid GT. In Figure 4.14 and Figure 4.15, to not mix benefits arising from cycle design and power management strategy, a continuous 1 MW on-take till battery discharges, is provided for both retrofit and redesign. Figure 4.14 and Figure 4.15 show the percentage difference in Normalized Energy and Normalized Fuel respectively between HEPS architectures (retrofit and redesign) and baseline engine.

$$[NormalizedEnergy] = [Energyconsumed/(Range * pax)] \tag{4.1}$$

$$[NormalizedFuel] = [Fuelconsumed/(Range * pax)] \tag{4.2}$$

It can be seen that even with a 750 Wh/kg assumption on the battery energy density, there is no benefit in normalized fuel burn for retrofit hybrid design relative to the baseline non-hybrid for all mission ranges. The same trend is observed in normalized energy consumption relative to the baseline, with penalties ranging from 0.2% to 36%. The redesigned GT brings a benefit of the order of 1-1.1% in block fuel burn relative to retrofit for all ranges when compared at the same payload. On a mission range of 400 nm, the redesigned HEPS provides a 1.8% fuel burn benefit relative to the baseline. Since the Fokker 100 flies 50% of the flights below 400 nm (based on data provided by sponsor), there is scope for fuel burn improvement with a properly designed engine cycle, optimally sized thermal management systems and optimally utilized electric powertrain. The quick outcome which can be seen when doing the sweep on battery energy density, is that 750 Wh/kg is the only option worth exploring as it is the only battery energy density where a significant fuel burn benefit can be obtained. The battery energy density is capped as 750 as the maximum possible upper limit battery pack value based on inputs from sponsor and studies

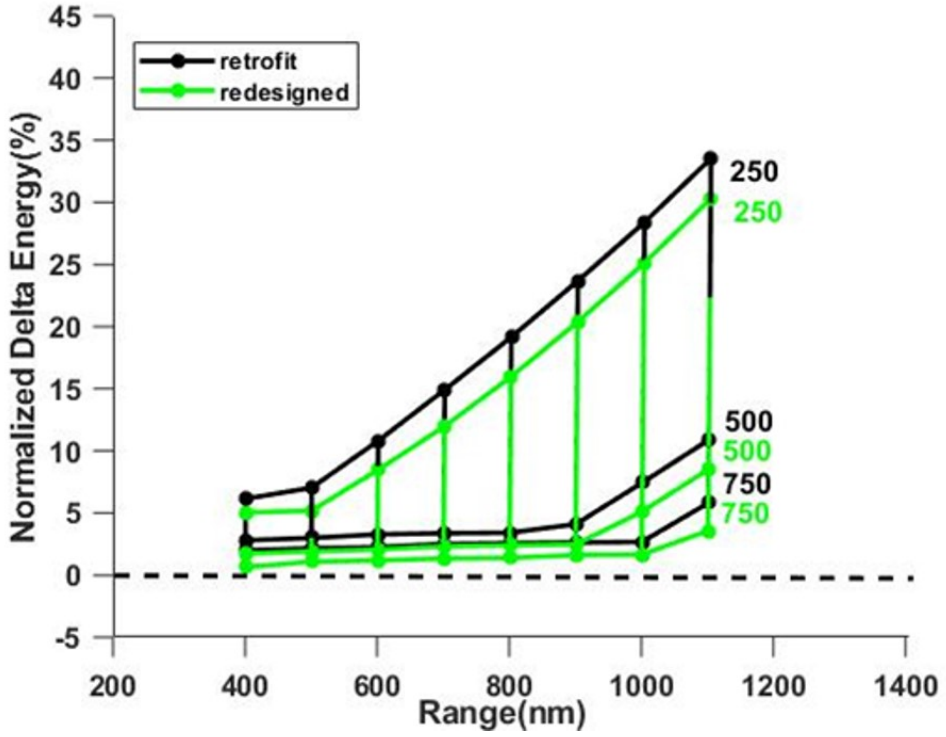


Figure 4.14: Normalized delta energy (%)

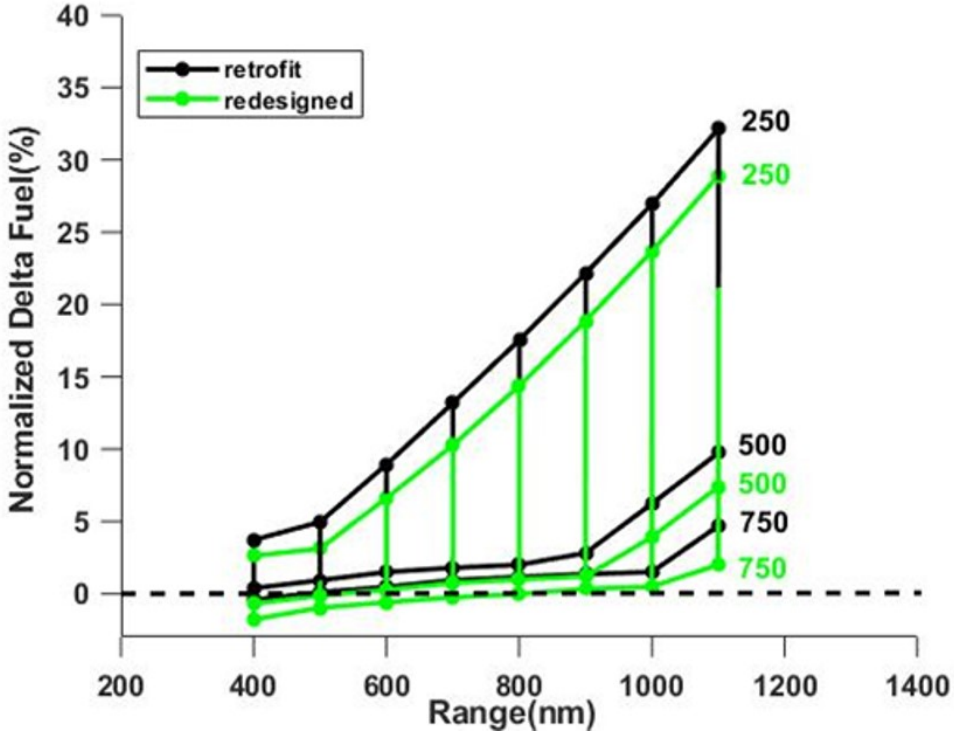


Figure 4.15: Normalized delta fuel (%)

from Boeing [167].

Sweep of battery weights and motor power

The next set of simulations is performed to identify the appropriate battery size and motor power for this aircraft using battery energy density of 750 Wh/kg and 2035 estimates on the electric powertrain. As the battery size increases, the maximum payload range of the aircraft reduces due to added weight and the energy consumption penalty also increases. In all the flight mission results considered herein, the genetic algorithm optimizer is employed to optimize the electrical power distribution along the flight mission. This is integrated and utilized with the cycle design method for the redesigned case studies. The individual benefit from optimizing the PMS is also benchmarked in the very next subsection 4.2.3.

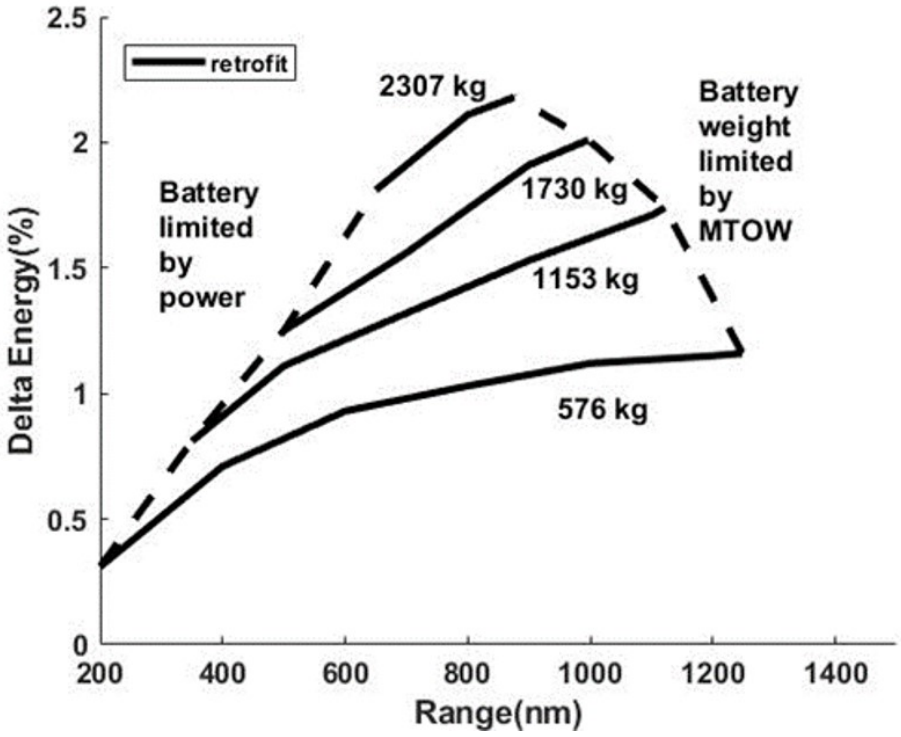


Figure 4.16: Battery weights vs range of ranges sweep for 0.5 MW retrofit

Starting with the retrofit trends for 0.5 MW, the line 'Battery limited by power' in Figure 4.16 is the maximum range below which the battery is not fully discharged (SoC>20%) and is oversized. This is a key parameter that reflects the need for a higher motor power to discharge the battery for lower flight mission ranges. The line 'Battery limited by MTOW' highlights the maximum flight mission range for maximum payload for different battery weights. So the aim should be identify how

high can you go on the motor power before the constraints reduce the benefit. The final comparison is made between 0.5 and 1 MW motor power for the sweep of battery sizes in Figure 4.17 and Figure 4.18. It is seen that retrofit hybrid with 0.5 MW consumes less block energy and fuel than 1 MW for the same battery size, but the trend is the opposite for redesigned hybrid. This shows that core size reduction has a more pronounced effect on fuel burn and energy consumption than electrical powertrain weight increment for the same battery size.

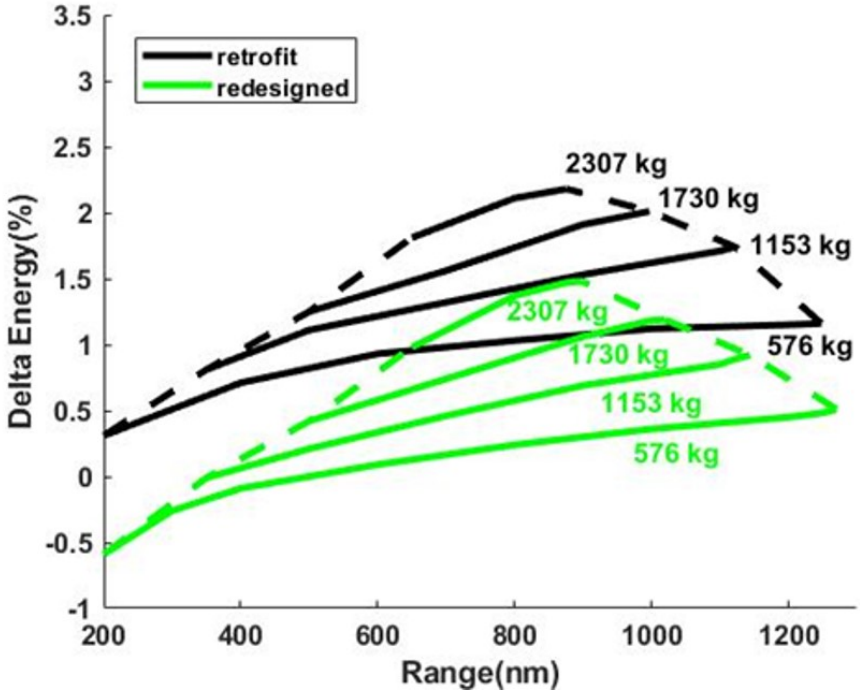


Figure 4.17: Delta energy % for 0.5 MW

A higher motor power on-take will improve the fuel burn benefit due to greater margin to redesign the engine cycle but will have operability issues and higher cruise turbine entry temperatures. The 1 MW redesigned hybrid has a roughly 45 K higher T40 than the baseline engine, while the 0.5 MW redesigned hybrid has roughly 22 K higher T40 than the baseline engine at cruise. This leads us to the conclusion that a higher power on-take would enable higher fuel burn benefits for redesigned cycles for the given case study. However, this power on-take may ultimately be limited by cruise turbine entry temperatures in cases where a higher margin for cycle redesign is available.

Finally, some light is shone on different power management strategies for the redesigned engine cycle. The difference between redesigned and retrofit delta energy is slightly higher for the results shown in 4.14 than Figure 4.18 by 0.2% corresponding

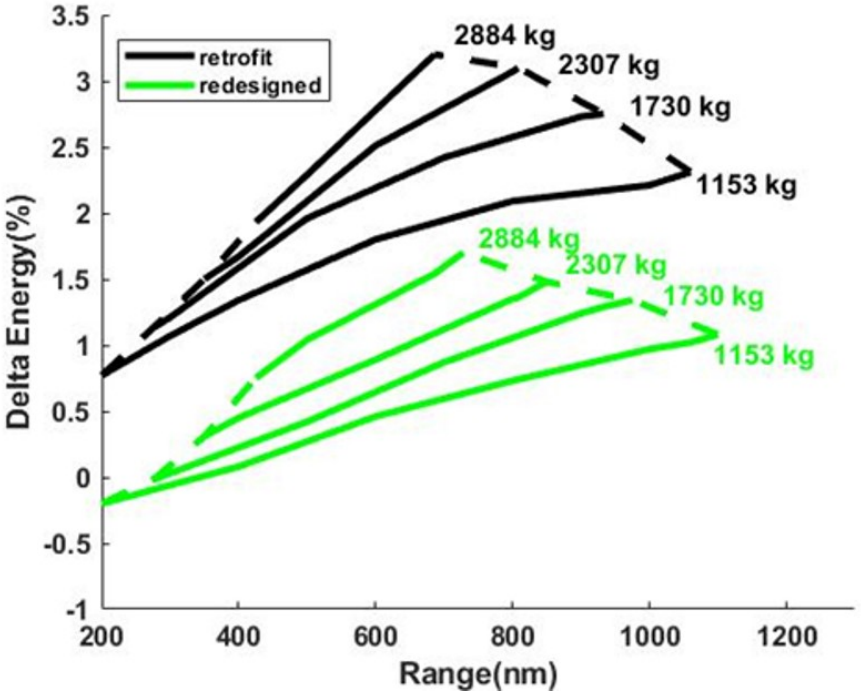


Figure 4.18: Delta energy % for 1 MW

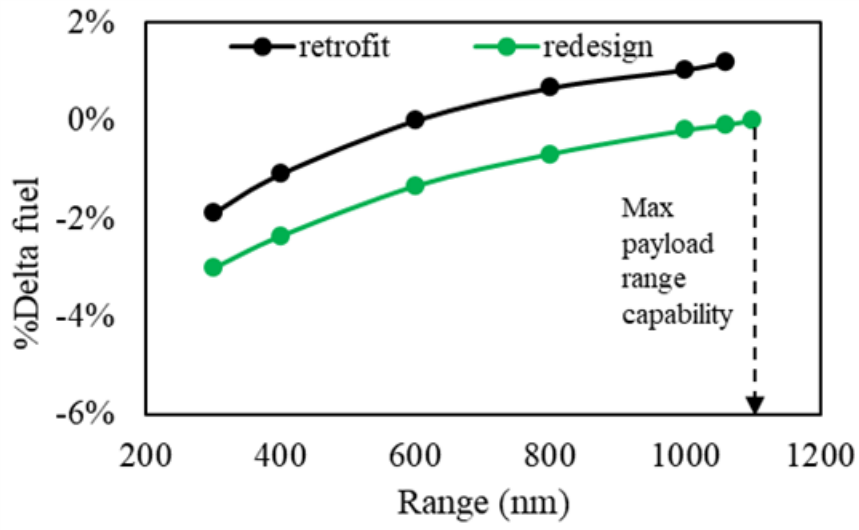


Figure 4.19: % Delta fuel burn for 1153 kg battery pack

to a battery size of 1153 kg. This difference is due to the better power management strategy of 1 MW and 400 kW at take-off and top of climb instead of 1 MW throughout, till the battery discharges. This difference of PMS is explained more in next sub-section. The identification of optimal battery size is heavily dependent on the operation of the aircraft fleet. It is seen from Figure 4.19 and Figure 4.20 that a 2307 kg battery pack has greater fuel burn benefit than an 1153 kg battery pack for

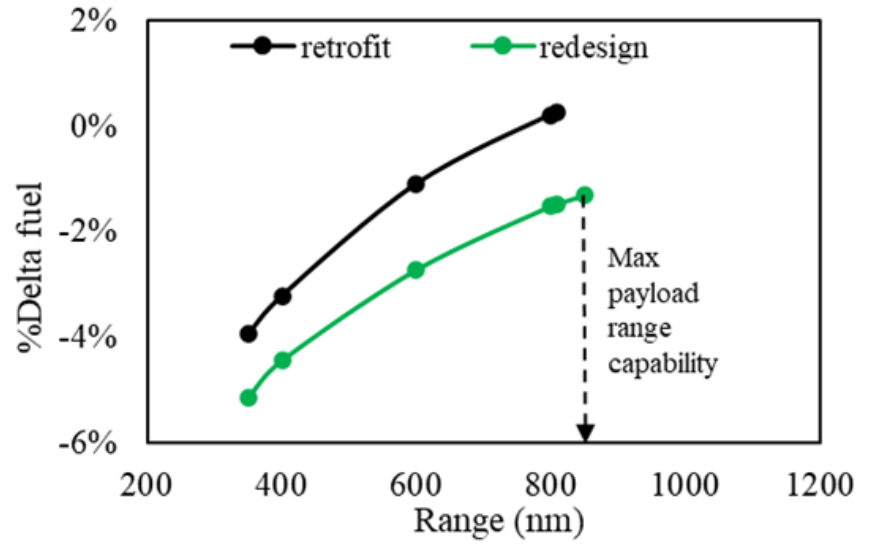


Figure 4.20: % Delta fuel for 2307 kg battery pack

all ranges below 800 nm but has a reduced maximum payload range capability by almost 300 nm. The push and pull between concentrated fuel burn benefit at lower ranges and greater penalty at higher ranges for different battery pack weights has been done in a more methodical manner in Section 4.3.

4.2.3 Impact of optimal PMS

This sub-section very briefly touches upon the impact of optimal PMS against a retrofit case. The same trends shown in Figure 4.16 are now recreated also with optimizing power management strategy.

Figure 14 illustrates the potential benefit arising from simply utilizing the battery in a more favorable manner albeit optimzing the PMS. The maximum fuel burn benefit from optimizing the power management strategy is on an average approximately 0.2-0.3%, which is less than the benefit from cycle redesign (0.9-1.0%). The power management trends are looked at and explained in detail in Section 2.2. This concludes the impact of assumptions on electrical systems sub-section. Next sub-section benchmarks the impact of GT technology level.

4.2.4 Impact of GT technology level

The TAY 651 hybrid results have been presented in the earlier sub-chapters. TAY 651 has been in service since 1990 [160] hence when hybridization will be applied, more efficient gas turbines will be available for the same thrust class. The next logical step would then be to analyze the impact of hybridization for a modern UHBR geared

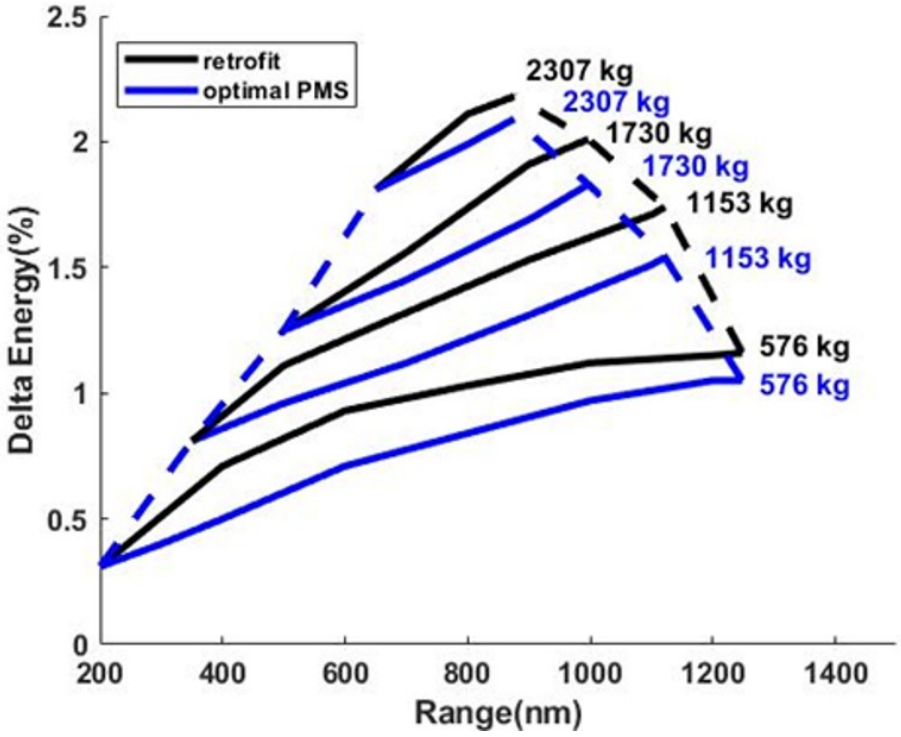


Figure 4.21: Retrofit vs Optimal PMS

turbofan engine with polytropic efficiency estimates for EIS 2035. In this section, hybrid engine cycle design is performed and presented for an entry into service 2035 turbofan engine. The engine cycle design and aircraft mission assessment methods are the same as described in the previous chapters. The engine cycle parameters are summarized in the Table 4.7. For the same electrical input power of 1 MW, the redesign cruise specific fuel consumption benefit is 0.97% relative to the retrofit cycle. This is slightly higher than the specific fuel consumption benefit which was obtained for the TAY redesign relative to retrofit. This brings us to a more fundamental understanding of parallel hybrid turbofan systems. It is intuitive to think that as the thermal efficiency of the gas turbine increases, the delta fuel burn percentage benefit of parallel hybrid electric systems should reduce. But the reduction in specific thrust has a greater impact than the improvement in thermal efficiency. Hence, for the same electrical power, there is a greater contribution to thrust from the electrical powertrain as lower specific thrust dominates thermal efficiency. This is the reason why EIS 2035 engine shows greater reduction in specific fuel consumption as compared to TAY 651 on application of same electrical power on-take.

The hypothesis proposed in the previous subsection is more easily understood

Parameter	Baseline	Retrofit, delta		Redesigned, delta	
CR BPR	13.8	13.8	0	14.9	8.2%
CR tsfc (g/kN.s)	13.4	13.4	0	13.27	-1%
CR OPR	41.5	41.5	0	43.2	4.3%
CR T40 (K)	1572	1572	0	1626	54
T/O T40 (K)	1800	1740	-60	1800	0
T/O T30 (K)	900	889	-11	900	0
TOC mass flow (kg/s)	150.4	150.8	0.3%	150.4	0
CR on-take (kW)	0	0	0	0	0
TOC on-take (kW)	0	400	400	400	400
T/O on-take (kW)	0	1000	1000	1000	1000

Table 4.7: Comparison of baseline, retrofit hybrid and redesigned hybrid engine cycles (EIS 2035)

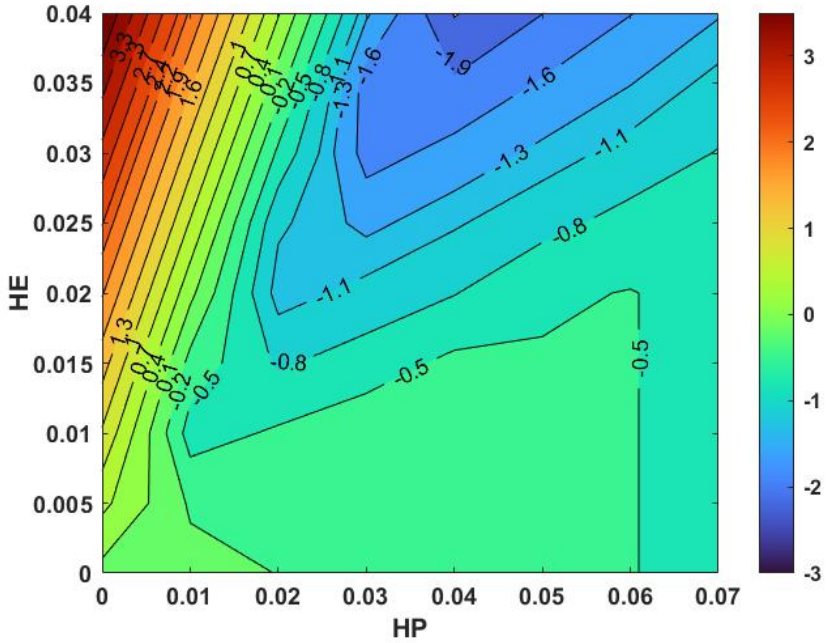


Figure 4.22: % Delta fuel burn hTAY vs cTAY

from the mission-level assessment. To cover the full design space for parallel hybrids, two specific parameters are used. These are HP and HE, called degree of hybridization by power and degree of hybridization by energy. Figure 4.22 shows the percentage delta fuel burn between hybrid retrofit TAY (hTAY) and baseline TAY (cTAY) on 500 nm. For 4% HP and 4% HE, the fuel burn benefit is 2.1% with a total battery weight of 2160 kg.

Figure 4.23 shows the percentage of delta fuel burn between hybrid retrofit EIS 2035 and conventional EIS 2035. For the same 4% HP and 4% HE, the percentage

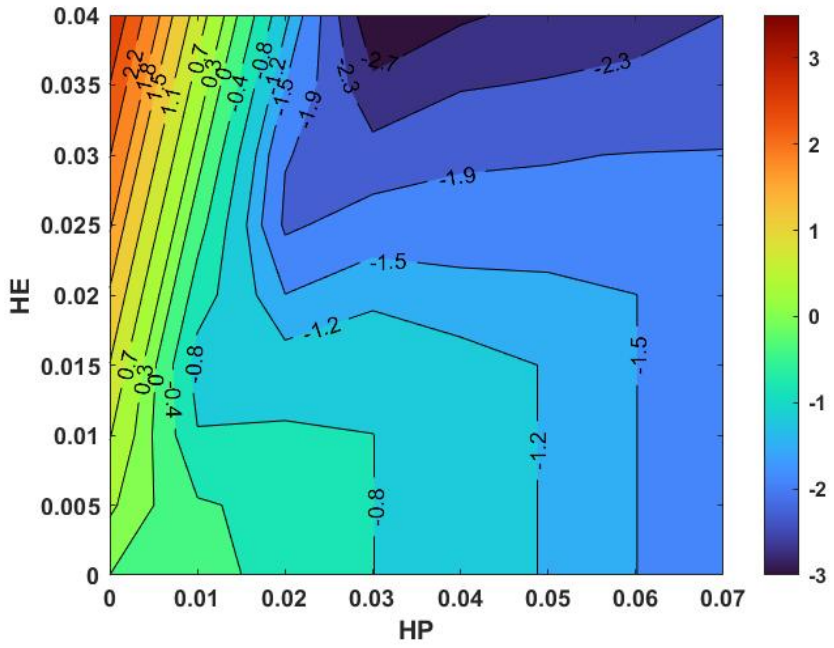


Figure 4.23: % Delta fuel burn, hybrid EIS2035 vs conventional EIS2035

fuel burn benefit is 2.8% with a total battery pack weight of 1400 kg. From these two contour plots, for the same HP and HE, hybrid EIS2035 has a greater fuel burn benefit than hybrid TAY relative to their respective basely baseline engines. This is reflected in the LP shaft power, as it reduces from 16.5 to 12 MW approximately from the TAY to EIS 2035. For the same HP and HE, hybrid EIS 2035 requires lighter battery and motor weights due to two reasons, lower shaft power requirement and higher shaft speed. The maximum LP shaft speed of the EIS 2035 is 11,200 RPM while TAY 651 is 8800 RPM [160]. The battery weights are only affected by the lower shaft power requirement and not the motor rotational speeds as line voltages are the same. The contribution of a higher motor power-to-weight ratio is much lower than the contribution of LP shaft power reduction to the fuel burn benefit for EIS 2035. The reduction in motor and inverter weights due to higher shaft speeds is only around 40 kg so it is safe to assume most of the fuel burn benefit for the hybrid EIS 2035 as compared to hybrid TAY 651 comes from the lower shaft power requirement.

Reduction in weights mainly due to lower shaft power requirement means that less fuel burn penalty is paid to carry the dead weight in the case of EIS 2035, and this is reflected in delta mission fuel burn in Figure 4.23. The trend of the energy burn is similar in both cases and is shown below in Figure 4.24 and Figure 4.25. But it can be seen even in energy burn, hybrid EIS 2035 has a significantly lower energy penalty than hybrid TAY. Figure 4.20 showed that 2-5% fuel burn can be saved with

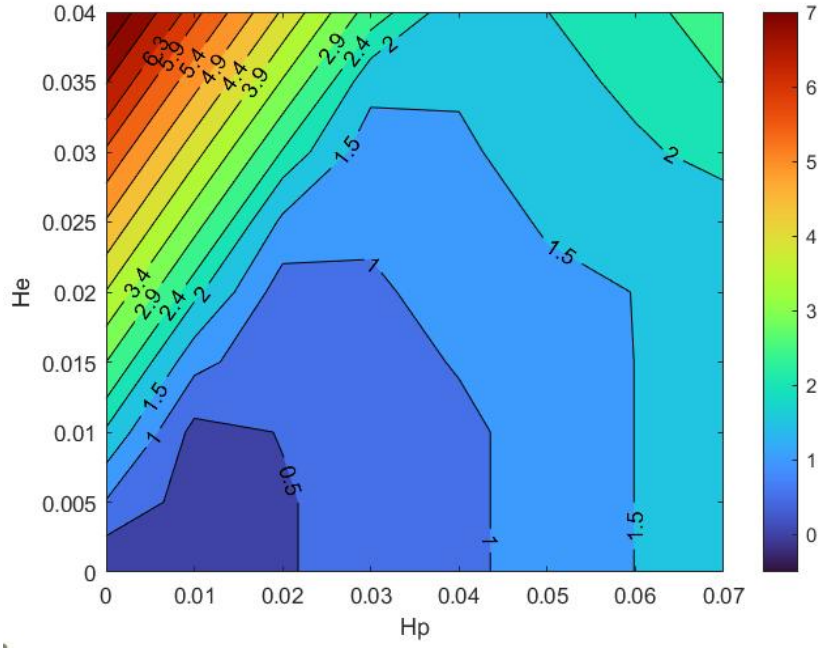


Figure 4.24: Delta energy burn (%), hTAY vs cTAY

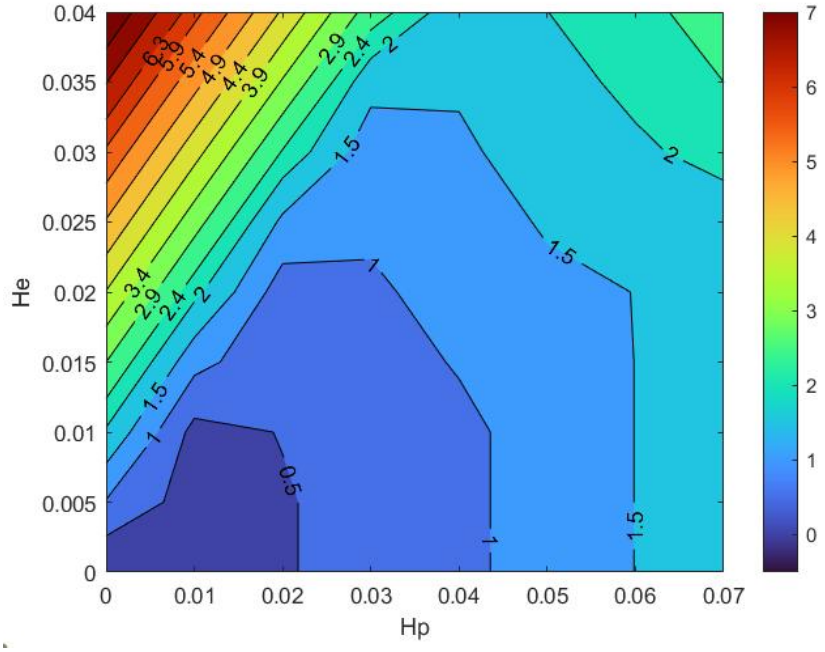


Figure 4.25: Delta energy burn (%), hybrid EIS2035 vs conventional EIS2035

a 2307 kg battery pack on a redesigned TAY. Since the benefit is 0.7-0.8% more on a hybrid redesigned EIS 2035 (difference between Figure 19 and Figure 20), the total benefit jumps to approximately 3-6%.

This concludes this section of the results where impact of all design parameters

has been quantified and the major conclusions were the requirement of battery energy of 750 Wh/kg, need for redesigned GT and integration of PMS with it to obtain the right combination of battery weight and motor power. Taking the learnings from this section, a more methodical integrated assessment is now performed in the next section where the focus is on electrifying EIS 2035 GT assuming a battery energy density upwards of 500 Wh/kg.

4.3 Integrated multi-mission assessment across aircraft classes

This section shows the 2nd major part of results, the integrated multi-mission assessment across aircraft classes. The inferences from previous section are directly implemented here so all the assessment is now only done for EIS 2035 baseline GT and EIS 2035 assumptions on electrical powertrain. The cycle design space is shown for SMR and regional turboprop platform, and then the optimal PMS trends are shown for redesigned and retrofit GT. Finally the maximum fuel burn possible is shown for all three aircraft, if a bespoke design is used for each mission range. Post this, the results from the multi mission assessment are shown and design scenarios are shown, and direct operating cost scenarios are shown. The results are shown more extensively for the two extremes of the design space, as Fokker 100 is explored in the previous chapter. Post the multi-mission and DOC assessment, a synthesis is performed showing a pareto front of DOC vs fuel burn benefit. The main purpose of the synthesis was to rationalize retrofit and redesigned HEPS across aircraft classes.

4.3.1 Gas turbine cycle design

Starting with the cycle design, the 3-point cycle design approach is again followed to redesign the gas turbine thermodynamic cycles with electrification. The results and trends are described for both SMR and turboprop test cases.

SMR test case

For the SMR test case, both retrofit and redesigned gas turbine cycle information are computed based on two gas turbine technology levels – EIS 2010 and EIS 2035. The thrust requirements for the three design points (MTO, MCL, CRZ) are shown in Table 4.8. Both the technology levels are just shown to once again prove the

inference obtained in section 4.2.4, so only EIS 2035 engine is used for later integrated calculations.

MTO Thrust (kN)	95
MCL Thrust (kN)	25
CRZ Thrust (kN)	18.8

Table 4.8: SMR thrust requirements

The temperature reduction for the retrofit case and specific fuel consumption benefit for the redesigned case as compared to the baseline is shown in Table 4.10. Both the cases are shown with T/O power on-take of 1.5 MW on the LP shaft, corresponding to 7% degree of electrification. The degree of hybridization by power at T/O and ToC is the same (7%) as explained in the previous section on Fokker 100 case study. The cycle-level benefit extracted from the EIS 2035 gas turbine is slightly higher than the EIS 2010 (Table 4.9) gas turbine, due to motor power being a greater fraction of LP shaft power. Again this is similiar to previous section, where lower specific thrust and improved core efficiency lead to a lower power requirement. The key point to note is that in the case of EIS 2035 SMR, redesign provides a benefit of 0.9% sfc benefit for a motor power of 1500 kW.

Parameter	**Baseline**	**Retrofit, delta**		**Redesigned, delta**	
CR BPR	5.7	5.7	0	6.1	7%
CR tsfc (g/kN.s)	16.6	16.6	0	16.5	-0.8%
CR OPR	24.7	24.7	0	25.6	3.6%
CR T40 (K)	1288	1288	0	1332	54
T/O T40 (K)	1641	1584	-57	1641	0
T/O T30 (K)	860	852	-8	860	0
Fan diameter (m)	1.65	1.65	0	1.65	0
CR on-take (kW)	0	0	0	0	0
TOC on-take (kW)	0	600	600	600	600
T/O on-take (kW)	0	1500	1500	1500	1500

Table 4.9: EIS 2010 SMR GT cycle data

The operability constraints on the compressors again remain same as the previous subsection. The impact of providing electric power on-take on the LP & HP shaft at top of climb is shown in 4.27 and 4.26. Only the top of climb is presented as it is the sizing point for compressors. The surge margin for the booster reduces on increasing electrical power on the LP shaft due to the components rematching. The booster surge margin drops to 10% on application of 1.5 MW at top of climb (14% degree

Parameter	Baseline	Retrofit, delta		Redesigned, delta	
CR BPR	15.8	15.8	0	17	7.6%
CR tsfc (g/kN.s)	13.2	13.2	0	13.1	-0.9%
CR OPR	39	39	0	40.5	3.8%
CR T40 (K)	1536	1536	0	1585	59
T/O T40 (K)	1890	1830	-60	1890	0
T/O T30 (K)	940	931	-9	940	0
Fan diameter (m)	1.98	1.98	0	1.98	0
CR on-take (kW)	0	0	0	0	0
TOC on-take (kW)	0	600	600	600	600
T/O on-take (kW)	0	1500	1500	1500	1500

Table 4.10: EIS 2035 SMR GT cycle data

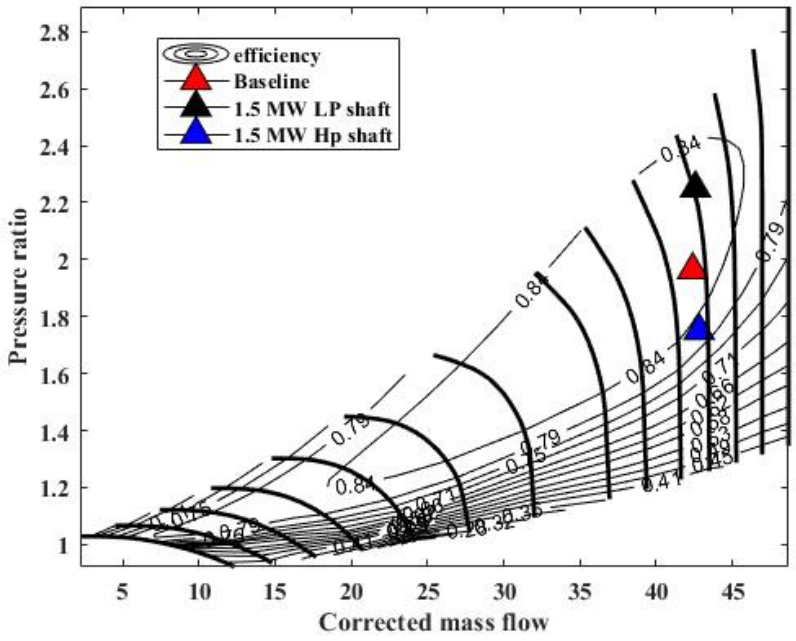


Figure 4.26: EIS 2010 SMR retrofit booster operating points, top of climb

of hybridization). It should be noted that this would not occur if it were a 3-spool or turboprop configuration where the LPC and fan are driven by different turbines, as explained in previous sections.It is possible that this margin can be increased by powering the HP shaft but this should be avoided to not overspeed HP shaft. There is potential for a combination of LP and HP power on-take to have best performance and this is recommended for future work and elaborated in the concluding section.

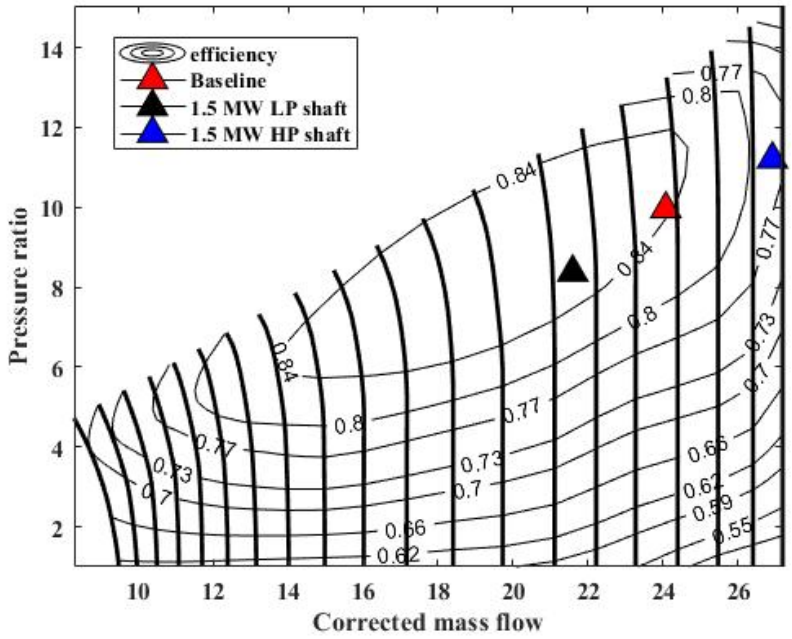


Figure 4.27: EIS 2010 SMR retrofit HPC operating points, top of climb

Regional turboprop test case

Within the regional turboprop case study, for the case that the electric power train drives the power turbine, the degree of electrification is not limited by component operability but by the power/thrust ratios, compressor polytropic efficiency and thermal management requirements for peak heat loads. Because the low pressure compressor and propeller are driven by their own turbines, the impact on operability is not extreme like before. Snyder[168] suggested a relationship for centrifugal compressor polytropic efficiency change with corrected exit mass flow. This relationship is used when assessing the hybrid cycle design space for the turboprop case. Figures 4.29 and 4.28 shows the cruise sfc for different target T40 and T30 at MTO for three degrees of hybridization. It can be seen from Figure 4.28 and Figure 4.29, that when the effect of resizing on compressor polytropic efficiency is considered the benefit in specific fuel consumption for redesigning for Hp=30% drops from 5.1% (Figure 4.28) to 3.7% (Figure 4.29). This drops shows that the benefit from cycle benefit diminishes for very high degrees of hybridization by power. The other parameter to consider is also the high CRZ temperatures on cycle redesign.

The CRZ T40 variation for the sweep of all T40, T30 and degrees of hybridization is shown in Figure 4.30. Beyond 30% Hp, the cruise temperatures will be very high (as seen from 4.30 and will dictate the core size. Hence after considering all factors,

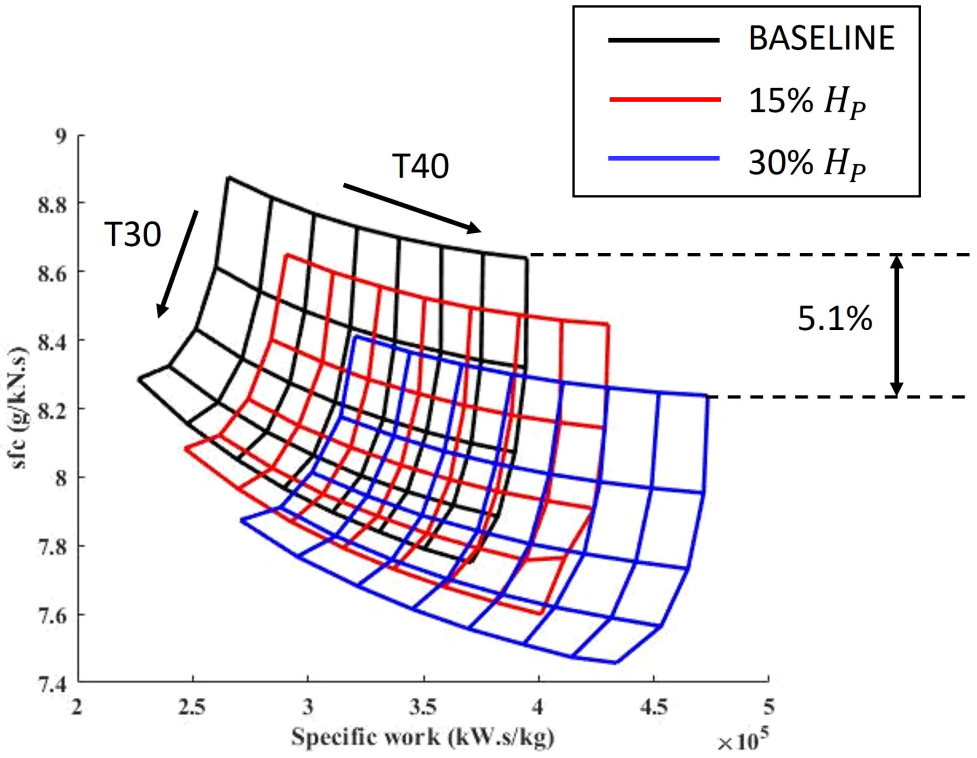


Figure 4.28: Turboprop cycle design space without efficiency correction

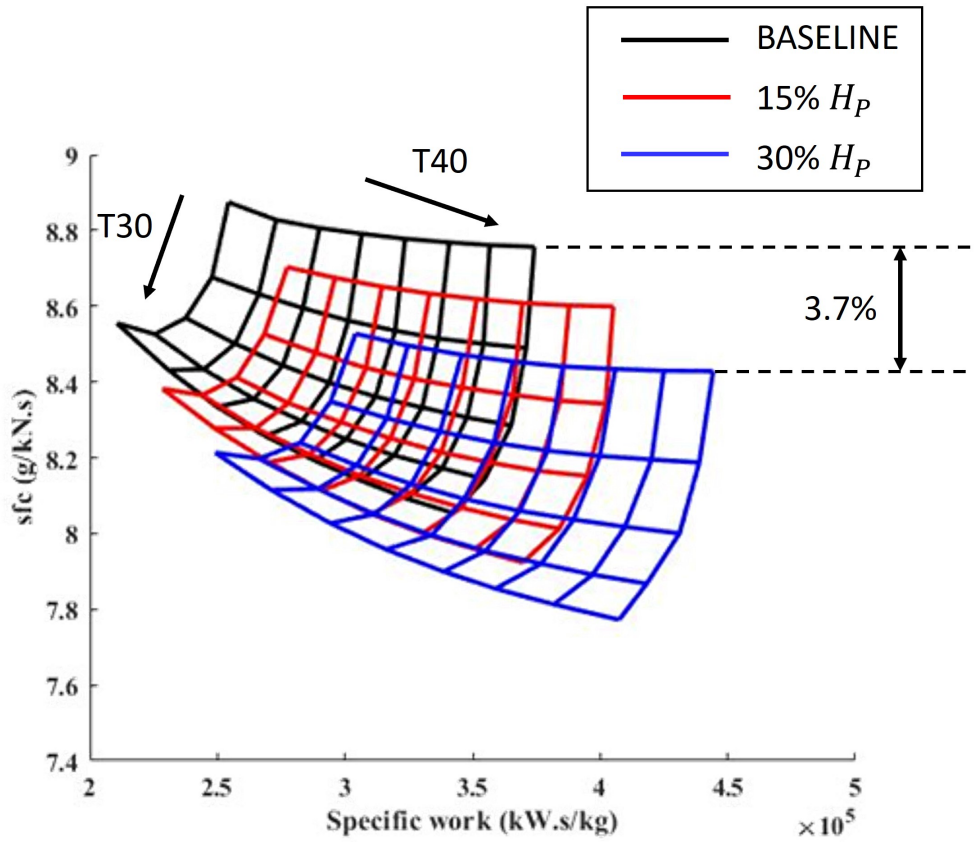


Figure 4.29: Turboprop cycle design space with efficiency correction

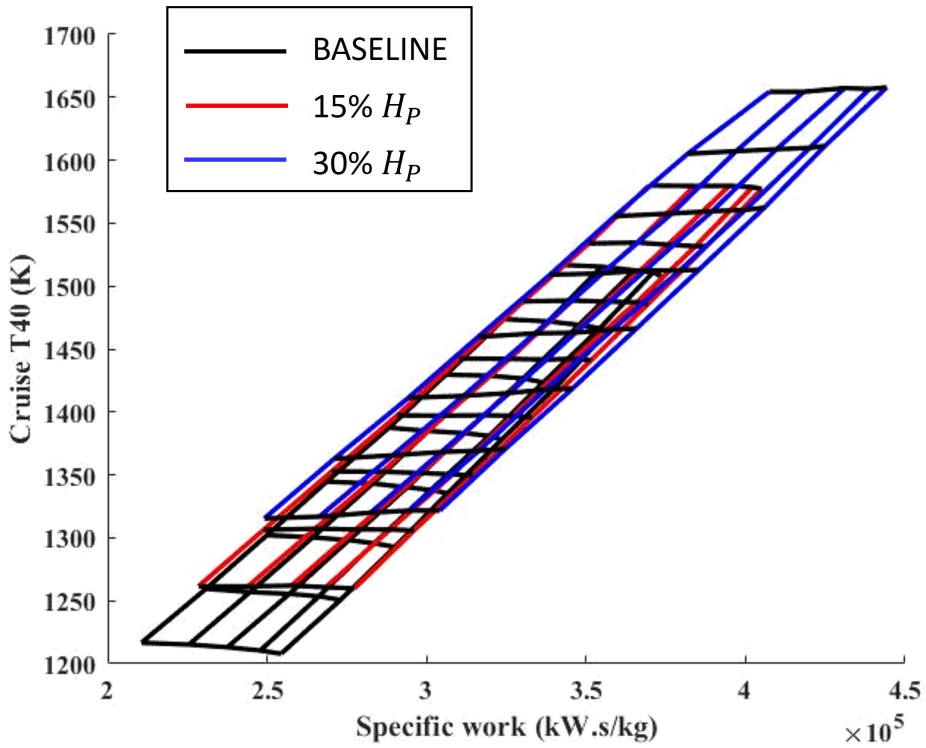


Figure 4.30: Cruise T40 variation with degree of hybridization

Parameter	Baseline	Retrofit, delta		Redesigned, delta	
T/O core flow (kg/s)	5.6	5.27	-6%	4.9	-13%
CR tsfc (g/kN.s)	8.4	8.4	0	8.25	-1.7%
CR OPR	18	18	0	19.1	6.1%
CR T40 (K)	1298	1298	0	1397	54
T/O T40 (K)	1600	1537	-63	1600	0
T/O T30 (K)	780	760	-20	780	0
CR Hp	0	0	0	0	0
T/O Hp	0.15	0.15	0.15	0.15	0.15

Table 4.11: EIS 2035 Turboprop GT cycle data

30% Hp is a limit on redesigning the turboprop engine cycle, with take-off and climb hybridization. Ultimately, the gas turbine cycle data for 15% Hp is summarized in Table 4.11. The trend remains the same as previous, and trade here is essentially between 1.7% sfc benefit from redesigning for 15% degree of hybridization against a saving of 63 K at MTO. This ends the cycle design section for the other two platforms, the next sub-section focuses on the optimal combination of PMS and cycle design for the platforms when minimization of fuel burn and direct operating cost. All the aircraft use EIS 2035 gas turbine as the baseline GT and the hybrid versions are compared against that.

4.3.2 PMS optimization and fuel burn benefit trends

The limits on electrification mentioned in the previous section, namely 10% DoH by power for both the SMR and regional turbofan, and 30% for the turboprop, are now applied at an aircraft mission level for all three test cases. The integrated PMS and cycle design methodology is utilized to optimize the combination of electric powertrain and gas turbine cycle for each mission range. Optimized power management strategy trends and fuel burn benefits for both retrofit and redesigned gas turbines are presented. EIS 2035 estimations of the electrical powertrain power density are used in the simulations as summarized previously in Table 4.6. The trends in optimal power management strategies are presented first and then fuel burn benefits are presented. There are variations in power management distributions due to different thrust/power ratios across aircraft classes. But the global trends are similar for all aircraft classes hence are bunched together. The power management strategy trends are assessed for three different purposes:

- To understand the difference in power management strategies between redesigned and retrofit gas turbines.
- To understand the difference in power management strategy trends with change in gas turbine technology.
- To understand the difference in power management strategies with different objective functions: direct operating cost, fuel burn or energy consumption.

PMS Variation with redesigned/retrofit

First up, the optimal power management strategies are compared for the retrofit and redesigned case for the SMR test case (Figure 4.31 & Figure 4.32).

The three main factors which dictate the optimal PMS are the electrical powertrain added weight, the benefit gained from core re-sizing and the battery efficiency. It can be noticed that the redesigned case always favors higher fraction of take-off and initial climb power on-takes as opposed to retrofit case. Take-off and initial climb power on-takes dictate the core size as shown previous section, hence the benefit coming from reduced specific consumption. In retrofit's case, the optimizer always tries to reduce discharge rates for the battery to have better efficiency and lower powertrain weights hence cruise is the favored flight segment. The lower discharge rates come from the lower currents which in turn come from the lower peak electrical powers.

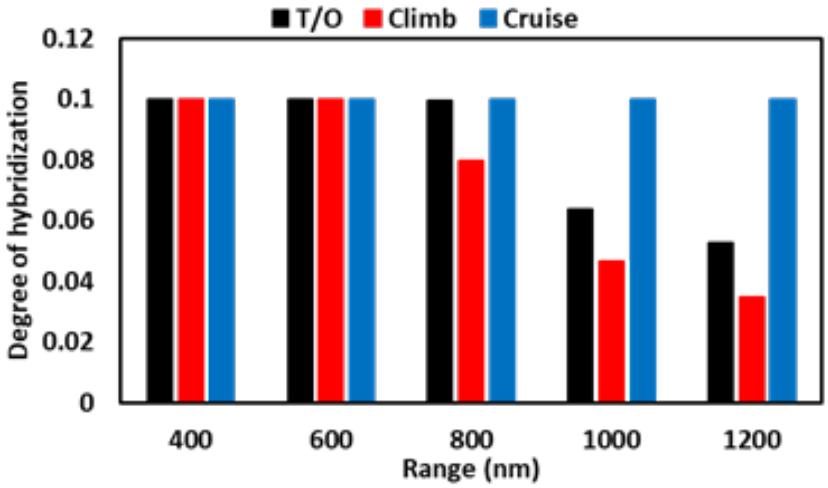


Figure 4.31: SMR Optimal PMS EIS 2035 (retrofit)

The distribution of battery and powertrain weights for the redesigned case are shown in Figure 4.33 and Figure 4.34 respectively.

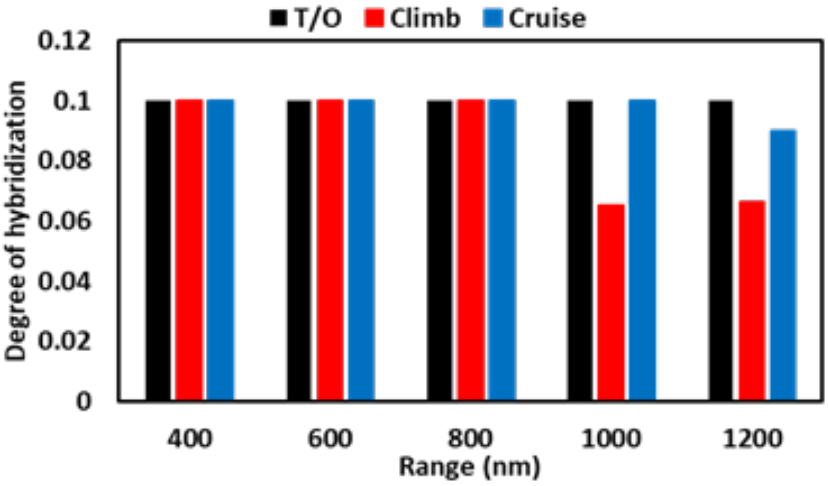


Figure 4.32: SMR Optimal PMS EIS 2035 (redesigned)

Parameter	Retrofit	Redesigned
Peak Motor power (kW)	1150	1950
Battery weight (kg)	2300	2400
EOR temperature (K)	1840	1880

Table 4.12: Comparison between redesigned and retrofit

It can be noticed that the battery weight consistently keeps increasing across mission ranges due to increase in cruise time resulting in a bigger battery pack, while the electrical power train weight decreases slightly due to reduction in thermal

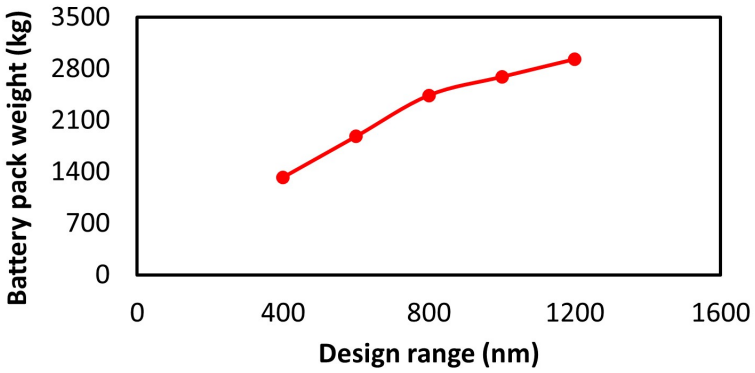


Figure 4.33: Battery pack weight variation across mission ranges (redesigned)

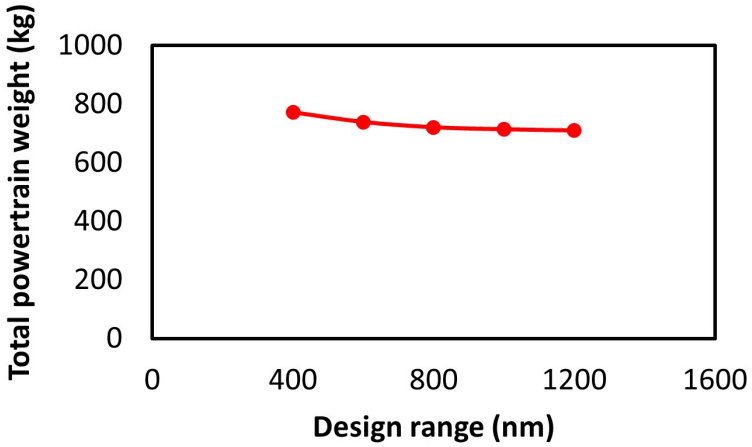


Figure 4.34: Electrical power train weight variation across mission ranges (redesigned)

management weight (this is due to bigger battery pack leading to greater efficiency due to lower currents). But, how about the comparison between redesigned and retrofit case in terms of power train weight, battery pack and gas turbine core temperatures. This comparison on 1000 nm mission range is shown in Table 4.12. It can be noticed that the retrofit case picks up similar levels of battery weight but is different in motor powers and cycle temperatures as discussed. The selection of battery weight becomes the crux of the multi mission assessment in section 4.3.3. Coming back to the PMS trends, the question which would arise at this point is whether these trends also hold true for the other test cases? The trends and comparison for the Turboprop EIS 2035 are shown in Figure 4.39 and Figure 4.38. The trends once again remain the same with redesigned hybrid optimal PMS having high take-off and climb power on-takes while retrofit hybrid having higher cruise power on-takes. It can be fairly understood

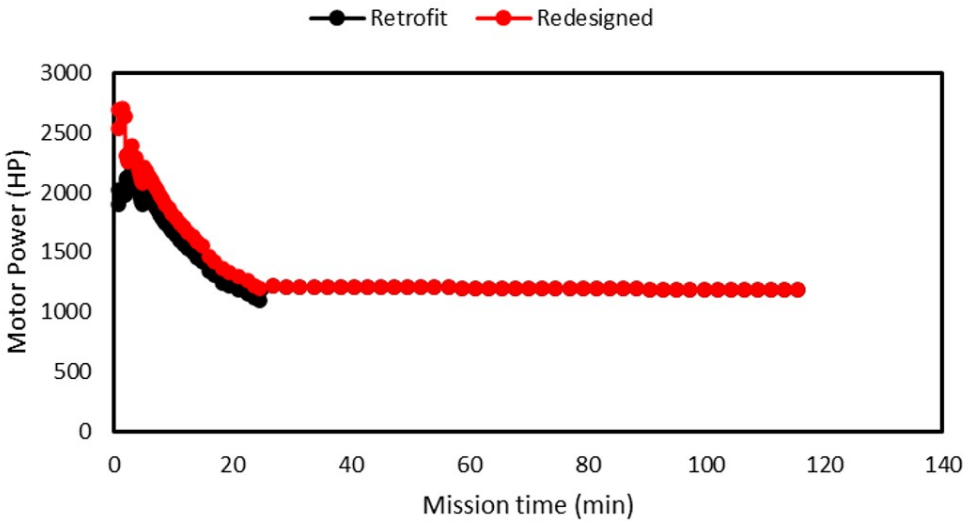


Figure 4.35: Motor power comparison on 1000 nm between redesigned and retrofit

that this a fundamental trade between take-off and climb on-take redesigned GT against cruise on-take driven retrofit GT. A comparison of motor power between retrofit and redesigned for SMR on 1000 nm is also shown on Figure 4.35. The difference between the motor powers at take-off and climb once again re-iterates the impact of cycle re-design. It should be noted that the retrofit trends shown in Figure 4.35 are also used for validation as described in Section 3.4. Now that the optimal PMS retrofit and optimal PMS redesigned have been described, the next sub-section deals with the PMS variation with GT technology.

PMS Variation with GT technology

Taking a step back to understand if the trends on PMS change with GT technology, EIS 2010 SMR GT is modelled and same integrated optimization is performed. The main aim to perform this exercise is to understand if the trends are same as EIS 2035 GT, then it can be safely extrapolated that off-design GT behaviour is not a dominating factor on the selection of optimal PMS strategy. Because there could be a potential difference that more efficient GT may lose more efficiency when run off-design as mentioned by Kyprianidis [78]. The figures below show the optimal power management strategies for EIS 2010 gas turbine technology (Figure 4.37 & Figure 4.36). The degree of hybridization increases as we move from EIS 2010 to 2035. This is due to the reduction in LP shaft power, which in turn is driven by reduction in specific thrust and improvement in thermal efficiency as mentioned but it can be also be seen that the difference in trends between redesigned and retrofit

remains the same as EIS 2035. Thereby, holding true the hypothesis which had been described in previous cycle design sections.

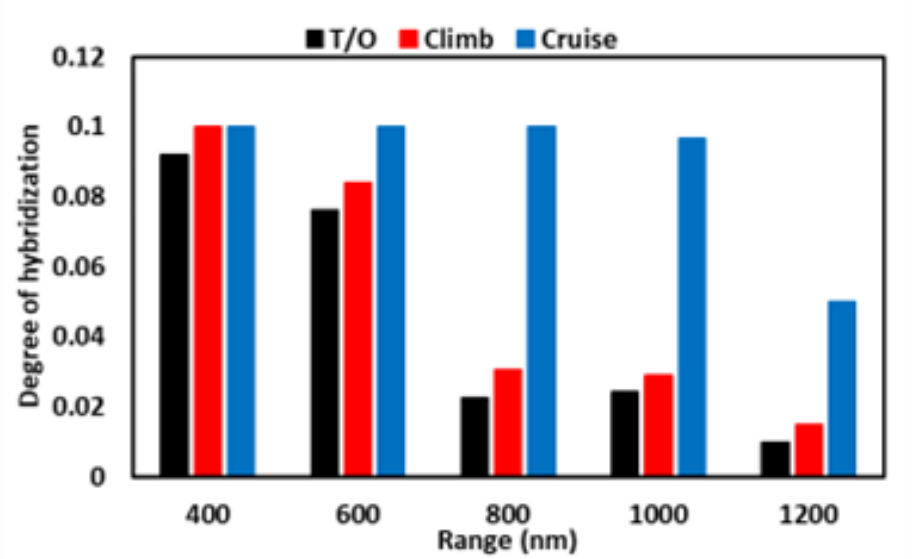


Figure 4.36: SMR Optimal PMS EIS 2010 (retrofit)

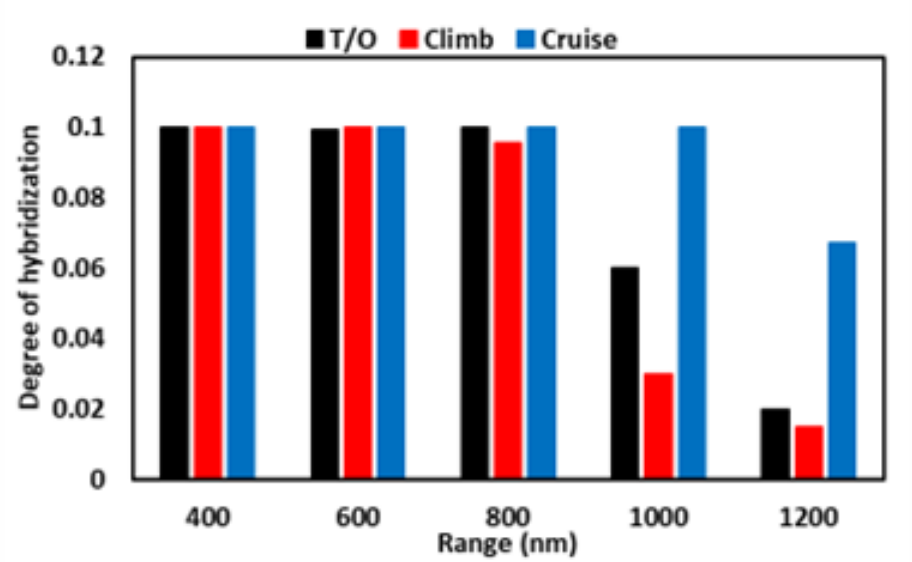


Figure 4.37: SMR Optimal PMS EIS 2010 (redesigned)

PMS Variation with objective function

The final sub section deals with the benchmarking the impact of objective function on optimal PMS. Two objective functions have been initially considered - Minimizing direct operating cost and fuel burn. This comparison is done only for the regional turboprop test case. This is because there is no direct operating cost benefit for

any hybrid SMR test case hence the optimizer always picks the non-hybrid baseline gas turbine as the best one. The DOC impact of HEPS on SMR test case has been explained later in detail in Section 3.5.

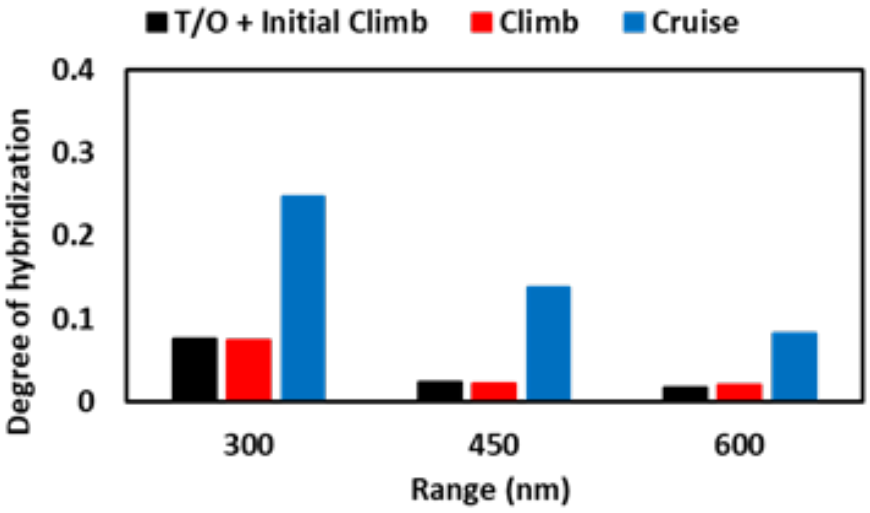


Figure 4.38: Regional Optimal PMS (retrofit)

The trends are initially shown for the retrofit (Figure 12) and redesigned (Figure 13) cases optimized for fuel burn. The trends are like the SMR test case favoring even greater hybridization fraction at cruise for retrofit and take-off for redesign. This is due to the lower non-dimensional cruise to take-off thrust ratio for the turboprop platform. For the case of DOC minimization, the trend changes significantly, as seen in Figure 14. The retrofit case is no longer favoring cruise but take-off and climb. This is due to the importance of gas turbine maintenance and battery replacement cost (explained in further detail in Section 4.3.4. The optimizer tries to pick a small battery pack just enough to reduce the number of HP turbine replacement cycles to get the turbine maintenance cost benefit(achieved by reduced take-off temperatures) and keep the battery acquisition and replacement cost low. This trade-off between turbine maintenance cost, fuel burn benefit and battery weight is essentially the driving factor behind HEPS design.

This concludes the PMS optimization trends, the next sub-section 4.3.2 deals with the maximum fuel burn benefit that can be obtained from redesigned HEPS across aircraft classes for different battery energy densities.

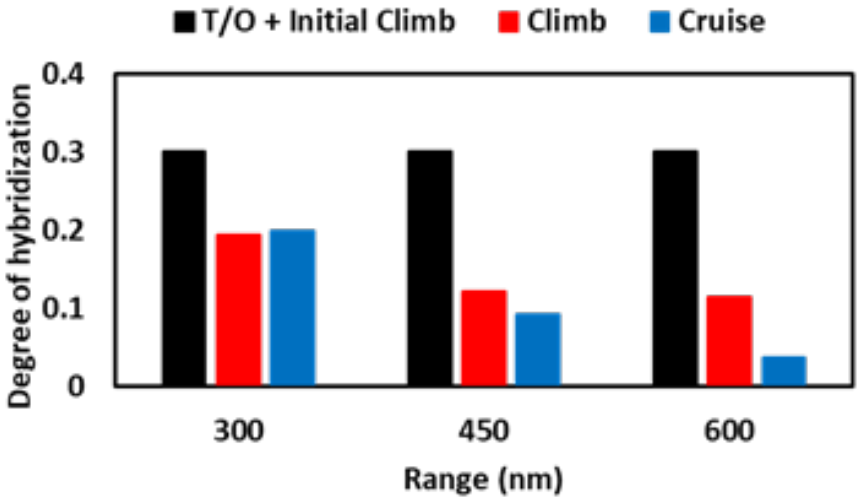


Figure 4.39: Regional Optimal PMS (redesigned)

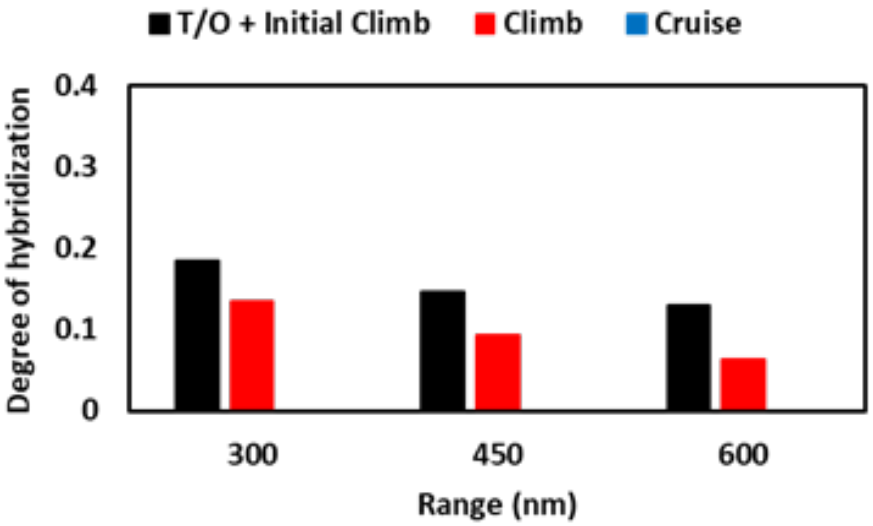


Figure 4.40: Regional Optimal DOC PMS (retrofit)

Comparison of fuel burn benefit for the two aircraft platforms

In this sub-section, the maximum potential percentage fuel burn benefit for the two aircraft platforms is shown (Figure 4.41). As explained before, EIS 2035 gas turbine technology level is used for all three platforms. The fuel burn benefit is calculated for 3 different design missions and for different battery technology level on three different aircraft cases. The caveats which should be kept in mind here is that each case corresponds to a unique redesigned propulsion system. Unique meaning that for each "design" range, a new propulsion configuration is selected. Let us now try to digress the results, it can be seen from the results that application of

electrification for the regional turboprop can offer substantial benefits, especially for short range missions, even for current and near future batteries technology. For the SMR as well as regional turbofan case the benefit is marginal for missions longer than 500nm and no benefit is calculated for any mission on current technology level batteries. The interesting thing to note here is that the level of benefit is similar for both SMR and regional turbofan case, showing that the size in fact isn't the driving factor in fuel burn benefit from HEPS but is instead the flight Mach and the aircraft power to weight ratio. The regional turboprop has a lower power to weight ratio which in essence drives a much lighter battery pack for a high level of degree of hybridization. Finally, it can be seen that 5-6% of fuel burn benefit can be obtained on 500 nm for both turbofan cases while the corresponding number is 12-16% for the turboprop case. Now, it remains to be seen that how much of this benefit remains intact after performing multi-mission assessment.

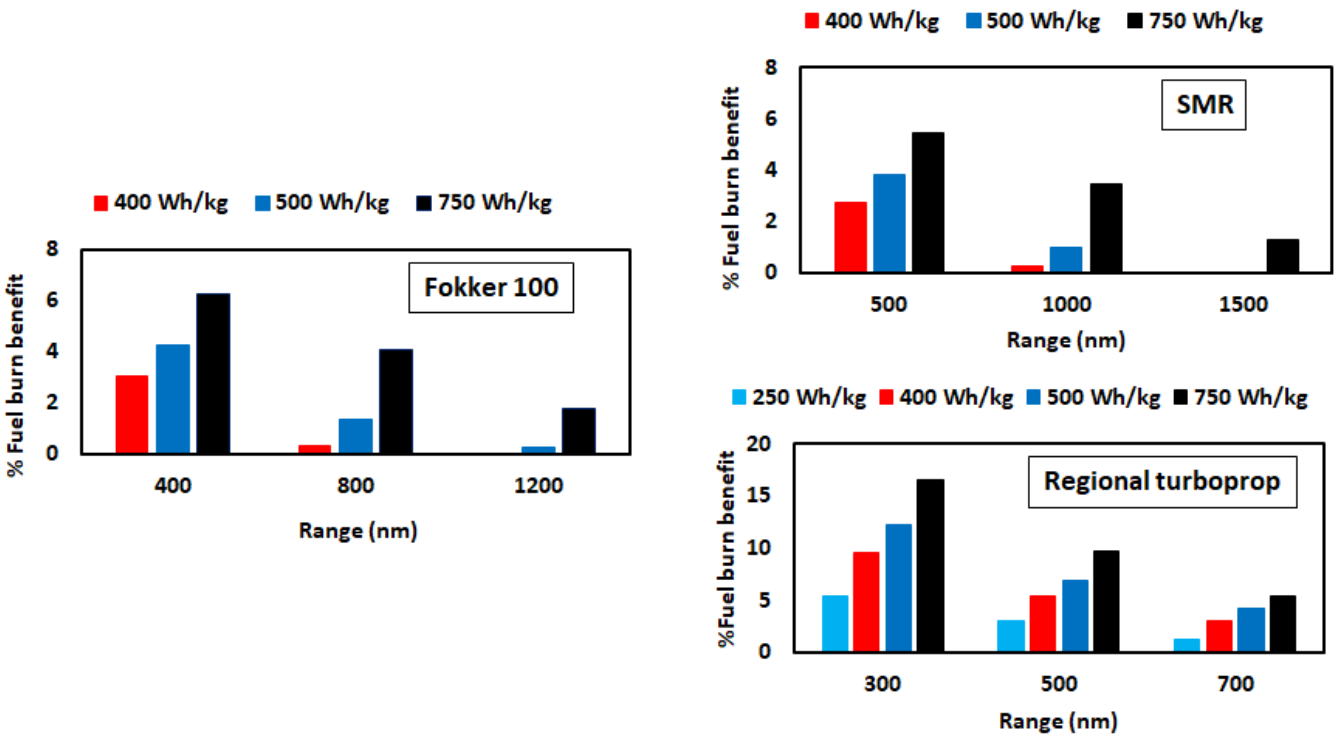


Figure 4.41: Percentage fuel burn benefit for SMR, regional turbofan and turboprop test case with varying battery energy densities

4.3.3 Multi mission assessment

This sun-section deals with the multi mission assessment of the two main aicraft - SMR and Turboprop. Given that regional turbofan had similar levels of benefit

as SMR, it makes sense to look at only SMR as the multi-mission trends would be similar. This multi-mission method (described in section 3.6) allows the identification of the optimum single configuration that can address the requirements of the relevant platform across a realistic off-design mission fleet cluster.

SMR test case

The designed propulsion configuration shown in Figure 4.33 is used for this assessment. Detailed off-design mission operation is only shown for two different design ranges of 400 nm and 600 nm, in Figure 4.42 & Figure 4.43, respectively. The results shown correspond to the redesigned case with battery energy density of 750 Wh/kg, on a baseline aircraft design range of 3200 nm. First thing that can be noticed is the loss of payload-range capability when sizing the HEPS at both design range of 400 nm and 600 nm as compared to baseline EIS 2035 max payload range of 3200 nm.

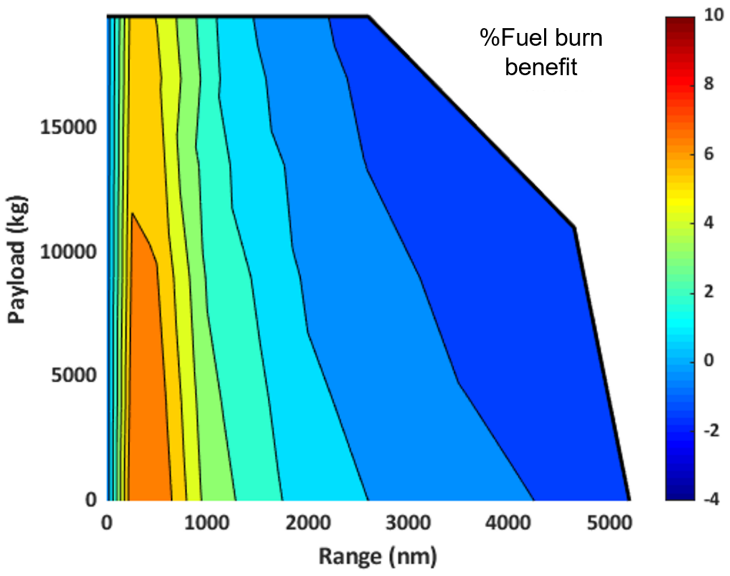


Figure 4.42: SMR test case, 400 nm design range, redesign

A HEPS design range of 600 nm has greater peaks of fuel burn benefit between 300-800 nm but beyond that it is worse and has higher penalties at longer ranges. From this it can be concluded that because the fuel burn benefit is in single digit for the SMR test case, it is better to go with as small a battery pack as possible to have no or little fuel burn penalty on slightly longer ranges. This would potentially lead us to select the 400 nm design configuration over others, which on 500 nm economic mission translates to 5% fuel burn benefit. This is slightly lower than the fuel burn

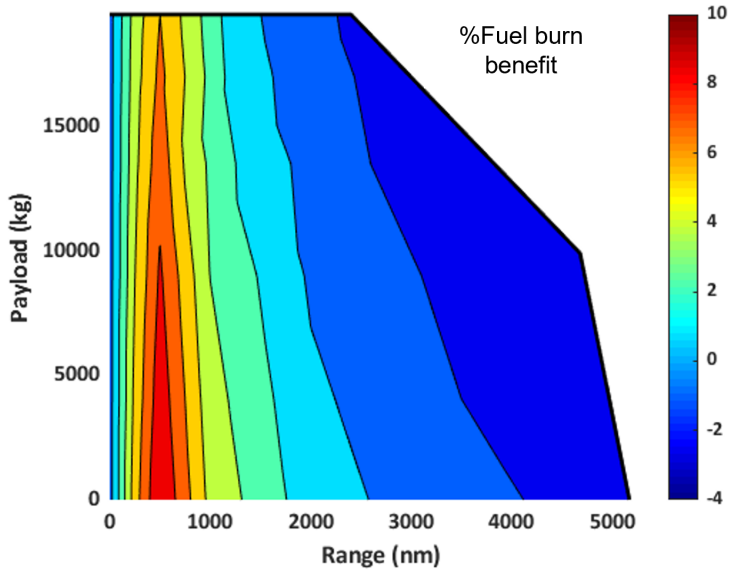


Figure 4.43: SMR test case, 600 nm design range, redesign

benefit of 5.5% obtained by the propulsion system that is designed for the 500 nm (Figure 4.41). When all the design configurations from 300 to 700 nm are run across off-design mission cluster, the actual average fuel burn benefit is shown in Figure 4.48.

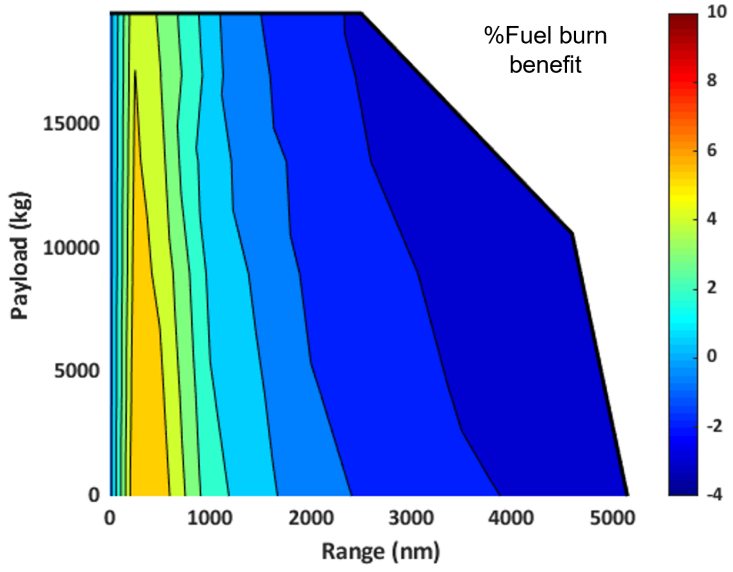


Figure 4.44: SMR test case, 400 nm design range, retrofit

Similar trends are also seen for the retrofitted case, where the HEPS design range of 400 nm (4.44) is again favorable against 600 nm (Figure 4.45) when a complete off-design operation is considered. Using the direct operating cost assumptions shown

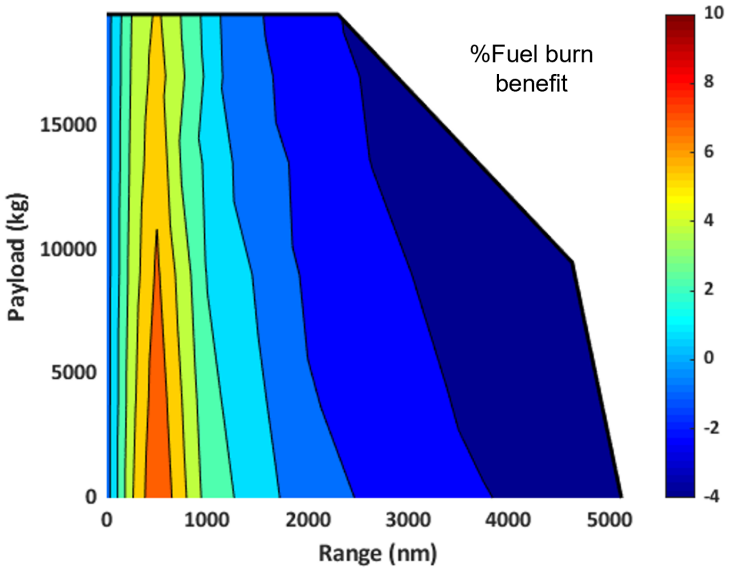


Figure 4.45: SMR test case, 600 nm design range, retrofit

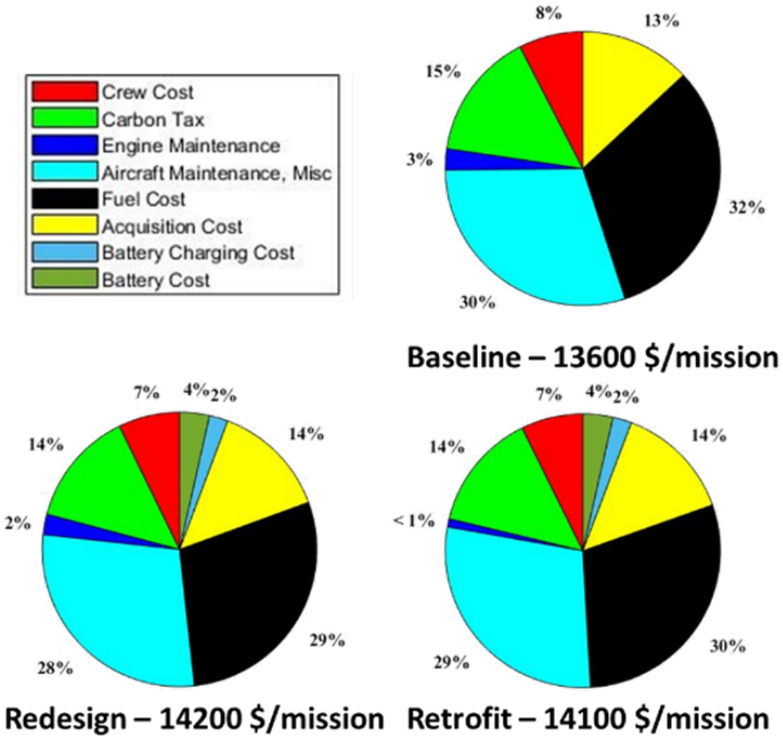


Figure 4.46: Direct operating cost comparison, SMR

in Section 3.5, the direct operating cost was evaluated based on a 500 nm mission for all 3 cases; baseline, retrofit and redesigned. This is presented in Figure 4.46 for the selected design configuration of 400 nm. The retrofit case has a penalty in DOC of 3.6% relative to baseline while the redesigned case has a penalty of 4.4%. The retrofit case has a lower penalty due lower turbine entry temperature translating in lower

engine maintenance cost. This difference can also be noticed in Figure 4.46, where if the pie charts between retrofit and redesigned are compared, the main differences are in the percentages of Engine maintenance cost (lower for retrofit) and fuel cost (lower for redesigned). Also when comparing either of the hybrid cases against baseline engine, the additional elements are the battery charging cost (electricity cost to recharge batteries) and battery cost (battery acquisition cost). The retrofitted case has an average of 1.5% lower fuel benefit than the redesigned case across the mission spectrum (average difference between Figure 4.42 & Figure 4.43). Since both the retrofit and redesigned cases have a penalty in DOC relative to baseline, it is better to go for the redesigned case due to higher fuel burn benefit.

Based on the observations and discussions above, two potential scenarios are devised, both utilizing redesigned parallel HEPS at 400 nm.

Scenario 1 : When all the different "design" range configurations were run at a set of off-design mission cluster (obtained from 3.6), a cumulative average fuel burn benefit can be obtained as seen in Figure 4.48.There is marginal difference between designs at 400 nm and 500 nm, but the lower battery pack of 400 nm makes that the selected "design" range configuration. The final outcome with the super imposed off-design mission cluster can be seen in Figure 4.47, with the final cumulative fuel burn benefit pegged at 2.6%, at a DOC penalty at of 4.4 % on economic mission (4.46. It was also estimated that this configuration gave an LTO NOx reduction of 4.7%.

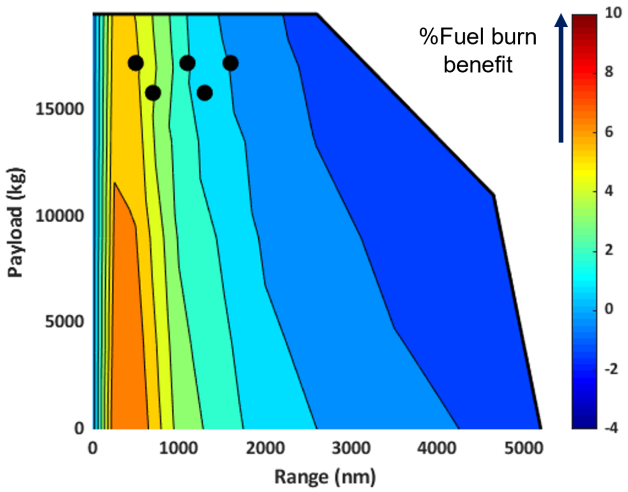


Figure 4.47: Scenario 1, SMR

Scenario 2 : Given that all the off-design mission cluster do not fly at peak payload capacity, a better idea could be the batteries can be placed in cargo hold

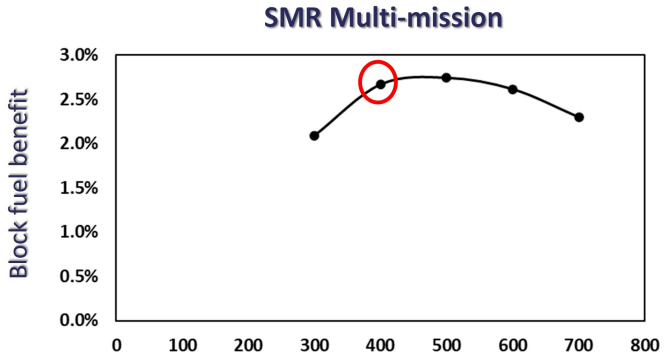


Figure 4.48: Multi mission fuel burn benefit, SMR

with reduced maximum payload capability. This will lead to lower landing gear and operating empty weight, translating in extra fuel burn benefit, albeit at the cost of reduced payload capacity. The payload capacity is still maintained such that it covers the off-design mission cluster capability. Performing this exercise using 400 nm design range configuration, translates into extra 0.6% fuel burn benefit as compared to Scenario 1.

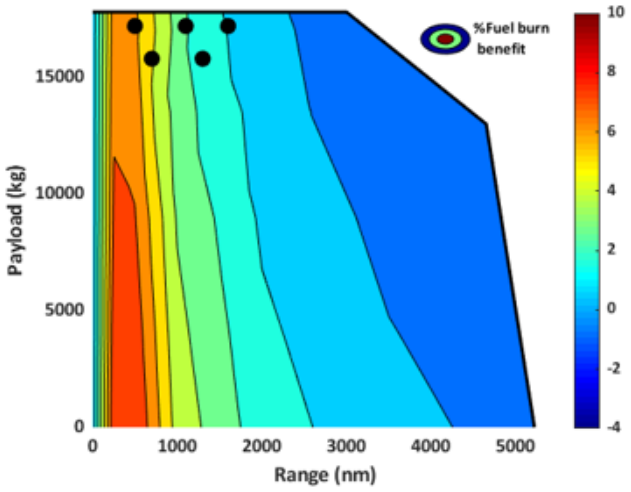


Figure 4.49: Scenario 2, SMR

Regional turboprop test case

Similar multi-mission exercise was also performed for regional turboprop test case using the off-design multi-mission cluster developed in 3.6. As the level of fuel burn benefit was an order of magnitude higher than the SMR test case, two extreme scenarios are proposed, one which targets high DOC benefit, time on wing and minimal fuel burn benefit. And second which targets maximum fuel burn benefit.

For regional turboprop studies to target an earlier EIS, 500 Wh/kg battery energy density is used.

Scenario 1 : This is the scenario which targets a high time on wing, and direct operating cost benefit (this the set where PMS is optimized for DOC, seen in Figure 4.40.

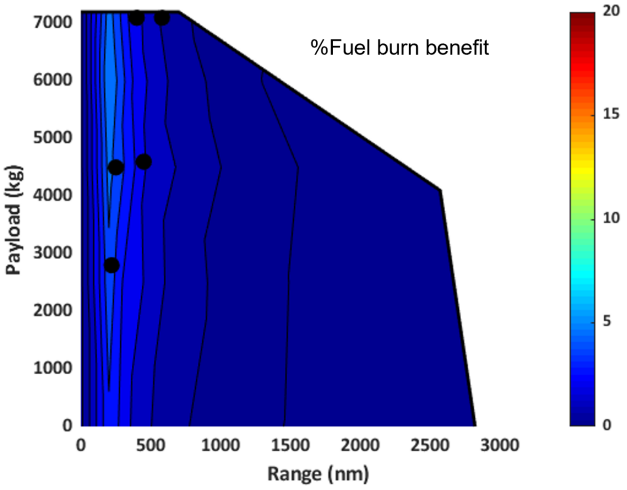


Figure 4.50: Overall fuel burn benefit, regional turboprop, Scenario 1

In this scenario as small battery packs were used, they have been put in cargo baggage and payload is slightly penalized. This allows for minimal to no changes on both the aircraft and engine side. The outcome can be visualized in Figure 4.50, with all the off-design mission cluster covered. The cumulative % fuel burn benefit across the cluster was found to be 3% and 3% DOC benefit was also obtained. As a high degree of hybridization is applied during take-off and climb as visualized in Figure 4.40, a 15% LTO NOx benefit can also be obtained in this scenario. The final outcome is visualized in Figure 4.50.

Scenario 2 : This is the scenario which targets maximum fuel burn benefit. Because the off-design mission cluster for ATR is concentrated at low ranges, 300 nm "design" range configuration was found to be the most beneficial in terms of fuel burn benefit. By utilizing this configuration, a cumulative average 10% fuel burn benefit and 2.4% direct operating cost penalty can be obtained compared to the baseline non-hybrid. Even though the gas turbine cycle is re-sized, the LTO NOx emissions reduction is 16% as compared to the baseline engine. This is all driven by the lower tsfc at take-off and climb.

Finally the DOC breakdown is also shown on economic mission for all three cases,

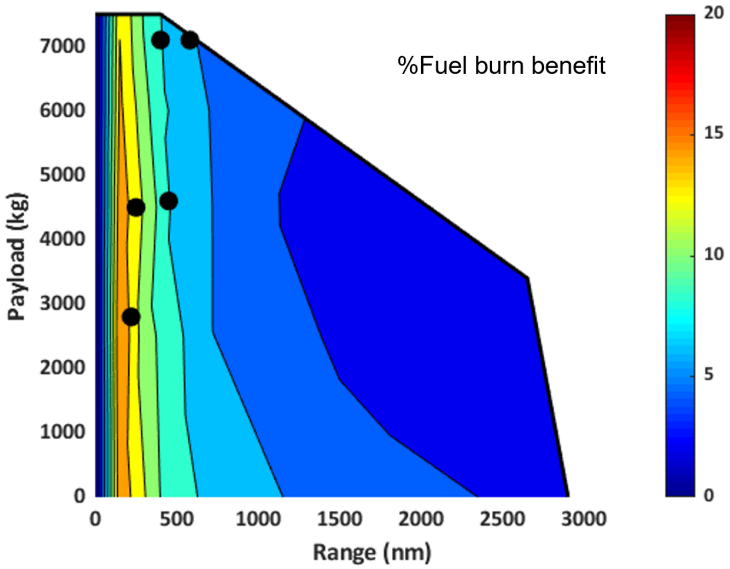


Figure 4.51: Overall fuel burn benefit, regional turboprop, Scenario 2

baseline, optimal retrofit and redesigned case using the data and method from 3.5. This is visualized in Figure 4.52. The big difference clearly is in the maintenance cost between retrofit and redesigned engine. Another difference is also the reduced fuel burn cost, once again highlighting the push and pull between fuel burn and direct operating cost reduction. These trends are synthesized in Section 4.3.5, but before that a short section is provided which expands on the direct operating trends variations and variation of optimal PMS in different scenarios.

4.3.4 Direct operating cost trends

This sub-section deals with the some trends on direct operating cost to understand how the DOC design space changes with variations in assumptions on number of battery life cycles, HPT maintenance cost, fuel price, battery acquisition cost and carbon tax. Once the single variable trends are shown, the the variables with highest impact on DOC are selected and simple two variable outcomes are shown. Post this, the optimal PMS trends journey towards minima DOC are shown for the regional turboprop.

SMR test case

The initial set of DOC sweeps are shown for the SMR test case, using the baseline numbers from Table 3.10. It should be noted that the starting numbers in Figure 4.53 are different than the numbers from 4.46 as the PMS used is different. The

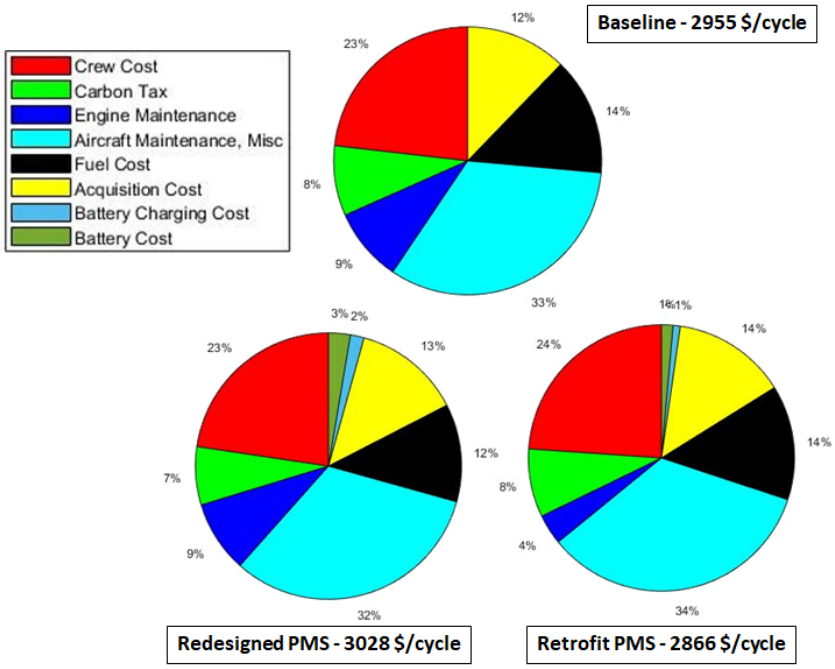


Figure 4.52: Direct operating cost comparison, Regional turboprop

sweeps produced in Figure 4.53 use only a take-off and climb 10% HP boosting as the aim was to get minimal DOC penalty starting points. All the plots in Figure 4.53 use a parameter called Delta DOC, which is defined as the difference between HEPS DOC and baseline non hybrid DOC.

Starting with the Delta DOC variation against engine overhaul cost/turbine maintenance cost, it can be seen the delta DOC for the retrofit case changes drastically with this parameter, while the delta DOC for the redesigned case remains same. This makes sense as the redesigned GT essentially has the same number of HPT cycles while the main selling point of the retrofit case is the high HPT cycles which translates into low maintenance cost. The impact of carbon tax is more significant for the redesigned case as the fuel burn benefit is greater compared to the retrofit case. Similar trend is also observed with changes in fuel price for the same reason. The trends of both battery acquisition cost and battery cycles to failure are the same for both retrofit and redesigned HEPS as both have the same battery pack sizes. It can be noticed is that the parameters which have the maximum impact on DOC are the battery cycles, fuel price and engine overhaul cost(retrofit). So, now 2 variable contour sweeps are performed to get the delta DOC numbers for different scenarios.

The impact of dual variations in battery cycles and fuel price can be visualized in Figure 4.54. It can be seen that even for extremely optimistic assumptions on either of the two parameters, the delta DOC is always penalizing for redesigned HEPS case.

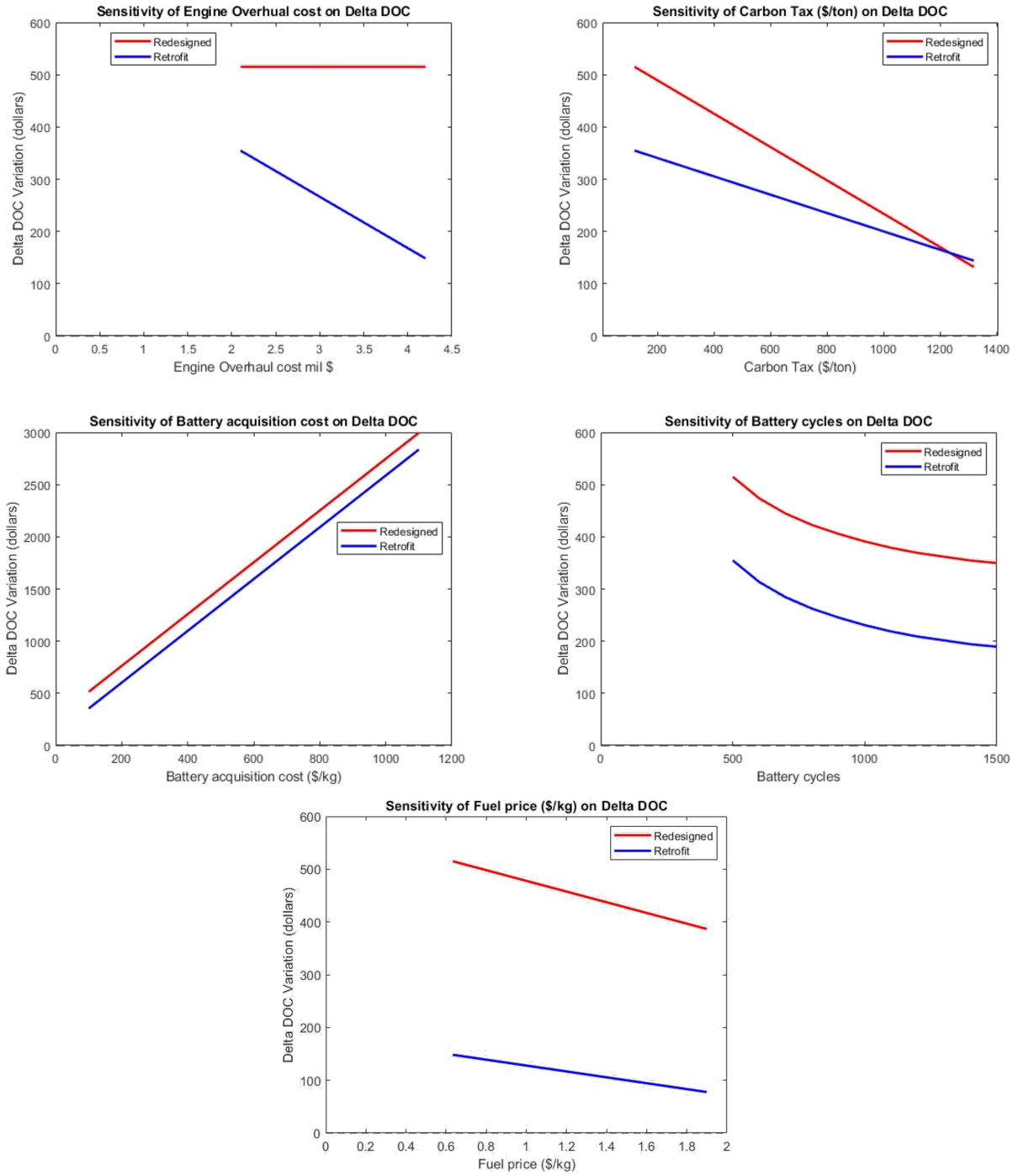


Figure 4.53: Delta DOC trends for single variable variations

Similar trends are also obtained for the retrofit case in Figure 4.55 but the real game changer is when the retrofit sweep is repeated for twice the turbine maintenance cost. This can be seen in Figure 4.56, where some regions in the top breakeven on DOC or even have a slight DOC benefit. This is an important inference and which might push for a retrofit HEPS case as the turbine maintenance cost increases.

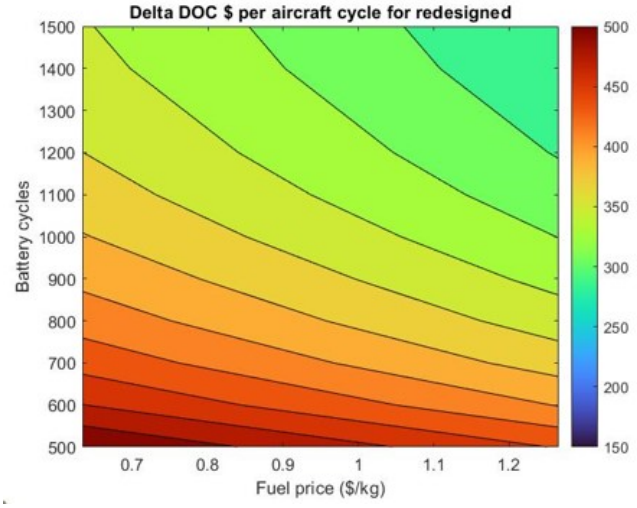


Figure 4.54: Delta DOC variation for redesigned

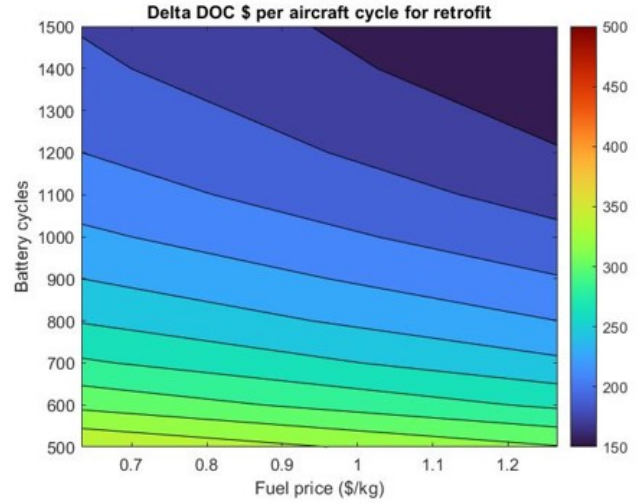


Figure 4.55: Delta DOC variation for retrofit

Regional Turboprop test case

Now moving onto the regional turboprop test case, the trends for optimal PMS are shown with varying objective functions (from min fuel to min total DOC). The trends for retrofit HEPS is shown in Figure 4.57 while the trends for redesigned HEPS are shown in Figure 4.58. Optimal PMS trends are performed for four objective functions - minimization of fuel burn, minimization of maintenance cost and fuel price, minimization of DOC with carbon tax and without carbon text. Focussing initially on the trends for retrofit, it can be seen that the trends in PMS almost reverses from cruise power on-takes to T/O and climb power ontakes. The T/O and climb on-takes are even more extreme when only maintenance cost and fuel price is considered, as the battery size isnt accounted for in this objective function. The

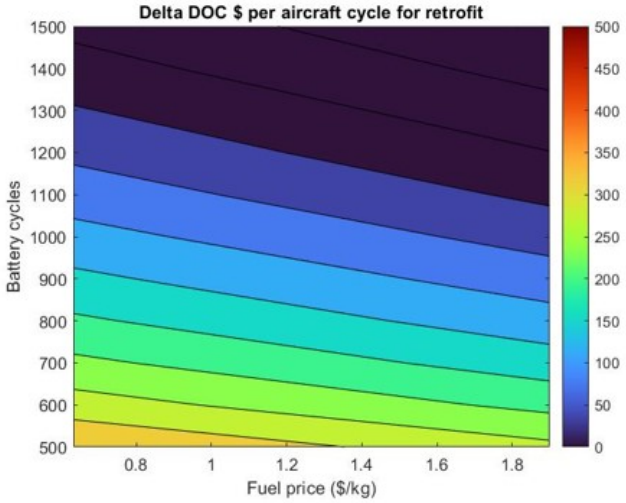


Figure 4.56: Delta DOC variation for retrofit for double overhaul cost

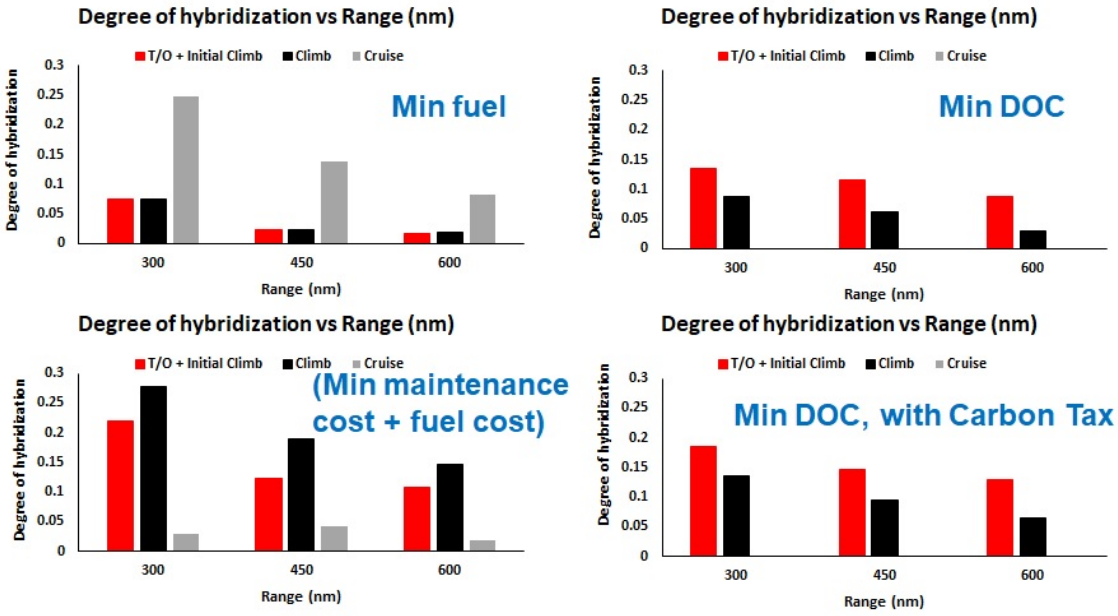


Figure 4.57: Optimal PMS ATR retrofit

optimal PMS for total DOC in the end show that effectively the strategy is to get the HPT maintenance cost/life benefit but at as small battery pack as possible, hence not that high T/O and climb on-takes.

Looking at the trends for redesigned case (Figure 4.58, the variation isn't as drastic as the retrofit trends but the trends variations are in reverse with the change from T/O and climb on-takes to climb and cruise on-takes. This is due to the extra benefit obtained from cycle re-design in the loop. This concludes the sub-section on DOC trends but a clear synthesis will be helpful to understand the final design trade choices across the aircraft classes.

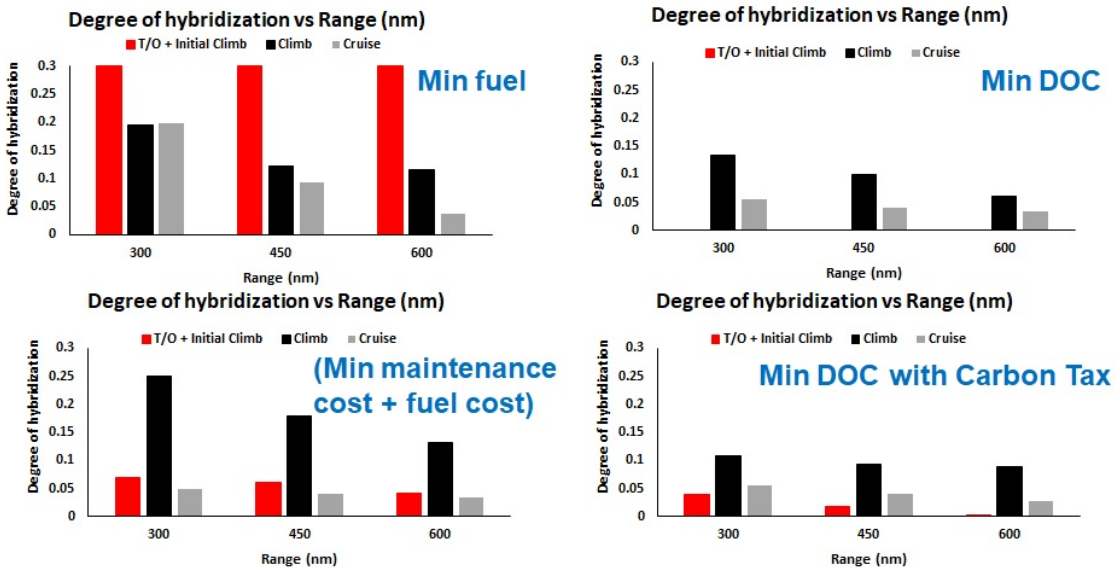


Figure 4.58: Optimal PMS ATR redesigned

4.3.5 Synthesis

In the previous subsections, three aspects of HEPS – gas turbine cycle design, optimal PMS, multi-mission assessment and DOC trends were covered for both test cases. In this section, a synthesis of those is provided and explicit trends between direct operating cost and fuel burn benefit are presented. A pareto front was obtained by exploring a full factorial on degree of hybridization across the design space. For a fair comparison, a 500 Wh/kg of battery energy density is used for both SMR and regional turboprop platforms. The regional turbofan has similar performance to SMR case, hence the pareto isn't developed for it.

Figure 4.59 summarizes all the trends for both aircraft classes. An explanation is now provided each of the trends:

- In all 3 pareto fronts, the maximum fuel burn benefit is restricted by the maximum aircraft ramp weight limit and maximum degree of hybridization by power. But this number is more critical for SMR as the max ramp weight essentially prevents putting bigger battery packs on. On the other hand, the maximum DOC benefit is limited by the turbine replacement cycles and battery cycles.

- Between redesigned and retrofit, the trade-off is primarily between significant fuel burn benefit and marginal DOC penalty as seen from the blue and red coloured fronts in Figure 4.59. The difference between them is primarily

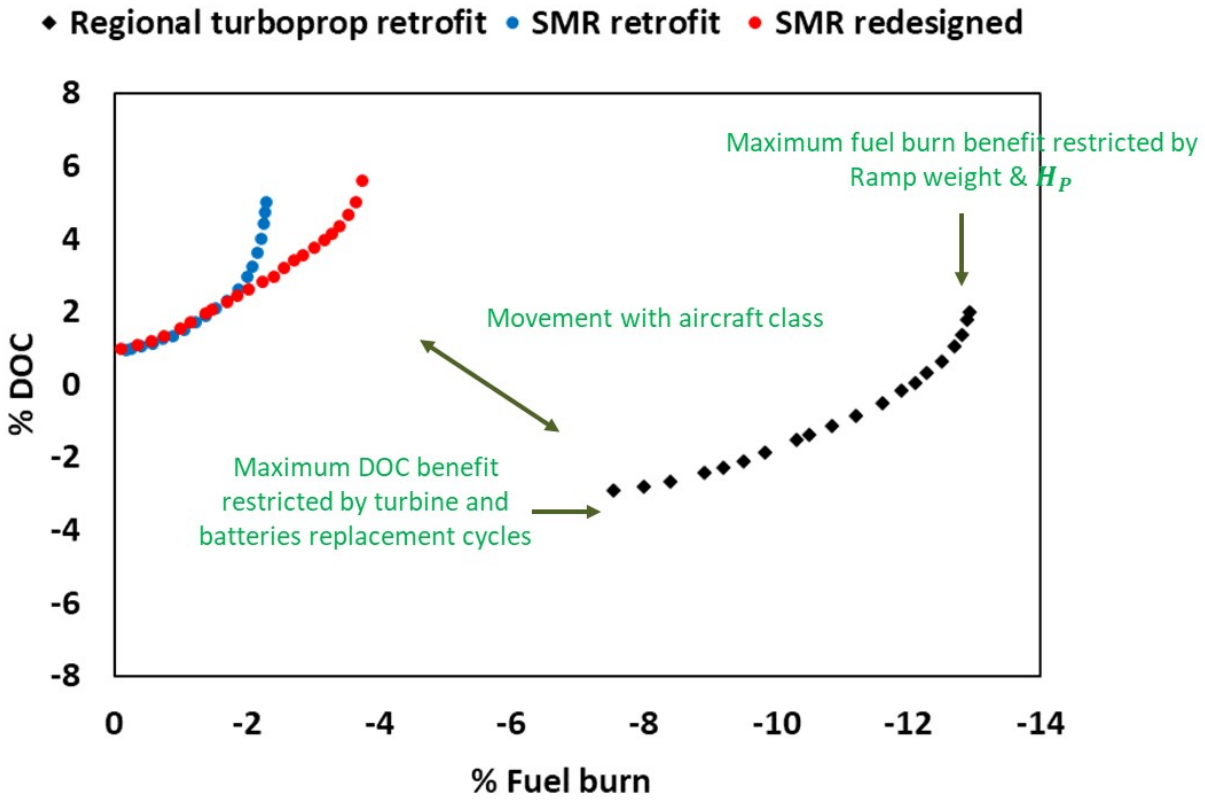


Figure 4.59: DOC vs Fuel burn benefit pareto

dependent on the thrust ratios between T/O and cruise. The greater the normalized difference between the two flight points, the greater will be the benefit gained from redesigning the gas turbine.

- When a direct comparison is made between the retrofit regional turboprop (black) and SMR (blue), it can be clearly seen that the regional turboprop is much more favorable than SMR test case. This difference can be attributed to the power to weight ratio of the aircraft, which in turn is driven by flight Mach number and engine specific thrust. The turboprop being the lowest possible specific thrust and flown at lower Mach will always be much more suitable for electrification. The fuel burn benefit becomes greater as the power to weight ratio of the aircraft reduces and hence, the electrification weight penalty reduces. This is also the reason why regional turbofan doesn't give drastically greater benefit than the SMR test case as it flies at same flight Mach and has similar Power to weight ratio. Hence, there is a misconception in open literature that size of the aircraft would drive electrification. It really isn't the size which drives but simply the propulsion power to aircraft weight ratio which drives it.

Flight Mach number and low specific thrust propulsion systems are the way to manipulate this propulsion power to aircraft weight ratio.

This concludes this section of the thesis and next section looks at TMS design space exploration.

4.4 TMS design and optimization

This section consists of design space exploration for both vapor compression cycle and liquid coolant-ram air thermal management architectures. A fuel cell and battery powered ATR 72 design space is explored with the relationship between the design parameters: Condenser/HEX frontal area, Refrigerant/coolant mass flow, compressor pressure ratio and condenser/HEX pinch temperature. The impact of these variables on aircraft energy penalty and also the weight, power off-take and drag penalty is quantified. This is done for varying levels of heat loads, power management strategies and also quality of heat loads. Once the broad space is show, the optimal design space is shown, concluding with the optimal set of TMS combinations for the turboprop heat loads. Before diving into the mission results with TMS in the next section 4.5.3, a short study is done on the parallel hybrid SMR test case. This is done to understand the impact of TMS on selection of PMS and fuel burn penalty. The main mission results of fuel-cell battery powered architectures are discussed in the next and final section of results.

4.4.1 TMS design space

The TMS design space sub-section is divided into two main categories, one covering liquid coolant ram air HEX and two covering the vapour compression cycle design space.

Liquid coolant ram air HEX

The liquid coolant ram air HEX design space exploration is done initially at design level to understand how flight conditions affect design of a heat exchanger. This is followed by showing complete mission energy penalty functions for different design parameters for ATR 72 PEM FC test case. And finally the optimal set of energy penalty functions are shown for different PMS and the breakdown of drag, weight and off-take penalty is shown.

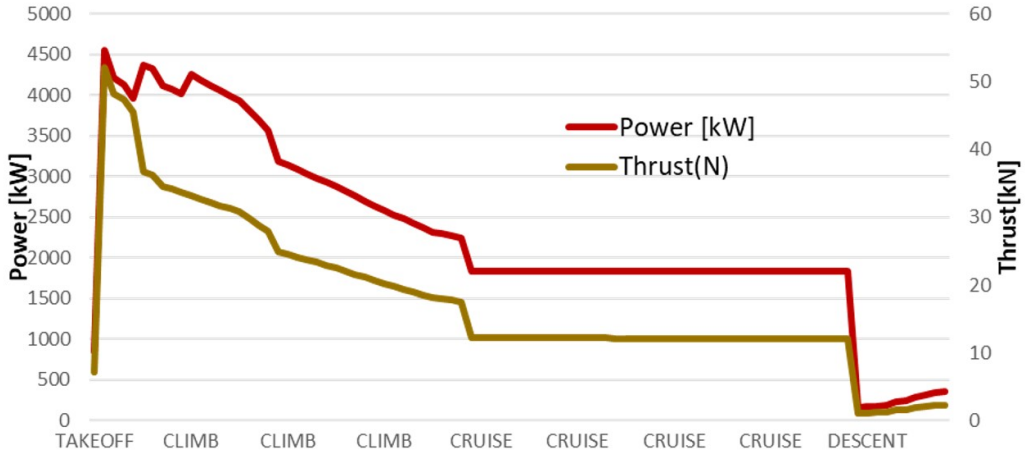


Figure 4.60: ATR 72 power profile

Starting with the impact of flight conditions on HEX design, series of Figures from 4.61 to 4.64 are generated to identify some trends. A flight shaft power profile for ATR 72 is shown in 4.60, which shows the total output power requirement from the motor, hence giving us some bounds on level of fuel cell heat loads. Keeping this in mind the fuel cell is swept for 0.5-2 MW heat loads for different altitude and Mach conditions.

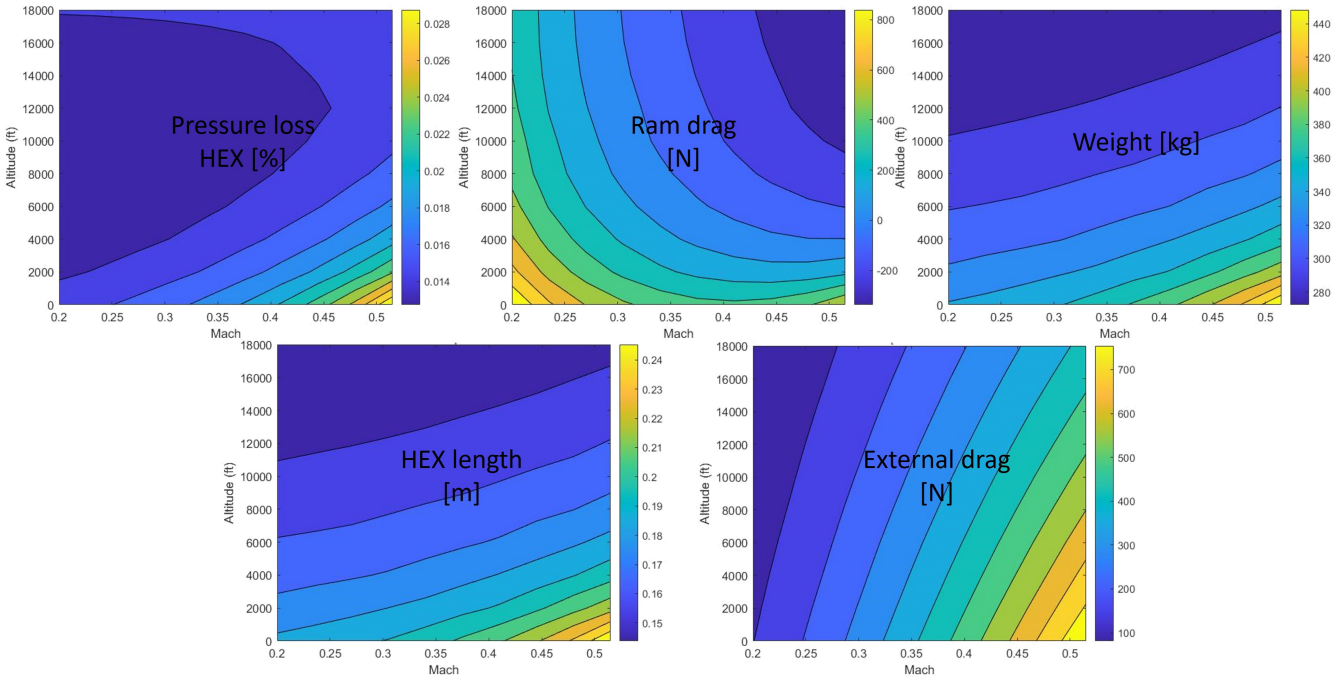


Figure 4.61: 2 MW fuel cell cell DSE

It can be noticed that the basic trends of HEX pressure loss, ram drag, weight, length and external drag are same with different heat load but simply scaled up

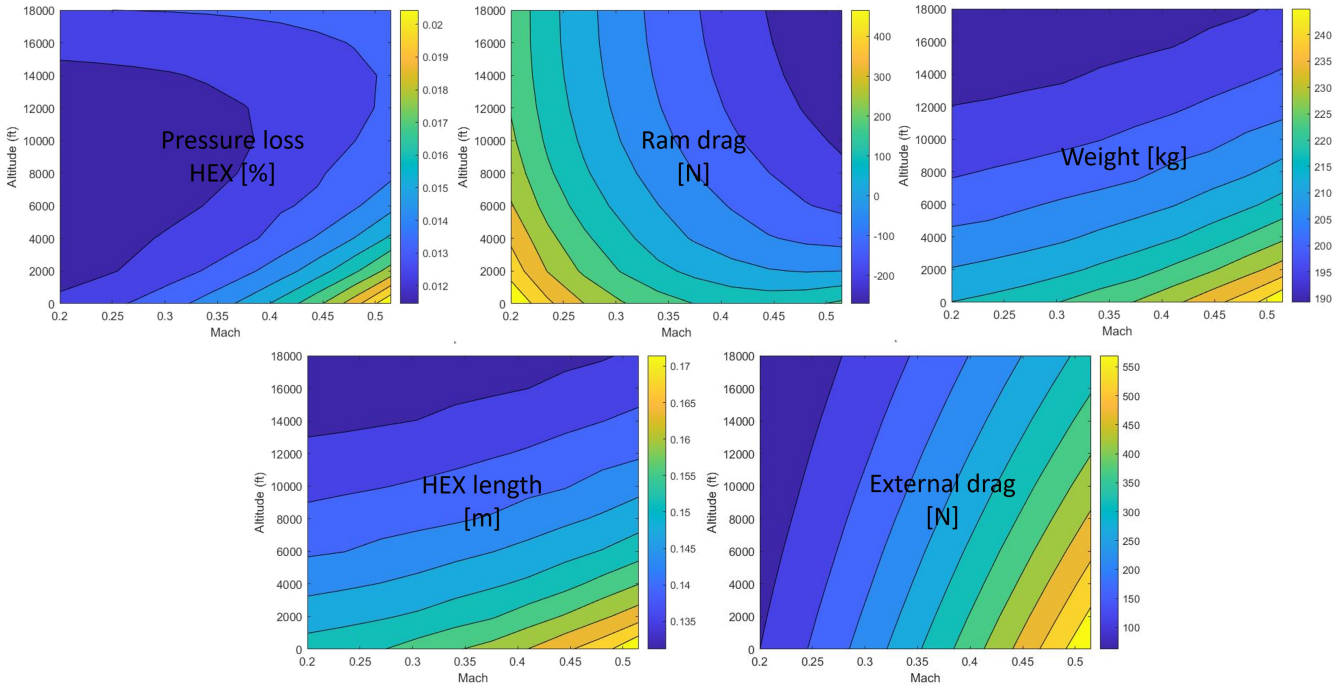


Figure 4.62: 1.5 MW fuel cell cell DSE

by corresponding numbers. It should also be noted that when the design space exploration is performed from Figures 4.61 to 4.64, the condenser area is scaled keeping the same heat load to area ratio, while the coolant mass flow and pinch temperature is kept fixed at maximum value (15 kg/s) and minimum value (10 K) respectively. Let us now start to look at the initial HEX trends across one heat load, it can be seen that the ram drag and external drag behave differently with increasing Mach at given flight conditions. This makes sense as the external drag varies as a square of flight Mn while ram drag would consistently improve due to Meredith effect. The HEX length and pressure loss increases with increasing Mach as higher Mach means a lower temperature gradient, which then translates to greater heat transfer length requirement if same pinch temperature is targeted. The increasing length also translates into greater HEX weight on a fixed frontal area.

The pressure loss does get some improvement as higher altitudes enable lower outside temperatures leading to better heat transfer. But it needs to be understood that in a typical aircraft mission scenario, with increasing altitude, the flight Mach also increases to maintain the same equivalent speed. This would then mean that the sizing point of the HEX isn't exactly intuitive as if a point say at 1500 ft, 0.20 Mn is compared against 5,000 ft, 0.30 Mn, the length and weight are very close to each other. This once again brings the importance of bringing off-design flight mission

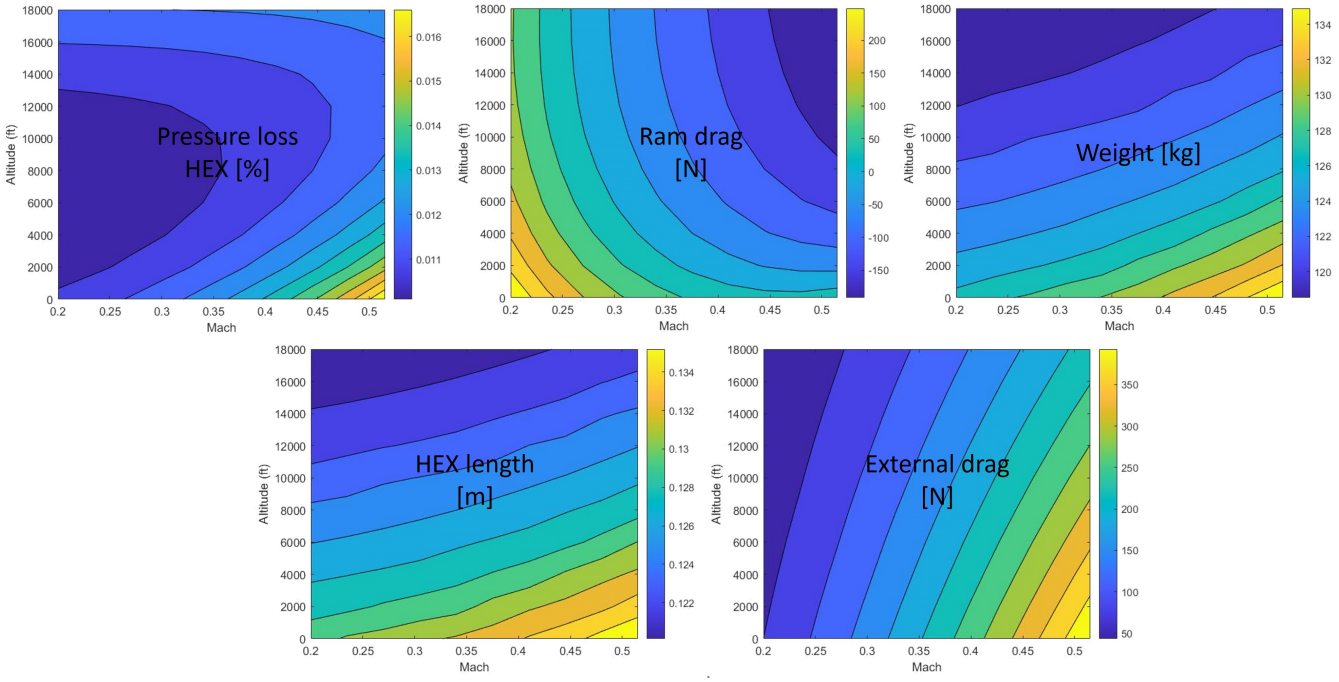


Figure 4.63: 1 MW fuel cell cell DSE

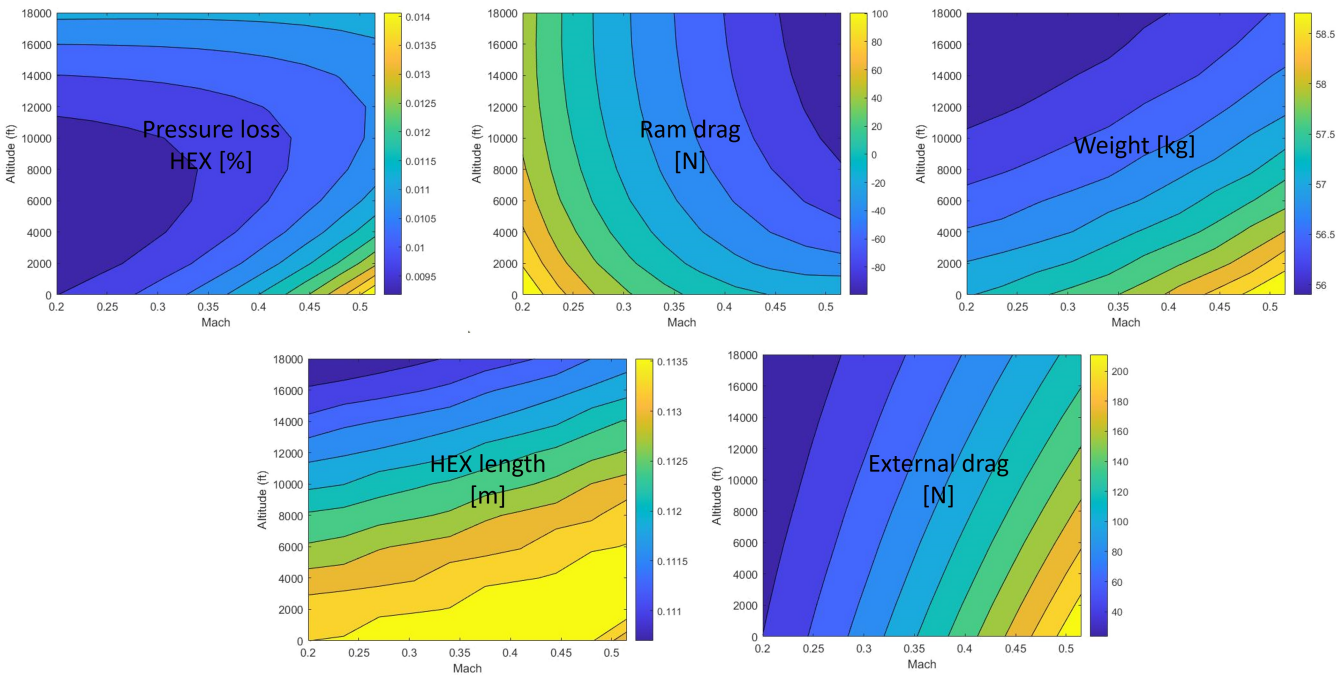


Figure 4.64: 0.5 MW fuel cell cell DSE

behaviour.

The next set of discussion is around the sweep of HEX design parameters accounting for off-design flight mission behaviour (using method discussed in Section 3.9 for an ATR 72 completely powered by PEM fuel cell. Given the mission profile

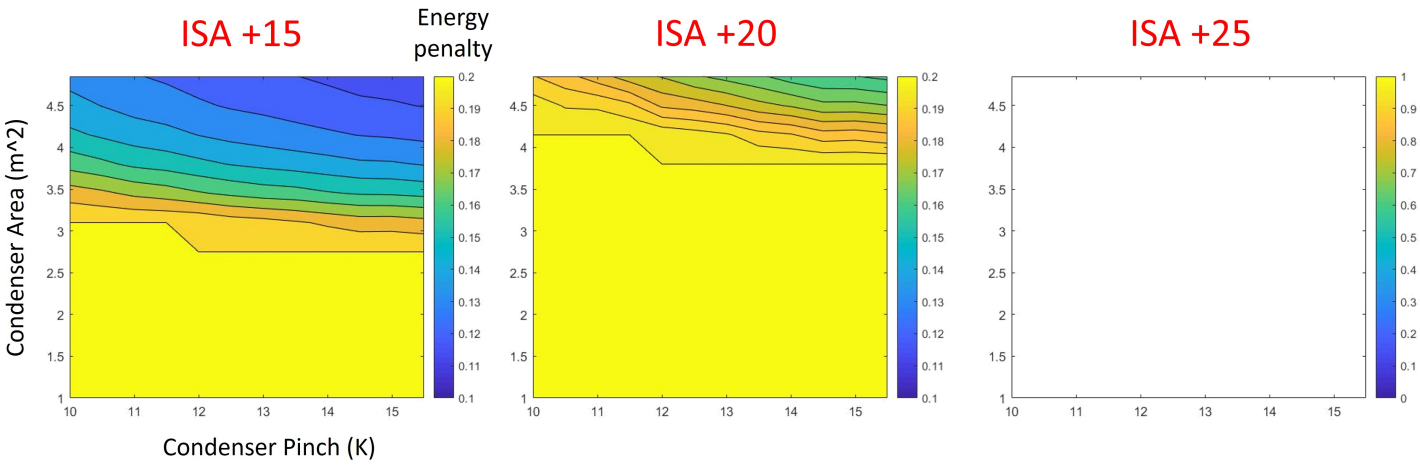


Figure 4.65: RA HEX energy penalty compared at ISA +15, +20 and +25

in Figure 4.60, for now ignoring the extra power off-take penalty, if this power is directly given by the fuel cell, we have a 100% hybridized fuel cell case. This case is now sized by a ram air HEX for three different dT ISA rating +15, +20 and +25 and the energy penalty is shown in Figure 4.65. The energy penalty here is the total energy penalty as defined in Section 3.9. In all the three plots, all energy penalty over 20% are counted as infeasible solutions and the coolant mass flow is assumed to be at 20 kg/s. The penalty function is parametrized against condenser area and condenser pinch from maximum and minimum bounds. The very interesting trend here is that ISA +25, there actually exists no thermal management solution which is feasible, meaning that essentially a 100% fuel cell ATR 72 cooled by ram air HEX is completely non viable. But there still exists some solutions at ISA + 15 and ISA +20 and the energy penalty varies from 11-15%. This is an important number as this number will be compared against VCC energy penalty.

VCC design space

This sub-section explores the VCC design space and the optimal configurations of VCC for both fuel cell and battery level heat loads for an ATR 72 class of aircraft. Initially for a fuel cell and battery powered ATR, extensive design space contours are shown to understand the behaviour of VCC design space and how it changes with quality and quantity of heat load. Post the design space, the optimal VCC designs are obtained using the method shown in Section 3.9 for a sweep of PMS. Finally, a breakdown of drag, power off-take and weight contribution to energy penalty is shown.

Starting the VCC design space exploration for the same initial test case as

described in Figure 4.65, that is 100% Fuel cell ATR 72. The 100% HP case is swept for three main design parameters - sizing point compressor pressure ratio, condense frontal area and sizing point pinch. The refrigerant mass flow was found to be 20 kg/s such that the exit of evaporator is always on the P-h saturation curve. It is to be noted that this value is linearly increased with different degree of hybridization like in Figure 3.50. Coming back to the trends in the 100% DoH case, visualized in Figure 4.67. The energy penalty is shown as a function of 3 design parameters, with any number above penalty of 0.20 showing an unfeasible TMS solution. It can be seen that the minima in energy penalty comes at high condenser area, low pressure ratio and pinch of around 15 K and the penalty number is around 10%. In order to understand more on why the trends are so, a breakdown of off-take, drag and weight penalty is provided, which ultimately contributes to the total energy penalty. The breakdown can be seen in Figure 4.67. It can be seen that optimizing for power off-take is what drives the design as the optimal point for minimal power off-take penalty is also the optimal point for minimal energy penalty. This makes sense as the quantity of fuel cell heat load is so high that any extra compression has a big knock-on effect on energy penalty.

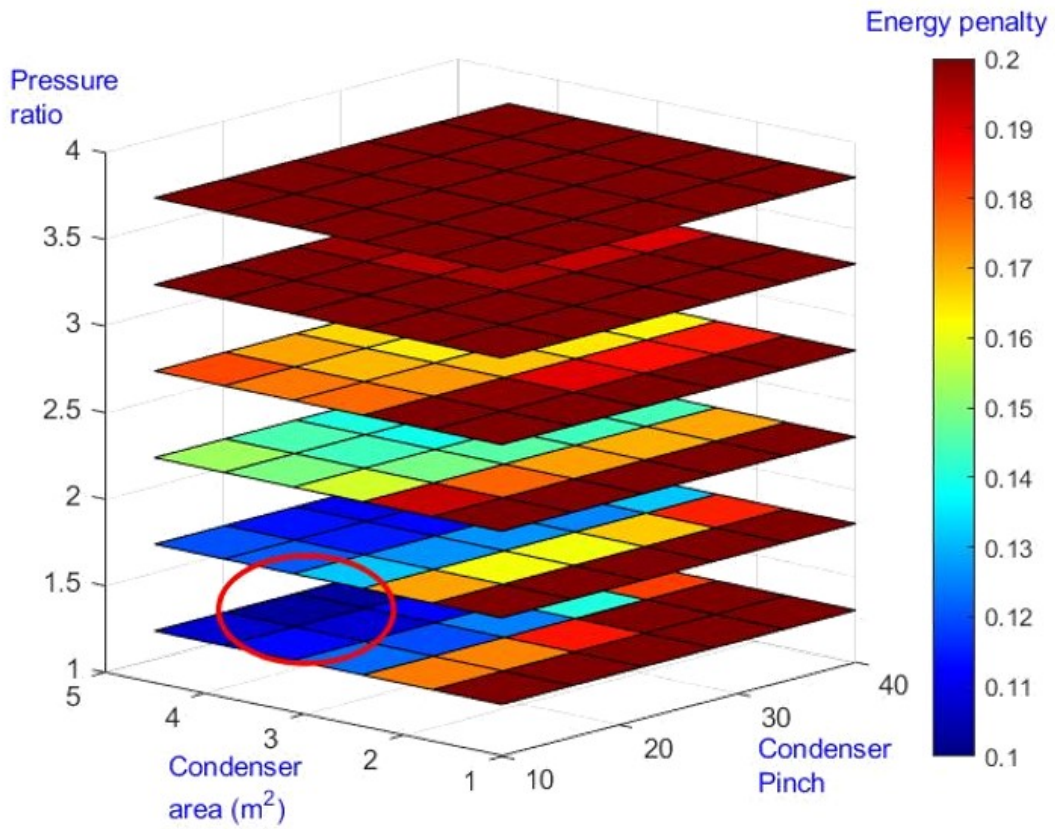


Figure 4.66: VCC energy penalty for FC loads, HP = 1.0, optimal PR

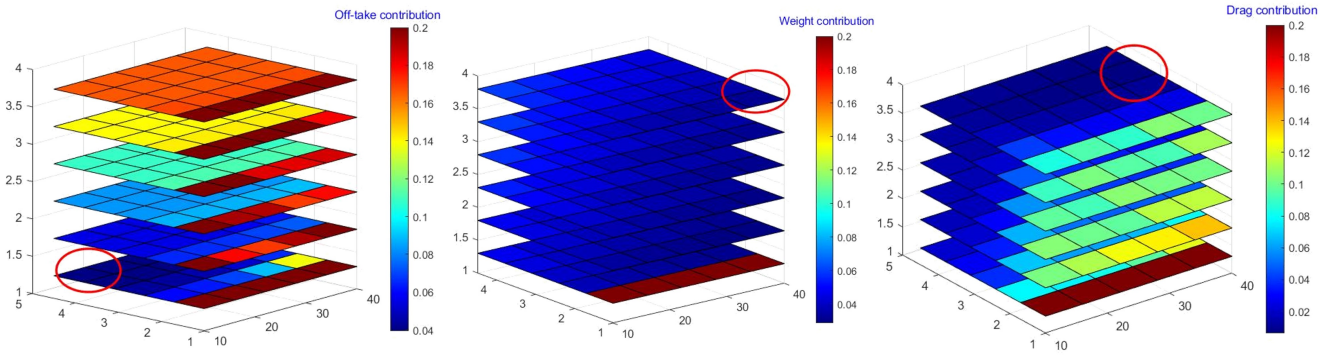


Figure 4.67: VCC energy penalty for FC loads breakdown, HP = 1.0, optimal PR

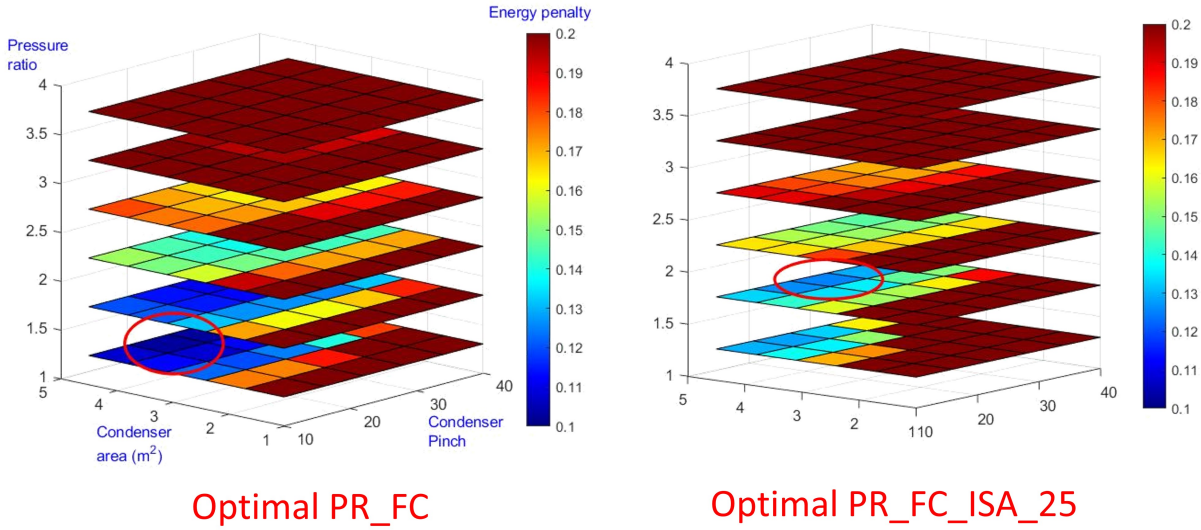


Figure 4.68: Energy penalty comparison between VCC sized for ISA 15 and 25

It almost seems that to dump fuel cell heat load (at 353 K) at outside air temperature of ISA+15, VCC is not really required and ram air HEX would do the job itself. But applying VCC at ISA +25 has a much bigger advantage over ram air HEX as can be seen in Figure 4.68. An extra 4% energy penalty when sizing for ISA +25 over ISA +15. So this gives us some numbers before hand on what to expect mission level, given that at ISA +15, VCC has 2% benefit over ram air HEX while at ISA +25, VCC is only viable solution. The next comparison is now made between fixing compressor pressure and optimizing pressure during off-design flight points along the mission profile. This comparison can be seen in Figure 4.69, where fixing the pressure ratio has a small 1.5% penalty over optimizing pressure ratio. The penalty is low as the design itself optimized at a low pressure ratio not giving enough opportunity for pressure ratio optimization.

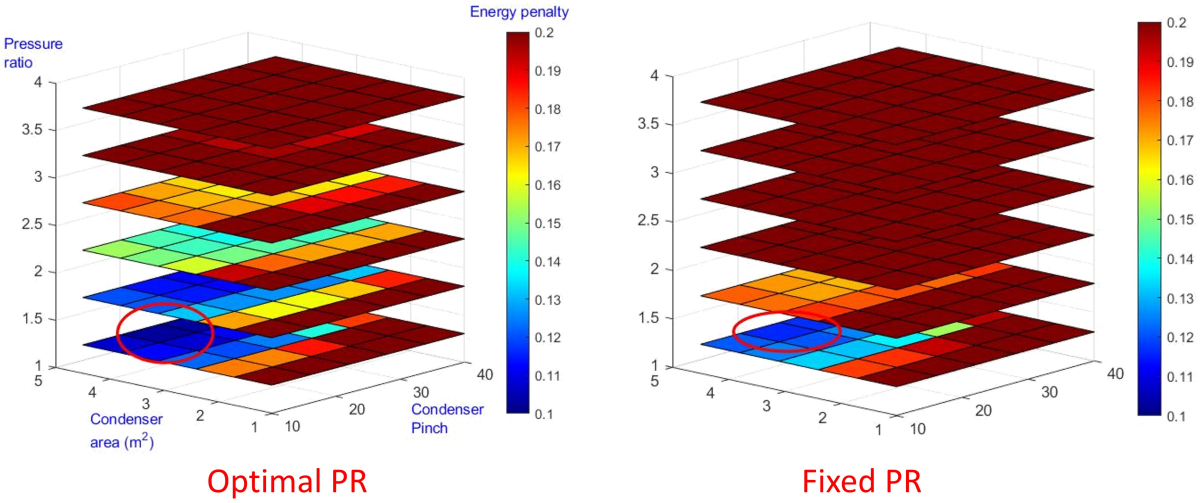


Figure 4.69: VCC energy penalty comparison between fixed and optimal PR

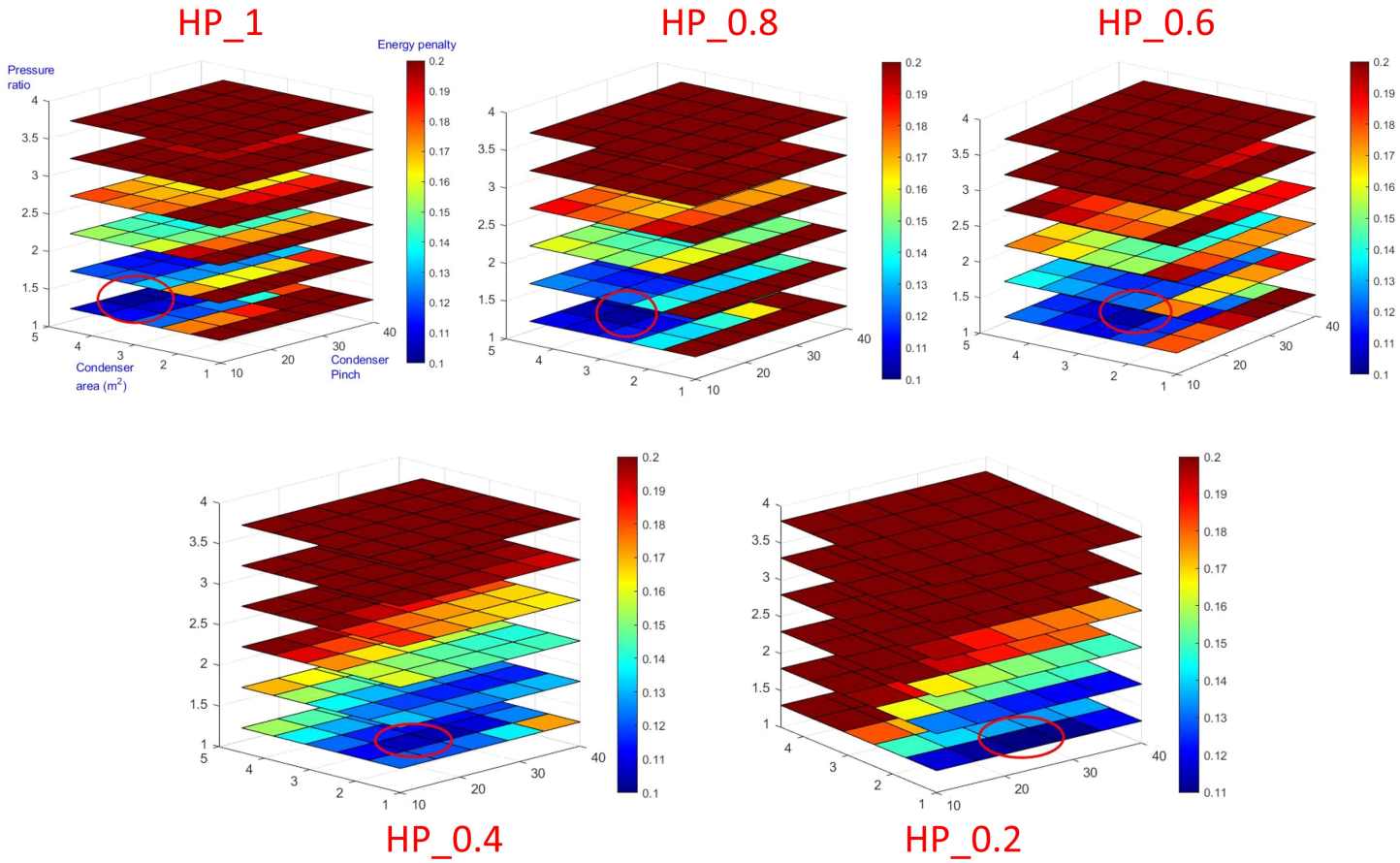


Figure 4.70: VCC energy penalty for FC with varying HP

The next sweep is done on different degrees of hybridization as can be seen in Figure 4.70. It is interesting to see that the energy penalty which is paid for different

fixed T/O, climb and cruise degrees of hybridization is more or less constant. This means that assuming a fixed power density as typically used in open literature isn't necessarily too far off as it seems HEX and VCC both scale linearly for consistent heat load distribution. This isn't true if the system isnt used consistently meaning that if battery or fuel cell is used only during certain flight phases, the penalty functions are no longer linear as will be seen later in Figure 4.72.

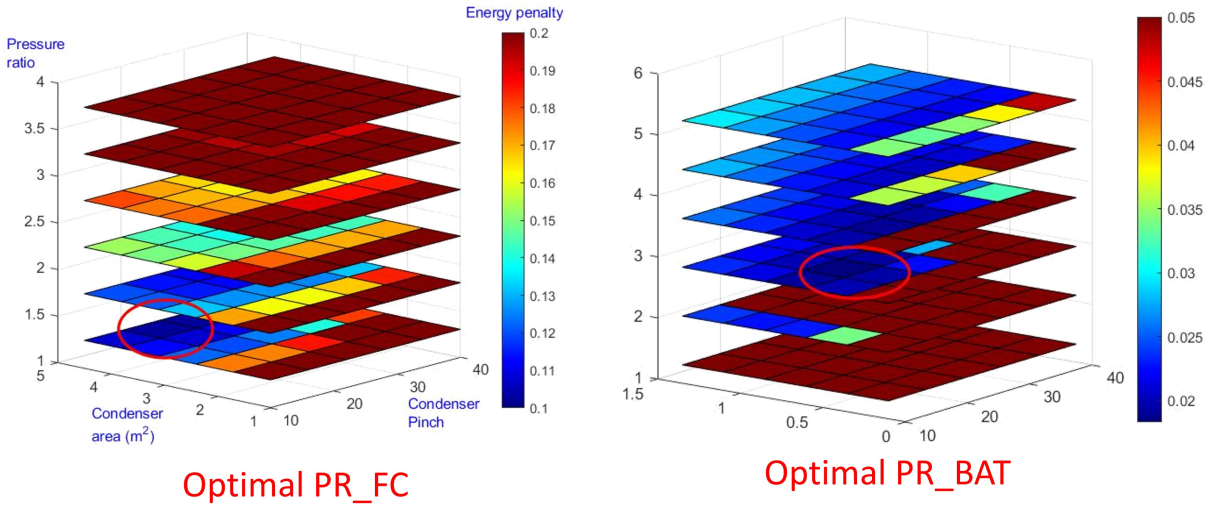


Figure 4.71: Energy penalty comparison between Battery and Fuel cell

The next comparison is now done between fuel cell and battery heat loads, and can be seen in Figure 4.71. It can be quickly noticed the battery optimal energy penalty comes at a higher pressure ratio of between 2.5-3 owing to the lower operating temperature (298 k against 353 K), while the selection of pinch remains at the same level. Regarding the condenser area, the area scales with quantity of heat load and hence optimizes at a much lower frontal area. And finally how about the numbers themselves? A quick look at the energy penalty which is 2% roughly translates to 0.6-0.7 kW/kg of thermal power. This number is also what Lents [32] and Kellerman [63] came up with, showing again that the numbers are in the right ballpark.

Now an analysis is done for fuel cell test case for optimal TMS solutions for different PMS. This is shown in Figure 4.72. Essentially what was done was a sweep of 125 power management strategies, with 20% DoH intervals on T/O, climb and cruise was run and within each PMS, the VCC system was optimized for energy penalty fraction. The bounds on the sweep are shown in Table 4.13. If one now looks at the trends in Figure 4.72, it can be that the energy penalty are extremely high for some PMS. This happens in some extreme combinations like 80% DoH during one flight segment and 20% in another, which means that the VCC is oversized leading to

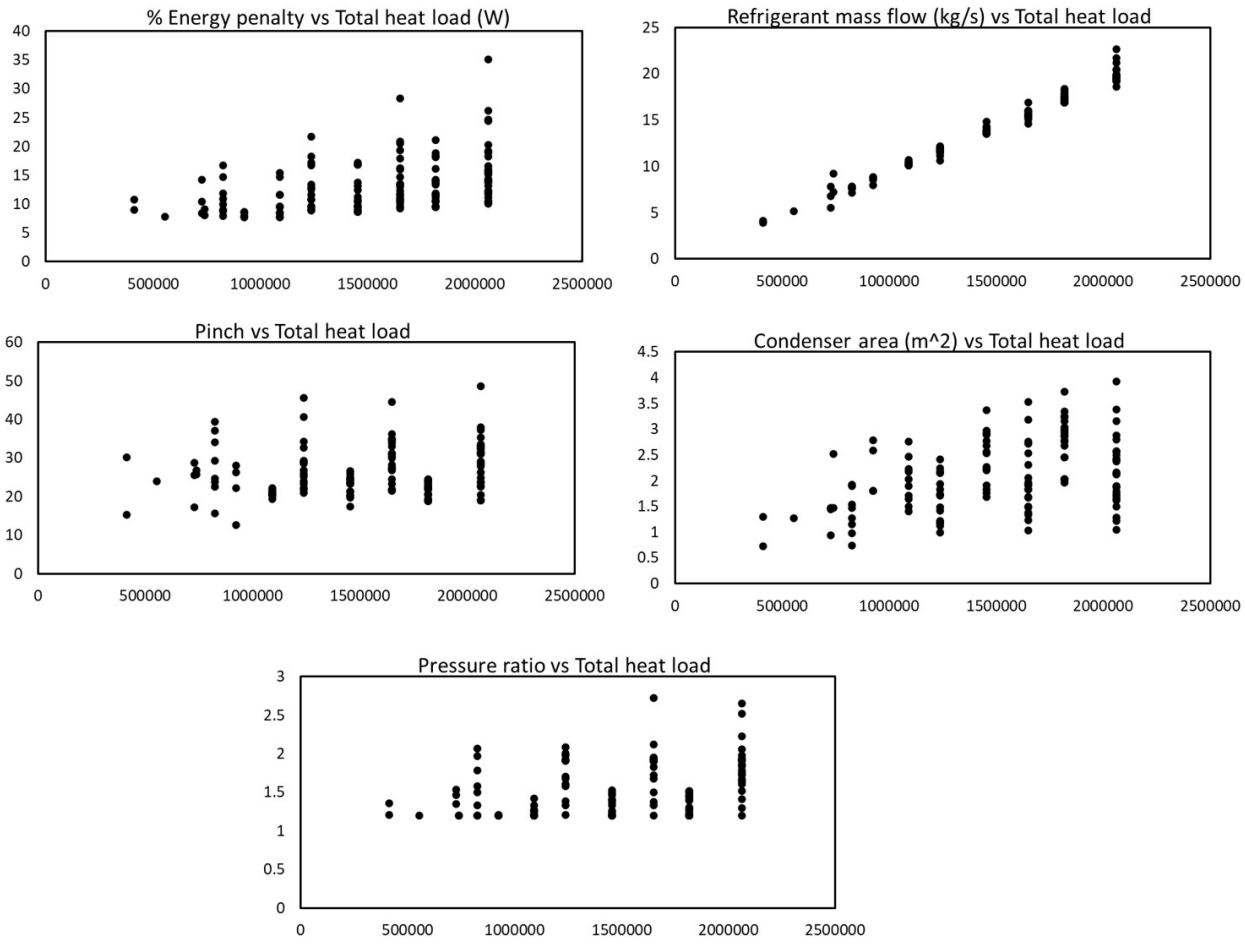


Figure 4.72: Optimal Parameters variation with sweep on PMS for Fuel cell splits

very high penalties when the propulsion system itself is non-utilized. The mass flow variation is linear as it only depends on the quantity heat load and is independent of flight conditions. Rest of the parameters have a very similar behaviour as the energy penalty as all these are outcomes of different DoH during the flight segments.

Parameter	Lower bound	Upper bound	Gap
T/O DoH	0.2	1.0	0.2
Climb DoH	0.2	1.0	0.2
Cruise DoH	0.2	1.0	0.2

Table 4.13: PMS bounds

Finally a breakdown of different contributors to energy penalty is shown in Figure 4.73. The breakdown is shown for all 3 cases, VCC for 100% DoH FC, RA for 100% DoH FC and 100% DoH battery. As expected VCC for fuel cell has maximum power off-take contribution and least drag contribution (due to higher ram recovery), while the opposite is true for battery case. This concludes the sub-section on TMS design

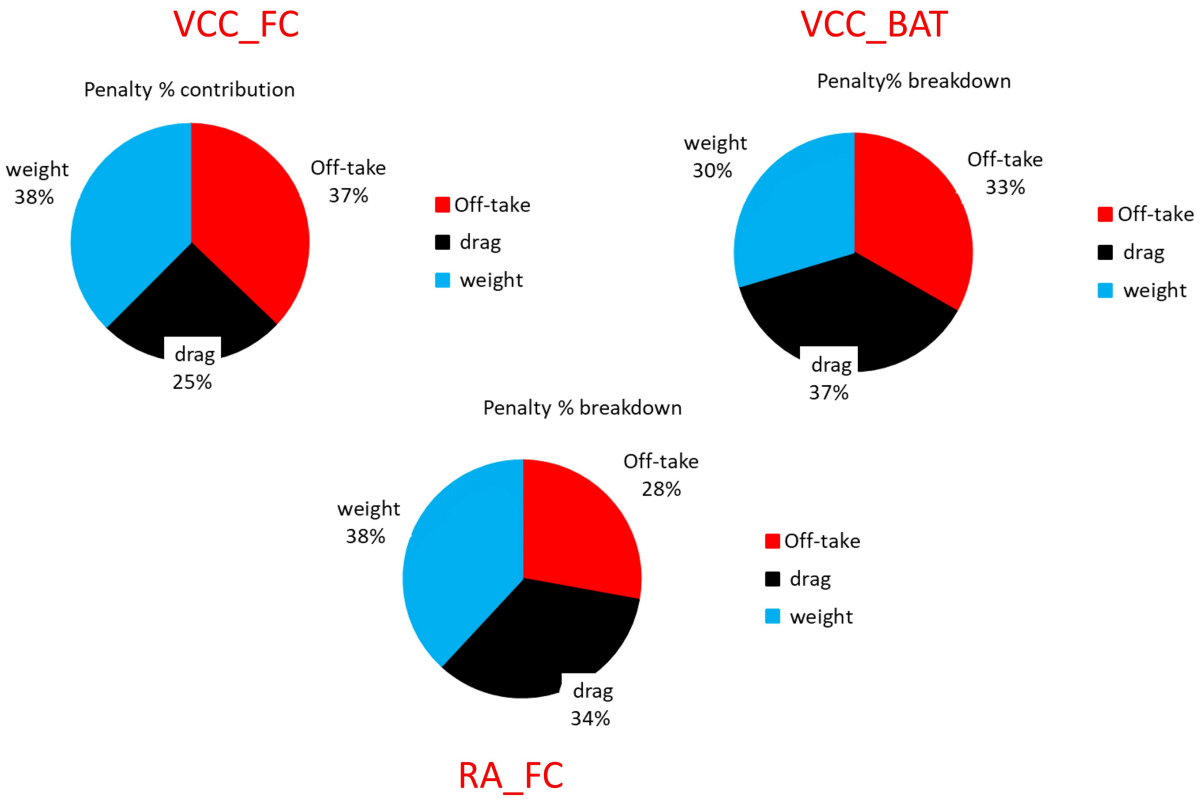


Figure 4.73: Penalty breakdown

space exploration.

4.4.2 TMS impact mission level

This subsection shows the impact on fuel burn for SMR PHEPS test case due to VCC TMS and also the change in optimal PMS. For this study, the VCC compression power is taken from the GT rather than the battery pack itself and option 1 (Figure 3.50) VCC pack is used for this case. This is because the parallel HEPS with batteries have much lower degree of hybridization than the ATR test case. But the design method remains same but simply put assumptions are different as described above. Moving onto the results, the optimal PMS trends are shown in Figure 4.74 and 4.75.

The trends shown in Figure 4.74 are the optimal PMS trends with no TMS assumptions for redesigned test case as also developed in Section 4.3.2 while Figure 4.75 shows the optimal PMS trends after implementing VCC TMS. As expected, because of the difficulty to remove heat at lower altitudes, implementation of TMS would always favour cruise power on-takes over take-off and climb on-takes. This trend is common across all design ranges and the corresponding fuel burn penalty is

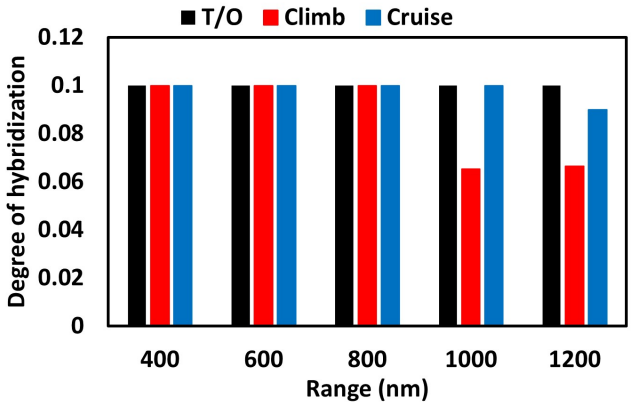


Figure 4.74: PMS without TMS

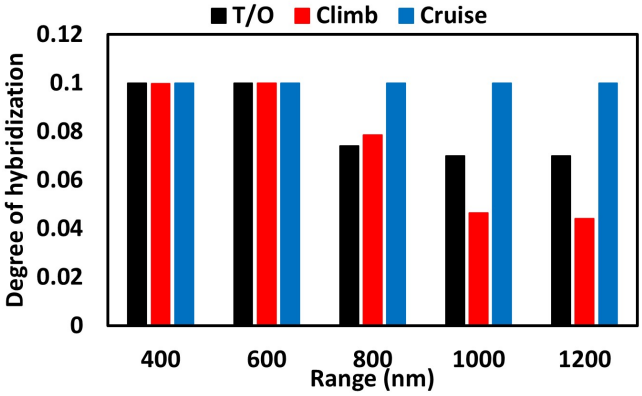


Figure 4.75: PMS with TMS

shown in Figure 4.76. A 0.6-0.8% fuel burn penalty due to VCC can be seen across all ranges.

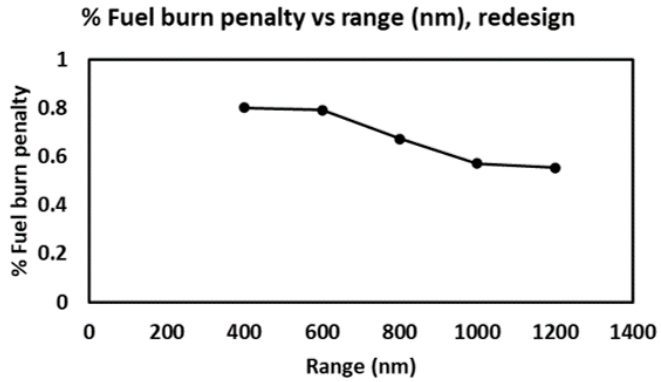


Figure 4.76: Fuel burn due to TMS

This concludes the sub-section on TMS penalty for the SMR test case. The next section moves to the Final technological evaluation implementing TMS.

4.5 Final Technology Evaluation

This section of results deals with the comparison of different HEPS propulsion configurations for the regional turboprop test case. The main propulsion configurations compared in are the kerosene EIS 2010, 2035 GT, hydrogen powered 2035 GT, parallel HEPS architecture with 2035 GT (batteries with VCC cooling loop), fuel cell and battery powered electric architecture (fuel cells cooled by VCC and ram air and batteries cooled by VCC). The fuel cell and GT parallel hybrid architecture is not pursued after some quick studies on SMR test case. It is explained why limited benefits can be obtained by a parallel hybrid configuration with fuel cells. Before going to that discussion, the LH2 GT is briefly explored to understand the impact of switching to hydrogen combustion on turbine and corresponding compressor rematch. The author did several hydrogen design space exploration studies during Flyzero project and those can be found in detail [35]. Over here, only the aspects related to hydrogen powered ATR 72 are discussed.

4.5.1 LH2 GT

The EIS 2035 kerosene GT cycle assumptions and thrust and shaft power requirements were used and then the full design space was swept for various T30 and T41 similar to Figure 4.29 and 4.28, albeit this time with hydrogen. For LH2 GT, two options are pursued, one where the same actual physical engine is kept except for change in combustor (LH2 switch) and one where the whole engine, gas path is re-sized to match the target temperatures at take-off (LH2 redesign). The reason why two options are explored is to benchmark the impact of fuel properties and the benefit coming from redesigning the cycle. It is assumed that hydrogen is fed into the combustor at 250 K and an electric heater is assumed to heat up this fuel from the tank to the combustor [33]. The LH2 switch cycle will have the turbine life benefit over the LH2 redesigned cycle due to lower temperatures coming from a bigger core, and we have seen in Section 4.3.4, that direct operating cost does have a high impact on ultimate selection of cycle.

All three engines, kerosene, LH2 redesigned and LH2 switch cycle are designed for same thrust ratios to understand impact of switch in fuel and the difference between swicth and redesigned. LH2 having a higher energy density compared to kerosene leads to less drop in weight across the aircraft mission hence a higher CRZ to MTO thrust ratio compared to kerosene. Figure 4.77 ([39]) illustrates the cruise ESFC against core specific work for varying MTO T40 and T30. For the LH2 switch cycle,

the gas turbine will run at reduced core temperatures due to the higher specific heat of flue gases on the hot end [35]. This reduction in temperatures is depicted in Figure 4.78([39]). It is observed that for the LH2 switch cycle, the reduction in cruise T40 is varies proportionally with change in take-off T40, with reduction of approximately 70 K on target T40 of 1800 K. Thus, if the same cycle is kept, this reduction will result in reduced T41 and increased turbine time on wing. On the other hand, for the LH2 redesigned case, the cycle is pushed to the original cycle temperatures. This push and pull between redesigned and switch LH2 is similar to the trade-offs between retrofit and redesigned hybrid GTs.

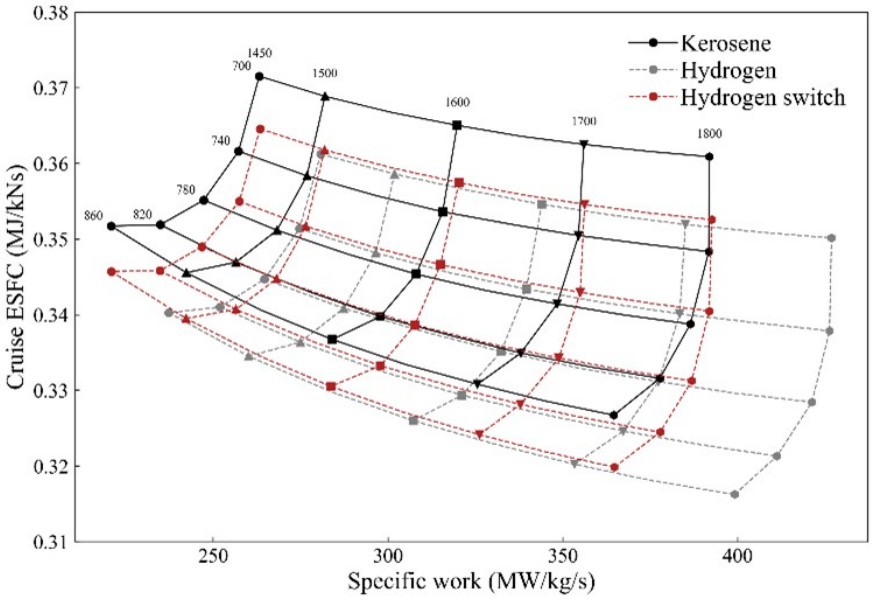


Figure 4.77: Comparison of cruise esfc against core specific work [39]

At cruise, owing to higher Cp on the hot end, an average of 2% reduction in energy specific fuel consumption is obtained across the for T40 and T30 spectrum compared to the kerosene baseline. The LH2 redesigned cycle on the other hand results in higher ESFC benefit of 3% by pushing the core to hotter CRZ temperatures. It should be noted that in this comparison, the reduced polytropic efficiency due smaller cores hasn't been accounted for as in Figure 4.29. So essentially the switch to LH2 brings benefit in three steps, one the benefit coming from higher Cp on the turbine side, 2 the additional core size reduction benefit enable by step 1 and finally the corresponding thrust ratios benefit. The final LH2 cycle used is sized at same levels of T30 and T40 as shown in Table 4.11 and this is the cycle used as EIS 2035 HY cycle in section 4.5.3. This concludes the sub-section on LH2 GT.

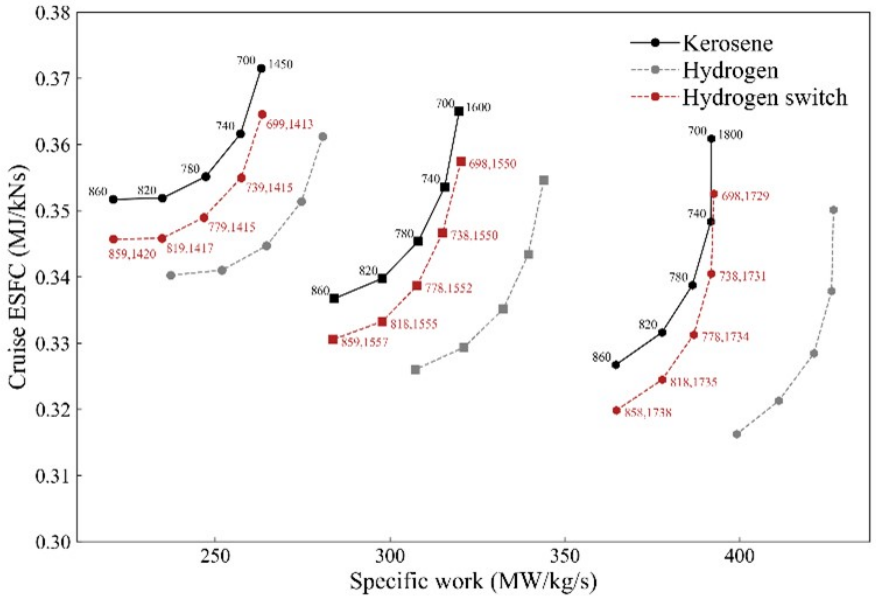


Figure 4.78: Comparison of cruise esfc against core specific work highlighting LH2 switch temperatures [39]

4.5.2 LH2 GT PEM FC hybrid

This sub-section deals with the assessment of parallel HEPS architecture with fuel cell. This architecture was covered for SMR test case as well as the other regional turbofan case (BAe 146). In order to have a back-to-back comparison, the corresponding hydrogen GT counterparts were also modelled for each aircraft. From the assessment of this architecture on the turbofan test cases, it was concluded that limited to no benefit can be obtained by this architecture hence only fuel cell or fuel cell-battery configuration is pursued for the regional turboprop case.

SMR Turbofan

As explained in the previous subsection, burning hydrogen has a drop in T40 and T30 compared on kerosene on same thrust due to higher Cp of the flue gases. The hybrid LH2 propulsion system on the aircraft can be visualized in Figure Before comparing the hydrogen GT aircraft against hydrogen GT-PEM FC hybrid, a table is shown comparing the hydrogen cycle and kerosene cycle.

The LH2 tank in all the cases is kept in the fuselage, with it extended to meet the design range of the corresponding kerosene aircraft. It is to be noted that this is the only place where the fuselage is extended and this isnt done for the turboprop studies. The additional fuselage weight is added by using correlations provided by

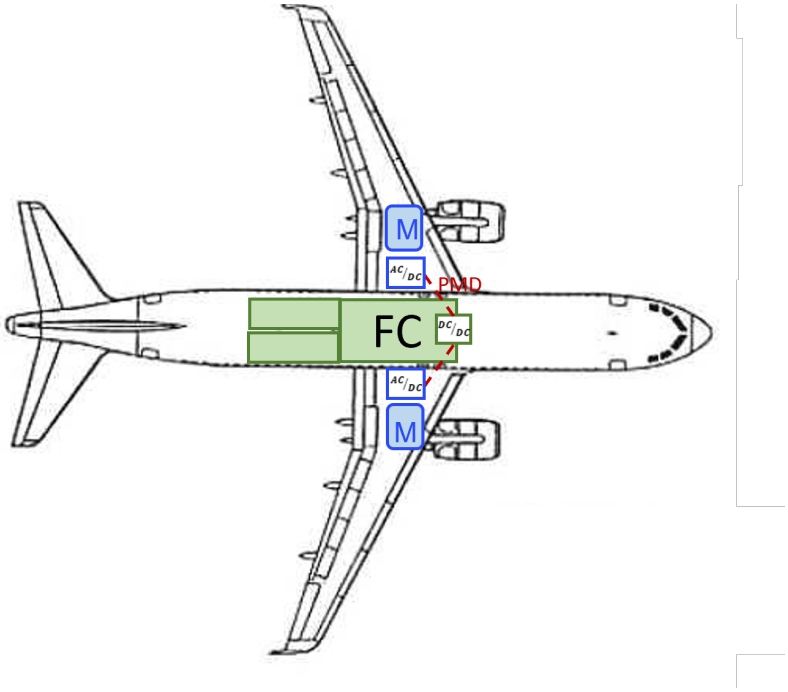


Figure 4.79: PEM FC hybrid aircraft

NASA FLOPS [86]. One interesting thing to note from Table 4.14, is that HY thrust requirements at MTO and MCL are lower than baseline kerosene (4.8), while CRZ thrust is higher. This is due to assumption of 60% GI for LH2 tanks, which leads to aircraft being lighter at take-off (as total fuel, tanks and fuselage weight is lesser than kerosene fuel weight) and climb. While the almost 3 times lower heating value of KE than HY leads to a higher aircraft weight at mid-cruise and also additional fuselage drag, ultimately translates to a higher mid cruise thrust.

MTO Thrust (kN)	89.5
MCL Thrust (kN)	24.5
CRZ Thrust (kN)	19.6

Table 4.14: HY SMR thrust requirements

Comparing the two cycle in Table 4.15, shows the higher BPR and T40 of HY at CRZ due to the thrust ratios and higher Cp of flue gases. The final hydrogen engine cycle has a 3.1% lower energy specific fuel consumption than kerosene cycle. Similarly, an EIS 2035 LH2 cycle is also obtained.

Now moving to the analysis of PEM FC - LH2 GT hybrid, this exercise was done without utilizing TMS design in previous section and a fixed value of 2 kW/kg balance of plant is assumed for the fuel cell at a sizing point efficiency of 49 % (this translates to 60-65 % efficiency at low power settings). This back to back comparison against

Parameter	Baseline KE	LH2
CR BPR	5.7	6.47
CR tsfc (g/kN.s)	16.6	5.78
CR OPR	24.7	27.7
CR T40 (K)	1288	1346
T/O T40 (K)	1641	1641
T/O T30 (K)	860	860
Fan diameter (m)	1.65	1.65

Table 4.15: EIS 2010 SMR GT cycle data (KE and HY)

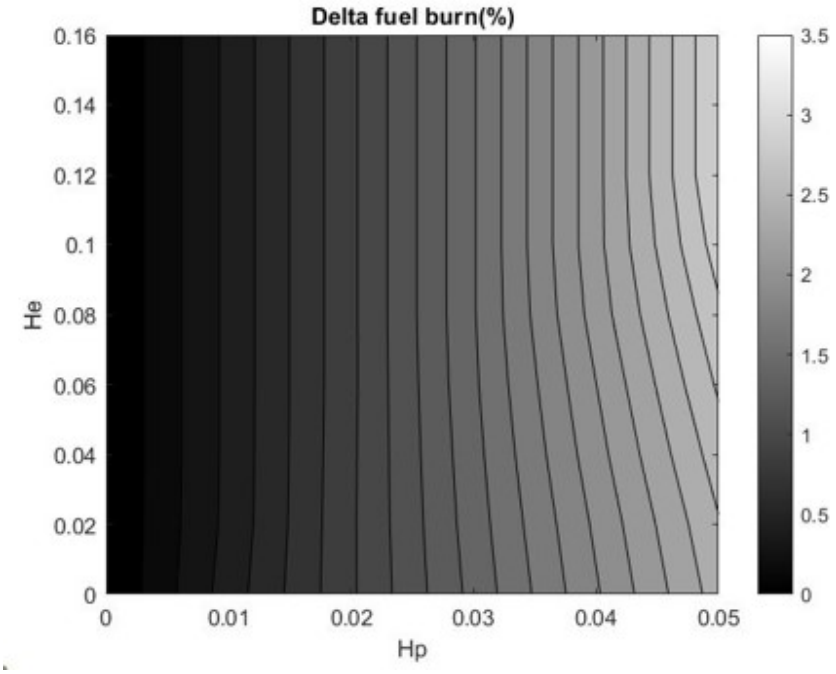


Figure 4.80: Delta Fuel burn for FC wrt LH2 GT, CFM

LH2 GT on 1000 nm is shown in Figure 4.80, where the contour is essentially the fuel burn delta between the hybrid and LH2 GT for varying degree of hybridization by power and energy. It can be quickly noticed the penalty of fuel burn keeps increasing as the degree of hybridization by power increases. But the interesting thing to understand is whether this picture change. A simple exercise was done to understand these trends without assuming any fuel cell weight which can be seen in Figure 4.81. The delta fuel burn penalty drops to zero, showing that the hybrid system is practically at the same efficiency level. The same exercise was repeated also for EIS 2035 GT case and is shown in Figures 4.82 and 4.83. From Figure 4.83, it can be seen that in fact there is now a penalty in fuel burn even when the weight of fuel cell is not considered.

The reason behind this is that the fuel cell power plant total efficiency is around

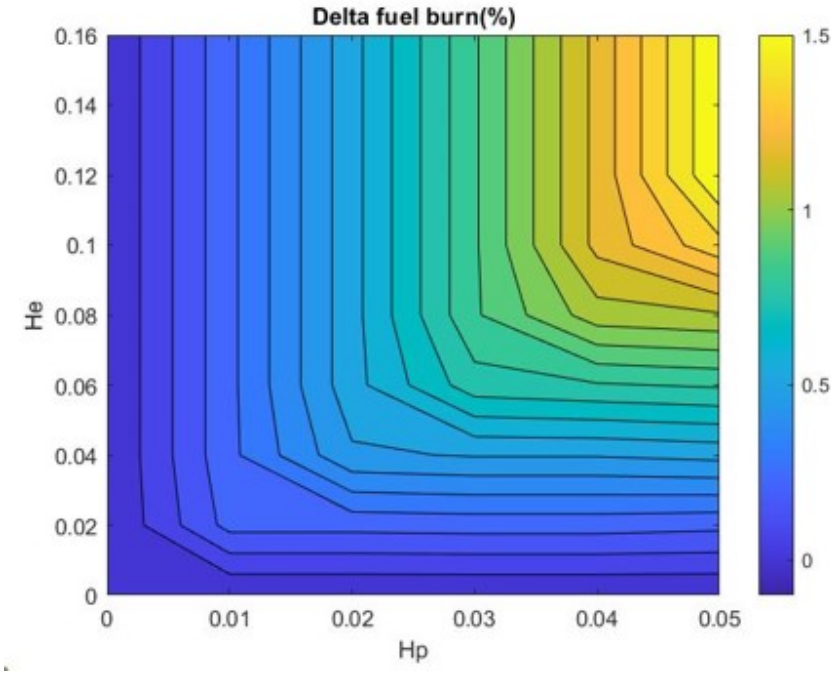


Figure 4.81: Delta Fuel burn for FC wrt LH2 GT, CFM, no FC weight

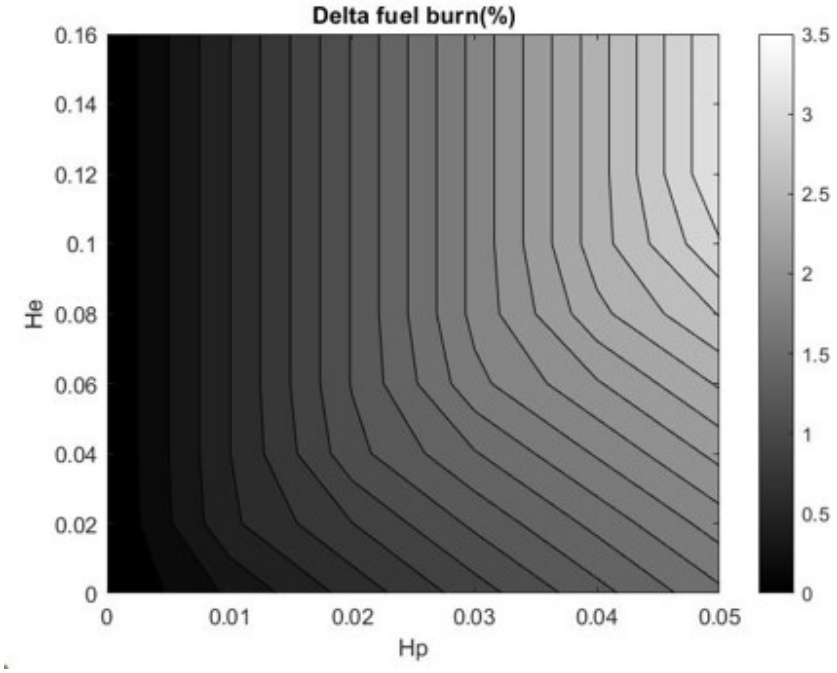


Figure 4.82: Delta Fuel burn for FC wrt LH2 GT, GTF

43% at MTO and 55% at CRZ, the true GT numbers to compare this would be the thermal efficiency without accounting for fan bypass efficiency. The GT 2010 number for MTO is 45% at MTO and 51% at CRZ, showing the rather small jump which the fuel cell actually brings. In fact when the fuel cell is ran with GT, the thermal

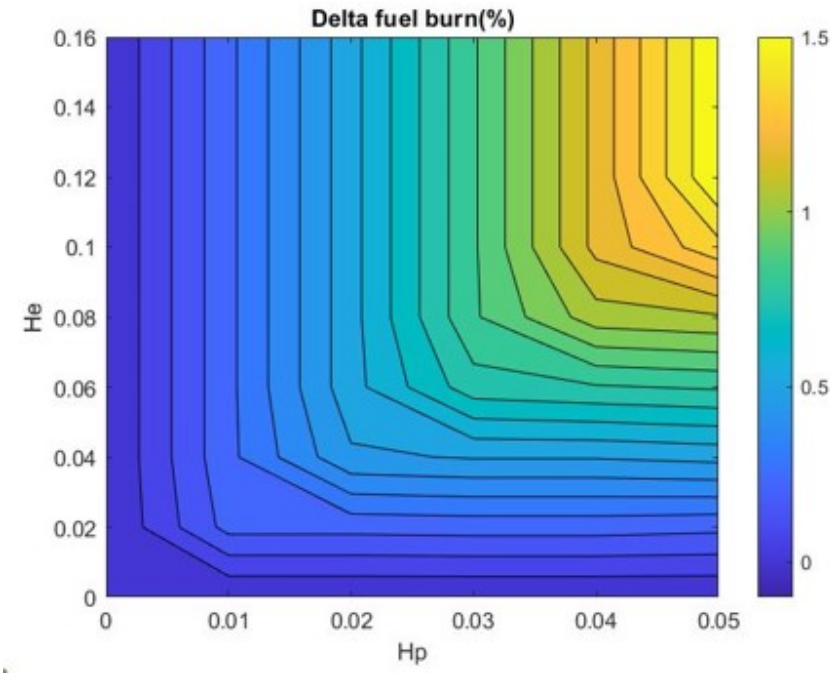


Figure 4.83: Delta Fuel burn for FC wrt LH2 GT, GTF, no FC weight

efficiency at CRZ drops due to lower temperatures showing the non-synergistic benefit on gas turbine (completely opposite to battery GT parallel HEPS architecture). The 2035 GT numbers for the same are 48% and 55% at MTO and CRZ, clearly showing why at lower ranges, fuel cell hybrid GT will never show a benefit over non hybrid LH2 GT.

There have been few studies which have tried to exploit water injection fuel cell hybrid GT [51], but condensing the water from fuel cell exhaust and then pumping into the gas turbine is a much bigger technological hurdle for 2035 entry into service. There could be reasons to use fuel cell to reduce LTO NOx emissions but it can argued that batteries are much better suited to this purpose. Due to these reasons, the fuel cell hybrid isn't pursued further and the next sub-section deals with completely fuel cell powered regional turbofan.

Regional Turbofan

A very quick assessment was done for one of the regional turbofan aircraft, BAe146 to understand the potential for a complete fuel cell powered aircraft. The study was done with varying levels on all tank and fuel cell parameters, gravimetric efficiency, fuel cell stack power density, TMS power density and fuel cell sizing point efficiency, seen in Table 4.16. The total weight of the propulsion system is seen in Figure 4.84, showing the extreme weight numbers for balance of plant. The least heavy propulsion

system including the tanks comes at around 14 tonnes.

Parameter	Lower bound	Upper bound
Stack power density (kW/kg)	2	4
TMS power density (kW/kg)	2	4
Fuel cell sizing point efficiency	0.5	0.6
LH2 tank GI	0.30	0.60

Table 4.16: Parameter bounds

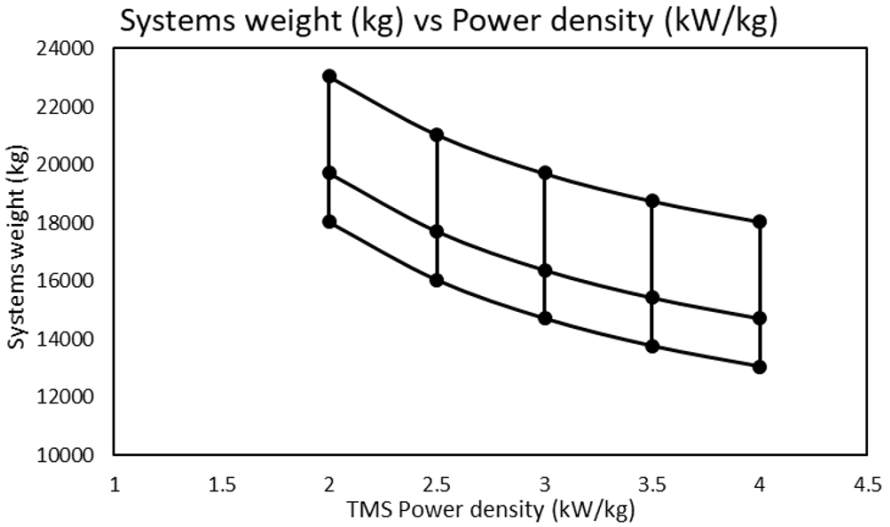


Figure 4.84: Total Balance of power plant weight for complete fuel cell aircraft

Taking the maximum bounds on TMS and stack power density and running the full aircraft mission leads to trends seen in Figures 4.85 and 4.86 for two different fuel cell efficiencies. Essentially two constraints applied the volumetric constraint (in this case fuselage length is kept fixed) and MTOW constraint and simply because of the massive weight of the fuel cell propulsion system the, the maximum allowable payload drops to 1800 kg from 7800 kg for tank gravimetric efficiency of 50%. The number doubles for 60% fuel cell efficiency as TMS weight drops but the maximum allowable is still much lower than max fuselage pax capacity.

Understanding the trends from this plots, it becomes clear that fuel cell may potentially only have application for replacement of GT on low power, high range aircraft. High Mach number, high power requirement turbofan engines will impose massive penalty on fuel cell weights and volume, thereby killing any potential application. It was then deemed that it would be really worth to assess potential application of fuel cell-battery hybrid powerplant on regional turboprop and the final section is dedicated completely to that.

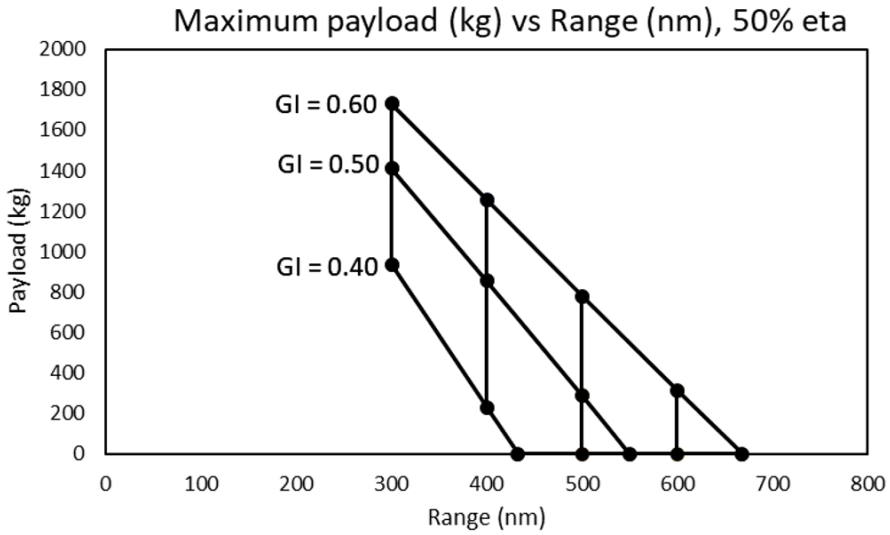


Figure 4.85: Maximum payload vs range for 50% FC eta

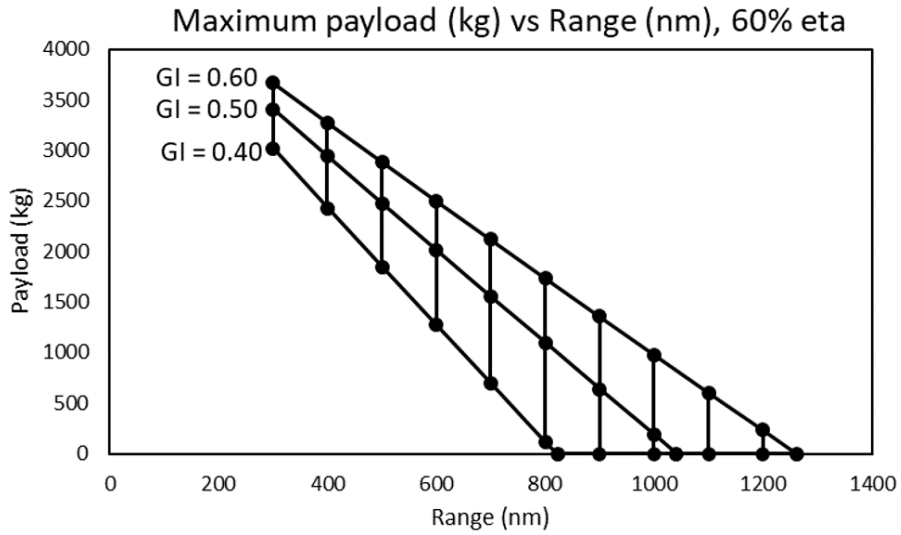


Figure 4.86: Maximum payload vs range for 60% FC eta

4.5.3 Regional Turboprop Architectural Comparison

This is the final section of the results which compares different architectures on the regional turboprop test case. The main objectives to perform this was to compare VCC and ram air HEX fuel cell powered aircraft, compare fuel cell against fuel cell and battery hybrid and finally compare all of this combinations against EIS 2035 hydrogen and kerosene powered GT. The propulsion configurations compared are summarized below and are as follows:

- Kerosene EIS 2035 GT.
- LH2 EIS 2035 GT.

- 100% Fuel cell powered ATR 72 cooled by VCC loop.
- 100% Fuel cell powered ATR 72 cooled by RA HEX.
- Fuel cell and battery powered hybrid architecture(Arch. 3 within 3.2, Fuel cell and batteries cooled by VCC loop
- Fuel cell and battery powered hybrid architecture(Arch. 3 within 3.2, Fuel cell cooled by RA HEX and batteries cooled by VCC loop
- 100% Fuel cell powered ATR 72 cooled using TMS assumptions in open literature.
- 100% Fuel cell powered ATR 72 cooled using no TMS assumptions.

Two main terms are defined here which are: $DeltaFPX$ and $DeltaEPX$ and these are defined using equations 4.3 and 4.4 respectively. It should be noted that all the hybrid architectures use LH2, it made sense to compare against LH2 EIS 2035 GT as the baseline hence the definition of $DeltaFPX$, while the total energy comsumed onboard the aircraft is normalized against Kerosene EIS 2035 GT hence the definition of $DeltaEPX$. It should also be noted that all the hydrogen architectures use fuselage mounted tanks hence the method described in Section 3.10 is used to get reduction in PAX with increasing tank fuel capacity. It is assumed that the fuel cell stack has a power density of 3 kW/kg, battery has an energy density of 500 Wh/kg and LH2 tank has a tank gravimetric index of 40%.

$$DeltaFPX = (\frac{Fuelburn}{PAX})_{Arch} - (\frac{Fuelburn}{PAX})_{LH2_{2035}} \tag{4.3}$$

$$DeltaEPX = (\frac{Energyconsumed}{PAX})_{Arch} - (\frac{Energyconsumed}{PAX})_{KE_{2035}} \tag{4.4}$$

Starting with the Delta FPX trends in Figure 4.87, it can be seen that the architecture that has the the maximum benefit across all ranges is the 100% fuel cell architecture without any TMS assumptions and it makes sense as without any TMS assumptions, the fuel cell without any TMS has the same weight density as small turboprop GT and also in turboprop class, it is better on thermal efficiency and also has significant benefits compared to the GT at lower descent and idle power settings. The next is the 100% FC with 3 kW/kg case which uses an assumption in

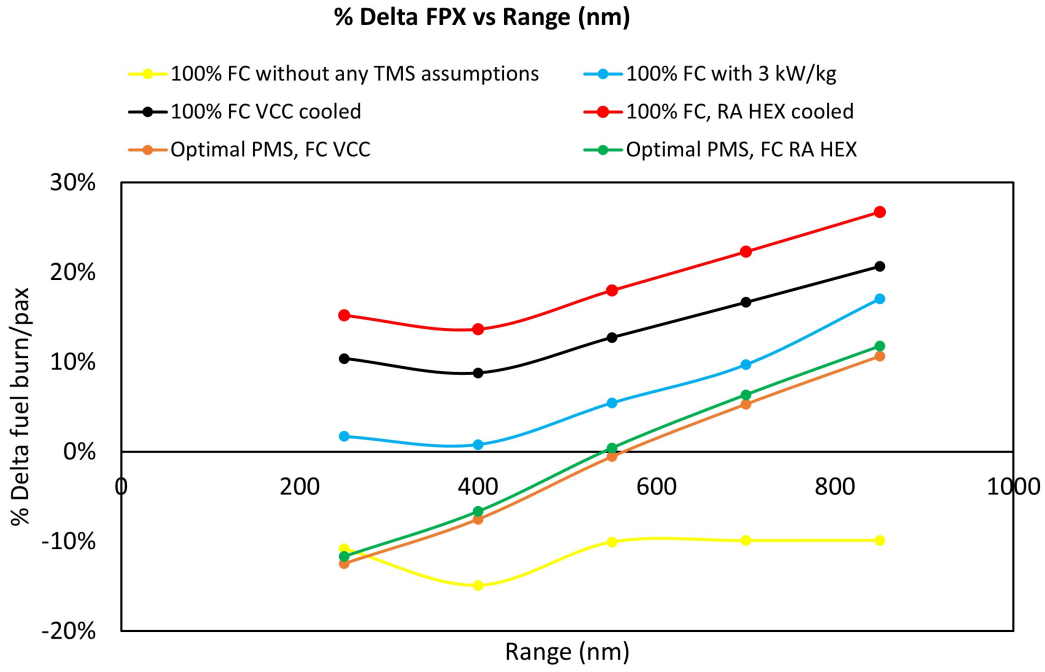


Figure 4.87: Delta Fuel burn for FC wrt LH2 GT

open literature to size the TMS and we can see the whole yellow curve (100% FC with no assumptions) shifts up and this case is consistently penalizing as compared to LH2 EIS 2035 GT. Another interesting thing to note is that both these cases have similar payload capacity as can be seen in Figure 4.89, showing that this case is volume constrained and not weight constrained. The real discussion though starts when the fuel cell cases with TMS are discussed, it can be seen that these cases are no longer volume constrained but are weight constrained as can be seen from Figure 4.89, as the weight consistently drops across the ranges to accomodate fuel and tanks. This happens as every architecture has an LH2 tank resized for each "design" range mission. It can be noticed that both the RA HEX and VCC cooled 100% FC propulsion systems have a consistent penalty in FPX ranging from 15-25%, showing the big power off-take and drag impact from Section 4.4. The numbers in open literature especially for fuel cell are greatly underpredicted and a true accounting in off-take, drag and weight makes a complete fuel cell aircraft non-viable due to big drops in PAX and increases in fuel burn. But how about a battery and fuel cell hybrid? Using the TMS integration ANN method (shown in 3.9), a split between battery and fuel cell was optimized keeping TMS design in the loop. These gave interesting trends which can be seen in Figure 4.88.

The optimizer always predicts maximum bounds on degree of hybridization by

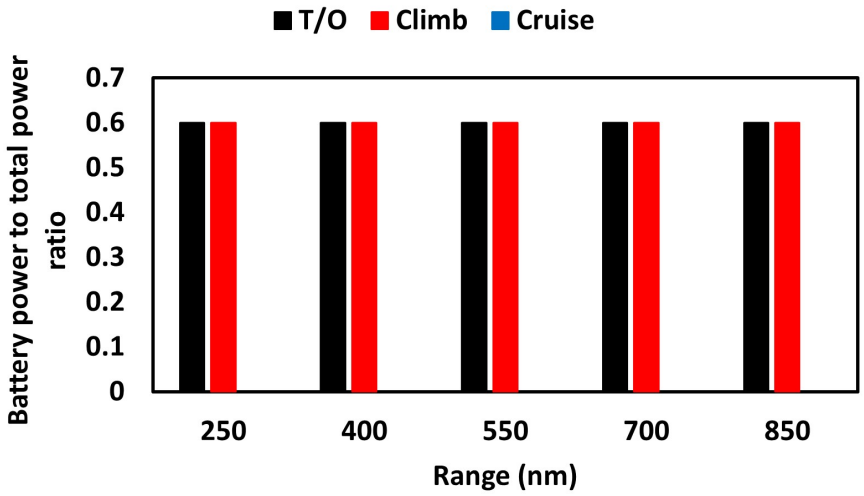


Figure 4.88: Optimal PMS for BAT FC architecture

power on the battery during take-off and climb segments while a full fuel cell powered cruise is predicted. This makes sense as the main idea would be to drop peak fuel cell heat loads such that the TMS penalty goes down drastically. The same PMS trends are observed for both ram air HEX and VCC and ram air HEX is predicted to be 1-1.5% worse than the VCC which is something which was also noticed in section 4.4.

It can also be noticed that all VCC and RA HEX cases with and without battery form a cluster (dotted ellipse) in Figure 4.89, meaning that the optimizer tends to put battery packs such that they have the same weight as the TMS packs sized for 100% DoH. Both RA HEX and VCC BAT-FC hybrid have a benefit in FPX ranging from 0-12% below 600 nm compared to LH2 EIS 2035 GT. This is a positive outcome and shows the potential for a PEM FC-battery hybrid case to be analyzed in future. But how about the energy consumption? as FPX doesnt account for the battery energy consumed.

The EPX outcomes are shown in Figure 4.90. It should be noted that the EPX is computed against kerosene EIS 2035 GT. It can be noticed that all architectures are at a penalty here, primarily due to drop in PAX capacity. HY EIS 2035 GT is at a penalty of 15-20% compared to kerosene EIS 2035 and all is attributed to reduced payload. It would be interesting to know what penalty a fuselage extension to keep same payload as kerosene would incur and should be done as future work. Coming back to the key hybrid and PEM FC architectures, it can be seen that both RA HEX and VCC only FC architectures have a penalty ranging from 30-50% while hybrid RA HEX and VCC have EPX penalty ranging from 15-40%. It should be noted that all these outcomes are for ISA +15 and the numbers especially for RA HEX will be

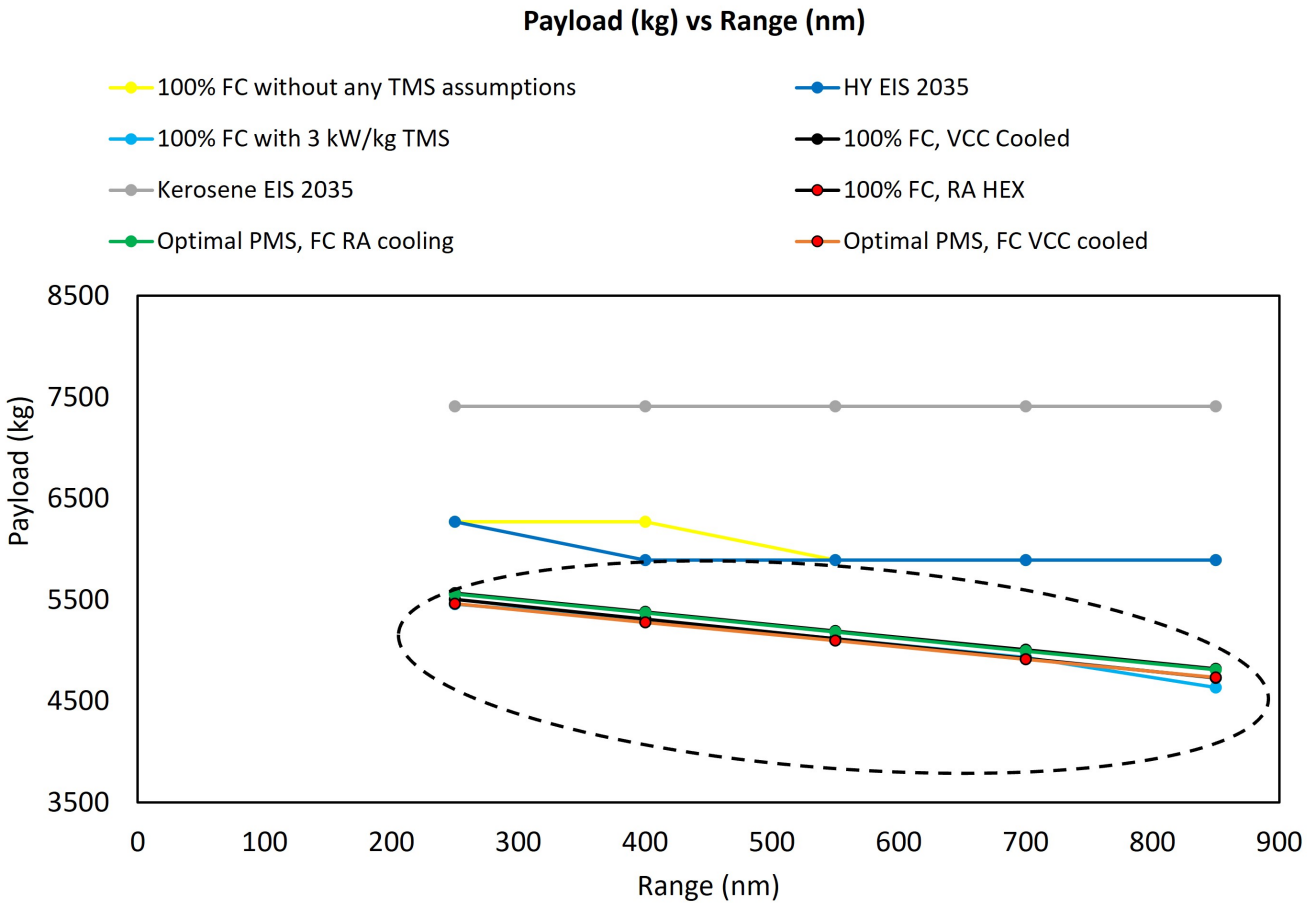


Figure 4.89: Payload comparison for all architectures

very different from these. This brings us to end of the results section of the thesis given that all architectures have now been compared with varying levels of details across the design space.

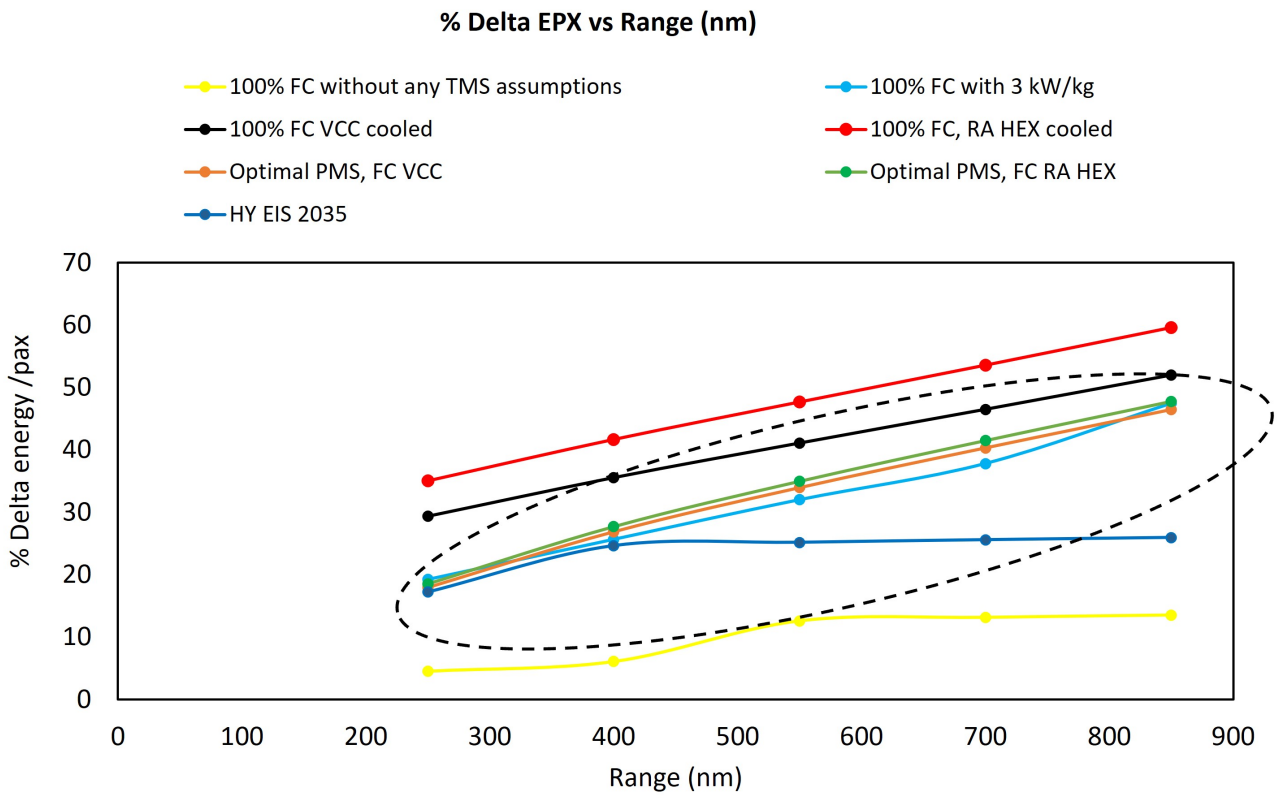


Figure 4.90: Delta EPX for all architectures

Chapter 5

Summary, Conclusions & Future Work

This chapter provides a final summary of the work done, achieved objectives, conclusions from the research and recommendations for future work.

Contents

5.1 Summary 169

5.2 Conclusions 171

5.3 Future Work 172

5.1 Summary

The thesis started by providing an introduction and context of the work. It was briefly shown the requirement for electrification of the gas turbines and the corresponding HEPS architectures and airframes envisioned. In order for transition to happen with minimal change to the airframe and to certify with maximum reliability, parallel hybrid architecture was the most preferred one. Literature review of the work done in open literature showed a research gap in a truly integrated assessment of parallel HEPS architectures. It was found that no study considered the integration of thermal management, gas turbine cycle and energy management in a single design loop. The main aim was formulated to do a comprehensive assessment of parallel HEPS architectures across the regional aircraft putting all the aforementioned elements in a simultaneous design and optimization loop. The objectives were then formulated such that the impact of each element could be separated and reasoned. The methodology

followed was then shown along with the aircraft design space.

The 3-point gas turbine cycle design approach was then shown for developing a database of designed gas turbine cycles for different degrees of hybridisation. This database was then trained using neural network to have a surrogate of design and off-design performance as a function of take-off, climb and cruise degree of hybridization for each gas turbine technology level and aircraft to be assessed. This engine performance surrogate was then called in the mission run (ORION) for each power management strategy giving all the outcomes for fuel burn, emissions, direct operating cost. The power management strategy was further optimized using genetic algorithm optimization scheme. Furthermore, a multi mission framework was then utilized to get the optimal propulsion system depending on the objective function of minimization of fuel burn or direct operating cost. The results were intially shown for regional turbofan case and the final outcomes were shown for all 3 test cases, regional turbofan (Fokker 100), regional turboprop (ATR 72) and SMR turbofan (A320). It was then concluded that there are limited scenarios where parallel HEPS on SMR aircraft had a substantial advantage in fuel burn. There would be potential scenario of application if NOx benefit is quantified and also time on wing benefits are appreciated. There could also be a potential scenario of application if idle and descent was electrified too but this needs to be quantified. There was a fuel burn benefit on the regional turboprop but it reaches a point where it is understood that full electrification is the way to go, in order to reduce operating cost.

This lead to an assessment of fuel cell hybrid architectures which required a complete development and integration of thermal management system models. Two TMS architectures were utilized in this study, vapour compression cycle utilizing R134a and liquid coolant ram air HEX. An energy penalty function accounting for contribution of ram drag, external drag, power off-take and weight was then developed for each aircraft and architecture to be assessed. Both the TMS architectures were then optimized for each PMS within an architecture using the energy penalty function. A TMS surrogate was again developed to get the optimal design variables as a function of PMS from the database developed. Finally, a back to back comparison was performed of different hybrid architectures against hydrogen and kerosene baseline GT architectures for regional turboprop aircraft. It showed a potential for a fuel cell and battery powered hybrid aircraft.

5.2 Conclusions

The final conclusions from the research can be summarized as below:

- Engine redesign offers sfc and weight benefits, while retrofitting turbine life benefit. A maximum of 1.5% fuel burn benefit can be obtained from redesigning the GT against retrofitting for SMR and regional turbofan test case.
- The potential benefits from hybridization increases with improvement in engine technology as improvement in GT technology improves reduces the power requirement, thereby dropping electrical system weights.
- Retrofitted engines favor low DoH by power during take-off and climb and high DoH by power during cruise.
- Redesigned cycles favor high DoH by power during take-off and climb and correspondingly lower DoH by power during cruise.
- Reduction in LPC Surge margin at ToC and increase in T40 at cruise will ultimately limit the percentage of hybridization into the LP Shaft for redesigned engine cycle, thereby also capping the redesign fuel burn benefit.
- A multi-mission assessment showed 10% DoH across T/O, climb and cruise flight phases and designed for 400 nm to be the optimal to maximize the fuel burn benefit.
- For SMR and regional turbofan powered aircraft maximum potential benefit of electrification is in the range of 5-6% for 750Wh/kg and EIS 2035. But this number post performing a multi-mission assessment, was found to be 2.6%.
- For SMR and regional turbofan powered aircraft maximum potential benefit of electrification is in the range of 12-14% for 500Wh/kg and EIS 2035. But this number post performing a multi-mission assessment, was found to be 10%.
- No direct operating cost benefit was found for any of the SMR or regional turbofan case but a benefit of 3% was found for the regional turboprop case.
- A new/modified airframe is required to justify hybrid electrification for regional Turboprop and no potential was found for SMR turbofan cases up to 750 Wh/kg battery energy density, when final integrated assessment was done.

- Implementing VCC TMS on SMR test case dropped fuel burn benefit by another 0.6-0.8% on SMR test case.

- No potential application scenario was found for either fuel cell GT hybrid or complete fuel cell turbofan test case.

- Performing the full TMS DSE showed the requirement to have VCC to cool fuel cells if aircraft is rated at ISA +20, while at ISA +15, both ram air HEX and VCC have similar levels of energy penalty for PEM FC case.

- For the VCC TMS, Optimizing the compressor pressure ratio against a fixed pressure ratio provides an extra 2-3% minimal energy penalty reduction and also a much more flexible design space.

- Performing a full architectural assessment showed a potential for battery fuel hybrid on regional turboprop with potential fuel burn per pax benefit up to 0-12% for ranges below 600 nm compared to LH2 GT.

- Complete fuel cell powered turboprop was found to be highly penalizing in the order to 15-25% compared to LH2 GT.

5.3 Future Work

Despite all the efforts to capture all the elements of HEPS architecture in the design loop, there is scope for extension to the framework. The future work should focus on solving these limitations and then apply it to selected case studies based on the conclusions of this work. First the modelling limitations are described followed by the future case studies.

5.3.1 Modelling limitations

The modelling limitations and potential additions to the framework are listed below.

- GT cycle design - In this study, the thrust ratios weren't varied with electrification due to the assumptions made on MTOW, but ideally design space should have even more freedom. A correct aircraft and cycle design optimization loop should be setup to cycle and match the design point thrusts, altitude and Mach.

- GT cycle design - A transient model should be developed and looped around the steady state model to get the compressor surge margin limits for both HPC and IPC and apply this with different degrees of hybridization.
- GT cycle design - Optimal T41 and T30 should be identified with electrification rather than use the baseline target T41 and T30.
- PMS Optimization - A generic surrogate and genetic algorithm based optimizers were used in this study as no design rules were known beforehand on where the optima would fall and whether the function is convex or non convex. Future work should take outcomes and trends from this study and develop some optimal control logic making the process quicker and streamlined.
- RA HEX TMS - A proper topology and fin optimization should be performed to modify HEX design with different mass flows and pinch temperature. Pumping the coolant power penalty is accounted for but the weight hasn't been considered, which should be added in the future. The modelling of the HEX on the heat load side needs greater attention with coolant lines through the load not modelled. The external drag modelling and diffuser modelling should be extended considering higher fidelity methods.
- VCC TMS - Compressor efficiency variation with pressure ratio should be included in future studies, along with different models for reciprocating and centrifugal compressors. The study should be extended to other refrigerants and in order to do that, heat transfer coefficients should be modified based on rig data especially for CO2. Cascaded cycles should be assessed as well.
- Multi-mission and TMS integration - The penalty function used to identify optimal TMS configurations should be revised to account for payload penalty on top of fuel burn.For this power off-take, drag and weight weightings should be changed.
- Fuel system modelling - In future, both compressed H2 and LH2 options should be pursued for FC-battery hybrid configurations and in order to do that, fuel tank storage should be modelled.
- Electrical systems modelling - Deterioration models of battery and fuel cell stack should be added to get better estimate of cycles to failure. Fuel cell BoP should be modelled in higher detail to more accurately estimate the power density for different designs.

The final framework after implementing the changes is shown in Figure 5.1.

5.3.2 Case studies

Based on the outcomes of this study, a list of future case studies which should be looked at are as follows:

- Fuel cell and battery powered turboprop should be investigated in future in more detail after clearing some of the modelling limitations in previous sub-section.
- LP-HP shaft power transfer and using electrification as a means of engine control should be pursued.
- Electric idle and secondary aircraft systems electrification should be pursued and some of the potential benefits from these should be quantified.
- A case can also be made for a fuel cell and battery hybrid slower turbofan and this should also potentially be pursued.

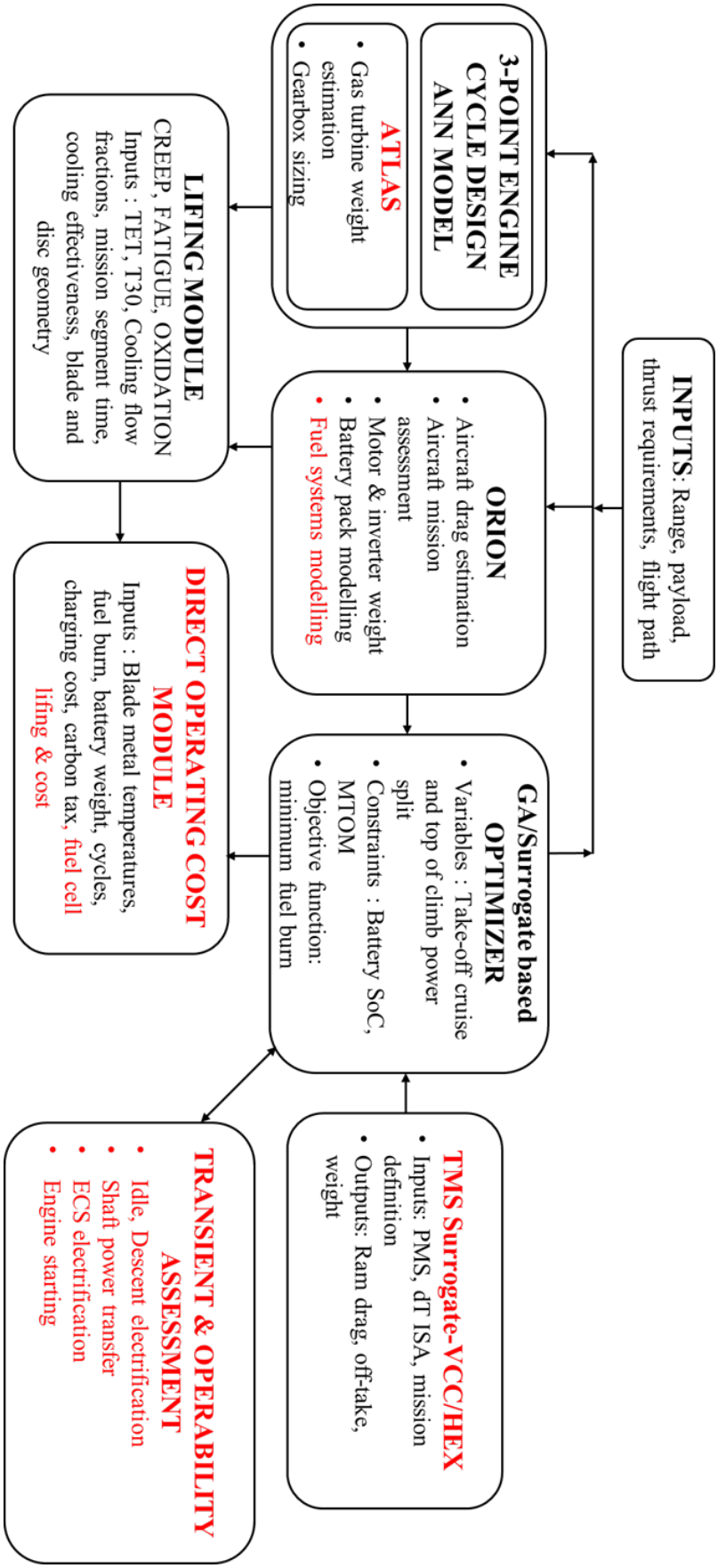


Figure 5.1: Future framework

Bibliography

[1] IATA, "Global Outlook for Air Transport - Sustained Recovery Amidst Strong Headwinds," no. December, 2022.

[2] Roland Berger, "Roadmap to True Zero . A path-breaking approach to bring down aviation ' s total climate impact .," Tech. Rep.

[3] SNETP, "SNETP Strategic Research and Innovation Agenda," no. February, 2013.

[4] Clean Aviation JU, "An Ambitious Vision for Clean Aviation," no. January, pp. 1–7, 2020.

[5] European Commission Decision C, "Climate, Energy and Mobility," Tech. Rep. July 2021, 2022, p. 2023.

[6] A. T. Institute, "ACCELERATE ZERO-CARBON EMISSION AIR TRAVEL," Tech. Rep. March, 2022.

[7] C. Lawson, I. Madani, R. Seresinhe, and D. K. Nalianda, "Trajectory Optimization of Airliners to Minimize Environmental Impact," *SAE Technical Papers*, vol. 2015-September, no. September, 2015, ISSN: 01487191. DOI: 10.4271/2015-01-2400.

[8] NASA, *NASA-DLR Study Finds Sustainable Aviation Fuel Can Reduce Contrails*. [Online]. Available: https://www.nasa.gov/news-release/nasa-dlr-study-finds-sustainable-aviation-fuel-can-reduce-contrails/.

[9] N. A. Cumpsty, "Preparing for the future: Reducing gas turbine environmental impact-IGTI scholar lecture," *Journal of Turbomachinery*, vol. 132, no. 4, pp. 1–17, 2010, ISSN: 0889504X. DOI: 10.1115/1.4001221.

[10] J. Whurr, "Future Civil Aeroengine Architectures & Technologies Chief Project Engineer, Future Programmes," 2013.

[11] A. Epstein, "Aeropropulsion: Advances, Opportunities, and Challenges," vol. 44, pp. 2694–5126, 2020. [Online]. Available: www.generations.asaging.org.

[12] K. G., "Future Aero Engine Designs: An Evolving Vision," *Advances in Gas Turbine Technology*, no. June, 2011. DOI: 10.5772/19689.

[13] A. Kharina and D. Rutherford, "Fuel efficiency trends for new commercial jet aircraft: 1960 to 2014," *International Council on Clean Transportation (ICCT)*, no. August, p. 27, 2015. [Online]. Available: www.theicct.org.

[14] N. Aeronautics and S. Administration, 2013. DOI: https://www1.grc.nasa.gov/aeronautics/eap/.

[15] K. R. Antcliff, "Mission Analysis of Hybrid Electric Regional Aircraft," *AIAA SciTech Forum*, no. January, pp. 1–18, 2016.

[16] K. P. Duffy, "Turboelectric and Hybrid Electric Aircraft Drive Key Perfomance Parameters AIAA Electric Aircraft Technologies Symposium," *AIAA Electric Aircraft Technologies Symposium*, pp. 1–23, 2018. [Online]. Available: https://ntrs.nasa.gov/search.jsp?R=20180007414.

[17] D. E. Culley, J. L. Kratz, and G. L. Thomas, "Turbine electrified energy management (TEEM) for enabling more efficient engine designs," in *2018 Joint Propulsion Conference*, 2018, pp. 1–17, ISBN: 9781624105708. DOI: 10.2514/6.2018-4798.

[18] J. L. Felder, H. D. Kim, and G. V. Brown, "Turboelectric distributed propulsion engine cycle analysis for hybrid-wing-body aircraft," *47th AIAA Aerospace Sciences Meeting including the New Horizons Forum and Aerospace Exposition*, pp. 1–25, 2009. DOI: 10.2514/6.2009-1132.

[19] R. H. Jansen, C. Bowman, A. Jankovsky, R. Dyson, and J. Felder, "Overview of NASA electrified aircraft propulsion research for large subsonic transports," *53rd AIAA/SAE/ASEE Joint Propulsion Conference, 2017*, 2017. DOI: 10.2514/6.2017-4701.

[20] G. D. Brewer, *Aircraft Technology*. 2018, ISBN: 0849358388. DOI: 10.5772/intechopen.70078.

[21] C. Goldberg, "Techno-economic, Environment and Risk Analysis of an Aircraft Concpet with Turbo-electric Distributed Propulsion," Ph.D. dissertation, Cranfield UNI.

[22] D. Verstraete, "On the energy efficiency of hydrogen-fuelled transport aircraft,"

[23] D. Verstraete, "The Potential of Liquid Hydrogen for long range aircraft propulsion," Ph.D. dissertation.

[24] P. C. Vratny, "Conceptual Design Methods of Electric Power Architectures for Hybrid Energy Aircraft," Ph.D. dissertation, TU Munich, 2018, pp. 1–166.

[25] A. Seitz, M. Nickl, A. Stroh, and P. C. Vratny, "Conceptual study of a mechanically integrated parallel hybrid electric turbofan," *Proceedings of the Institution of Mechanical Engineers, Part G: Journal of Aerospace Engineering*, vol. 232, no. 14, pp. 2688–2712, 2018, ISSN: 20413025. DOI: 10.1177/0954410018790141.

[26] J. L. Kratz, D. E. Culley, G. L. Thomas, and N. Glenn, "Evaluation of Electrical System Requirements for Implementing Turbine Electrified Energy Management," no. August, pp. 1–19, 2019. DOI: 10.2514/6.2019-4502.

[27] J. L. Kratz and D. L. Simon, "Failure Modes and Mitigation Strategies for a Turboelectric Aircraft Concept with Turbine Electrified Energy Management," *AIAA Science and Technology Forum and Exposition, AIAA SciTech Forum 2022*, pp. 1–17, 2022. DOI: 10.2514/6.2022-1191.

[28] S. Sahoo, X. Zhao, and K. Kyprianidis, "A review of concepts, benefits, and challenges for future electrical propulsion-based aircraft," *Aerospace*, vol. 7, no. 4, 2020, ISSN: 22264310. DOI: 10.3390/aerospace7040044.

[29] C. A. H. powered aviation, 2020. DOI: https://www.clean-aviation.eu/hydrogen-powered-aviation.

[30] E. Partnership and H. Europe, "European Partnership under Horizon Europe Integrated Air Traffic Management," no. July, pp. 1–43, 2020.

[31] C. Perullo, D. Trawick, M. Armstrong, J. C. Tai, and D. N. Mavris, "Cycle selection and sizing of a single-aisle transport with the Electrically Variable Engine (EVE) for fleet level fuel optimization," in *AIAA SciTech Forum - 55th AIAA Aerospace Sciences Meeting*, 2017, pp. 1–17, ISBN: 9781624104473. DOI: 10.2514/6.2017-1923.

[32] C. Lents, L. Hardin, J. Rheaume, and L. Kohlman, "Parallel hybrid gas-electric geared turbofan engine conceptual design and benefits analysis," in *52nd AIAA/SAE/ASEE Joint Propulsion Conference, 2016*, 2016, pp. 1–12, ISBN: 9781624104060. DOI: 10.2514/6.2016-4610.

[33] C. A. Saias, "SIMULATION FRAMEWORK DEVELOPMENT FOR MULTIDISCIPLINARY DESIGN OF NOVEL PROPULSION SYSTEMS FOR ROTORCRAFT," Ph.D. dissertation, Cranfield University, 2022, p. 224.

[34] T. Delaney, "Hybrid Electric Propulsion & Thermal Management Architectures," Ph.D. dissertation, Cranfield University, 2021, p. 350.

[35] P. Vassilios, R. Ioannis, N. Devaiah, M. Christos, H. Jon, S. A. Chana, G. Raj, and S. Sarath, "Gas Turbine & Advanced Propulsion Cycles," Tech. Rep., 2021.

[36] R. Ghelani, I. Roumeliotis, C. A. Saias, C. Mourouzidis, V. Pachidis, J. Norman, and M. Bacic, "Design Methodology and Mission Assessment of Parallel Hybrid Electric Propulsion Systems," *Journal of Engineering for Gas Turbines and Power*, vol. 145, no. 3, pp. 1–10, 2023, ISSN: 15288919. DOI: 10.1115/1.4055635.

[37] R. Ghelani, I. Roumeliotis, C. Mourouzidis, C. A. Saias, V. Pachidis, M. Bacic, and J. Norman, "INTEGRATED HYBRID ENGINE CYCLE DESIGN AND POWER MANAGEMENT," *Journal of Engineering for Gas Turbines and Power*, pp. 1–11, accepted, 2023.

[38] R. Ghelani, D. Obertino, M. Righi, I. Roumeliotis, E. Anselmi Palma, M. Bacic, and J. Norman, "METHODOLOGY TO INTEGRATE THERMAL MANAGEMENT STRATEGIES WITHIN AIRCRAFT PROPULSION SYSTEM DESIGN LOOP," *Applied Thermal Engineering*, vol. preparation,

[39] C. A. Saias, R. Ghelani, I. Roumeliotis, and N. Grech, "Multi-point cycle design and mission assessment of hydrogen-powered regional aircraft," *International Journal of Hydrogen Energy*, preparation.

[40] R. Ghelani, I. Roumeliotis, C. Mourouzidis, C. A. Saias, V. Pachidis, M. Bacic, and J. Norman, "Design Methodology and Mission Assessment of Parallel Hybrid Electric Propulsion Systems," in *Proceedings of the ASME Turbo Expo*, vol. 1, 2022, pp. 1–13, ISBN: 9780791885970. DOI: 10.1115/GT2022-82478.

[41] R. Ghelani, I. Roumeliotis, C. Mourouzidis, C. A. Saias, V. Pachidis, M. Bacic, and J. Norman, "INTEGRATED HYBRID ENGINE CYCLE DESIGN AND POWER MANAGEMENT," in *ASME Turbo Expo 2023*, 2023, pp. 1–11.

[42] A. S. J. V. Heerden, S. Sasi, R. Ghelani, D. Sanders, and I. Roumeliotis, "A SCALABLE HYDROGEN PROPULSION SYSTEM FOR CIVIL TRANSPORT AIRCRAFT,"

[43] V. Lhote, *Hydrogen Based Powertrain Design for a 19-Seater Aircraft*, 2021.

[44] A. Contreras, *Hydrogen fuel cell-based powertrain design for a 19-seater aircraft*, 2021.

[45] S. khaja Dudekula, *ASSESSING GREEN PROPULSION SYSTEMS FOR EXTENDED RANGE (DUAL FUEL PROPULSION SYSTEMS)*, 2023.

[46] M. Voskuijl, J. van Bogaert, and A. G. Rao, "Analysis and design of hybrid electric regional turboprop aircraft," *CEAS Aeronautical Journal*, vol. 9, no. 1, pp. 15–25, 2018, ISSN: 18695590. DOI: 10.1007/s13272-017-0272-1.

[47] G. Cinar, "A Methodology for Dynamic Sizing of Electric Power," Ph.D. dissertation, Georgia Tech, 2018, pp. 1–366.

[48] R. de Vries, M. T. Brown, and R. Vos, "A preliminary sizing method for hybrid-electric aircraft including aero-propulsive interaction effects," in *2018 Aviation Technology, Integration, and Operations Conference*, 2018, ISBN: 9781624105562. DOI: 10.2514/6.2018-4228.

[49] C. Pornet, "Conceptual Design Methods for Sizing and Performance of Hybrid-Electric Transport Aircraft," Ph.D. dissertation, TECHNISCHE UNIVERSITÄT MÜNCHEN, 2018, p. 144.

[50] S. Sahoo, K. Kyprianidis, and X. Zaho, "Performance assessment of an integrated parallel hybrid-electric propulsion system aircraft," in *ASME Turbo Expo 2019*, 2019, pp. 8–12.

[51] A. Seitz, M. Nickl, F. Troeltsch, and K. Ebner, "Initial Assessment of a Fuel Cell—Gas Turbine Hybrid Propulsion Concept," *Aerospace*, vol. 9, no. 2, 2022, ISSN: 22264310. DOI: 10.3390/aerospace9020068.

[52] M. Sielemann, C. Coïc, X. Zhao, D. E. Diamantidou, and K. Kyprianidis, "Multi-point design of parallel hybrid aero engines," *AIAA Propulsion and Energy 2020 Forum*, pp. 1–18, 2020. DOI: 10.2514/6.2020-3556.

[53] M. Sielemann, J. Gohl, X. Zhao, K. Kyprianidis, G. Valente, and S. Sumsurooah, "ON the SHAFT SPEED SELECTION of PARALLEL HYBRID AERO ENGINES," *Proceedings of the ASME Turbo Expo*, vol. 1, 2021. DOI: 10.1115/GT2021-59500.

[54] P. C. Vratny, C. Gologan, C. Pornet, A. T. Isikveren, and M. Hornung, "Battery Pack Modeling Methods for Universally-Electric Aircraft," in *Ceas 2013*, 2013, pp. 525–535.

[55] J. Zhang, I. Roumeliotis, and A. Zolotas, "Nonlinear Model Predictive Control-Based Optimal Energy Management for Hybrid Electric Aircraft Considering Aerodynamics-Propulsion Coupling Effects," *IEEE Transactions on Transportation Electrification*, vol. 8, no. 2, pp. 2640–2653, 2022, ISSN: 23327782. DOI: 10.1109/TTE.2021.3137260.

[56] D. Trawick, C. Perullo, M. Armstrong, D. Snyder, J. C. Tai, and D. Mavris, "Development and Application of GT-HEAT to design of the Electrically Variable Engine (EVE)," in *AIAA SciTech Forum*, 2017.

[57] D. R. Trawick, "A Methodology for the Determination of Optimal Operational Schedules of Hybrid Electric Architectures," Ph.D. dissertation, Georgia Tech, 2018, pp. 1–228.

[58] A. Spinelli, H. B. Enalou, B. Zaghari, T. Kipouros, and P. Laskaridis, "Application of Probabilistic Set-Based Design Exploration on the Energy Management of a Hybrid-Electric Aircraft," *MDPI Aerospace*, 2022.

[59] M. Doff-Sotta, M. Cannon, and M. Bacic, "Predictive Energy Management for Hybrid Electric Aircraft Propulsion Systems," *IEEE Transactions on Control Systems Technology*, pp. 1–22, 2022, ISSN: 15580865. DOI: 10.1109/TCST.2022.3193295. arXiv: 2103.07909.

[60] J. Zhang, I. Roumeliotis, X. Zhang, and A. Zolotas, "Techno-economic-environmental evaluation of aircraft propulsion electrification: Surrogate-based multi-mission optimal design approach," *Renewable and Sustainable Energy Reviews*, vol. 175, no. May 2022, p. 113 168, 2023, ISSN: 18790690. DOI: 10.1016/j.rser.2023.113168. [Online]. Available: https://doi.org/10.1016/j.rser.2023.113168.

[61] E. J. Adler, B. J. Brelje, and J. R. R. A. Martins, "Thermal Management System Optimization for a Parallel Hybrid Aircraft Considering Mission Fuel Burn," *Aerospace 2022, MDPI*, 2022. [Online]. Available: https://doi.org/10.3390/aerospace9050243.

[62] H. Kellermann, S. Fuhrmann, M. Shamiyeh, and M. Hornung, "Design of a Battery Cooling System for Hybrid Electric Aircraft," pp. 1–31, 2021. DOI: 10.2514/6.2021-3138.

[63] H. Kellermann, M. Lüdemann, M. Pohl, and M. Hornung, "Design and Optimization of Ram Air – Based Thermal Management Systems for Hybrid-Electric Aircraft," *MDPI Aerospace*, pp. 1–21, 2021.

[64] J. M. Rheaume and C. E. Lents, "Commercial hybrid electric aircraft thermal management system design, simulation, and operation improvements," in *AIAA Propulsion and Energy Forum and Exposition, 2019*, 2019, pp. 1–23, ISBN: 9781624105906. DOI: 10.2514/6.2019-4492.

[65] J. M. Rheaume and C. E. Lents, "Commercial hybrid electric aircraft thermal management sensitivity studies," in *AIAA Propulsion and Energy 2020 Forum*, 2020, pp. 1–6, ISBN: 9781624106026. DOI: 10.2514/6.2020-3558.

[66] I. Roumeliotis, T. Nikolaidis, V. Pachidis, O. Broca, and D. Unlu, "DYNAMIC SIMULATION OF A ROTORCRAFT HYBRID ENGINE IN SIMCENTER AMESIM," September, 2018, pp. 18–21.

[67] G. L. Thomas, D. E. Culley, J. L. Kratz, and K. L. Fisher, "Dynamic analysis of the hFan, a parallel hybrid electric turbofan engine," in *2018 Joint Propulsion Conference*, 2018, pp. 1–15, ISBN: 9781624105708. DOI: 10.2514/6.2018-4797.

[68] W Chapman, "A Study of Large-Scale Power Extraction and Insertion on Turbofan Performance and Stability," no. January, 2021.

[69] W Chapman, S. L. Schnulo, and M. P. Nitzsche, "Development of a Thermal Management System for Electrified Aircraft," no. March, 2020.

[70] J. W. Chapman, H. Hasseeb, and S. Schnulo, "Thermal management system design for electrified aircraft propulsion concepts," *AIAA Propulsion and Energy 2020 Forum*, no. March, pp. 1–23, 2020. DOI: 10.2514/6.2020-3571.

[71] A. Yoon, X. Yi, J. Martin, Y. Chen, and K. Haran, "A high-speed, high-frequency, air-core PM machine for aircraft application," *2016 IEEE Power and Energy Conference at Illinois, PECI 2016*, pp. 0–3, 2016. DOI: 10.1109/PECI.2016.7459221.

[72] Y. Chen, R. Sanchez, A. Yoon, and K. S. Haran, "Mechanical Design Considerations of an 'Ironless,' High-Specific-Power Electric Machine," *IEEE Transactions on Transportation Electrification*, vol. 3, no. 4, pp. 855–863, 2017, ISSN: 23327782. DOI: 10.1109/TTE.2017.2733763.

[73] X. Yi, T. Yang, J. Xiao, N. Miljkovic, W. P. King, and K. S. Haran, "Equivalent Thermal Conductivity Prediction of Form-Wound Windings with Litz Wire including Transposition Effects," *IEEE Transactions on Industry Applications*, vol. 57, no. 2, pp. 1440–1449, 2021, ISSN: 19399367. DOI: 10.1109/TIA.2021.3053500.

[74] Airbus, *Airbus E-Fan X*. [Online]. Available: https://www.airbus.com/en/innovation/low-carbon-aviation/hybrid-and-electric-flight/e-fan-x.

[75] Lilium, *Lilium*. [Online]. Available: https://lilium.com/jet.

[76] Joby, *Joby Aviation*. [Online]. Available: https://www.jobyaviation.com/.

[77] K. Kyprianidis, ""Multi-disciplinary conceptual design of future jet engine systems"," Ph.D. dissertation, Cranfield University, 2010. [Online]. Available: https://dspace.lib.cranfield.ac.uk/handle/1826/8041.

[78] K. G. Kyprianidis, "On Gas Turbine Conceptual Design," Ph.D. dissertation, Cranfield University, 2019.

[79] A. Guha, "Optimisation of aero gas turbine engines," *Aeronautical Journal of the Royal Aeronautical Society*, 2001.

[80] C. Mourouzidis, "Cycle Optimisation and preliminary design of very low specific thrust turbofan engines," Ph.D. dissertation, Cranfield University, 2016.

[81] A. Guha, D. Boylan, and P. Gallagher, "Determination of optimum specific thrust for civil aero gas turbine engines: A multidisciplinary design synthesis and optimisation," *Proceedings of the Institution of Mechanical Engineers, Part G: Journal of Aerospace Engineering*, vol. 227, no. 3, pp. 502–527, 2013, ISSN: 09544100. DOI: 10.1177/0954410011435623.

[82] X Zhao, S. Sahoo, K. Kyprianidis, J. Rantzer, and M. Sielemann, "Off-design performance analysis of hybridised aircraft gas turbine," *Aeronautical Journal of the Royal Aeronautical Society*, no. July, pp. 1999–2018, 2019. DOI: 10.1017/aer.2019.75.

[83] S. Kang, I. Roumeliotis, J. Zhang, and V. Pachidis, "ASSESSMENT OF ENGINE OPERABILITY AND OVERALL PERFORMANCE FOR PARALLEL HYBRID," in *Proceedings of the ASME Turbo Expo*, 2021.

[84] H. Balaghi Enalou and S. Bozhko, "Performance improvement of the CFM56-3 aircraft engine by electric power transfer," *13th European Turbomachinery Conference on Turbomachinery Fluid Dynamics and Thermodynamics, ETC 2019*, pp. 1–11, 2019. DOI: 10.29008/etc2019-004.

[85] P. C. Vratny, S. Kaiser, A. Seitz, and S. Donnerhack, "Performance Investigation of Cycle-Integrated Parallel Hybrid Turboshafts," vol. 139, no. March, pp. 1–9, 2017. DOI: 10.1115/1.4034498.

[86] T. M. Lavelle and B. P. Curlett, "Aircraft Performance and Sizing Code," no. October, 1994.

[87] J. Zamboni, R. Vos, M. Emeneth, and A. Schneegans, "A method for the conceptual design of hybrid electric aircraft," *AIAA Scitech 2019 Forum*, no. January, 2019. DOI: 10.2514/6.2019-1587.

[88] G. Cinar, E. Garcia, and D. Mavris, "A Framework for Electrified Propulsion Architecture and Operation Analysis," *Aircraft Engineering and Aerospace Technology*, vol. 92, no. 5, pp. 675–684, 2019.

[89] G. Cinar, Y. Cai, M. V. Bendarkar, A. I. Burrell, R. K. Denney, and D. N. Mavris, "System Analysis and Design Space Exploration of Regional Aircraft with Electrified Powertrains," *Journal of Aircraft*, 2022.

[90] M. K. Bradley and C. K. Droney, "Subsonic Ultra Green Aircraft Research: Phase I Final Report," *NASA technical report*, vol. CR-2011-21, no. April 2011, p. 207, 2011.

[91] M. K. Bradley, T. J. Allen, and C. K. Droney, "Subsonic Ultra Green Aircraft Research: Phase II – Volume II – Hybrid Electric Design Exploration," *NASA Technical Report*, vol. CR–2015-21, no. April, p. 76, 2015.

[92] D. Trawick, "A Method for Determining Optimal Power Management Schedules for Hybrid Electric Airplanes," in *AIAA Propulsion and Energy Forum 2019*, 2019, pp. 1–21.

[93] A. T. Isikveren, S. Kaiser, C. Pornet, and P. C. Vratny, "Pre-design strategies and sizing techniques for dual-energy aircraft," *Aircraft Engineering and Aerospace Technology*, vol. 86, no. 6, pp. 525–542, 2014, ISSN: 00022667. DOI: 10.1108/AEAT-08-2014-0122.

[94] A. T. Isikveren, "FUNDAMENTALS , PRE-DESIGN METHODS AND VARIOUS STUDIES OF HYBRID / ELECTRIC," Ph.D. dissertation, ISAE Supaero, 2019.

[95] C. A. Saias, I. Goulos, I. Roumeliotis, V. Pachidis, and M. Bacic, "Preliminary Design of Hybrid-Electric Propulsion Systems for Emerging Urban Air Mobility Rotorcraft Architectures," *Journal of Engineering for Gas Turbines and Power*, vol. 143, no. 11, 2021, ISSN: 0742-4795. DOI: 10.1115/1.4052057.

[96] T. Donateo, C. L. D. Pascalis, L. Strafella, and A. Ficarella, "Off-line and on-line optimization of the energy management strategy in a Hybrid Electric Helicopter for urban air-mobility," *Aerospace Science and Technology*, vol. 113, 2021.

[97] J. Zhang, I. Roumeliotis, and A. Zolotas, "Model-based fully coupled propulsion-aerodynamics optimization for hybrid electric aircraft energy management strategy," *Energy*, vol. 245, p. 123 239, 2022, ISSN: 03605442. DOI: 10.1016/j.energy.2022.123239. [Online]. Available: https://doi.org/10.1016/j.energy.2022.123239.

[98] J. P. S. Pinto Leite and M. Voskuijl, "Optimal energy management for hybrid-electric aircraft," *Aircraft Engineering and Aerospace Technology*, vol. 92, no. 6, pp. 851–861, 2020, ISSN: 17488842. DOI: 10.1108/AEAT-03-2019-0046. arXiv: 2004.02582.

[99] J. Zhang, I. Roumeliotis, and A. Zolotas, "Sustainable Aviation Electrification: A Comprehensive Review of Electric Propulsion System Architectures, Energy Management, and Control," *Sustainability (Switzerland)*, vol. 14, no. 10, 2022, ISSN: 20711050. DOI: 10.3390/su14105880.

[100] W. A. Jr, R. T. Tavares, and F. R. Barbosa, "System architectures for thermal management of System architectures for thermal management of hybrid-electric aircraft - FutPrInt50," 2022. DOI: 10.1088/1757-899X/1226/1/012062.

[101] C. Lents, Z. Baig, and R. Taylor, "Parallel hybrid propulsion & secondary power system architecture exploration and evaluation," in *AIAA Propulsion and Energy 2020 Forum*, 2020, pp. 1–7, ISBN: 9781624106026. DOI: 10.2514/6.2020-3555.

[102] J. W. Chapman, G. L. Thomas, and B. P. Malone, "Development and Integration of a Thermal Management," pp. 1–19, 2021. DOI: 10.2514/6.2021-3336.

[103] C. E. Lents, "Impact of Weight, Drag and Power Demand on Aircraft Energy Consumption," pp. 1–6, 2021. DOI: 10.2514/6.2021-3322.

[104] Dragan Kozulovic, "HEAT RELEASE OF FUEL CELL POWERED AIRCRAFT," in *GPPS-CH-2020-0099*, 2020.

[105] C. A. Saias, I. Goulos, V. Pachidis, and M. Bacic, "On the Effects of Optimal Implementation of Variable Rotor Speed and Power Management on Hybrid-Electric Rotorcraft," *Journal of Engineering for Gas Turbines and Power*, vol. 145, no. 3, Feb. 2023, 031028, ISSN: 0742-4795. DOI: 10.1115/1.4056855.

eprint: https://asmedigitalcollection.asme.org/gasturbinespower/article-pdf/145/3/031028/6991114/gtp_145_03_031028.pdf. [Online]. Available: https://doi.org/10.1115/1.4056855.

[106] C. A. Saias, I. Roumeliotis, I. Goulos, V. Pachidis, and M. Bacic, "Assessment of hydrogen fuel for rotorcraft applications," *International Journal of Hydrogen Energy*, vol. 47, no. 76, pp. 32 655–32 668, 2022, ISSN: 03603199. DOI: 10.1016/j.ijhydene.2022.06.316. [Online]. Available: https://doi.org/10.1016/j.ijhydene.2022.06.316.

[107] C. A. Saias, I. Roumeliotis, I. Goulos, V. Pachidis, and M. Bacic, "Design Exploration and Performance Assessment of Advanced Recuperated Hybrid-Electric Urban Air Mobility Rotorcraft," *Journal of Engineering for Gas Turbines and Power*, vol. 144, no. 3, pp. 1–11, 2022, ISSN: 15288919. DOI: 10.1115/1.4052955.

[108] F. Cappuzzo, O. Broca, and I. Roumeliotis, "Application of Model Based Systems Engineering for the Conceptual Design of a Hybrid-Electric ATR 42-500," Tech. Rep., 2020, pp. 1–13.

[109] I. Roumeliotis, C. Mourouzidis, M. Zaffereti, D. Unlu, O. Broca, and V. Pachidis, "Assessment of Thermo-Electric Power Plants for Rotorcraft Application," *Journal of Engineering for Gas Turbines and Power*, vol. 142, no. May, pp. 1–12, 2020. DOI: 10.1115/1.4045103.

[110] J. C. Gladin, "A Parametric Study of Gas Turbine Propulsion as a Function of Aircraft Size Class and Technology Level," no. January, pp. 1–37, 2017.

[111] H. Lee, C. Harris, J. Gladin, and D. N. Mavris, "A method for simultaneous optimization of power split and flight path trajectories for hybrid electric aircraft," *AIAA Scitech 2021 Forum*, no. January, pp. 1–23, 2021. DOI: 10.2514/6.2021-1010.

[112] J. M. Vegh, E. Botero, M. Clarke, J. Smart, and J. Alonso, "Current Capabilities and Challenges of NDARC and SUAVE for eVTOL Aircraft Design and Analysis," in *AIAA*, 2019.

[113] M. Clarke and J. J. Alonso, "Lithium – Ion Battery Modeling for Aerospace Applications," vol. 58, no. 6, 2021. DOI: 10.2514/1.C036209.

[114] N. Moebs, D. Eisenhut, E. Windels, J. V. D. Pols, and A. Strohmayer, "Adaptive Initial Sizing Method and Safety Assessment for Hybrid-electric Regional Aircraft," *MDPI Aerospace*, pp. 1–26, 2022.

[115] B. Zaghari, T. Zhou, H. B. Enalou, E. Pontika, and P. Laskaridis, "The Impact of Multi-Stack Fuel Cell Configurations on Electrical Architecture for a Zero Emission Regional Aircraft," no. January, pp. 1–14, 2023. DOI: 10.2514/6.2023-1593.

[116] E. Pontika, B. Zaghari, T. Zhou, H. B. Enalou, and P. Laskaridis, "Integrated Mission Performance Analysis of Novel Propulsion Systems: Analysis of a Fuel Cell Regional Aircraft Retrofit," in *AIAA SciTech Forum*, 2023, pp. 1–32. DOI: 10.2514/6.2023-0840.

[117] A. Elena, S. Dimitar, and T. Mirko, "Environmental life cycle assessment and operating cost analysis of a conceptual battery hybrid - electric transport aircraft Association of European Airlines," *CEAS Aeronautical Journal*, vol. 13, no. 1, pp. 215–235, 2022, ISSN: 1869-5590. DOI: 10.1007/s13272-021-00556-0. [Online]. Available: https://doi.org/10.1007/s13272-021-00556-0.

[118] D. Vries, D. Version, and D. Vries, "Aerodynamic Performance and Conceptual Design," Ph.D. dissertation, 2022, ISBN: 9789463842877. DOI: 10.4233/uuid.

[119] W. Ng and A. Datta, "Hydrogen fuel cells and batteries for electric-vertical takeoff and landing aircraft," *Journal of Aircraft*, vol. 56, no. 5, pp. 1765–1782, 2019, ISSN: 15333868. DOI: 10.2514/1.C035218.

[120] B. J. Brelje and J. R. Martins, "Electric, hybrid, and turboelectric fixed-wing aircraft: A review of concepts, models, and design approaches," *Progress in Aerospace Sciences*, vol. 104, no. March 2018, pp. 1–19, 2019, ISSN: 03760421. DOI: 10.1016/j.paerosci.2018.06.004. [Online]. Available: https://doi.org/10.1016/j.paerosci.2018.06.004.

[121] D. F. Finger, C. Braun, and C. Bil, "Comparative assessment of parallel-hybrid-electric propulsion systems for four different aircraft," *AIAA Scitech 2020 Forum*, vol. 1 PartF, no. January, 2020. DOI: 10.2514/6.2020-1502.

[122] V. G. Gkoutzamanis, S. E. Tsentis, O. S. Mylonas, Kalfas, Anestis I., Kyprianidis, Konstantinos G., Tsirikoglou, Panagiotis, and M. Sielemann, "Thermal Management System Considerations for a Hybrid-Electric Commuter Aircraft," *Journal of Thermophysics and Heat Transfer*, vol. 36, no. 3, 2022. DOI: 10.2514/1.T6433.

[123] D. Mo, I. Roumeliotis, C. Mourouzidis, S. Kissoon, and Y. Liu, "Assessment of Performance Boundaries and Operability of Low Specific Thrust GUHBPR

Engines for EIS2025," *Journal of Engineering for Gas Turbines and Power*, vol. 144, no. 7, pp. 1–11, 2022, ISSN: 15288919. DOI: 10.1115/1.4054405.

[124] S. Ippedico, "Cabin Blower System Analysis," Ph.D. dissertation, 2019, pp. 1–317. [Online]. Available: http://www.scopus.com/inward/record.url?eid=2-s2.0-84865607390&partnerID=tZOtx3y1%0Ahttp://books.google.com/books?hl=en&lr=&id=2LIMMD9FVXkC&oi=fnd&pg=PR5&dq=Principles+of+Digital+Image+Processing+fundamental+techniques&ots=HjrHeuS_.

[125] A. Guha, D. Boylan, and P. Gallagher, "Determination of optimum specific thrust for civil aero gas turbine engines: A multidisciplinary design synthesis and optimisation," *Proceedings of the Institution of Mechanical Engineers, Part G: Journal of Aerospace Engineering*, vol. 227, no. 3, pp. 502–527, 2013, ISSN: 09544100. DOI: 10.1177/0954410011435623.

[126] C. Svoboda, "Turbofan engine database as a preliminary design tool," *Aircraft Design*, vol. 3, no. 1, pp. 17–31, 2000, ISSN: 13698869. DOI: 10.1016/S1369-8869(99)00021-X.

[127] D. P. Raymer, *Aircraft Design: A Conceptual Approach*. 2004, ISBN: 0-930403-51-7.

[128] E. Torenbeek, *Synthesis of Subsonic Airplane Design*. 1982, ISBN: 9024727243. DOI: 10.1007/978-94-017-3202-4.

[129] Boeing Military Airplane Development, "A Method to Estimate Weight and Dimensions of Aircraft Gas Turbine Engine," Tech. Rep., 1977.

[130] P. Lolis, "Development of a Preliminary Weight Estimation Method for Advanced Turbofan Engines," Ph.D. dissertation, 2014, p. 214. [Online]. Available: https://core.ac.uk/download/pdf/29409793.pdf%0Ahttps://dspace.lib.cranfield.ac.uk/handle/1826/9244.

[131] MATLAB, *Trainlm*. [Online]. Available: https://www.mathworks.com/help/deeplearning/ref/trainlm.html.

[132] A. Seitz, "Advanced Methods for Propulsion System Integration in Aircraft Conceptual Design," Ph.D. dissertation, TECHNISCHE UNIVERSITAT MUNCHEN, 2012, pp. 1–181. [Online]. Available: http://mediatum.ub.tum.de/node?id=1079430.

[133] K. Deb, "Multi-objective optimisation using evolutionary algorithms: An introduction," in *Multi-objective Evolutionary Optimisation for Product Design and Manufacturing*, L. Wang, A. H. C. Ng, and K. Deb, Eds. London: Springer London, 2011, pp. 3–34, ISBN: 978-0-85729-652-8. DOI: 10.1007/978-0-85729-652-8_1. [Online]. Available: https://doi.org/10.1007/978-0-85729-652-8_1.

[134] MATLAB, *Surrogate optimization*. [Online]. Available: https://www.mathworks.com/help/gads/surrogateopt.html.

[135] C. Y. Justin and D. N. Mavris, "Aircraft and engine economic evaluation for fleet renewal decision-making and maintenance contract valuation," *Proceedings of the Institution of Mechanical Engineers, Part G: Journal of Aerospace Engineering*, vol. 229, no. 11, pp. 2051–2055, 2015, ISSN: 20413025. DOI: 10.1177/0954410014564403.

[136] T. Carpentier, I. Roumeliotis, S. Van Heerden, and J. Zhang, "PERFORMANCE AND ECONOMIC ASSESSMENT OF MECHANICALLY INTEGRATED PARALLEL HYBRID AIRCRAFT," in *Proceedings of the ASME Turbo Expo*, 2022.

[137] H. Hanumanthan, "Severity estimation and shop visit prediction of civil aircraft engines, Ph.D Thesis," Ph.D. dissertation, 2009.

[138] M. Elter, J. M. Sebastiampillai, D. K. Nalianda, and D. Chatzianagnostou, "Development of an aero engine life prediction methodology for preliminary design optimisation assessments," *Proceedings of the 27th ISABE Conference*, pp. 1–11, 2017.

[139] United States Department of Transportation, *Bureau of Transportation Studies*. [Online]. Available: https://www.transtats.bts.gov/.

[140] FlyZero, "FZO-AIN-REP-0007-FlyZero-Zero-Carbon-Emission-Aircraft-Concepts-2," Tech. Rep., 2022.

[141] D. Juschus, *Preliminary Propulsion System Sizing Methods for PEM Fuel Cell Aircraft*, 2021. [Online]. Available: http://repository.tudelft.nl/..

[142] *CHARGED ELECTRIC VEHICLES MAGAZINE*, 2014. [Online]. Available: https://chargedevs.com/features/high-voltage-ev-battery-packs-benefits-and-challenges-more-voltage-more-better/.

[143] S. Stückl, "Methods for the Design and Evaluation of Future Aircraft Concepts Utilizing Electric Propulsion Systems," Ph.D. dissertation, 2016, pp. 1–173. [Online]. Available: https://d-nb.info/1107543258/34.

[144] K. Ibrahim, S. Sampath, and D. Nalianda, "Optimal Voltage and Current Selection for Turboelectric Aircraft Propulsion Networks," *IEEE Transactions on Transportation Electrification*, vol. 6, no. 4, pp. 1625–1637, 2020, ISSN: 23327782. DOI: 10.1109/TTE.2020.3004308.

[145] H. Neudorfer, "Weiterentwicklung von elektrischen antriebssystemen für elektro- und hybridstraßenfahrzeuge," de, Darmstadt, Techn. Univ., Habil.-Schr., 2008, habilitation, 2008. [Online]. Available: http://tubiblio.ulb.tu-darmstadt.de/36652/.

[146] J. Rucker, "Design and Analysis of a Permanent Magnet Generator for Naval Applications," Ph.D. dissertation, 2004.

[147] M. D. Bogomolov, "Concept study of 20 MW high- speed permanent magnet synchronous motor for marine propulsion," Ph.D. dissertation, 2013, ISBN: 9789044411911.

[148] Panasonic, "NCR20700A data sheet," Tech. Rep., 2020.

[149] W. Bhatti, W. Wu, F. Doyle, J. Llambrich, and H. Webber, "Fuel Cells Technical Analysis," no. March, 2022.

[150] K. Guo, "Optimisation of Plate/ Plate Fin Heat Exchanger Design," Ph.D. dissertation, University of Manchester, 2015.

[151] H. Peng and X. Ling, "Optimal design approach for the plate-fin heat exchangers using neural networks cooperated with genetic algorithms," vol. 28, pp. 642–650, 2008. DOI: 10.1016/j.applthermaleng.2007.03.032.

[152] M Youse, R Enayatifar, and A. N. Darus, "Optimal design of plate- fin heat exchangers by a hybrid evolutionary algorithm," vol. 39, pp. 258–263, 2012. DOI: 10.1016/j.icheatmasstransfer.2011.11.011.

[153] M. Picón-Núñez, G. T. Polley, and M. Medina-Flores, "Thermal design of multi-stream heat exchangers," *Applied Thermal Engineering*, vol. 22, no. 14, pp. 1643–1660, 2002, ISSN: 13594311. DOI: 10.1016/S1359-4311(02)00074-1.

[154] L. T. Kosters, X. Liu, D. Ko, J. Friedrichs, and X. Gao, "ScienceDirect Comparison of phase-change-heat-pump cooling and liquid cooling for PEM fuel cells for MW-level aviation propulsion," vol. 7, 2022. DOI: 10.1016/j.ijhydene.2022.06.235.

[155] NIST, *NIST Reference Fluid Thermodynamic and Transport Properties Database (REFPROP): Version 10*. [Online]. Available: https://www.nist.gov/srd/refprop.

[156] S. Kabelac, "Boiling of R134a in a Plate-Fin Heat Exchanger Having Offset Fins," vol. 137, no. 1718, pp. 1–10, 2015. DOI: 10.1115/1.4030910.

[157] Hoerner, *Fluid Dynamic Drag*. 2018. DOI: 10.1093/benz/9780199773787.article.b00088376.

[158] Panagiotis Giannakakis, "Design space exploration and performance modelling of advanced turbofan and open-rotor engines," Ph.D. dissertation, Cranfield University.

[159] L. Jenkinson, P. Simpkin, and D. Rhodes, *Civil Jet Aircraft Design*. 1999. DOI: 10.2514/4.473500.

[160] Jane's Aircraft Engines, "Aero-Engines - Turbofan - Rolls-Royce Tay," Tech. Rep., 2020, pp. 1–11.

[161] Statista, *Distribution of commercial aviation emissions worldwide in 2022, by aircraft type*. [Online]. Available: https://www.statista.com/statistics/1330955/aviation-emissions-shares-by-aircraft-type/%0A.

[162] M Voskuijl, "Fokker 100," 2014.

[163] Airbus SAS, "Airbus A320 - Aircraft Characteristics, Airport and Maintenance Planning," *Issue: Sep 30/85, Rev: Dec 01/20*, pp. 1–387, 2020.

[164] Francesco S. Mastropierro and D. Nalianda, "BAe 146-100 Electric Fan," Tech. Rep.

[165] P. Pilidis, "MSc Thermal Power - Gas Turbine Performance Notes," 2003.

[166] D. D. Niklas Hansson, Marty Bradley, Matt Campbell, De'Andre J. Cherry, Kelsea Cox and J. Z. Joseph Gonzalez, Curtis Moore, "Environmental Impacts of Aerospace Batteries," *Boeing Technical Journal*, 2018. [Online]. Available: https://www.boeing.com/resources/boeingdotcom/features/innovation-quarterly/aug2018/BTJ_Batteries_AUG2018_FULL.pdf.

[167] D. D. Niklas Hansson, Marty Bradley, Matt Campbell, De'Andre J. Cherry, Kelsea Cox and J. Z. Joseph Gonzalez, Curtis Moore, "Environmental Impacts of Aerospace Batteries," *Boeing Technical Journal*, 2018. [Online]. Available: https://www.boeing.com/resources/boeingdotcom/features/innovation-quarterly/aug2018/BTJ_Batteries_AUG2018_FULL.pdf.

[168] C. A. Snyder, "Exploring advanced technology gas turbine engine design and performance for the Large Civil Tiltrotor (LCTR)," *50th AIAA/ASME/SAE/ASEE Joint Propulsion Conference 2014*, no. July 2014, 2014. DOI: 10.2514/6.2014-3442.